A FUNCTIONAL ROLE FOR DYSTROGLYCAN AT INHIBITORY SYNAPSES ACROSS MULTIPLE BRAIN REGIONS

By

Jennifer N. Jahncke

A DISSERTATION

Presented to the Neuroscience Graduate Program
at the Vollum Institute and the
Oregon Health & Science University
School of Medicine
in partial fulfillment of
the requirements for the degree of

Doctor of Philosophy

March 2024

Advisor, Kevin Wright, PhD

Member & Chair, Tianyi Mao, PhD

Member, Eric Schnell, MD, PhD

Member, Skyler Jackman, PhD

Member, Swetha Murthy, PhD

Table of Contents

Acknowledgements

This dissertation, though written by me, was the product of many people and I cannot reasonably acknowledge them all individually here. I hope you know who you are: thank you.

Before graduate school I had fantastic mentors who were willing to put in the time to teach me concepts and techniques when I had absolutely no experience: Brian Trainor, Katharine Campi, James Trimmer, Hannah Bishop, Michael Crump, Karen Zito, Ivar Stein, Lin Tian, and others. Each offering unique expertise. Each wishing to help me achieve my goals, not theirs. I want to thank everyone for their time and support. They are the reason I got into graduate school in the first place.

My graduate school experience would not have been the same without the various past and present members of the Wright lab who made coming to work every day something to look forward to. First and foremost, I want to thank Kevin Wright who has been the most supportive mentor, who believed in me, who made a safe space, who took to the bench to train me personally, and who brought in many delicious spicy snacks (brain food). In no particular order: Patrick Kerstein, Daniel Miller, Matthew Pomaville, Marissa Co, Alejandra Fernandez, Yessica Santana Agreda, Teva Bracha, Arielle Isakharov, Nina Luong - thank you for lending your expertise, for stepping in to support me when I needed help, and for bringing laughter to the lab (also, more snacks). Thank you for continuing to love me and giving me space to turn into a gremlin as I got closer to my defense date.

I benefited from a dissertation advisory committee stacked with brilliant scientists who were not only genuinely excited about my project, but always had my best interests in mind. Thank you to Tianyi Mao, Eric Schnell, and Skyler Jackman. A special thank you to Eric, and members of the Schnell lab (William Hendricks, Kathleen Beeson,

Corwin Butler), for providing me with an electrophysiology rig and teaching me all things electrophysiology. I will never forget balancing rig time during the COVID shutdown wherein Cory and I were separated by a wall and Kathleen and I separated by a hanging sheet of plastic. We persevered. I also want to thank the Schnell and Westbrook labs for giving me a regular spot in their lab meeting lineup and providing outside expertise on my project.

Much of my microscopy data was generated using microscopes managed by the OHSU Advanced Light Microscopy core. Thank you to core staff (Stefanie Kaech Petrie, Brian Jenkins, Hannah Bronstein, Felice Kelly) for all the work you do to keep the facilities running smoothly. Thank you for your time, expertise, equipment, enthusiasm, and most importantly for adding to the rigor of my experiments.

Over the course of my dissertation I maintained 10+ different lines of genetically modified mice. These animals were bred for science and I want to acknowledge that my dissertation and my doctorate would not exist without their unwitting sacrifice. I have nothing but respect and appreciation for my colony. I hope that my findings with regards to the mechanism Dystroglycan's function in the brain will inform impactful therapies for patients diagnosed with dystroglycanopathies such that the lives of these laboratory animals will have a purpose beyond just me.

The majority of this dissertation was written at Upper Left Roasters (1204 SE Clay St, Portland, OR 97214). Thank you, Upper Left, for the caffeine, toast, Wi-Fi, music, and bustling atmosphere. Also, a thank you to Yessica for recommending this spot to me in the first place.

The two dogs in my life, Ollie and Dipper, took my dissertation writing very seriously. They both offered me toys and snuggles for support. One is a better lap dog than the other but I'm not naming names. I appreciate both of their contributions to my writing.

A big thank you to my parents, Jim and Christa Jahncke, who have always been supportive of my love of brains. They gave me space and opportunity to explore my interests and have been my cheerleaders along the way. My parents respect my independent nature but I always knew I could call on them for help and they'd be there. My grandparents, Robert and Elizabeth Jahncke and Hellmut and Margarete Heinisch, have been my other cheerleaders from afar. A special acknowledgment for my Omi and Opa: they immigrated from Austria in 1971 with two young children to give them the opportunity to have a better life. One of those children was my mother, who was the first in her family to go to college, paving the way for me and my siblings.

And finally, I want to thank my husband, Ramiro Romo Jr. When I was accepted into graduate school we had been dating for only a year and half but you took a chance, moving states to be with me. I wasn't sure I would be able to handle the stress of grad school, but you were there with a hot water bag, a cookie, tea, and a pile of blankets. You picked me up from campus to alleviate the commute time after a long day. You made sure I never ran out of bagels. You made me not one, but two, coffees every morning to meet my caffeine needs. You took off your therapist hat and just let me complain, not understanding a word I said, when my cells were garbage. You listened to each of my lectures multiple times to give me an audience to practice in front of (CCK baskets! Puncta!). It wasn't always easy, but you were always there. Thank you.

List of Figures

List of Tables

List of Abbreviations

AAV	Adeno-associated virus
AChE	Acetylcholinesterase
AChR	Acetylcholine Receptor
B4gat1	Beta-1,4-glucuronyltransferase 1
BAC	Bacterial Artificial Chromosome
BC	Basket Cell
CA1	Cornu Ammonis 1
Calb1	Calbindin
CAM	Cell Adhesion Molecule
CB_1R	Cannabinoid Receptor 1
CCh	Carbachol
CCK	Cholecystokinin
CGE	Caudal Ganglionic Eminence
CNS	Central Nervous System
Cntnap1	Contactin associated protein 1
Dag1	Dystroglycan
DCN	Deep Cerebellar Nuclei
DGC	Dystrophin Glycoprotein Complex
DMD	Duchenne Muscular Dystrophy
Dmd	Dystrophin
ECM	Extracellular matrix
Emx1	Empty Spiracles Homeobox 1
En1	Engrailed 1
ER	Endoplasmic Reticulum
Fkrp	Fukutin Related Protein
GABA	γ-Aminobutyric acid
$GABA_AR$	$GABA_A$ Receptor
GAD67	Glutamic Acid Decarboxylase 67
ICD	Intracellular Domain
IIH6	Matriglycan antibody
IML	Inner Molecular Layer
IN	Interneuron
IP	Immunoprecipitation
L7	Purkinje Cell Protein 2
LG	Laminin G
LGMD	Limb Girdle Muscular Dystrophy
LSL	lox-stop-lox
MAGUK	Membrane-Associated Guanylate Kinase
mIPSC	Miniature Inhibitory Postsynaptic Current
MLI	Molecular Layer Interneuron
NEX	Neurogenic differentiation factor 6 (NeuroD6)
NF-M	Neurofilament medium chain
Nlgn	Neuroligin
NMJ	Neuromuscular junction
Nrxn	Neurexin
OPC	Oligodendrocyte Precursor Cell
PC	Purkinje Cell
Pcp2	Purkinje Cell Protein 2
Pomt2	Protein O-mannosyltransferase 2
PV	Parvalbumin
RRP	Readily Releasable Pool
SC	Stellate Cell
sIPSC	Spontaneous Inhibitory Postsynaptic Current
SO	Stratum Oriens
SP	Stratum Pyramidale
SR	Stratum Radiatum
S-SCAM	Synaptic Scaffolding Molecule (MAGI-2)
TCS	Tonic-Clonic Seizure
VGAT	Vesicular GABA Transporter
VGluT1	Vesicular Glutamate Transporter 1
VGluT2	Vesicular Glutamate Transporter 2
Wnt1	Wnt Family Member 1
WT	Wild-type
ZT	Zeitgeber Time

Abstract

Neurons canonically communicate through chemical synapses whose structure is formed, refined, and maintained through the coordination of pre- and post-synaptic scaffolding molecules that interact across the synaptic cleft. One such trans-synaptic molecule, Dystroglycan (Dag1), is expressed throughout the body where it is important for muscle integrity, neuronal migration, regulation of the blood-brain barrier, axon targeting, and, as we have recently come to appreciate, the formation of inhibitory synapses. Dystroglycan is composed of two subunits: an extracellular alpha subunit and a transmembrane beta subunit. α-Dystroglycan is extensively glycosylated through the coordination of at least 19 different genes. Mutations resulting in hypoglycosylation lead to dystroglycanopathy, a class of muscular dystrophy characterized by muscular and neurological defects. Dystroglycan localizes to inhibitory synaptic populations throughout the brain, and in this dissertation I explore the mechanism through which Dystroglycan acts at inhibitory hippocampal CCK^{+}/CB_1R^{+} basket synapses (CCK:PyN) and cerebellar molecular layer interneuron synapses onto Purkinje cells (MLI:PC). In Chapter 2, I show that Dystroglycan is required for CCK:PyN axon targeting, synapse formation, and synapse function. This is dependent on Dystroglycan glycosylation, however, mild defects in Dystroglycan glycosylation do not affect synapse function. The Dystroglycan intracellular domain is required for the function, but not formation of CCK:PyN synapses. Furthermore, I show that loss of either extracellular glycosylation or the intracellular domain of Dystroglycan results in increased seizure susceptibility. In Chapter 3, I characterize a suite of *Cre* driver lines for conditional genetic deletion in cerebellar Purkinje cells, which allow me to dissect Dystroglycan's synaptic function at different stages of development. In Chapter 4, I show that Dystroglycan is required for MLI:PC synapse formation, function, and maintenance. Glycosylation is required for MLI:PC

synapse formation and function while the intracellular domain is required for synapse function but not formation. In Chapter 5, I use an unbiased proteomics screen to identify novel interacting partners of Dystroglycan in an effort to understand the composition of Dystroglycan-containing synaptic complexes. Collectively, these results advance our knowledge of the molecular mechanism behind inhibitory synapse development and will inform targeted treatments for synaptic defects in dystroglycanopathy.

Chapter 1: Introduction

Jennifer N. Jahncke[1], Kevin M. Wright[2]

[1] Neuroscience Graduate Program, Oregon Health & Science University, Portland, OR, 97239

[2] Vollum Institute, Oregon Health & Science University, Portland, OR, 97239

Adapted from:

Jahncke, J.N., Wright, K.M. (2023). “The many roles of dystroglycan in nervous system development and function”. *Developmental Dynamics*. 252(1): 61- 80. doi:10.1002/dvdy.516

During neural circuit development, neurons are born, must migrate to the correct location, send axons to distal targets, elaborate dendritic arbors with specific morphologies, and form synapses with a high degree of fidelity. This requires complex interactions between cell surface receptors and molecules in the extracellular environment. These can include extracellular matrix proteins that provide a substrate for migration and axon guidance and can also organize secreted cues. The complexity of the nervous system and the relatively limited number of molecules involved requires that many of these molecular pathways are used reiteratively throughout different stages of development and can often have disparate roles within different cell types. One such protein is Dystroglycan (Dag1), which plays complex roles at multiple stages of neural circuit development, including neuronal migration, axon guidance, synapse formation and maintenance, and a variety of roles in non-neuronal cells within the nervous system.

Dystroglycan Structure and Glycosylation

Dag1 was originally discovered as the Dystrophin-associated glycoprotein component of the Dystrophin glycoprotein complex (DGC) (Ibraghimov-Beskrovnaya et al., 1992). The DGC is composed of Dystroglycan, Dystrophin, Dystrobrevin, Sarcoglycans, Syntrophins, nNOS, and other adapter proteins with the exact composition varying between tissues (**Figure 1.1**). Dag1 is the transmembrane and extracellular portion of the DGC that serves to link the extracellular environment to the actin cytoskeleton. The *DAG1* gene is comprised of two coding exons spliced to form a single mRNA transcript that is initially translated as a single polypeptide (Ibraghimov-Beskrovnaya et al., 1992). This is subsequently processed through an autoproteolytic cleavage event to form an extracellular alpha subunit and a transmembrane beta subunit that are non-covalently associated at the plasma membrane (Akhavan et al., 2008;

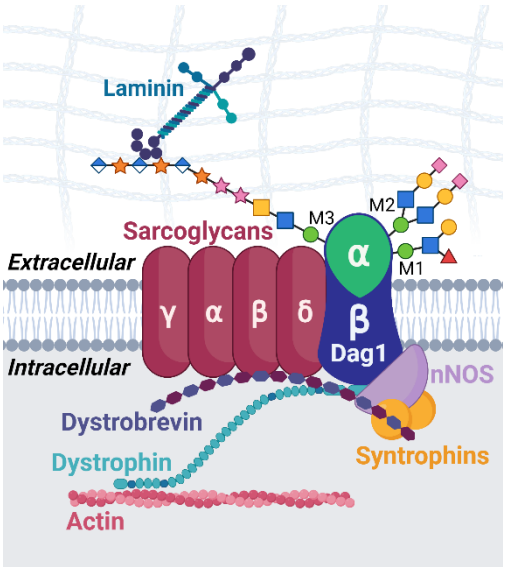

Figure 1.1 Structure of Dystroglycan and the Dystrophin glycoprotein complex (DGC).

The Dystrophin glycoprotein complex (DGC) is composed of Dystroglycan (Dag1), Dystrophin, Dystrobrevin, Sarcoglycans, Syntrophins, neuronal Nitric Oxide Synthase (nNOS) and other adapter proteins. The precise composition of the DGC varies between tissues. The glycoprotein Dystroglycan is composed of an extracellular alpha subunit that is non-covalently bound to the transmembrane beta subunit. α-Dag1 undergoes *O*-glycosylation, forming three core glycan motifs: Cores M1, M2, and M3. Core M3 is extended with a "matriglycan" chain, which interacts with proteins such as the extracellular matrix protein Laminin. The intracellular domain of β-Dag1 directly interacts with Dystrophin, which mediates the interaction with the actin cytoskeleton.

Esapa et al., 2003; Holt et al., 2000). α-Dag1 is comprised of a central mucin-like domain that is flanked by two globular domains. Within the mucin-like domain are multiple sites for post-translational glycosylation, which are essential for Dag1's ligand-binding function. The C-terminal portion of α-Dag1 mediates its binding to the N-terminal portion of β-Dag1 on the extracellular plasma membrane. β-Dag1 contains a short extracellular N-terminal region, a single-pass transmembrane domain, and a short 120 amino acid intracellular domain that contains binding sites for cytosolic proteins, including Dystrophin and several signaling adaptor proteins.

As it is trafficked through the endoplasmic reticulum and Golgi apparatus, Dag1 undergoes extensive glycosylation. The unprocessed core molecular weight of α-Dag1 is predicted to be ~70kD but migrates at anywhere between 100-200kD by western blot, depending on the tissue. While there are multiple sites for *N*- and *O*-glycosylation in the alpha subunit, removal of *N*-glycans only slightly reduces the molecular weight and does not affect its ability to bind extracellular ligands (Ervasti and Campbell, 1993, 1991). In contrast, complete chemical deglycosylation of *N*- and *O*-linked glycans reduces Dag1's molecular weight to the predicted size and results in a loss of ligand binding capacity

(Ervasti and Campbell, 1993). These results suggested that the ligand binding glycans on Dag1 were predominantly mediated by *O*-glycan chains, specifically *O*-mannosyl chains (Chiba et al., 1997; Sasaki et al., 1998; Smalheiser et al., 1998). Subsequent studies found that ligand binding glycans on Dag1 arise from a phosphorylated (GalNAc)-β3-(GlcNAc)-β4-Mannose structure, referred to as Core M3, synthesized by the coordinated action of at least 19 genes (**Figure 1.2**) (Yoshida-Moriguchi et al., 2013). (See Kanagawa and Toda, 2018 for a detailed review.) Core M3 serves as an attachment site for a GlcA-Xyl disaccharide repeat referred to as "matriglycan" that is extended by the dual xylosyltransferase and glucuronyltransferase activity of the enzyme LARGE1 (Inamori et al., 2012). Matriglycan repeats bind directly to Laminin G (LG) domain containing proteins in the extracellular environment (Briggs et al., 2016). The length of the matriglycan chain is proportional to Dag1's ligand binding capacity, suggesting that it can function as a "tunable" scaffold that can bind multiple LG domain containing proteins simultaneously (Goddeeris et al., 2013; Sheikh et al., 2021). In addition to Core M3, there are also two other types of *O*-mannosyl linked glycans referred to as Core M1 and Core M2 on α-Dag1, although these do not appear to directly mediate ligand binding (Combs and Ervasti, 2005; Hinou et al., 2019).

Dag1 is ubiquitously expressed throughout the body, and is particularly enriched in skeletal muscle, the central and peripheral nervous system, and in epithelial structures (Cohen et al., 1995; Durbeej et al., 1998; Gee et al., 1993; Ibraghimov-Beskrovnaya et al., 1992). In the nervous system, Dag1 is initially expressed early in development in neuroepithelial cells throughout the central nervous system (CNS), where Dag1 protein localization is enriched at basal laminar structures (Anderson et al., 2007; Schröder et al., 2007). At subsequent stages of neurodevelopment, Dag1 expression increases and remains elevated in subsets of neurons, where it is localized predominantly to inhibitory synapses (Lévi et al., 2002; Zaccaria et al., 2001). Dag1 is also expressed in glial cells

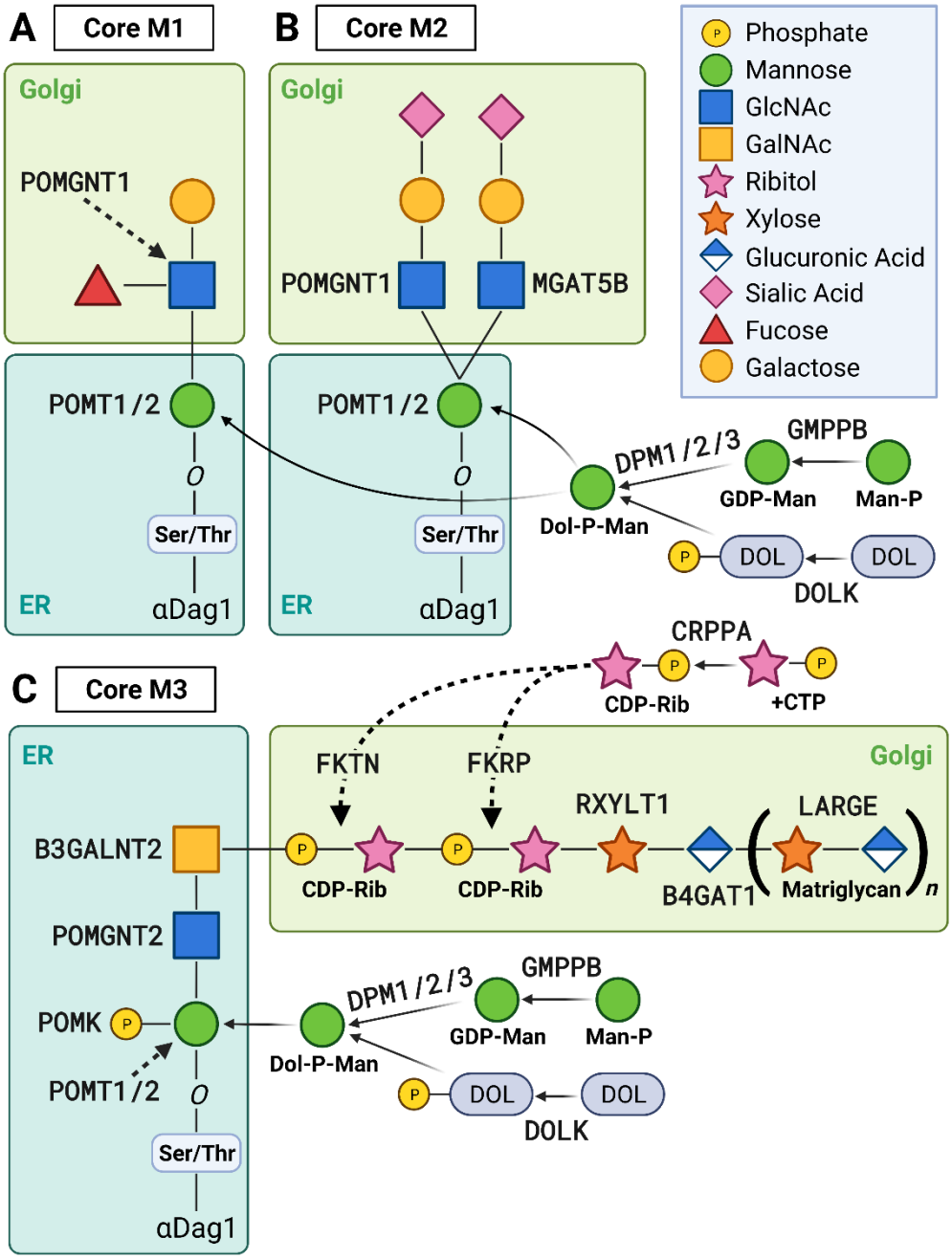

Figure 1.2 The Dystroglycan glycosylation pathway.

α-Dag1 undergoes *O*-glycosylation, forming three possible core motifs: **(A)** Core M1, **(B)** Core M2, and **(C)** Core M3. Extracellular interacting proteins bind to the "matriglycan" repeats on Core M3. Glycosylation of Dystroglycan requires the coordinated activity of at least 19 genes (see **Table 1.1**). Modification occurs in the endoplasmic reticulum (ER) and Golgi apparatus prior to trafficking to the cell surface.

and endothelial cells in the adult nervous system (Menezes et al., 2014; Tian et al., 1996). The apparent molecular weight of glycosylated Dag1 is different depending on the tissue examined, suggesting cell-type or tissue specific differences in glycosylation: skeletal muscle Dag1 migrates at ~156kD; Dag1 migrates in a broad band ranging from 120-150kD in forebrain lysates, with the higher molecular weight Dag1 originating from excitatory neurons; Dag1 in cerebellar Purkinje neurons migrates at ~180kD (Satz et al., 2010). The molecular basis for these cell-type differences in glycosylation and how they affect Dag1 function remains unknown.

Interacting Proteins

Extracellular Interactions

To date, nearly every protein identified as a binding partner for the extracellular component of Dag1 contains at least one Laminin G (LG) domain. These interacting proteins include Laminins (Ibraghimov-Beskrovnaya et al., 1992; Tian et al., 1996) Agrin (Campanelll et al., 1994; Gee et al., 1994; Sugiyama et al., 1994), Perlecan (Talts et al., 1999), Neurexins (Sugita et al., 2001), Pikachurin (Sato et al., 2008), Slit2 (Wright et al., 2012), and Celsr3/Adgrc3 (Lindenmaier et al., 2019). Biglycan is an exception to the rule, as it binds to α-Dag1 independent of Dag1 glycosylation (Bowe et al., 2000). The matriglycan repeats on glycosylated α-Dag1 constitute the LG-domain binding site. The minimum length of matriglycan appears to be around 4 repeats, with longer chains showing enhanced binding (Sheikh et al., 2021). With the extension of matriglycan repeats, Dag1 is capable of binding multiple proteins simultaneously (Goddeeris et al., 2013). It is thought that the multiple repeats of matriglycan increase the affinity for LG domains by permitting rapid rebinding after disassociation (Nagae and Yamaguchi,

2014). Considering that the degree of glycosylation varies across tissues this could result in variable binding capacities of Dag1 in different contexts.

Not all LG domains are capable of binding Dag1. Binding to Dag1 is Ca^{2+}-dependent and often requires the coordination of tandem LG domains (Briggs et al., 2016). Thus far the only known protein capable of binding Dag1 with a single LG domain is Slit2 (Wright et al., 2012). The LG4-5 domains of Laminin α2 represent the canonical Dag1 binding site, and although all 5 Laminin alpha chain isoforms each contain multiple LG domains, not all alpha chain isoforms bind Dag1 (reviewed in Dempsey et al., 2019). It is interesting that α4 and α5 chains bind Dag1, as they are not predicted to have the conserved Ca^{2+}-binding pocket needed for interaction with Dag1 (Hohenester et al., 1999). Ca^{2+}-binding is not necessary for the proper folding of the β-sandwich that makes up LG domains, but the presence of the cation likely stabilizes the structure (Stetefeld et al., 2004). It is possible that another divalent cation, such as Mg^{2+}, could also stabilize the structure enough to permit LG domain interactions with matriglycan.

Intracellular Interactions

Soon after the identification of Dag1 as a component of the DGC it was shown that intracellular domain of β-Dag1 interacts with Dystrophin directly (Rosa et al., 1996; Suzuki et al., 1994). Since the initial discovery, other intracellular Dag1 interacting proteins have been identified. The adapter protein Grb2 is one such protein, which interacts with β-Dag1 in both muscle and brain and likely acts to couple Dag1 to various signaling cascades. For example, both Grb2 and focal adhesion kinase $p125^{FAK}$ (FAK) were isolated from synaptosomal extracts by chromatography on immobilized recombinant β-Dag1. FAK is known to be at the crossroads of multiple signaling pathways including the Ras/MAPK pathway (Cavaldesi et al., 1999; Yang et al., 1995). The juxtamembrane region of β-Dag1 binds the ERM domain protein Ezrin to regulate Cdc42 activation and the formation of filopodia (Batchelor et al., 2007; Spence et al.,

2004). A recent study using an unbiased proteomics screen in the adult *Drosophila* nervous system identified an interaction between Dg (the *Drosophila* homologue of *DAG1*) and the exocyst complex that is necessary for Dg transport to the plasma membrane (Yatsenko et al., 2021).

Disease Phenotypes

Throughout the body, glycosylated Dag1 serves to connect cells to the extracellular matrix, and in particular, basement membranes. Prominent examples of this includes the sarcolemma of muscle fibers and the neuroepithelial cells in the CNS. Accordingly, mutations that affect Dag1 function result in a form of progressive congenital muscular dystrophy referred to as dystroglycanopathy. Primary dystroglycanopathy results from mutations in Dag1 itself, although examples of this are very rare (Brancaccio, 2019). Rather, the majority of mutations resulting in dystroglycanopathy are in one of 19 genes required for the functional glycosylation of Dag1 (**Table 1.1**). These are categorized as secondary dystroglycanopathy when the mutation affects an enzyme that acts directly in the glycan synthesis pathway, or tertiary dystroglycanopathy when the mutated gene is required for precursor molecules required for glycan chain extension (Kanagawa and Toda, 2017). Dystroglycanopathy is typically diagnosed based on hypoglycosylation of Dag1 by western blotting or immunohistochemistry on muscle biopsy tissue.

The clinical manifestations of dystroglycanopathy can have a wide range of severity, from a mild form of adult-onset limb-girdle muscular dystrophy to severe forms that are accompanied by widespread neurological abnormalities that can be terminal early in life. In addition to the prominent muscular and neurological symptoms, cardiac dysfunction is often observed in patients with dystroglycanopathy. The heterogenous

Table 1.1 Genes involved in the glycosylation of dystroglycan.

Gene symbol	Full Gene Name	Core	Location	Dystroglycan-opathy Degree	Previous Symbols
DAG1	Dystroglycan 1	*NA*	*NA*	primary	
GMPPB	GDP-mannose pyrophosphorylase B	M1, M2, M3	Cytosol	tertiary	
DOLK	Dolichol kinase	M1, M2, M3	Cytosol	tertiary	*TMEM15, DK1*
DPM1	Dolichyl-phosphate mannosyltransferase subunit 1	M1, M2, M3	Cytosol	tertiary	*MPDS*
DPM2	Dolichyl-phosphate mannosyltransferase subunit 2	M1, M2, M3	Cytosol	tertiary	
DPM3	Dolichyl-phosphate mannosyltransferase subunit 3	M1, M2, M3	Cytosol	tertiary	
POMT1	Protein-O-mannosyltransferase 1	M1, M2, M3	ER	secondary	
POMT2	Protein-O-mannosyltransferase 2	M1, M2, M3	ER	secondary	
MGAT5B	α-1,6-mannosylglycoprotein 6-β-N-acetylglucosaminyltransferase B	M2	Golgi	secondary	*GnT-VB, GnT-IX*
POMK	Protein-O-mannose kinase	M3	ER	secondary	*SGK196*
POMGNT1	Protein-O-mannose β-1,2-N-acetylglucosaminyltransferase 1	M1, M2	Golgi	secondary	*MEB*
POMGNT2	Protein-O-mannose β-1,4-N-acetylglucosaminyltransferase 2	M3	ER	secondary	*GTDC2, C3ORF39*
B3GALNT2	β-1,3-N-Acetylgalactosaminyltransferase 2	M3	ER	secondary	
CRPPA	CDP-L-ribitol pyrophosphorylase A	M3	Cytosol	tertiary	*ISPD*
FKTN	Fukutin	M3	Golgi	secondary	*FCMD*
FKRP	Fukutin-related protein	M3	Golgi	secondary	
RXYLT1	Ribitol xylosyltransferase 1	M3	Golgi	secondary	*TMEM5*
B4GAT1	β-1,4-Glucuronyltransferase 1	M3	Golgi	secondary	*B3GNT1, B3GNT6*
LARGE1	LARGE xylosyl- and glucuronyltransferase 1	M3	Golgi	secondary	*LARGE*
LARGE2	LARGE xylosyl- and glucuronyltransferase 2	M3	Golgi	secondary	*GYLTL1B*

range of symptoms does not necessarily reflect on the specific gene mutated in the glycosylation pathway, but rather the nature of the mutation, how it affects the enzymatic activity of the resulting gene product, and the resulting level of Dag1 hypoglycosylation. The neurological involvement in severe forms of dystroglycanopathy can include brain malformations that manifest as type II lissencephaly or focal pachygyria/polymicrogyria, midbrain/pontine/cerebellar hypoplasia, hydrocephalus, white matter abnormalities, and retinal dysplasia (Bönnemann et al., 2014; Devisme et al., 2012). The majority of patients with abnormal MRI findings have moderate to severe intellectual disability (Brun

et al., 2017; Messina et al., 2010), and epilepsy is seen in roughly 30% of patients with detectable brain malformations (Specht and Straub, 2021). Intellectual disability is also frequently observed in dystroglycanopathy patients with normal MRI, potentially highlighting an important role for Dag1 beyond regulating early structural development of the brain (Mercuri et al., 2009).

Conservation and Expression

Dystroglycan is highly conserved among metazoans as far back as porifera (sponges). The most highly conserved regions are the binding site between the alpha and beta subunits, C-terminal portion of the alpha subunit, the cytoplasmic domain, and the C-terminal end of the beta subunit. The intracellular binding partner Dystrophin is similarly conserved among metazoans (Adams and Brancaccio, 2015). Many of the glycosyltransferases responsible for extending the glycan chains on α-Dag1 are conserved even further back than *DAG1* itself. These enzymes are present in choanoflagellata, a single-celled eukaryotic precursor to metazoa that do not express *DAG1* (Bigotti and Brancaccio, 2021). Thus, it seems likely that Dag1 co-opted existing enzymes for its own purposes. The nematode *C. elegans* represents an interesting outlier case, given that almost none of the Dag1-associated glycosyltransferases are present in the *C. elegans* genome. Consistent with this, the *DAG1* homolog in *C. elegans* lacks the mucin-like domain where *O*-mannosyl chains are attached in other species (Adams and Brancaccio, 2015; Bigotti and Brancaccio, 2021; Johnson et al., 2006) and does not undergo *O*-glycosylation, instead exhibiting *N*-glycosylation.

The high degree of gene conservation among metazoans allows for researchers to take advantage of a wide variety of model systems and the genetic tools available to each system. There are conditional deletion tools and point mutations in nematodes,

Drosophila, zebrafish, and mouse. Nematodes do not express *DAG1* in muscle but remain useful for studying Dag1 function in the nervous system. Though zebrafish express Dag1 in both muscle and nervous tissue, the published literature using zebrafish models to date focuses predominantly on muscle phenotypes (Di Costanzo et al., 2014; Parsons et al., 2002).

In mammals *DAG1* is expressed by a multitude of cell types throughout the body but is most frequently studied in the context of the muscular or nervous systems. Within the brain *DAG1* is expressed in the hippocampus, cerebellum, cerebral cortex, basal ganglia, thalamus, hypothalamus, olfactory bulb, retina, and brain stem (C.górecki et al., 1994; Omori et al., 2012; Tian et al., 1996; Zaccaria et al., 2001). Within these regions, *DAG1* is expressed by neuroepithelial cells, neurons, glia, and blood vessels. Because constitutive loss of Dag1 function results in early embryonic lethality and it is expressed in a wide array of tissues and cell types, targeted genetic manipulations are invaluable for understanding its function in development and adulthood. During early nervous system development, Dag1 plays a critical role in cellular migration, dendrite morphology, and axon guidance. The subsequent expression of Dag1 in neurons during the period of synaptogenesis that is sustained into adulthood has prompted further work that shows that Dag1 holds structural and functional importance at both the neuromuscular junction (NMJ) and central synapses. These many roles of Dag1 are outlined in further detail below.

Central Nervous System Development

Cellular Migration

Type II lissencephaly is a hallmark of congenital muscular dystrophies including dystroglycanopathy and is characterized by the ectopic migration of neuronal cells into

the subarachnoid space. Mouse models of dystroglycanopathy faithfully recapitulate the phenotype observed in human patients. *DAG1* is expressed by neuroepithelial cells important for proper cell migration including radial glia in cortex and hippocampus and Bergmann glia in the cerebellum (Henion et al., 2003; Myshrall et al., 2012; Tian et al., 1996). Dag1 protein is enriched at the radial glial endfeet abutting the basement membrane at the cortical surface. Brain-specific deletion of *DAG1* results in disruptions in the basal lamina, with clear breaks in the localization of Laminin at the cortical surface, leading to the ectopic migration phenotype (Li et al., 2011; Moore et al., 2002; Myshrall et al., 2012; Nguyen et al., 2014; Satz et al., 2010, 2008).

In neocortex, the impaired integrity of the neuroepithelial scaffold in models of dystroglycanopathy results in fusion of the cortical hemispheres and a type II lissencephaly phenotype in which the cortical layers fail to delineate properly (Booler et al., 2016; Myshrall et al., 2012; Pawlisz and Feng, 2011; Satz et al., 2010, 2008). Hippocampal dentate gyrus granule cells show a similar migration phenotype, with granule cell ectopia observed in the inferior blade (Li et al., 2011). During cerebellar development, granule cells fail to properly migrate inward along Bergmann glia, resulting in ectopic granule cell heterotopia (Moore et al., 2002; Satz et al., 2010). While Purkinje neurons largely develop normally, they do occasionally overmigrate into the molecular layer. Fusion of cerebellar lobules and fusion between the midbrain and adjacent lobules is also evident with regional differences in severity between cerebellar lobules (Nguyen et al., 2014). In the retina, inner retinal neurons are disorganized with ectopic cells migrating through breaches in the inner limiting membrane (Clements et al., 2017; Satz et al., 2008).

Much of the work done to tease apart the role of Dag1 in different cellular populations has been done using conditional *DAG1* deletion in mice. Conditional deletion leverages the now widely available *Cre-lox* system. Various *Cre* driver lines

have been used to excise *DAG1* from neuroepithelial cells and their resulting progeny, either throughout the brain (*Nestin*^{Cre}, *hGFAP*^{Cre}) or selectively in the dorsal forebrain (*Emx1*^{Cre}) [1]. This results in the cortical migration phenotypes that resemble type II lissencephaly (Moore et al., 2002; Myshrall et al., 2012; Nguyen et al., 2014; Pawlisz and Feng, 2011; Satz et al., 2010). In contrast, when deletion of *DAG1* is restricted to newly born pyramidal neurons using *NEX*^{Cre}, cortical migration is normal (Früh et al., 2016; Miller and Wright, 2021; Satz et al., 2010). This demonstrates that the neuronal migration phenotype in *DAG1* mutants is non-cell autonomous, with neuroepithelial cells playing the primary role as a scaffold to support proper neuronal migration. Similarly, in the cerebellum, *Nestin*^{Cre} and *hGFAP*^{Cre} conditional mutants show the above-described granule cell migration phenotype while *L7*^{Cre} (Purkinje neurons) and *mAlpha6*^{Cre} (granule cells) conditional knockouts exhibit normal Purkinje neuron and granule cell development (Nguyen et al., 2014). For a comparison of the effects of deleting *DAG1* with different *Cre* lines see **Appendix A**.

Genetic dissection shows that Dag1 requires proper glycosylation to orchestrate neuronal migration in all brain regions described, while intracellular signaling appears to be dispensable. Mutation in any of the genes involved in the glycosylation of α-Dag1 results in hypoglycosylation to varying degrees. Similar to *DAG1* itself, complete

[1] **Conditional genetics: The *Cre-lox* system.** In the *Cre-lox* system, a driver line is engineered to express the bacterial *Cre recombinase* sequence under the control of a specific promoter or gene regulatory sequence. Cre recombinase binds a 34-base pair loxP recognition sequence. When two loxP sites in the same orientation are bound, the intervening sequences are excised from the genome, leaving a single loxP site "scar" (Orban et al., 1992). In the case of Dystroglycan, *DAG1* conditional knockout mice were designed to have loxP sites flanking exon 2, which contains most of the coding sequence for the gene (Cohn et al., 2002). When *DAG1* conditional knockout mice are crossed to a *Cre* driver line, *DAG1* is excised from *Cre* positive cells, but its expression is retained in *Cre* negative cells. This allows researchers to avoid the embryonic lethality associated with global deletion of *DAG1*. Given the ubiquitous expression of *DAG1*, the *Cre-lox* system allows for careful dissection of Dag1's role in a specific cell population.

knockout of these genes is early embryonic lethal, however many point mutants, chimeras, and conditional knockout mouse lines have been generated to study the role of Dag1 glycosylation in the musculoskeletal and central nervous systems. These mouse lines tend to exhibit similar cortical, cerebellar, and hippocampal migration phenotypes seen with neuroepithelial-specific deletion of *DAG1*. However, the severity of the phenotype seen varies with the specific mutation and correlates with the degree of retained functional glycosylation. (For a review of existing glycosylation mutants and their central nervous system defects see Nickolls and Bönnemann, 2018.) Conversely, mice expressing truncated Dag1 lacking the intracellular domain but with normal alpha-subunit glycosylation (*Dag1*$^{\Delta cyto}$) exhibit normal cellular migration throughout the central nervous system (Lindenmaier et al., 2019; Satz et al., 2010, 2009).

Axon Guidance

A forward genetic screen designed to identify novel genes involved in peripheral nervous system development identified an unexpected role for Dag1 in axon guidance (Wright et al., 2012). Mice with point mutations in *Crppa* (*Crppa*^{L79*}) and *B4gat1* (*B4gat1*^{M155T}) were originally identified based on defects in the development of descending longitudinal axonal tracts in the hindbrain. Both *Crppa*^{L79*} and *B4gat1*^{M155T} mutants exhibit hypoglycosylation of Dag1. To confirm that these axon guidance phenotypes were mediated by defective Dag1 function, *Sox2*^{Cre};*Dag1*^{cKOs} (epiblast deletion) were generated and shown to have identical phenotypes. In addition to the initial axon guidance phenotypes, several other longitudinal axon tracts in the spinal cord are abnormal in all three mutants. The dorsal funiculus of the spinal cord, comprised of centrally-projecting axons from sensory neurons in the dorsal root ganglia, has a patchy and discontinuous appearance. *Crppa*^{L79*}, *B4gat1*^{M155T}, and *Sox2*^{Cre};*Dag1*^{cKOs} also showed defective floor plate crossing by spinal cord commissural axons. In wildtype mice, commissural neurons in the dorsal spinal cord project their axons to the ventral

midline, cross through the floor plate, and turn rostrally upon exiting the floor plate. In contrast, *Crppa*^{L79*}, *B4gat1*^{M155T}, and *Sox2*^{Cre};*Dag1*^{cKO} mutants all exhibit axon stalling within the floor plate and randomized turning upon exiting the floorplate (**Figure 1.3 A**) (Wright et al., 2012). Subsequent work showed that these defects are non-cell autonomous, as commissural axons show normal floor plate crossing and anterior turning when *DAG1* is deleted from the commissural neurons (*Wnt1*^{Cre}) and in *Dag1*$^{\Delta cyto}$ mutants, which lack the intracellular domain (Lindenmaier et al., 2019).

Mechanistically, Dag1 localized to the floor plate neuroepithelial cells non-cell autonomously regulates commissural axon guidance in multiple ways. In wildtype mice, commissural axons crossing the floor plate are in close contact with the basal lamina in the ventral spinal cord. As they navigate through the floor plate, commissural axons encounter the secreted repulsive Slit proteins, which signal through Robo receptors to expel them from the floor plate and prevent recrossing (Brose et al., 1999; Long et al., 2004). Upon exiting the floor plate, Celsr3/Adgrc3 localized on the growth cones of commissural axons mediates anterior turning in response to a gradient of Wnt (Lyuksyutova et al., 2003; Shafer et al., 2011). In the absence of functional Dag1, extracellular matrix (ECM) proteins are disorganized and the basal lamina is fragmented, depriving axons of their growth substrate (Wright et al., 2012). In addition, Dag1 directly binds to Slit2 to restrict its localization to the floor plate (Wright et al., 2012). Finally, Dag1 in neuroepithelial cells also forms a *trans* interaction with Celsr3/Adgrc3 to mediate post-crossing anterior turning (Lindenmaier et al., 2019; Wright et al., 2012).

Since the initial discovery of a role for Dag1 in axon guidance in the spinal cord, additional work has identified the importance of Dag1 for axon guidance in the internal capsule, lateral olfactory tract, anterior commissure, and optic chiasm, supporting a conserved role for Dag1 in axon guidance across multiple systems (Clements and Wright, 2018; Früh et al., 2016; Lindenmaier et al., 2019; Miller and Wright, 2021).

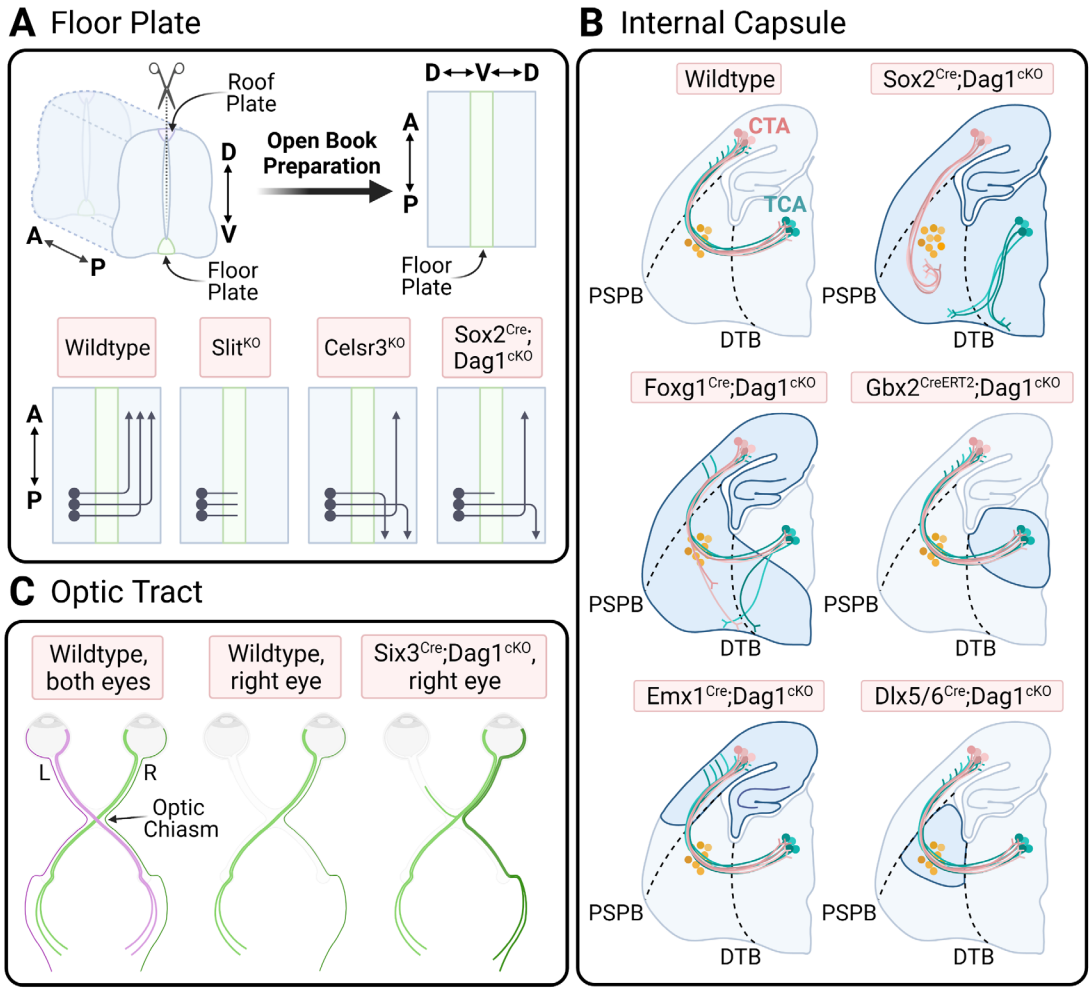

Figure 1.3 Axon guidance phenotypes in Dystroglycan mutants.

(A) Spinal commissural axons of *Dystroglycan* conditional knockouts exhibit both stalling at the floor plate and post-crossing randomized turning. This phenotype is a combination of the stalling phenotype observed in Slit KOs and the randomized turning phenotype observed in Celsr3 KOs. **(B)** The internal capsule contains descending corticothalamic axons (CTAs) and ascending thalamocortical axons (TCAs). "Corridor" cells are depicted in orange. Shaded blue regions depict areas of *Cre* recombination in various *Dystroglycan* conditional knockouts. Epiblast *Dystroglycan* conditional knockouts ($Sox2^{Cre}$) develop abnormal CTA and TCA trajectories. Neuroepithelial *Dystroglycan* is required for CTA/TCA targeting ($Foxg1^{Cre}$). Dystroglycan is not required in CTA axons ($Emx1^{Cre}$), TCA axons ($Gbx2^{CreERT2}$ + E10 tamoxifen), or corridor cells ($Dlx5/6^{Cre}$). PSPB = pallial-subpallial boundary; DTB = diencephalon-telencephalon boundary. (Figure adapted from Lindenmaier et al. 2019.[35]) **(C)** Under wildtype conditions, most retinal ganglion cell (RGC) axons primarily project from the retina to contralateral retinorecipient brain regions, crossing at the optic chiasm. A small proportion of RGC axons project ipsilaterally. In $Six3^{Cre};Dag1^{cKOs}$ (retinal neuroepithelial cells), RGCs project equally to the contra- and ipsilateral brain, as well as to the contralateral eye.

The internal capsule is comprised of descending corticothalamic axons (CTAs) and ascending thalamocortical axons (TCAs). A third population of “corridor cells” acts as an intermediate target to facilitate the guidance of CTAs and TCAs as they navigate through the ventral forebrain. Epiblast deletion of *DAG1* using *Sox2*^{Cre} results in mistargeting of both CTAs and TCAs. Descending CTAs largely fail to cross the pallial-subpallial border (PSPB), and those that do form large ectopic bundles in the ventral forebrain. The majority of TCAs make an incorrect turn at the diencephalon-telecephalon border (DTB), and rather than projecting dorsolaterally through the corridor, they project ventrally into the optic tract. The few TCAs that do successfully project into the cortex send premature misprojections into the upper layers of the cortex, rather than staying confined to the intermediate zone. Due to the ubiquitous expression of *DAG1* throughout the brain, a battery of *Cre* driver lines were used to genetically dissect where Dag1 functions to coordinate the correct assembly of the internal capsule. Internal capsule formation was normal when *DAG1* was deleted from cortical neurons (*Emx1*^{Cre}), thalamic neurons (*Gbx2*^{CreERT2} + E10.5 tamoxifen administration), and corridor cells (*Dlx5/6*^{Cre}), demonstrating that it functions non-cell autonomously. Instead, neuroepithelial Dag1 in the ventral telencephalon (*Foxg1*^{Cre}) mediates internal capsule axon guidance, possibly by regulating the formation of the permissive corridor (**Figure 1.3 B**) (Lindenmaier et al., 2019).

In the developing visual system, axons from retinal ganglion cells (RGCs) initially grow along the inner limiting membrane towards the optic nerve head, where they exit the retina. They then navigate through the optic chiasm in the ventral forebrain before projecting to one of 30 retinorecipient areas. In mice, ~90% of RGC axons cross through the chiasm and project to contralateral brain regions, while 10% project ipsilaterally (Petros et al., 2008). Deletion of *DAG1* from retinal neuroepithelial cells and the ventral forebrain using *Six3*^{Cre} disrupts the formation of the inner limiting membrane, resulting in

disorganized intraretinal axon guidance due to the loss of growth substrate (Clements et al., 2017). RGC axons in *Six3*^{Cre}*;Dag1*^{cKOs} also fail to navigate through the chiasm properly. Many axons stall within the chiasm, and those that do exit project equally to both the contralateral and ipsilateral optic tract, resulting in abnormal bilateral innervation of retinorecipient brain regions. In addition, there are aberrant projections to the contralateral eye (**Figure 1.3 C**). Both the intraretinal axon disorganization and missorting of axons at the optic chiasm are dependent on appropriate glycosylation of Dag1 as *Crppa*^{L79*} point mutants phenocopy the *DAG1* conditional knockouts (Clements and Wright, 2018).

In addition to regulating long-range axon guidance events connecting disparate regions of the nervous system, Dag1 can also regulate axon targeting in local circuits. In the hippocampus, *DAG1* is expressed by pyramidal neurons in CA1-CA3 and is required for the perisomatic innervation of these neurons by presynaptic CCK$^+$ basket interneurons. Postsynaptic deletion of *DAG1* from pyramidal cells (*NEX*^{Cre}) results in the total loss of CCK$^+$ basket interneuron axons as determined by immunostaining with markers for the specific population (VGluT3, CB_1R), whereas the PV$^+$ population of basket interneurons remains unaffected (Früh et al., 2016; Miller and Wright, 2021).

Axon guidance phenotypes have also been identified in *DAG1* mutants in both *Caenorhabditis elegans* and *Drosophila melanogaster*, indicating an evolutionarily conserved mechanism (Johnson and Kramer, 2012; Yatsenko et al., 2021). In *C. elegans*, the homologues of *DAG1* (*DGN-1*) and *Celsr3/Adgrc3* (*FMI-1*) are both required for follower axons along pioneer axons (Johnson and Kramer, 2012; Steimel et al., 2010). In *D. melanogaster*, the homologues of *DAG1* (*Dg*), *Slit/Robo*, and *Celsr3/Adgrc3* (*Flamingo*) are all required for proper targeting of photoreceptor axons to the optic lobe (Chen and Clandinin, 2008; Lee et al., 2003; Senti et al., 2003; Shcherbata et al., 2007; Tayler et al., 2004).

Synapse development and function

The Neuromuscular Junction

The first role for Dag1 in the organization of synapses was described in the 1990s when it was found that Dag1 is involved in the clustering of acetylcholine receptors (AChRs) at the neuromuscular junction (NMJ) across multiple model systems including mouse, chick, electric ray, *Xenopus*, and *Drosophila*. Dag1 was found to colocalize with AChRs at the NMJ by immunofluorescence (Cohen et al., 1995; Montanaro et al., 1998; Sugiyama et al., 1994). Agrin released from presynaptic motor neurons induces the accumulation of postsynaptic AChRs into aggregates (Reist et al., 1992). It was soon found that the application of Agrin to myotubes competes with an α-Dag1-specific antibody for binding to Dag1 (Campanelll et al., 1994; Sugiyama et al., 1994). Application of the canonical binding partner of Dag1, Laminin, also induces AChR aggregation and appears to stabilize the AChR clusters; a property which is enhanced by the application of Agrin (Cohen et al., 1997; Montanaro et al., 1998). Dag1 is therefore able to simultaneously bind at least two independent extracellular molecules at the NMJ to support its structure (**Figure 1.4 A**).

As genetic tools for manipulating *DAG1* expression became available, studies showed that deletion of *DAG1* affected AChR clustering at the NMJ. Chimeric *DAG1* knockout mice exhibited fragmented nerve terminals, and AChRs appeared in microclusters that failed to stabilize (Côté et al., 1999; Jacobson et al., 2001). Dag1 is also required for the proper localization of Acetylcholinesterase (AChE) (the enzyme responsible for rapidly breaking down acetylcholine in the synapse after presynaptic release) at the NMJ via its interactions with the heparan-sulfate proteoglycan Perlecan (Peng et al., 1999).

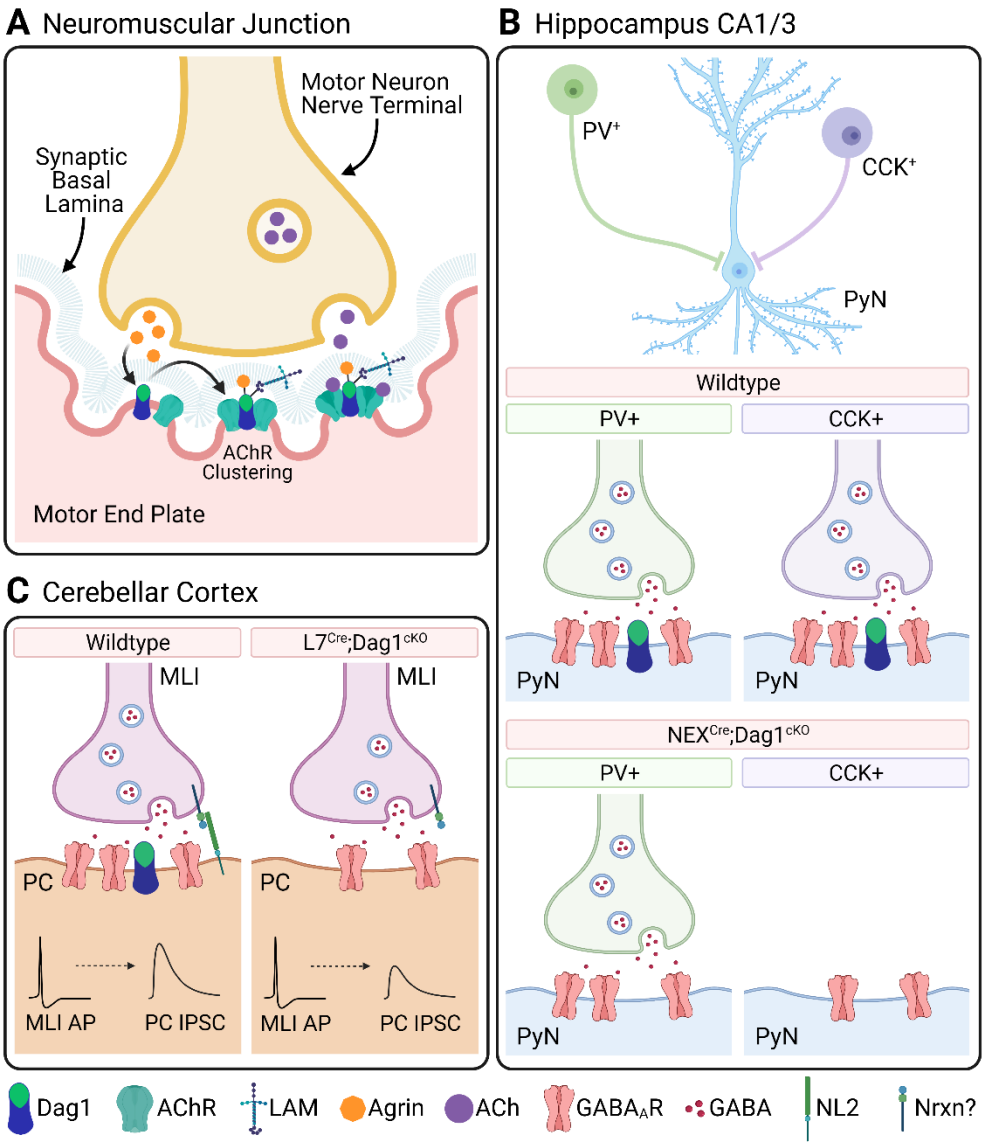

Figure 1.4 A role for Dystroglycan at synapses.

(A) Dystroglycan is localized postsynaptically at the neuromuscular junction (NMJ) end plate. Secreted neuronal Agrin binds to Dystroglycan to induce acetylcholine receptor (AChR) cluster formation. AChR clusters are then stabilized by Laminin associated with the synaptic basal lamina. **(B)** Hippocampal pyramidal neurons (PyNs) receive inhibitory perisomatic input from two classes of interneurons: PV+ and CCK+ basket interneurons. Dystroglycan is selectively required at CCK+ basket synapses. Postsynaptic deletion of *DAG1* (*NEX*^{Cre}) results in the loss of CCK+ basket synapses without affecting the PV+ population. $GABA_AR$ clustering is mildly affected. **(C)** Purkinje cells (PCs) receive inhibitory somatodendritic input from molecular layer interneurons (MLIs). PC deletion of *DAG1* (*L7*^{Cre}) results in a decrease in presynaptic inputs, fewer presynaptic vesicles in MLIs, reduced density of synaptic $GABA_ARs$, and reduced density of Neuroligin 2 (NL2), which is presumed to interact with a presynaptic scaffolding molecule such as Neurexin (Nrxn). Electrophysiological recordings from PCs show reduced IPSC frequency and amplitude. *Additional abbreviations: LAM = Laminin; AP = Action Potential, IPSC = Inhibitory Postsynaptic Current.*

The electrophysiological consequence of deleting *DAG1* at the NMJ has not been studied in depth. The only direct evidence that Dag1 is important for NMJ electrophysiological function is from a study done in *Drosophila*, where homologs of the mammalian DGC are also expressed at the *Drosophila* NMJ. In contrast to the mammalian NMJ, which is cholinergic, the *Drosophila* NMJ is glutamatergic. RNAi knockdown of *Dg* was found to affect the postsynaptic clustering of glutamate receptors, similar to the AChR-clustering role of Dag1 in other organisms. Electrophysiological recordings revealed a reduction in the amplitude of evoked junctional currents (EJCs), although miniature EJC amplitude was unchanged. It was determined that the quantal content in presynaptic vesicles was reduced. Driving *Dg* RNAi in the nervous system using elav-GAL4 did not show a electrophysiological phenotype, whereas RNAi-mediated knockdown in muscle using 24B-GAL4 recapitulated the phenotype of the global RNAi-mediated knockdown, indicating that postsynaptic Dg in muscle mediates presynaptic motoneuron release (Bogdanik et al., 2008).

In mammals, Dystrophin-deficient *mdx* mice, which show similar postsynaptic fragmentation and impaired AChR clustering (Grady et al., 2000; van der Pijl et al., 2016), have also been shown to have impaired NMJ electrophysiological function. Several studies report a decrease in the amplitude of the miniature endplate potential (mEPP) and changes in quantal content, with some studies reporting an increase in quantal content while others see a decrease or even no change (Carlson and Roshek, 2001; Lyons and Slater, 1991; Nagel et al., 1990; van der Pijl et al., 2016). This discrepancy could be explained by differences in the type of muscle or time point examined, or may be due to differences in the method of calculating quantal content.

Central Synapses

Given Dag1's role in postsynaptic receptor clustering at the NMJ and its expression at postsynaptic specializations in cortex, hippocampus, and cerebellum

(Zaccaria et al., 2001), it was hypothesized that Dag1 may function as a synaptic organizer at central synapses. Dag1 colocalizes with markers of GABAergic synapses (Briatore et al., 2020, 2010; Lévi et al., 2002; Pribiag et al., 2014; Uezu et al., 2019), but its importance at inhibitory synapses was unclear, as deletion of *DAG1* in cultured neurons did not affect inhibitory synapse differentiation (Lévi et al., 2002). Subsequent studies showed that Dag1 plays a role in regulating inhibitory synaptic scaling *in vitro*. Chronic treatment of primary hippocampal neurons with the GABA receptor antagonist bicuculline increases the amount of surface $GABA_A$ receptors ($GABA_A$Rs) as a mechanism of restoring homeostasis, leading to an increase in miniature inhibitory postsynaptic current (mIPSC) amplitude. Dag1 surface expression increases with bicuculline treatment, and RNAi-mediated knockdown of *DAG1* blocks this synaptic scaling response. Knockdown of the glycosyltransferase *LARGE1* also blocks synaptic scaling, indicating that the response requires proper glycosylation of Dag1. This suggests that an extracellular interaction mediates the effect. The responsible ligand may be Agrin, as chronic treatment with Agrin is sufficient to induce the $GABA_A$R accumulation and synaptic scaling in a Dag1-dependent manner (Pribiag et al., 2014).

In vivo studies have clarified the role of Dag1 at synapses. Early work looking at the functional consequence of *DAG1* deletion in the brain focused on hippocampal long-term potentiation (LTP). Deletion of *DAG1* from neuroepithelial/radial glial cells (and their resulting progeny) using $hGFAP^{Cre}$ results in impaired LTP (Moore et al., 2002). Postsynaptic deletion of *DAG1* from pyramidal neurons using NEX^{Cre} also results in impaired LTP, confirming that Dag1 is functioning within neurons to regulate synaptic function. The same phenotype was found in $Large^{myd}$ mice which have significantly reduced matriglycan chains on α-Dag1, showing that Dag1's role at the synapse is glycosylation dependent (Satz et al., 2010). The precise mechanism by which Dag1 supports synapse function differs between brain regions. Genetic deletion of *DAG1*

results in a decrease in $GABA_AR$ cluster size and density in specific neuronal populations (Briatore et al., 2020; Früh et al., 2016). In the hippocampus, postsynaptic deletion of *DAG1* from pyramidal neurons using NEX^{Cre} causes the loss of presynaptic inputs from CCK^+ basket interneurons. Baseline spontaneous IPSCs remain unchanged and the number of presynaptic GABAergic terminals appear relatively normal, with only slight changes to $GABA_AR$ cluster size (**Figure 1.4 B**) (Früh et al., 2016). This is likely due to the selective loss of inputs from the CCK^+ basket interneurons, while PV^+ basket interneurons remain unaffected. In the cerebellum, however, deletion of *DAG1* from Purkinje neurons using $L7^{Cre}$ results in a decrease in the number of inhibitory inputs from molecular layer interneurons, a decrease in $GABA_AR$ density, fewer presynaptic vesicles, and a progressive decrease in spontaneous IPSC amplitude with an increase in IPSC inter-event-interval (**Figure 1.4 C**) (Briatore et al., 2020). In the retina, Dag1 is located presynaptically at photoreceptor ribbon synapses – the only known instance of presynaptic Dag1. Conditional deletion of *DAG1* from photoreceptors using Crx^{Cre} results in the reduced amplitude and prolonged implicit time of the electroretinogram b-wave (Omori et al., 2012; Sato et al., 2008). In this context, the secreted, LG-domain containing molecule Pikachurin provides a link between presynaptic Dag1 and the postsynaptic transmembrane receptor GPR179 (Orlandi et al., 2018).

Many of the findings regarding Dag1's function at synapses are recapitulated in the Dystrophin-deficient *mdx* mouse. Dystrophin, a principal component of the DGC, colocalizes with Dag1 and markers of inhibitory synapses (Briatore et al., 2020; Knuesel et al., 1999; Lévi et al., 2002). $GABA_AR$ density and intensity is reduced in both hippocampus and cerebellum of *mdx* mice compared to wild-type controls (Knuesel et al., 1999). Consistent with this finding, both spontaneous and miniature IPSCs recorded from *mdx* cerebellar Purkinje neurons show a decrease in frequency and amplitude (Anderson et al., 2003; Kueh et al., 2011, 2008; Wu et al., 2022). Paired recordings

between Purkinje neurons and molecular layer interneurons (MLIs) revealed a decrease in the evoked IPSC amplitude, partially due to an increase in the synaptic failure rate in *mdx* mice. It was determined that the presynapse had a smaller readily releasable pool, reduction in the number of vesicles released, and a decrease in quantal size. Electron microscopy revealed fewer somatodendritic inputs onto Purkinje neurons (Wu et al., 2022). Electron microscopy in $L7^{Cre}$;$Dag1^{cKOs}$ (lacking Purkinje neuron Dag1) also showed fewer presynaptic vesicles at MLI:Purkinje neuron synapses (Briatore et al., 2020). Altogether this points to a role for the DGC in not only postsynaptic receptor clustering, but synapse structure and function as well.

It has been proposed that Dag1 acts as a synaptic adhesion molecule capable of supporting synapse formation or maintenance. Dag1 interacts with the presynaptic scaffolding molecule Neurexin *in vitro* (Sugita et al., 2001) and Dag1 has been shown to compete with both Neurexophilin and Neuroligin for Neurexin binding (Reissner et al., 2014), indicating that Dag1 can act as a synaptic adhesion molecule. A T190M point mutation in *DAG1* resulting in hypoglycosylated Dag1 reduces the ability of Dag1 to bind Neurexin (Hara et al., 2011). However, presynaptic innervation of pyramidal neurons in the hippocampus appears normal in these mice (Früh et al., 2016), suggesting that there may be an unknown presynaptic interacting partner of Dag1.

Discussion

Dystroglycan's primary role as the transmembrane component of the DGC is to connect the extracellular matrix to the actin cytoskeleton. The ubiquitous expression of *DAG1* throughout the body has given rise to many roles for Dag1 in muscle, the central and peripheral nervous systems, and beyond. During development of the nervous system, neuroepithelial Dag1 is required for neuronal migration in cortex, hippocampus,

cerebellum, and retina (Clements et al., 2017; Moore et al., 2002; Myshrall et al., 2012; Nguyen et al., 2014; Satz et al., 2010). Dag1 is also required non-cell autonomously for appropriate axon guidance in the spinal cord, internal capsule, and optic tract (Clements and Wright, 2018; Lindenmaier et al., 2019; Wright et al., 2012). Sustained neuronal Dag1 expression into adulthood indicates a role for Dag1 at both peripheral and central synapses. In the periphery, Dag1 is localized to the NMJ end plate where it clusters and stabilizes acetylcholine receptors (Cohen et al., 1997; Montanaro et al., 1998). In the central nervous system Dag1 is important at inhibitory synapses in the hippocampus and cerebellum and at photoreceptor synapses in the retina (Briatore et al., 2020; Früh et al., 2016; Omori et al., 2012). Dag1 is localized at synapses throughout the developing and adult brain, where it may play additional roles in synapse development and function that have not yet been studied in depth.

Is there a common mechanism for Dag1 function at synapses? Across multiple systems, Dag1 has repeatedly been shown to be involved in the clustering of receptors. Dag1/Dg induces postsynaptic acetylcholine and glutamate receptor aggregation at the mammalian and *Drosophila* NMJs, respectively (Bogdanik et al., 2008; Cohen et al., 1997; Montanaro et al., 1998). Dag1 also clusters sodium channels at nodes of Ranvier and the water channel Aquaporin-4 and the inward rectifying potassium channel Kir4.1 at the blood-brain barrier (Colombelli et al., 2015; Menezes et al., 2014; Nguyen et al., 2014; Noell et al., 2011; Satz et al., 2009). Given this conserved role for Dag1 in clustering receptors across multiple systems, it remains quite possible that Dag1 plays a similar role in clustering postsynaptic elements at inhibitory synapses in the brain. Evidence for this includes altered $GABA_A$ receptor cluster density or size in both the hippocampus and cerebellum of *DAG1* conditional knockouts (Briatore et al., 2020; Früh et al., 2016). Interestingly, conditional deletion of *GABRA1*, which encodes the $GABA_A\alpha1$ receptor subunit, from Purkinje neurons using $L7^{Cre}$ results in decreased Dag1

immunoreactivity in cerebellar cortex, suggesting a reciprocal relationship (Briatore et al., 2010). Additional work is required to understand the mechanism mediating this phenomenon. Recent work has identified an indirect interaction between Dag1 and InSyn1 through syntrophin and/or β-dystrobrevin that regulates the organization and subunit composition of GABA receptor complexes in the hippocampus (Uezu et al., 2019).

A key remaining question is whether the postsynaptic role of Dag1 requires its intracellular domain (ICD). It has long been known that the ICD of Dag1 directly binds Dystrophin, however it is unknown whether (1) Dag1 is required for the proper localization of synaptic Dystrophin, (2) Dystrophin is required for the proper localization of synaptic Dag1, or (3) both are reciprocally required for the proper localization of the DGC at synapses. Interestingly, Briatore et al. (Briatore et al., 2020) performed Dystrophin and Dag1 immunostaining in Purkinje neurons of the Dystrophin-deficient *mdx* mouse and showed that the extracellular α-Dag1 maintains proper localization at inhibitory synapses, while the transmembrane β-Dag1 is undetected. This result highlights the “chicken-and-egg” relationship between Dystroglycan and Dystrophin that requires further careful analysis (Krasowska et al., 2014).

What are the relevant extracellular binding partners for Dag1 at each step of neural circuit development? The long matriglycan chains allow Dag1 to bind multiple LG-domain containing proteins simultaneously. Defining which binding events are important at any one time or place is complicated, as loss of *DAG1* or its defective glycosylation affects all of these interactions. For example, Dag1 in the spinal cord floor plate governs axon guidance by simultaneously binding ECM proteins such as Laminin to regulate basal lamina integrity, coordinating distribution of secreted Slit proteins, and binding the axon guidance receptor Celsr3/Adgrc3 in *trans* (Lindenmaier et al., 2019; Miller and Wright, 2021). While Dag1 can bind presynaptic Neurexins, this is unlikely to be the sole

extracellular binding partner that mediates Dag1 function at inhibitory synapses (Sugita et al., 2001). While Neurexins have been shown to play a critical role at a number of inhibitory synapses, the specific inhibitory synapses known to be affected by loss of *Dag1* (hippocampal CCK^+ basket synapses, cerebellar MLI:Purkinje neuron synapses) have not yet been examined in *Neurexin* mutants. In addition, other known LG-domain containing Dag1-interacting proteins are also localized to synapses. Parsing the respective roles of these interactions requires careful genetic dissection of each specific extracellular binding partner.

Chapter 2: Hippocampal inhibitory CCK$^+$ basket synapse defects in mouse models of dystroglycanopathy

Jennifer N. Jahncke[1,], Daniel S. Miller[1,], Milana Krush[1], Eric Schnell[2,3], and Kevin M. Wright[4]

[1] Neuroscience Graduate Program, Oregon Health & Science University, Portland, OR 97239, USA

[2] Operative Care Division, Portland VA Health Care System

[3] Anesthesiology and Perioperative Medicine, Oregon Health & Science University, Portland, OR 97239, USA

[4] Vollum Institute, Oregon Health & Science University, Portland, OR 97239, USA

Adapted from:

Jahncke, J. N., Miller, D. S., Krush, M., Schnell, E., & Wright, K. M. (2024). Inhibitory CCK$^+$ basket synapse defects in mouse models of dystroglycanopathy. *Elife*, 12, RP87965. doi:10.7554/eLife.87965.3

Abstract

Dystroglycan (Dag1) is a transmembrane glycoprotein that links the extracellular matrix to the actin cytoskeleton. Mutations in *Dag1* or the genes required for its glycosylation result in dystroglycanopathy, a type of congenital muscular dystrophy characterized by a wide range of phenotypes including muscle weakness, brain defects, and cognitive impairment. We investigated interneuron (IN) development, synaptic function, and associated seizure susceptibility in multiple mouse models that reflect the wide phenotypic range of dystroglycanopathy neuropathology. Mice that model severe dystroglycanopathy due to forebrain deletion of *Dag1* or *Pomt2*, which is required for Dystroglycan glycosylation, show significant impairment of CCK^+/CB_1R^+ IN development. CCK^+/CB_1R^+ IN axons failed to properly target the somatodendritic compartment of pyramidal neurons in the hippocampus, resulting in synaptic defects and increased seizure susceptibility. Mice lacking the intracellular domain of Dystroglycan have milder defects in CCK^+/CB_1R^+ IN axon targeting, but exhibit dramatic changes in inhibitory synaptic function, indicating a critical postsynaptic role of this domain. In contrast, CCK^+/CB_1R^+ IN synaptic function and seizure susceptibility was normal in mice that model mild dystroglycanopathy due to partially reduced Dystroglycan glycosylation. Collectively, these data show that inhibitory synaptic defects and elevated seizure susceptibility are hallmarks of severe dystroglycanopathy, and show that Dystroglycan plays an important role in organizing functional inhibitory synapse assembly.

Introduction

The formation of neural circuits is a multistep process involving proliferation, migration, axon guidance, maturation of neuronal subtypes, and establishment of functional synaptic connections between neurons. The cell adhesion molecule Dystroglycan is widely expressed in muscle and brain. Within the forebrain, Dystroglycan is expressed in neuroepithelial cells, pyramidal neurons, astrocytes, oligodendrocytes, and vascular endothelial cells where it plays important roles in the formation of basement membranes during early brain development (Colognato et al., 2007; Nguyen et al., 2014; Nickolls and Bönnemann, 2018; Tian et al., 1996; Zaccaria et al., 2001). At later developmental stages, Dystroglycan is present at multiple synapses, including at photoreceptor ribbon synapses in the retina (Omori et al., 2012; Orlandi et al., 2018), inhibitory synapses in the cerebellum (Briatore et al., 2020, 2010; Patrizi et al., 2008), and inhibitory synapses onto pyramidal neurons (Brünig et al., 2002; Lévi et al., 2002).

Dystroglycan is a central component of the Dystrophin Glycoprotein Complex (DGC) known primarily for its role in the etiology of neuromuscular diseases including Duchenne muscular dystrophy (DMD), limb-girdle muscular dystrophy (LGMD), and congenital muscular dystrophy (CMD). The gene encoding *Dystroglycan* (*Dag1*) yields two subunits, the extracellular alpha Dystroglycan (α-Dag1) and the transmembrane beta Dystroglycan (β-Dag1). These two subunits are non-covalently bound, allowing Dystroglycan to function as a link between extracellular ligands and cytoskeletal and signaling proteins (Ervasti and Campbell, 1991; Holt et al., 2000; Ibraghimov-Beskrovnaya et al., 1992; Moore and Winder, 2010). Extracellular α-Dag1 interacts with multiple proteins in the nervous system through its extensive glycan chains (Jahncke and Wright, 2023). Mutations in any of the 19 genes involved in α-Dag1 glycosylation impair Dystroglycan function through reduced ligand binding and leads to a class of congenital muscular dystrophy termed dystroglycanopathy (Blaeser et al., 2013).

Patients with severe forms of dystroglycanopathy frequently present with structural brain abnormalities and experience seizures and cognitive impairments (Barresi and Campbell, 2006; Muntoni et al., 2011; Taniguchi-Ikeda et al., 2016). Dystroglycanopathy patients with moderate severity can exhibit cognitive impairments even in the absence of identifiable brain malformations, suggesting that Dystroglycan functions at later stages of neural circuit formation such as synapse formation and/or maintenance (Clement et al., 2008; Godfrey et al., 2007).

The dramatic structural and anatomical phenotypes of global *Dag1* deletion in mice has often precluded analysis of Dystroglycan's synaptic functions (Myshrall et al., 2012; Satz et al., 2010, 2008). Recent studies show that when *Dag1* is selectively deleted from postmitotic pyramidal neurons, neuronal migration and lamination is normal, however CCK^+/CB_1R^+ interneurons (INs) fail to populate the forebrain or form synapses in these mice (Früh et al., 2016; Miller and Wright, 2021). Furthermore, conditional deletion of *Dag1* from cerebellar Purkinje neurons leads to impaired inhibitory synaptic transmission and a reduction in the number of inhibitory synapses in cerebellar cortex (Briatore et al., 2020). These studies establish a role for Dystroglycan function at a subset of inhibitory synapses in the brain, but the critical features of Dystroglycan necessary for these functions, and the relationship between inhibitory synaptogenesis and neurological phenotypes in dystroglycanopathy, remains undefined.

Here, we use multiple mouse models that recapitulate the full range of dystroglycanopathy neuropathology to address several outstanding questions related to the role of Dystroglycan at inhibitory synapses. We find that CCK^+/CB_1R^+ IN axon targeting, synapse formation, and synapse function requires both glycosylation of α-Dag1 and interactions through the intracellular domain of β-Dag1, and that defects in synaptic structure and function is associated with increased seizure susceptibility in mouse models of dystroglycanopathy.

Results

Characterizing Dystroglycan localization and glycosylation in multiple models of dystroglycanopathy

While conditional deletion of *Dag1* from pyramidal neurons causes a loss of CCK^+/CB_1R^+ IN innervation in the forebrain, this has not been examined in dystroglycanopathy relevant mouse models exhibiting more widespread loss of functional Dystroglycan. We therefore generated five distinct mouse models; three to provide mechanistic insight into Dystroglycan function and two of which model mild dystroglycanopathy (schematized in **Figure 2.1 A**). Since complete loss of *Dag1* results in early embryonic lethality in mice, we generated forebrain-specific conditional knockouts by crossing $Emx1^{Cre}$ with *Dystroglycan* floxed mice ($Dag1^{flox/flox}$), to drive recombination in neuroepithelial cells in the dorsal forebrain beginning at embryonic day 10.5 (E10.5) (Gorski et al., 2002; Liang et al., 2012). We verified the recombination pattern of $Emx1^{Cre}$ with the mCherry reporter $ROSA26^{Lox\text{-}STOP\text{-}Lox\text{-}H2B:mCherry}$. H2B:mCherry signal was present in all excitatory neurons and astrocytes throughout the forebrain (**Supplementary Figure 2.1 A, B, D**) but not microglia or interneurons (**Supplementary Figure 2.1 C, E**).

To model loss of Dystroglycan glycosylation, $Emx1^{Cre}$ was crossed with $Pomt2^{flox/flox}$ conditional mice to generate $Pomt2^{cKOs}$. Pomt2 (protein *O*-mannosyltransferase 2) is a glycosyltransferase that functions in a heterocomplex with Pomt1 to add *O*-mannose at the beginning of the Dystroglycan glycan chain (Manya et al., 2004). Without the initial *O*-mannose, no additional sugar moieties can be added to the glycan chain, resulting in near complete loss of Dystroglycan glycosylation. This is

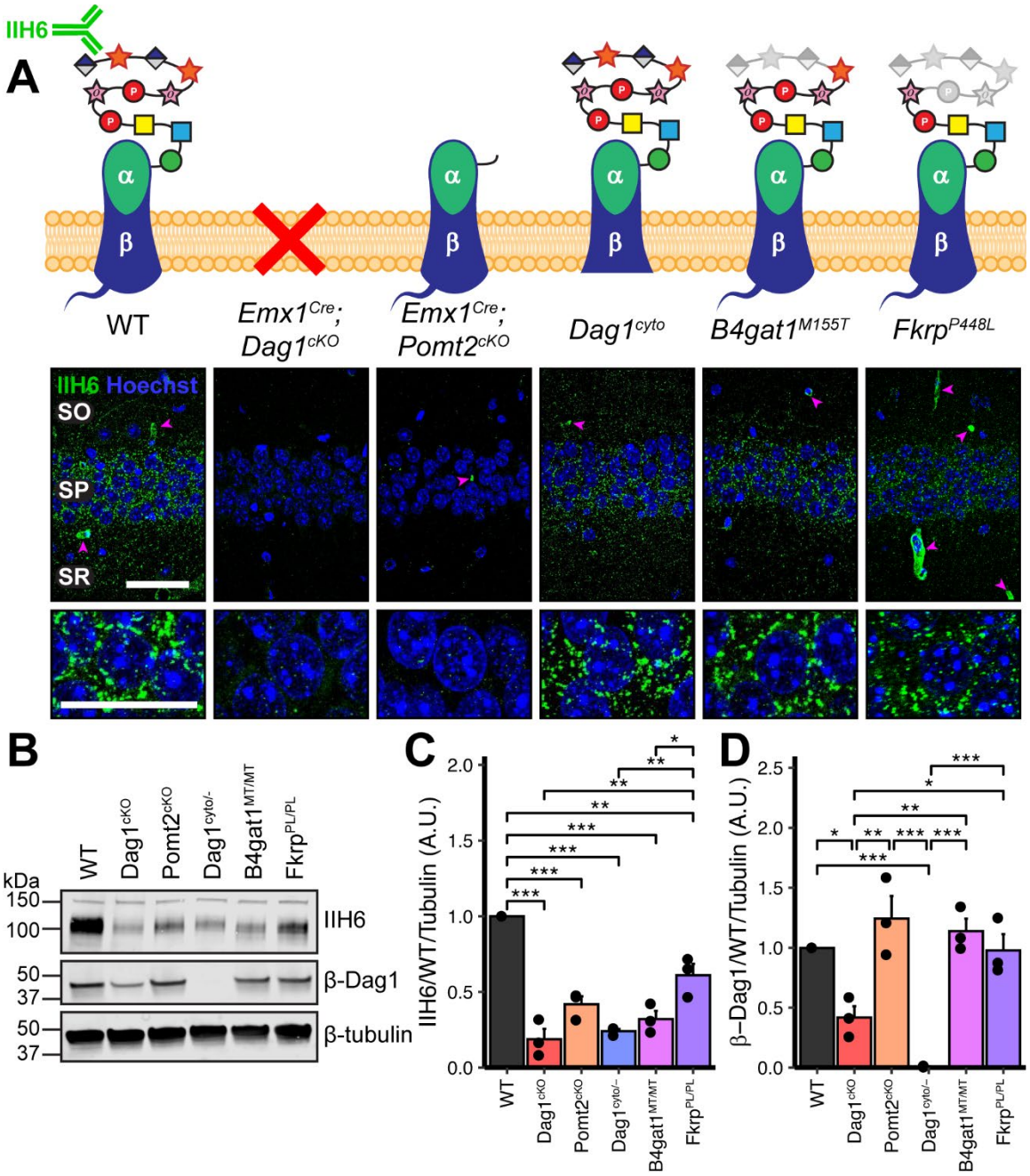

Figure 2.1 Dystroglycan synaptic localization and glycosylation in mouse models of dystroglycanopathy.

(A) Schematic depiction of Dystroglycan in different mouse models. The IIH6 antibody recognizes the matriglycan repeats on extracellular αDag1. Hippocampal CA1 of P30 mice immunostained for Dystroglycan glycosylation (IIH6, green) and nuclear marker Hoechst (blue) show puncta of glycosylated Dystroglycan localized to the perisomatic region of pyramidal cells and to blood vessels (magenta arrowheads); scale bar = 50μm. Lower panels show cell bodies in SP; scale bar = 25μm. CA1 layers: SO, stratum oriens; SP, stratum pyramidale; SR, stratum radiatum. **(B)** WGA-enriched lysates from P0 forebrain were immunoblotted for IIH6, β-Dag1, and β-tubulin. **(C-D)** Quantification of immunoblot in **(B)**. Error bars show mean + SEM.

lethal embryonically in a global *Pomt2* knockout, however *Emx1*^{Cre};*Pomt2*^{cKO} mice are viable and survive into adulthood (Hu et al., 2016; Reeuwijk et al., 2005; Yanagisawa et al., 2007).

In addition to binding extracellular ligands, Dystroglycan binds cytoskeletal proteins and signals through the intracellular tail of its β-subunit. To determine whether the intracellular domain of Dystroglycan is required for synaptic development and/or function, we examined mice in which one copy of *Dag1* was deleted, and the other copy lacks the intracellular domain of β-Dag1 (*Dag1*$^{cyto/-}$). These mice develop muscular dystrophy but show normal neuronal migration and axon guidance in regions throughout the central nervous system where Dystroglycan glycosylation is required (Lindenmaier et al., 2019; Satz et al., 2010, 2009).

To model mild forms of dystroglycanopathy, we examined mice expressing missense mutations in *B4gat1 (*β-1,4-glucuronyltransferase, *B4gat1*^{M155T}) and *Fkrp* (fukutin related protein, *Fkrp*^{P448L}), two genes required for Dystroglycan glycosylation. *B4gat1*^{M155T} mice were initially identified in a forward genetic screen and develop mild muscular dystrophy and have diminished ligand binding capacity due to reduced Dystroglycan glycosylation (Wright et al., 2012). The *Fkrp*^{P448L} missense mutation models a mutation found in a patient with dystroglycanopathy (Brockington et al., 2001). In mice, the *Fkrp*^{P448L} mutation leads to reduced glycosylation and mild muscular dystrophy, but no gross brain or eye malformations (Blaeser et al., 2013). While it is possible that *Pomt2*, *B4gat1*, and *Fkrp* could play a role in the glycosylation of proteins other than Dystroglycan, the identity of these proteins has not been described in neurons to date and we did not observe any emergent phenotypes that have not been observed in *Dag1* mutants (Gerin et al., 2016; Larsen et al., 2017a, 2017b; Willer et al., 2014).

We first examined the pattern of Dystroglycan localization in pyramidal neurons in CA1 of hippocampus in each of the five models by immunostaining adult (P30) mice

with the IIH6 antibody, which detects the terminal matriglycan repeats on the glycan chain on α-Dag1 (Sheikh et al., 2022; Yoshida-Moriguchi and Campbell, 2015). In wild-type (WT) mice, punctate IIH6 immunoreactivity was evident in the somatic and perisomatic compartment of CA1 pyramidal neurons (**Figure 2.1 A**). Immunoreactivity was also present in blood vessels, where *Dag1* is also expressed (Durbeej et al., 1998; Zaccaria et al., 2001). Neuronal immunoreactivity was undetectable in $Emx1^{Cre};Dag1^{cKOs}$ and $Emx1^{Cre};Pomt2^{cKOs}$, whereas blood vessel expression was maintained, illustrating the specificity of the conditional deletion (**Figure 2.1 A**). Punctate perisomatic IIH6 immunoreactivity was present in $Dag1^{cyto/-}$, $B4gat1^{M155T/M155T}$, and $Fkrp^{P448L/P448L}$ mice (**Figure 2.1 A**). To assess Dystroglycan localization in $Emx1^{Cre};Pomt2^{cKOs}$ we used an antibody that recognizes the intracellular C-terminus of β-Dag1. Although immunoreactivity for β-Dag1 was present and elevated above $Emx1^{Cre};Dag1^{cKO}$ or $Dag1^{cyto/-}$ levels, Dag1 localization did not appear punctate in $Emx1^{Cre};Pomt2^{cKOs}$ (**Supplementary Figure 2.2 A**). This apparent difference implies that Dag1 glycosylation, and by extension the extracellular interactions that matriglycan mediates, is required for proper Dag1 synaptic localization.

We next prepared WGA-enriched lysate from neonatal (P0) forebrain and immunoblotted for (1) IIH6, to quantify the degree of α-Dag1 glycosylation and (2) β-Dag1, to measure total Dystroglycan protein levels (**Figure 2.1 B**). Dag1 glycosylation was significantly reduced in $Emx1^{Cre};Dag1^{cKOs}$, $Emx1^{Cre};Pomt2^{cKOs}$, $Dag1^{cyto/-}$, $B4gat1^{M155T/M155T}$, and $Fkrp^{P448L/P448L}$ mice; however, the reduction in $Fkrp^{P448L/P448L}$ mice was less severe than the other models (**Figure 2.1 C**). The reduction in glycosylation observed in the $Dag1^{cyto/-}$ mice is surprising given that the mutation is restricted to the intracellular domain. *Dystroglycan* heterozygotes ($Dag1^{+/-}$) show no reduction in IIH6 levels compared to wild-types (data not shown), so the reduction in $Dag1^{cyto/-}$ mice can

be presumed to be due to the intracellular deletion. It is possible that the intracellular domain is required for the trafficking of Dystroglycan through the endoplasmic reticulum and/or Golgi apparatus, where Dystroglycan undergoes glycosylation, however additional work is needed to verify this. As expected, β-Dag1 immunoblotting was significantly reduced in *Emx^{Cre};Dag1^{cKOs}* and absent in *Dag1$^{cyto/-}$* mice but normal in the glycosylation mutants (**Figure 2.1 D**). The residual β-Dag1 in *Emx1^{Cre};Dag1^{cKO}* brain is likely due to *Dag1* expression in unrecombined cells, such as blood vessels, as well as unrecombined tissue that remained after the forebrain dissection.

We next examined Dag1 protein levels during synaptogenesis using WGA-enriched lysate from P21-P30 hippocampus. As expected, Dag1 glycosylation assessed by IIH6 immunoblotting was severely reduced in *Emx1^{Cre};Dag1^{cKOs}* and *Emx1^{Cre};Pomt2^{cKOs}* but normal in *Dag1$^{cyto/-}$* mice (**Supplementary Figure 2.2 B-C**). Immunoblotting for β-Dag1 showed a significant reduction in *Emx1^{Cre};Dag1^{cKOs}* and *Dag1$^{cyto/-}$* mutants but normal levels in *Emx1^{Cre};Pomt2^{cKOs}* (**Supplementary Figure 2.2 B, D**). Although localization of Dag1 was not punctate in *Emx1^{Cre};Pomt2^{cKOs}* (**Supplementary Figure 2.2 A**), the overall level of β-Dag1 was normal by WGA-enrichment, which enriches for proteins in the plasma membrane (**Supplementary Figure 2.2 B, D**). It therefore remains possible that Dag1 still trafficks to the cell surface in *Emx1^{Cre};Pomt2^{cKOs}* but fails to contact presynaptic axons and therefore does not permit synaptogenesis.

Dystroglycan is required for cortical neuron migration in a glycosylation-dependent manner

In neocortex, *Dag1* expression in radial glia is required for proper migration of neurons, with *Dag1* conditional deletion from neuroepithelial cells or radial glia resulting in Type II lissencephaly (Moore et al., 2002; Pawlisz and Feng, 2011; Satz et al., 2010,

2008). This requires proper Dystroglycan glycosylation, but not its expression in neurons (Chan et al., 2010; Holzfeind et al., 2002; Hu et al., 2011; Wright et al., 2012). To compare cortical migration across our five models of dystroglycanopathy, we performed immunostaining for the upper layer marker Cux1 (layers II/III-IV) and the deep layer marker Tbr1 (layers III, VI) in P30 somatosensory cortex (**Figure 2.2 A-B**). *Emx1*^{Cre}*;Dag1*^{cKOs} and *Emx1*^{Cre}*;Pomt2*^{cKOs} showed complete cortical dyslamination with 100% penetrance, whereas the cytoplasmic (*Dag1*$^{cyto/-}$) deletion mutants appeared normal (**Figure 2.2 C-D**). *B4gat1*$^{M155T/M155T}$ missense mutants showed a migration phenotype only at the cortical midline, while *Fkrp*$^{P448L/P448L}$ missense mutants did not show any cortical migration phenotype (**Figure 2.2 C-D**, **Supplementary Figure 2.3 A**). These results indicate that cortical migration depends on Dystroglycan glycosylation but does not require its cytoplasmic domain. Furthermore, taken with the data in **Figure 2.1 B-D**, they illustrate that the severity of the cortical migration phenotype scales with the degree of Dystroglycan hypoglycosylation; *Emx1*^{Cre}*;Dag1*^{cKOs} and *Emx1*^{Cre}*;Pomt2*^{cKOs} model a severe form of dystroglycanopathy (Walker-Warburg Syndrome, Muscle-Eye-Brain disease) and *B4gat1*$^{M155T/M155T}$ and *Fkrp*$^{P448L/P448L}$ mutants modeling a milder form of the disease.

To further assess the impact of our functional domain mutations, we assessed Laminin localization, the canonical interacting partner of Dystroglycan in the extracellular matrix (ECM), in adult neocortex (Ibraghimov-Beskrovnaya et al., 1992). Under WT conditions, Laminin immunoreactivity was evident at the pial surface where Laminin and Dystroglycan interact at the interface between radial glial endfeet and the cortical basement membrane (Satz et al., 2010). Laminin was also present in blood vessels, where Dystroglycan-expressing perivascular astrocytes contribute to the maintenance of water homeostasis (Menezes et al., 2014). In *Emx1*^{Cre}*;Dag1*^{cKO} cortex, Laminin immunoreactivity at the pial surface was patchy and vascular Laminin showed evidence

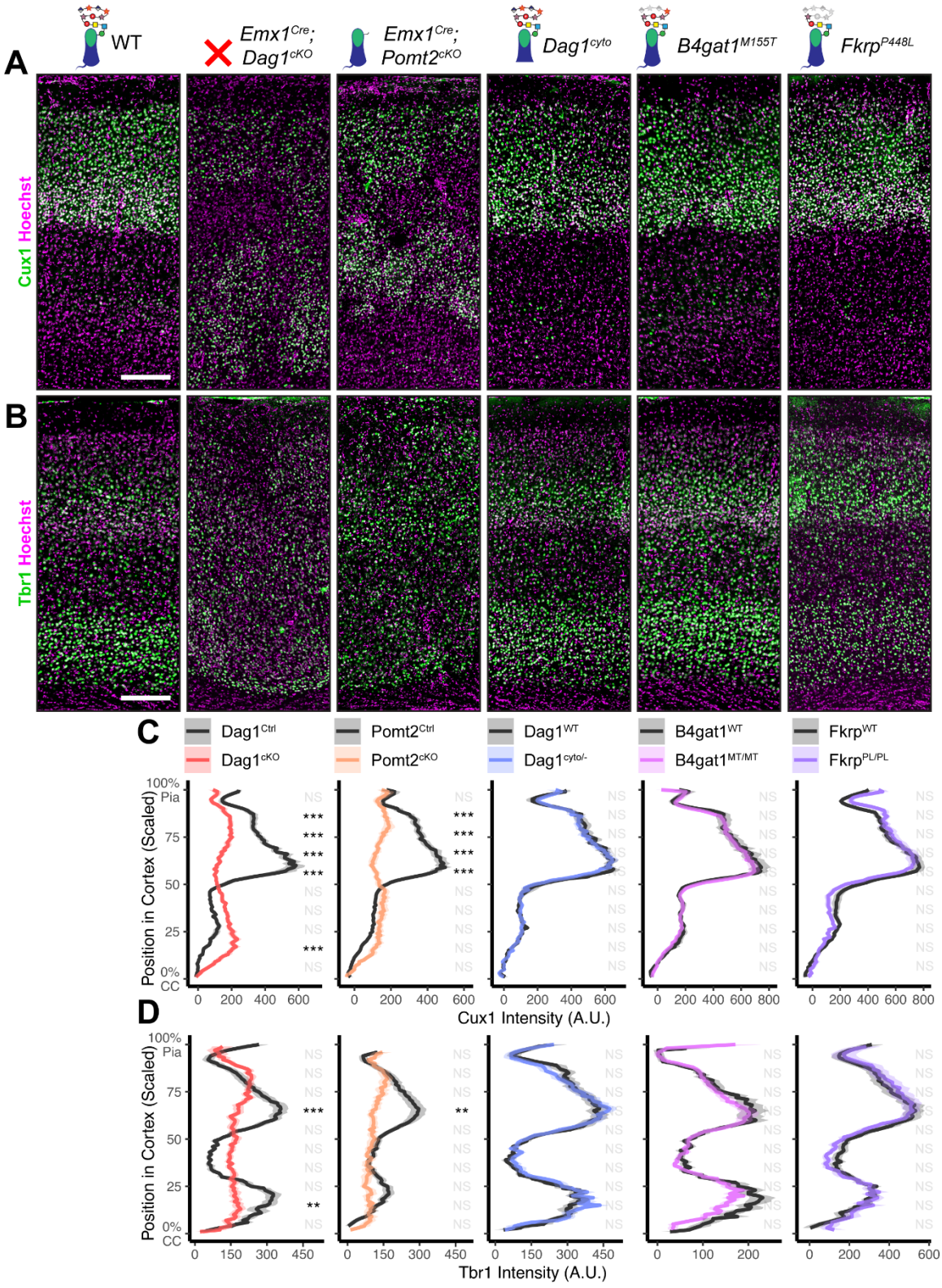

Figure 2.2 Dystroglycan is required for cortical neuron migration in a glycosylation-dependent manner and independent of intracellular interactions.

Immunostaining for cortical layer markers **(A)** Cux1 (layers 2-4) and **(B)** Tbr1 (layers 3

and 6) in P30 somatosensory cortex (scale bar = 200μm). Layer markers are shown in green. Nuclear marker Hoechst is shown in magenta. Quantification of fluorescence intensity of layer markers shown for **(C)** Cux1 and **(D)** Tbr1. Shaded regions of intensity profile illustrate ± SEM. Significance: * = $p < 0.05$, ** = $p < 0.01$, *** = $p < 0.001$, NS = $p \geq 0.05$. *Abbreviations: CC, corpus callosum; A.U., arbitrary units.*

---

of the neuronal migration phenotype described in **Figure 2.2** (**Supplementary Figure 2.4 A**). Laminin immunoreactivity in *Emx1^{Cre};Pomt2^{cKO}* cortex similarly showed a patchy appearance, albeit less severe than *Emx1^{Cre};Dag1^{cKOs}*, along with the evident cortical migration phenotype (**Supplementary Figure 2.4 B**). *Dag1$^{cyto/-}$* mutants, on the other hand, exhibited normal Laminin immunoreactivity both at the pial surface and with regards to vascular organization (**Supplementary Figure 2.4 C**).

Perisomatic CCK$^+$/CB$_1$R$^+$ interneuron targeting requires Dystroglycan in a non-cell autonomous manner

CCK$^+$/CB$_1$R$^+$ IN innervation is largely absent from the cortex and hippocampus when *Dag1* is deleted selectively from pyramidal neurons using *NEX^{Cre}* (Früh et al., 2016; Miller and Wright, 2021). However, the development and function of CCK$^+$/CB$_1$R$^+$ INs has not been examined in mouse models that more broadly lack *Dag1* throughout the central nervous system (CNS) and thus more accurately reflect the neuropathology of dystroglycanopathy. We focused our analysis on region CA1 of the hippocampus, as its overall architecture is grossly unaffected in each of our mouse models. Both *Emx1^{Cre};Dag1^{cKO}* and *Emx1^{Cre};Pomt2^{cKO}* mice exhibited a mild granule cell migration phenotype in dentate gyrus (**Figure 2.3 A**, yellow arrows), however CA1-CA3 showed normal pyramidal neuron organization.

In WT control mice, CCK$^+$/CB$_1$R$^+$ IN axon terminals were abundant throughout the hippocampus, with their highest innervation density in the CA1 pyramidal cell body layer (*stratum pyramidale*, SP) where they form characteristic basket synapses onto

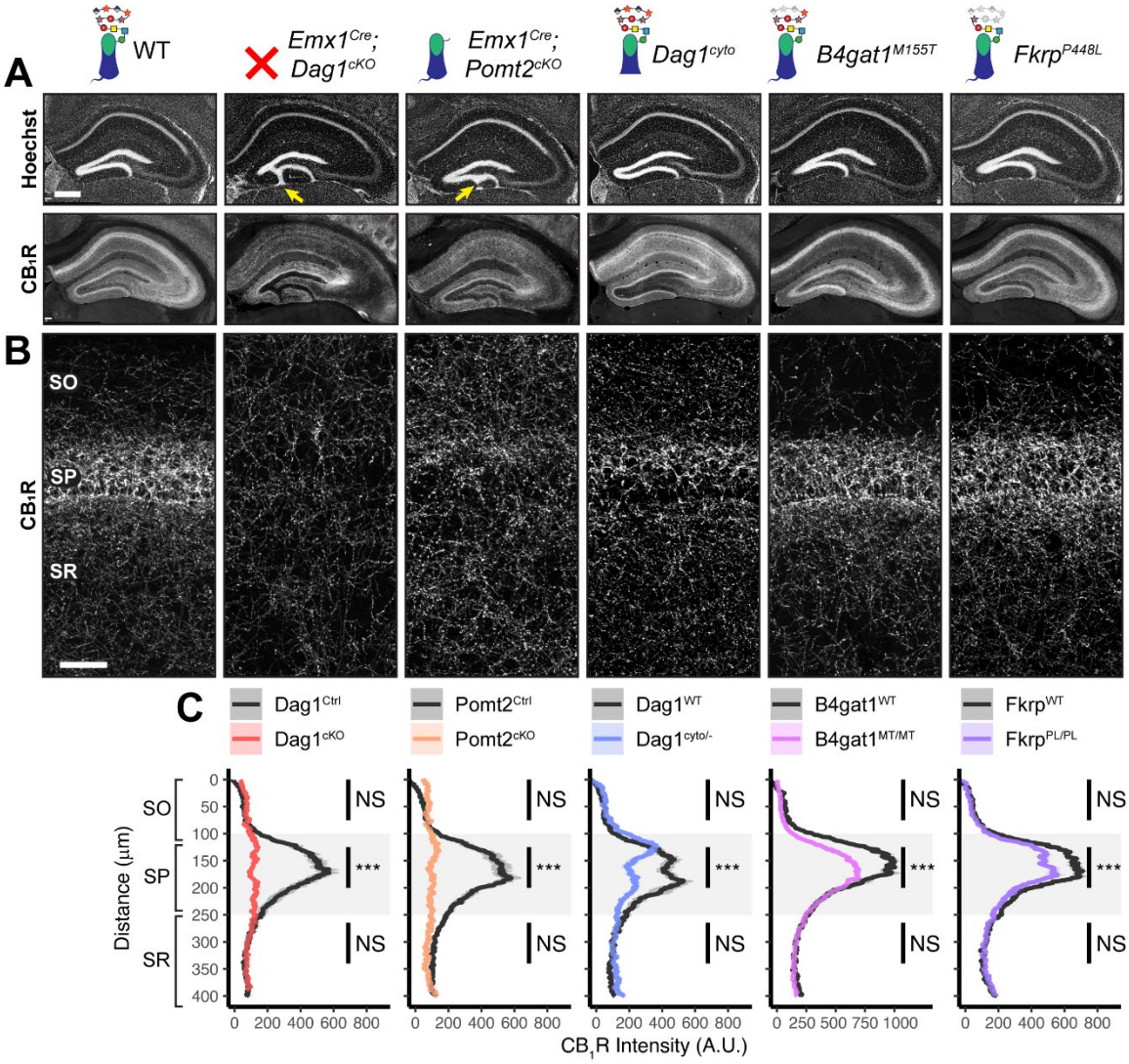

Figure 2.3 Dystroglycan is required for CCK⁺/CB₁R⁺ basket IN perisomatic axon targeting in stratum pyramidale of hippocampal CA1-3.

(A) Nuclear marker Hoechst (upper panels) shows hippocampal morphology. Granule cell migration is disrupted in dentate gyrus of *Emx1^{Cre};Dag1^{cKOs}* and *Emx1^{Cre};POMT2^{cKOs}* (yellow arrows). CA1-3 gross morphology is normal in all models. CB_1R immunostaining (lower panels) shows abnormal CCK^+/CB_1R^+ basket interneuron targeting in CA1-3 to varying degrees across models (scale bar = 400µm). **(B)** Higher magnification view of CB_1R immunostaining in CA1 (scale bar = 50µm). **(C)** Quantification of CA1 CB_1R fluorescence intensity profile. Shaded regions of intensity profile illustrate ± SEM. Gray region highlights SP. Significance: * = $p < 0.05$, ** = $p < 0.01$, *** = $p < 0.001$, NS = $p \geq 0.05$. *Abbreviations: A.U., arbitrary units; SO, stratum oriens; SP, stratum pyramidale; SR, stratum radiatum.*

pyramidal neurons (**Figure 2.3 A-C**, **Supplementary Figure 2.5 A**). In *Emx1^{Cre};Dag1^{cKO}* mice, CCK$^+$/CB$_1$R$^+$ axons were present but failed to target the pyramidal cell layer (**Figure 2.3 A-C**, **Supplementary Figure 2.5 A**), a surprising difference from the phenotype observed in *NEX^{Cre};Dag1^{cKO}* mice which lack CCK$^+$/CB$_1$R$^+$ IN innervation entirely (Früh et al., 2016; Miller and Wright, 2021) (**Supplementary Figure 2.5 C**). To confirm the CCK$^+$/CB$_1$R$^+$ IN innervation pattern in the context of widespread *Dag1* deletion, we generated *Nestin^{Cre};Dag1^{cKO}* mice. *Nestin^{Cre}*, similar to *Emx1^{Cre}*, drives *Cre* recombination in forebrain progenitors, however *Emx1^{Cre}* recombination begins around E10.5 and *Nestin^{Cre}* recombination begins around E11.5 (Liang et al., 2012; Tronche et al., 1999). *Nestin^{Cre};Dag1^{cKOs}* showed the same CCK$^+$/CB$_1$R$^+$ axon targeting phenotype as *Emx1^{Cre};Dag1^{cKOs}* (**Supplementary Figure 2.5 B**), further suggesting that the observed *Emx1^{Cre};Dag1^{cKO}* phenotype faithfully models dystroglycanopathy neuropathology.

It was previously reported that the lack of CCK$^+$/CB$_1$R$^+$ IN innervation of CA1 pyramidal neurons observed in *NEX^{Cre};Dag1^{cKOs}* was accompanied by reduced numbers of CCK$^+$/CB$_1$R$^+$ INs (Miller and Wright, 2021). We therefore sought to quantify CCK$^+$/CB$_1$R$^+$ IN cell density in *Emx1^{Cre};Dag1^{cKOs}* using both NECAB1 and NECAB2 antibodies (Miczán et al., 2021). As NECAB1 is expressed by both CCK$^+$/CB$_1$R$^+$ INs and PV$^+$ INs, we performed immunolabeling for both NECAB1 and PV and quantified the density of NECAB1$^+$;PV$^-$ cell bodies in CA1, finding no difference between *Emx1^{Cre};Dag1^{Ctrls}* and *Emx1^{Cre};Dag1^{cKOs}* (**Supplementary Figure 2.6 A-B**). To confirm this, we also quantified the density of NECAB2$^+$ cell bodies in CA1, again finding no difference between genotypes (**Supplementary Figure 2.6 C, E**). Thus, the observed change in CCK$^+$/CB$_1$R$^+$ IN axon targeting of CA1 pyramidal cells is not due to a reduction in cell numbers, but rather a failure to innervate the appropriate compartment.

Emx1^{Cre}*;Pomt2*^{cKO} mice fully phenocopied the aberrant *Emx1*^{Cre}*;Dag1*^{cKO} CB_1R^+ immunoreactivity pattern (**Figure 2.3 A-C**), demonstrating that proper CCK^+/CB_1R^+ IN basket axon targeting requires Dystroglycan glycosylation. Both the *B4gat1* and *Fkrp* mutants showed a normal distribution of CB_1R^+ axon targeting to the somatodendritic compartment of CA1 neurons, but with reduced CB_1R intensity in SP (**Figure 2.3 A-C**). The cytoplasmic domain of Dystroglycan also plays a role in the appropriate targeting of CB_1R immunoreactive axons, as the distribution of axons was perturbed in the *Dag1*$^{cyto/-}$ mutants, though with an intermediate phenotype in which the upper portion of SP appeared normal while the lower portion of SP showed loss of selective CB_1R^+ axon targeting (**Figure 2.3 A-C**).

Due to the axonal targeting defect in the CCK^+/CB_1R^+ IN population, we next examined the Parvalbumin (PV) population of interneurons in the hippocampus, as these cells also form perisomatic basket cell synapses on to CA1 pyramidal cells. There was no significant difference in the number of PV^+ INs in CA1 of *Emx1*^{Cre}*;Dag1*^{cKO} mice and littermate controls (**Supplementary Figure 2.6 D, F**). Furthermore, the distribution of PV^+ IN axons showed normal targeting to SP in all mouse models (**Supplementary Figure 2.7 A-B**), indicating that the axon targeting phenotype is specific to the CCK^+/CB_1R^+ IN population. Interestingly, *Emx1*^{Cre}*;Dag1*^{cKO} mice exhibited a slight increase in PV intensity in SP, perhaps indicating that there is a degree of compensation (**Supplementary Figure 2.7 A-B**).

Notably, CB_1R expression was also abnormal in brain regions outside of the hippocampus. In somatosensory cortex, CB_1R immunostaining reflected the dyslamination phenotype in both the *Emx1*^{Cre}*;Dag1*^{cKO} and *Emx1*^{Cre}*;Pomt2*^{cKO} mice throughout neocortex and the *B4gat1*$^{M155T/M155T}$ mice at midline, while it appeared normal in cortex of *Dag1*$^{cyto/-}$ and *Fkrp*$^{P448L/P448L}$ mice (**Supplementary Figure 2.8 A**). CB_1R staining was also reduced and disorganized in the basolateral amygdala (BLA) in

Emx1^{Cre}*;Dag1*^{cKO} and *Emx1*^{Cre}*;Pomt2*^{cKO} mice (**Supplementary Figure 2.8 B**). Interestingly, CB_1R immunostaining in the inner molecular layer (IML) of dentate gyrus appears normal in all mutants (**Figure 2.3 A**). In the IML, CB_1R is present in excitatory mossy cell axons targeting dentate granule cells whereas in both cortex and amygdala CB_1R expression is restricted to GABAergic interneurons (Földy et al., 2006; Katona et al., 2001; Monory et al., 2015). Therefore, glycosylated Dystroglycan instructs the development of inhibitory CB_1R^+ interneuron populations in multiple brain regions.

Dystroglycan is required for CCK^+/CB_1R^+ interneuron axon targeting during early postnatal development

During early postnatal development, CCK^+/CB_1R^+ IN axons undergo a dramatic laminar rearrangement, progressing from more distal localization amongst pyramidal cell dendrites, to eventually target pyramidal neuron cell bodies in the hippocampus (Miller and Wright, 2021; Morozov et al., 2009; Y. M Morozov and Freund, 2003; Yury M. Morozov and Freund, 2003). We examined the developmental time course of CCK^+/CB_1R^+ IN axon targeting in our *Emx1*^{Cre}*;Dag1*^{cKO} mice beginning at P5, when the axons are first readily identifiable (Berghuis et al., 2007; Eggan et al., 2010; Mulder et al., 2008; Vitalis et al., 2008). At P5 in control *Emx1*^{Cre}*;Dag1*^{Ctrl} mice, CCK^+/CB_1R^+ axons were initially concentrated in the *stratum radiatum* (SR) of the hippocampus (**Figure 2.4 A-C**). Between P10 and P30, the CCK^+/CB_1R^+ axons underwent developmental reorganization, with reduced innervation of SR coinciding with a progressive increase in innervation of SP. In contrast, overall CCK^+/CB_1R^+ innervation was initially reduced in the hippocampus of mutant *Emx1*^{Cre}*;Dag1*^{cKO} mice at P5, and these axons failed to undergo laminar reorganization as they developed (**Figure 2.4 A-C**). By P30, after IN synapse formation and targeting are largely complete in control mice, the density of CCK^+/CB_1R^+ axons in *Emx1*^{Cre}*;Dag1*^{cKO} mice was uniform across all hippocampal lamina

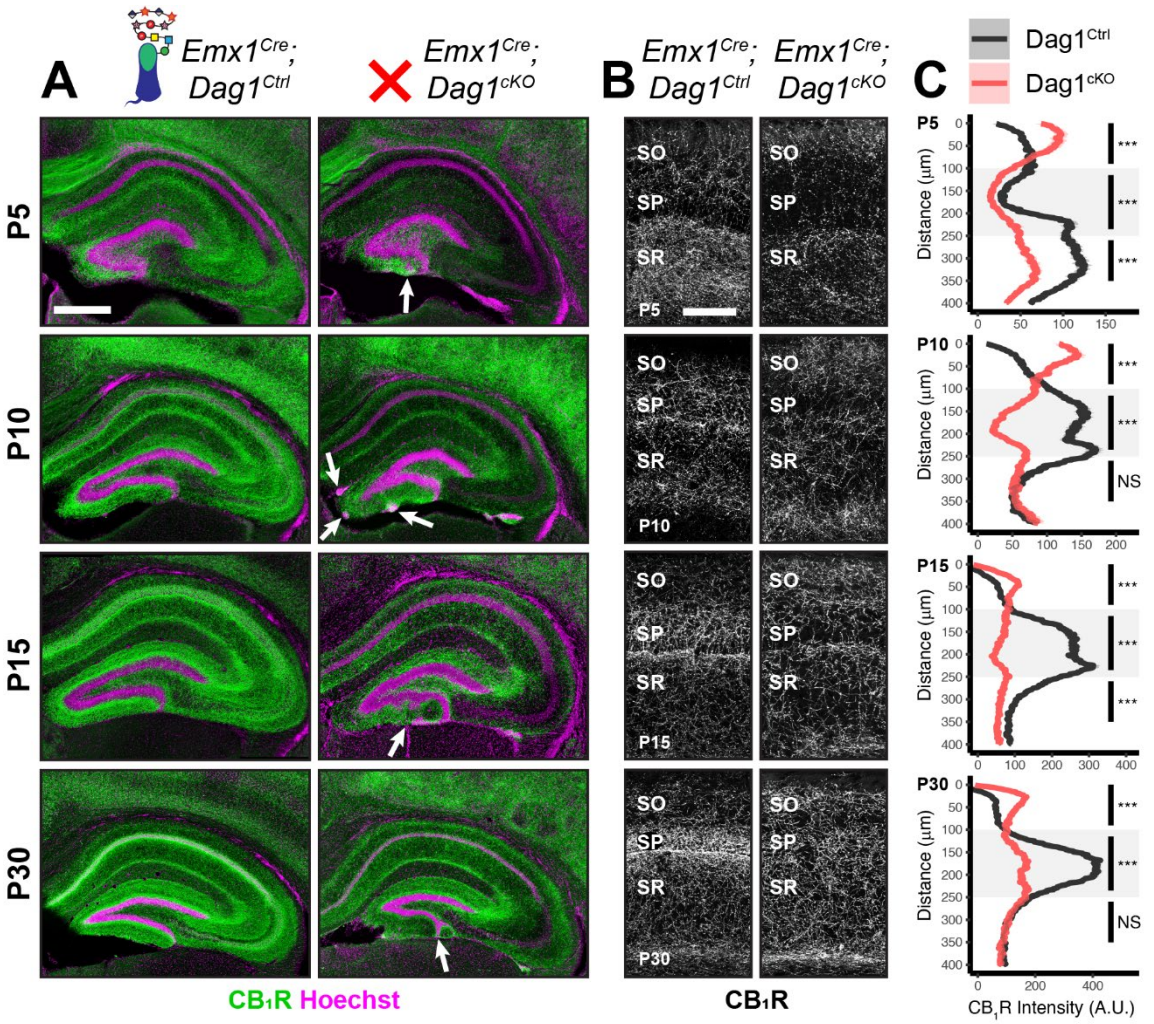

Figure 2.4 Dystroglycan is required for CCK⁺/CB₁R⁺ IN axon targeting during early postnatal development.

(A) Immunostaining for CB_1R^+ axon terminals (green) in the hippocampus of *Emx1^{Cre};Dag1* controls (left) and cKOs (right) at ages P5-P30. Nuclear marker Hoechst is shown in magenta. White arrowheads indicate migration errors in dentate granule cells *Emx1^{Cre};Dag1^{cKO}* mice. Scale bar = 500µm. **(B)** Higher magnification images of CB_1R^+ axon terminals in CA1 of *Emx1^{Cre};Dag1* controls (left) and cKOs (right) at ages P5-P30. Scale bar = 100µm. **(C)** Quantification of CB_1R fluorescence intensity profile in CA1. Shaded regions of intensity profile illustrate ± SEM. Gray region highlights SP. Significance: * = $p < 0.05$, ** = $p < 0.01$, *** = $p < 0.001$, NS = $p \geq 0.05$. *Abbreviations: A.U., arbitrary units; SO, stratum oriens; SP, stratum pyramidale; SR, stratum radiatum.*

(**Figure 2.4 A-C**). Therefore, Dystroglycan plays a critical developmental role during the first two postnatal weeks, for the proper laminar distribution and perisomatic targeting of CCK^+/CB_1R^+ IN axons in the hippocampus.

CCK$^+$/CB$_1$R$^+$ IN synapse formation requires postsynaptic glycosylated Dystroglycan

Given the perturbed distribution of CCK$^+$/CB$_1$R$^+$ IN axons in the hippocampus, we next wanted to determine whether the remaining CCK$^+$/CB$_1$R$^+$ IN axons were capable of forming synapses in dystroglycanopathy models. Using VGAT as a marker of inhibitory presynaptic terminals, we saw no difference in total VGAT puncta density in SP in any of the mouse models, indicating that the total number of inhibitory synapses is normal (**Figure 2.5 B-D**). Immunostaining for CB$_1$R showed a significant decrease in CB$_1$R in SP of *Emx1^{Cre};Dag1^{cKO}*, *Emx1^{Cre};Pomt2^{cKO}*, *B4gat1$^{M155T/M155T}$*, and *Fkrp$^{P448L/P448L}$* mutants, but not *Dag1$^{cyto/-}$* mutants (**Figure 2.5 E**). This suggests that the difference in CB$_1$R$^+$ axon distribution described in SP of *Dag1$^{cyto/-}$* mutants in **Figure 2.3 A-C** likely reflects a change in CCK$^+$/CB$_1$R$^+$ IN axon targeting but not synapse formation, whereas *Emx1^{Cre};Dag1^{cKO}* and all three glycosylation mutants exhibit a reduction in CCK$^+$/CB$_1$R$^+$ IN axon targeting and synapse number in SP. It should be noted that the data in **Figure 2.3 A-C** reflects axonal CB$_1$R intensity across all hippocampal layers, whereas the quantification in **Figure 2.5 E** reflects the density of axonal swellings within SP. These data therefore suggest that there is an overall reduction in CB$_1$R intensity in SP of *Dag1$^{cyto/-}$* mutants that does not influence the number of CB$_1$R$^+$ axonal swellings. In contrast to CCK$^+$/CB$_1$R$^+$ INs, the PV$^+$ population of basket interneurons showed no change in puncta density in SP in any of the models (**Supplementary Figure 2.10 A-E**; analysis of VGAT, CB$_1$R, and PV densities in SO and SR included in **Supplementary Figure 2.9 A-B** and **Supplementary Figure 2.11 A**.)

To better approximate the extent of basket synapse formation, we quantified the co-localization between VGAT and CB$_1$R or PV. In SP, the percent of CB$_1$R puncta co-localized with VGAT was reduced in the same models that showed a reduction in CB$_1$R density (*Emx1^{Cre};Dag1^{cKO}*, *Emx1^{Cre};Pomt2^{cKO}*, *B4gat1$^{M155T/M155T}$*, and *Fkrp$^{P448L/P448L}$*

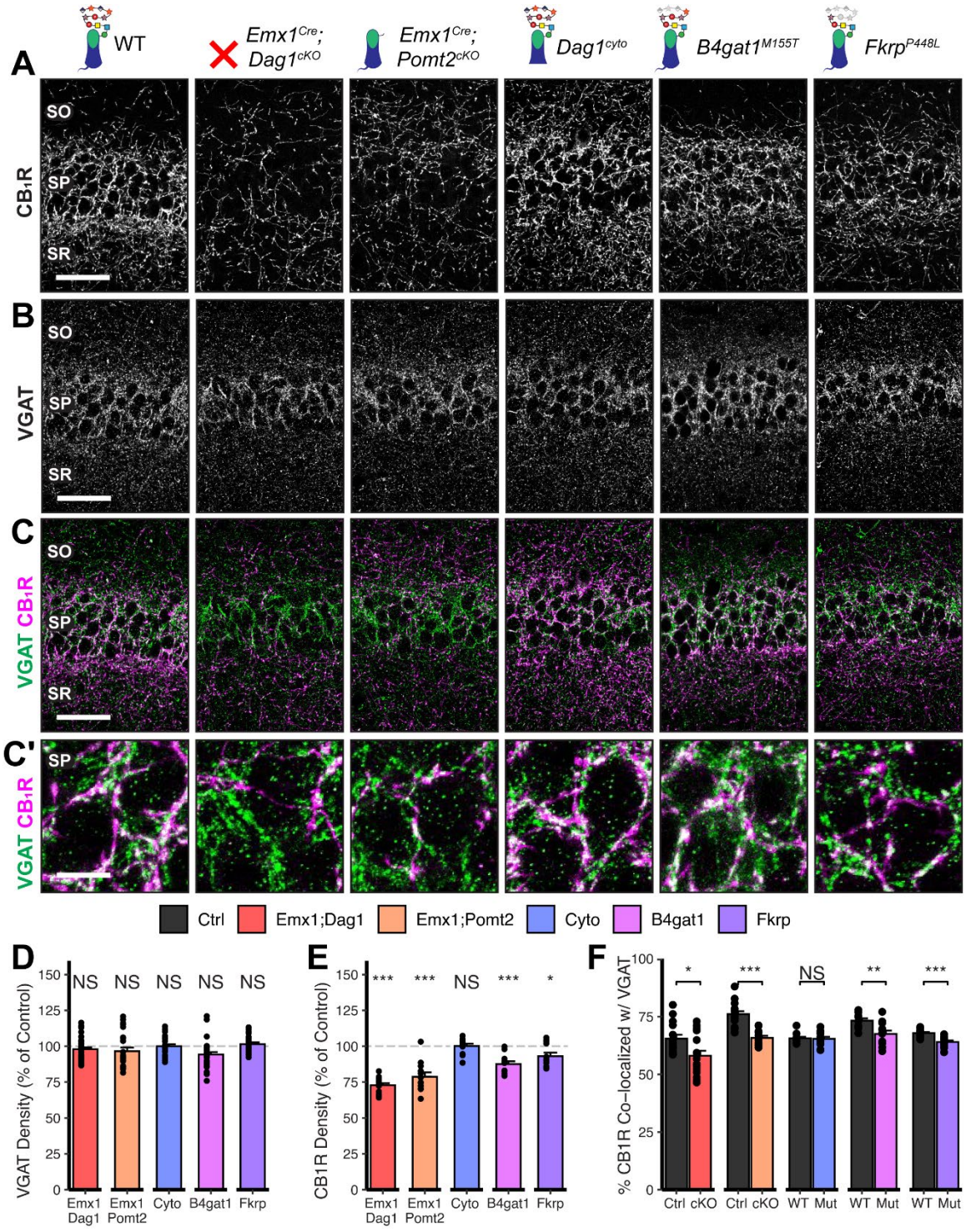

Figure 2.5 *Dag1* and *Pomt2* cKOs exhibit impaired CB1R$^+$ basket synapse formation in *stratum pyramidale* of hippocampal CA1.

P30 coronal sections immunostained for **(A)** CB_1R and **(B)** VGAT in hippocampal CA1; merged image in **(C)** shows CB_1R in magenta and VGAT in green. (A-C) Scale bar = 50μm. (Higher magnification view of SP in **(C')**; scale bar = 10μm.) **(D)** Quantification of VGAT puncta density in SP expressed as a percent of control. **(E)** Quantification of

CB_1R puncta density in SP expressed as a percent of control. **(F)** Quantification of co-localization between VGAT and CB_1R in SP to estimate putative CB_1R^+ basket cell synapse formation. Error bars show mean + SEM. (For quantification of puncta densities and co-localization in SO and SR see **Supplementary Figure 2.9**.) *Significance: * = $p < 0.05$, ** = $p < 0.01$, *** = $p < 0.001$, NS = $p \geq 0.05$. Abbreviations: SO, stratum oriens; SP, stratum pyramidale; SR, stratum radiatum.*

---

mutants) but not *Dag1$^{cyto/-}$* mutants (**Figure 2.5 C, F**), suggesting that CCK^+/CB_1R^+ INs require postsynaptic glycosylated Dystroglycan in order to form synapses whereas the cytoplasmic domain is required for axon targeting but not synapse formation.

Interestingly, the percent of PV co-localized with VGAT increased in the SP of *Emx1^{Cre};Dag1^{cKOs}* and *Emx1^{Cre};Pomt2^{cKOs}* mice, with no change in any of the other models (**Supplementary Figure 2.10 C, E**; analysis of co-localization in SO and SR included in **Supplementary Figure 2.9 C**, **Supplementary Figure 2.11 B**). It is possible that the reduction in inhibitory CCK^+/CB_1R^+ synapses prompts homeostatic compensation through an increase in PV^+ synapses. Alternatively, this may reflect competition between CCK^+/CB_1R^+ and PV^+ INs for physical space on the perisomatic region of pyramidal cells, with the decrease in CCK^+/CB_1R^+ synapses in *Emx1^{Cre};Dag1^{cKOs}* and *Emx1^{Cre};Pomt2^{cKOs}* allowing additional PV^+ IN synapses to form.

CCK^+/CB_1R^+ interneuron basket synapse function is dependent on Dystroglycan function

Perisomatic inhibitory basket cell synapses powerfully control activity in the hippocampal circuit (Freund and Katona, 2007). Previous studies in *NEX^{Cre};Dag1^{cKO}* mice, in which CCK^+/CB_1R^+ INs are absent, demonstrated reduced inhibitory synaptic function (Früh et al., 2016). In the current study, however, CCK^+/CB_1R^+ INs are present but mistargeted. Thus, we wanted to determine whether with the changes in CCK^+/CB_1R^+ basket synapse localization in our mouse models were associated with altered inhibitory synaptic function. CCK^+/CB_1R^+ IN basket cells can be selectively

activated by muscarinic receptor activation, which increases the rate of spontaneous inhibitory post-synaptic currents (sIPSCs) in nearby pyramidal cells (Früh et al., 2016; Nagode et al., 2014). To assay function at CCK^+/CB_1R^+ IN synapses, we performed whole cell patch clamp electrophysiology from CA1 pyramidal neurons in slices from control and mutant mice. After recording 5 minutes of baseline sIPSCs, the cholinergic receptor agonist Carbachol (CCh) was added to the bath and an additional 5 minutes of sIPSCs were recorded. While both *Emx1^{Cre};Dag1^{Ctrl}* and *Emx1^{Cre};Dag1^{cKO}* cells displayed a CCh-mediated change in sIPSC frequency, this response was dramatically attenuated in *Emx1^{Cre};Dag1^{cKOs}* mice compared to *Emx1^{Cre};Dag1^{Ctrl}* mice (**Figure 2.6 A-C**). Furthermore, in *Emx1^{Cre};Dag1^{Ctrls}*, 19/21 cells (90.5%) responded to CCh application (defined as a >20% increase in sIPSC frequency), whereas only 13/22 cells (59.1%) responded in *Emx1^{Cre};Dag1^{cKOs}* (**Supplementary Figure 2.12 B**). Proper Dystroglycan glycosylation was also required for CCK^+/CB_1R^+ IN synapse function, as *Emx1^{Cre};Pomt2^{cKO}* mice exhibited the same phenotype as *Emx1^{Cre};Dag1^{cKOs}*: a reduced response to CCh overall, and a reduced proportion of responsive cells (**Figure 2.6 A-C**, **Supplementary Figure 2.12 B**). CCh also increased the mean sIPSC amplitude in each of the controls (**Supplementary Figure 2.12 A**), which may reflect an increased contribution of larger-amplitude action potential-mediated perisomatic events elicited by CCh (Früh et al., 2016; Nagode et al., 2014). Consistent with the decreased function of CCK^+/CB_1R^+ IN synapses, a CCh-mediated change in sIPSC amplitude was also absent in each of these models (**Supplementary Figure 2.12 A**). Together, these data indicate that the altered perisomatic CCK^+/CB_1R^+ IN synaptic localization in CA1 is associated with a functional deficit in synaptic signaling.

Dag1$^{cyto/-}$ mutants also had a dramatically attenuated sIPSC response to CCh compared to WT controls (**Figure 2.6 C**). Notably, even baseline sIPSC frequency was

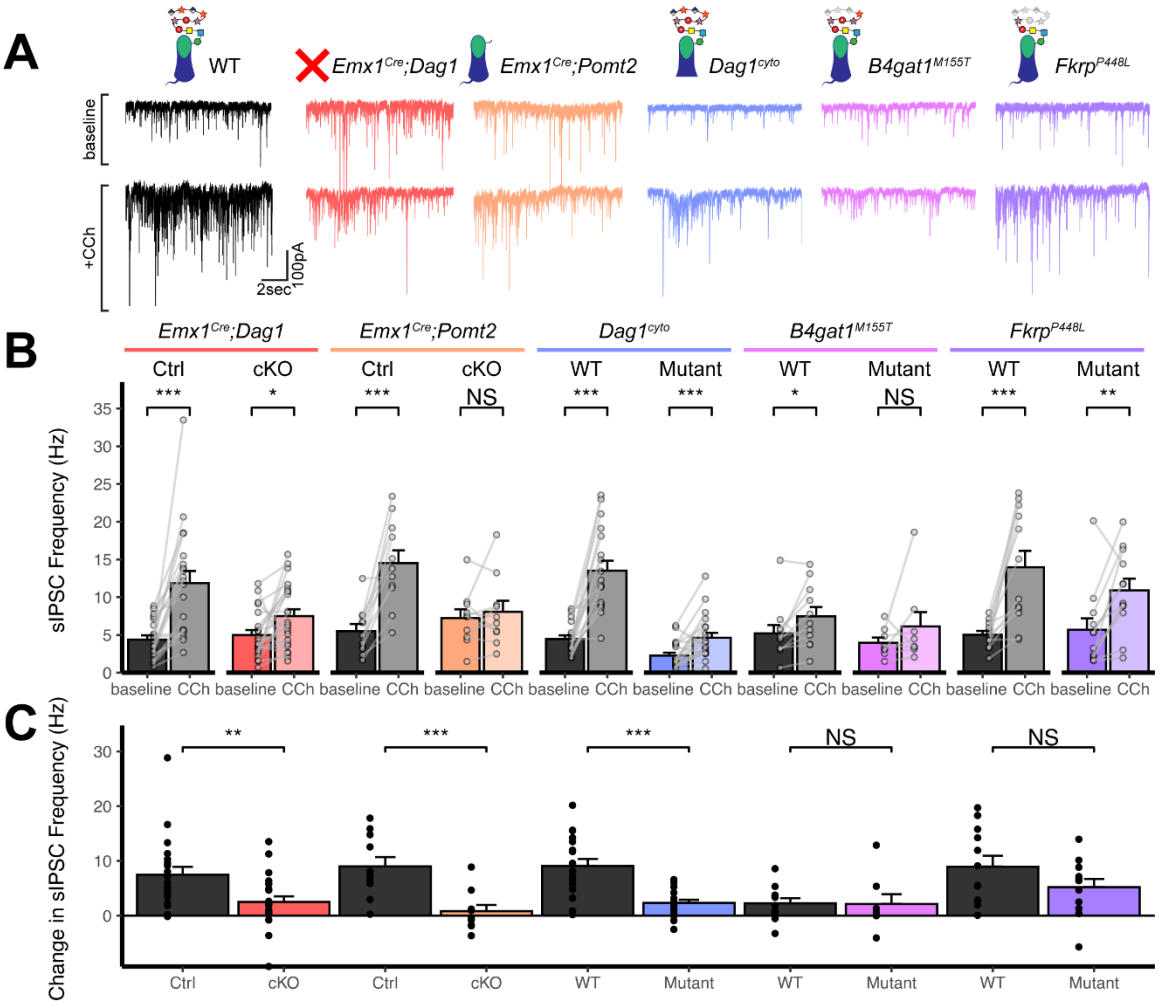

Figure 2.6 *Dag1* is required for CCK$^+$/CB$_1$R$^+$ IN synapse function in hippocampal CA1 in a manner dependent on both glycosylation and intracellular interactions.

(A) Representative traces showing 15 seconds of sIPSC recordings at baseline (top) and after the addition of carbachol (bottom). **(B)** Quantification of average sIPSC frequency at baseline and after the addition of carbachol. **(C)** Quantification of the change in sIPSC frequency with the addition of carbachol. Error bars show mean + SEM. Significance: * = $p < 0.05$, ** = $p < 0.01$, *** = $p < 0.001$, NS = $p \geq 0.05$. *Abbreviations: sIPSC, spontaneous inhibitory postsynaptic current; CCh, carbachol.*

reduced in *Dag1*$^{cyto/-}$ mutants (2.27±1.70 Hz) compared to WT controls (4.46±2.04 Hz, $p = 0.002$), whereas baseline sIPSC frequencies appeared normal in all other mutants when compared to their respective controls. Together with the finding that these mutants contain a normal number of CCK$^+$/CB$_1$R$^+$ basket synapses (as measured using immunohistochemistry; **Figure 2.5 A-D**), these results indicate that the cytoplasmic

domain of Dystroglycan may play a critical role in mediating the assembly of functional postsynaptic signaling/receptor complexes at these synapses.

Neither of the more mildly hypoglycosylated mutants (*B4gat1*$^{M155T/M155T}$, *Fkrp*$^{P448L/P448L}$) were different from their respective littermate controls in terms of the magnitude of the CCh effect on sIPSC frequency (**Figure 2.6 C**), although the *B4gat1*^{WT} mice appeared to possess a reduced effect of CCh compared to other control conditions (**Figure 2.6 A-C**). The *B4gat1* line is of a mixed genetic background, which could possibly explain the difference in CCh response. This finding is of unclear significance and may have obscured potential differences. Importantly, however, the marked functional synaptic differences observed between the *Emx1*^{Cre}*;Pomt2*^{cKO}, *Emx1*^{Cre}*;Dag1*^{cKO} and *Dag1*$^{cyto/-}$ mice when compared with each of their respective controls described above was not seen in either of these phenotypically milder mutants.

Together, these results suggest that Dystroglycan is required for the function of CCK^+/CB_1R^+ IN perisomatic basket synapses in a glycosylation-dependent manner, as evidenced by the *Emx1*^{Cre}*;Dag1*^{cKO} and *Emx1*^{Cre}*;Pomt2*^{cKO} synaptic phenotypes, and that the intracellular domain of Dystroglycan is also required for normal CCK^+/CB_1R^+ IN basket synapse function. However, we cannot rule out the possibility that CCK^+/CB_1R^+ INs are simply less responsive to CCh in the mutants, as we lack the tools to identify CCK^+/CB_1R^+ INs in live tissue for targeted recordings. In contrast, *B4gat1*$^{M155T/M155T}$ and *Fkrp*$^{P448L/P448L}$ hypomorphic mutants both appear to retain sufficient Dystroglycan glycosylation to maintain normal synapse function.

Increased seizure susceptibility in models of dystroglycanopathy

Human patients with dystroglycanopathy have an increased risk of seizures and epilepsy (Dhaibani et al., 2018; Di Rosa et al., 2011; Raphael et al., 2014; Yang et al., 2022), however the underlying cause has yet to be determined. The observed defects in

inhibitory basket synapse function suggest that alterations in neuronal circuit inhibition could potentially predispose mutant mice to seizures. To test whether mouse models of dystroglycanopathy exhibit a reduced seizure threshold, we exposed mice to the volatile chemoconvulsant flurothyl and measured the latency to generalized tonic-clonic seizure (TCS) (Egawa et al., 2021).

The latency to TCS was significantly faster in *Emx1^{Cre};Dag1^{cKO}* mice than their littermate controls (a 40.9% reduction on average, **Figure 2.7 A**), with no difference in seizure latency between sexes in either group (**Supplementary Figure 2.13 C**). *Emx1^{Cre};Pomt2^{cKOs}* and *Dag1$^{cyto/-}$* mutants also had a significantly shorter latency to TCS than littermate controls (42.9% and 33.6% reductions, respectively; **Figure 2.7 A**), indicating that the mechanism underlying Dystroglycan's role in seizure susceptibility requires both extracellular glycosylation and intracellular interactions. *B4gat1$^{M155T/M155T}$* mutants showed a small but significant reduction (16%) in seizure latency, despite exhibiting no detectable functional deficit by electrophysiology (**Figure 2.6 A-C**, **Figure 2.7 A**). Finally, *Fkrp$^{P448L/P448L}$* mutants showed no significant change in seizure susceptibility (**Figure 2.7 A**). Thus, the reduction in seizure latency reflects the severity of the synaptic phenotypes across the various models of dystroglycanopathy. These results demonstrate that disruptions in Dystroglycan function, including both its extracellular glycosylation and intracellular interactions, increase sensitivity to seizures.

Discussion

Recent work identified a key role for neuronal Dystroglycan in the establishment and function of CCK^+/CB_1R^+ inhibitory synapses in the forebrain (Früh et al., 2016; Miller and Wright, 2021). Deletion of *Dag1* selectively from pyramidal neurons (*NEX^{Cre};Dag1^{cKO}*) led to a near complete loss of CCK^+/CB_1R^+ INs during the first few

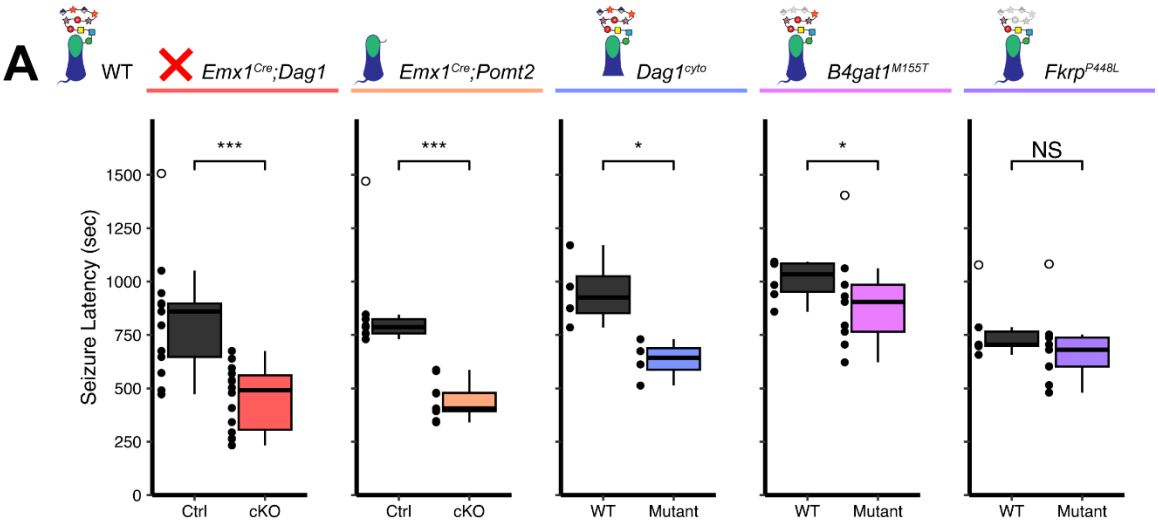

Figure 2.7 Reduced seizure induction threshold in models of dystroglycanopathy. **(A)** Quantification of latency (in seconds) to generalized tonic clonic seizure upon exposure to 10% flurothyl delivered at a constant rate. Open points denote statistical outliers. Significance: * = $p < 0.05$, ** = $p < 0.01$, *** = $p < 0.001$, NS = $p \geq 0.05$.

postnatal weeks. In this study, we sought to better understand how CCK^+/CB_1R^+ IN synapse formation is affected in mouse models that more accurately reflect dystroglycanopathy, in which Dystroglycan function is more broadly affected throughout the CNS (**Figure 2.1**, **Figure 2.2**). Using a model that deletes *Dag1* throughout the developing forebrain (*Emx1*^{Cre}*;Dag1*^{cKO}) we found that CCK^+/CB_1R^+ INs were present, but the laminar organization of their axon terminals and their ability to form functional basket synapses onto pyramidal neuron cell bodies in the hippocampus was impaired (**Figures 2.3**, **2.4**, **2.5**, **2.6**). The inability of CCK^+/CB_1R^+axon terminals to concentrate in the CA1-3 cell body layer began to manifest during the first postnatal week, when dynamic changes in laminar innervation by CCK^+/CB_1R^+ axons normally occur (**Figure 2.4**). Furthermore, these mice were found to exhibit a reduced seizure threshold compared to controls, showing for the first time that mouse models of dystroglycanopathy are vulnerable to seizures (**Figure 2.7**). Because *Emx1*^{Cre} (and *Nestin*^{Cre}) conditional deletion of *Dag1* or *Pomt2* leads to widespread loss of functional

Dystroglycan in the forebrain in contrast with the previously studied *NEX*^{Cre} conditional deletion, which targets pyramidal neurons, these models more accurately model dystroglycanopathy.

We found that CCK^{+}/CB$_1$R^{+} IN synapse formation and function are dependent on proper Dystroglycan glycosylation and appear to correlate with the degree of hypoglycosylation in different mutants. Complete reduction of glycosylation in *Emx1*^{Cre}*;Pomt2*^{cKO} mutants caused the same phenotypes seen in Dystroglycan conditional knockouts (*Emx1*^{Cre}*;Dag1*^{cKO}) (**Figures 2.1**, **2.2**, **2.3**, **2.5**, **2.6**), possibly due to the mislocalization of Dystroglycan. The finding that glycosylation is required for Dystroglycan synaptic localization in hippocampal pyramidal cells is similar to a previous finding in retinal photoreceptors in the context of *Pomt1* conditional deletion (Rubio-Fernández et al., 2018). In contrast, when *Fktn* deletion is induced in myotubes β-Dystroglycan localization is unchanged, suggesting that this phenomenon is unique to synaptic Dystroglycan (Beedle et al., 2012). One interpretation is that without matriglycan present to mediate interaction with presynaptic cells, Dystroglycan is no longer concentrated at synaptic sites, implicating it as a synaptic organizer. However, the miswiring of the CCK^{+}/CB$_1$R^{+} axons could also reduce the likelihood of postsynaptic Dystroglycan encountering a presynaptic axon, discouraging synaptic localization. Conversely, it is possible that glycosylation is required for trafficking to the surface in the first place, however this is less likely given that the levels of β-Dystroglycan were normal in membrane-enriched lysate (**Figure 2.1, Supplementary Figure 2.2**).

A milder reduction in glycosylation (*B4gat1*$^{M155T/M155T}$) resulted in a cortical migration phenotype that was restricted to midline (**Supplementary Figure 2.8**) and a small reduction in CCK^{+}/CB$_1$R^{+} axon terminals and synaptic puncta density in CA1 which did not appear to affect synapse function (**Figures 2.3**, **2.5**, **2.6**). The mildest reduction in glycosylation amongst our models was observed in *Fkrp*$^{P448L/P448L}$ mutants, which

exhibited normal cortical migration but the same mild defect in CCK^+/CB_1R^+ IN axon targeting and synaptic puncta density observed in *B4gat1*$^{M155T/M155T}$ mutants (**Figures 2.3**, **2.5**, **2.6**). Together, these three glycosylation mutants illustrate the degree of hypoglycosylation required for neurodevelopmental processes and show that defects in synaptic function only arise in the context of severely reduced glycosylation; the residual Dystroglycan function present in *B4gat1*$^{M155T/M155T}$ and *Fkrp*$^{P448L/P448L}$ mutants is sufficient for most aspects of brain development. Finally, using *Dag1*$^{cyto/-}$ mutants that lack the intracellular domain of Dystroglycan, we found that the intracellular domain plays a role in some, but not all, neurodevelopmental processes. The intracellular domain is not required for neuronal migration in neocortex or synapse formation in CA1 (**Figure 2.2** and **Figure 2.5**) but is required for the proper targeting of CCK^+/CB_1R^+ IN axons in CA1-3 (**Figure 2.3**) and for subsequent CCK^+/CB_1R^+ IN basket synapse function (**Figure 2.6**).

Dystroglycan is an essential transsynaptic organizing molecule for CCK^+/CB_1R^+ basket synapses

Synaptogenesis requires multiple distinct steps: (1) synaptic partner recognition, (2) recruitment and assembly of core pre- and post-synaptic machinery, (3) differentiation and maturation of synaptic identity, and (4) synaptic maintenance (Südhof, 2018). Based on data from this study (**Figure 2.4**) and previous work from our group and others, mice lacking *Dystroglycan* exhibit defects in CCK^+/CB_1R^+ IN development at the earliest time point they can be reliably identified (P0-P5), before the peak phase of inhibitory synapse formation (P9), suggesting that Dystroglycan functions at the earliest stages of synaptogenesis such as synaptic partner recognition (Favuzzi et al., 2019). Determining the precise onset of synapse targeting and formation for most IN subtypes, including CCK^+/CB_1R^+ INs, is limited by a lack of genetic tools for visualizing and manipulating IN subtypes during developmental stages.

The impairment in CCK^+/CB_1R^+ IN development throughout the forebrain suggests a trans-synaptic role for Dystroglycan (**Figure 2.3, Supplementary Figure 2.8**). The identity of the trans-synaptic binding partner between Dystroglycan-expressing cells and CCK^+/CB_1R^+ INs remains unknown. Our data in *Emx1*^{Cre}*;Pomt2*^{cKO} mice point to a critical role for the glycan chains on Dystroglycan mediating this binding. All proteins that bind to the glycan chains on Dystroglycan do so through at least one Laminin G (LG) domain. There are over 25 LG-domain containing extracellular or transmembrane proteins expressed in the hippocampus. Neurexins, a family of highly alternatively spliced synaptic cell-adhesion molecules (*NRXN1-3*) which each contain multiple LG domains, bind Dystroglycan in a glycosylation-dependent manner (Boucard et al., 2005; Fuccillo et al., 2015; Reissner et al., 2014; Sugita et al., 2001). The specific splice isoforms of *Nrxns* that bind Dystroglycan are expressed by CCK^+/CB_1R^+ INs (Fuccillo et al., 2015; Ullrich et al., 1995). *Neurexin-3* conditional knockout (targeting all *Nrxn3* isoforms) and CRISPR-mediated *Dag1* knockout both result in similar synaptic deficits in olfactory bulb and prefrontal cortex (Trotter et al., 2023). While a Dystroglycan knock-in mouse with reduced glycosylation that impairs Neurexin binding (*Dag1*^{T190M}) shows normal CCK^+/CB_1R^+ synapse formation by immunohistochemistry, the functionality of these synapses was not assessed by electrophysiology (Früh et al., 2016). Similar to *B4gat1*$^{M155T/M155T}$ and *Fkrp*$^{P448L/P448L}$ mutants, the *Dag1*^{T190M} mutation does not fully eliminate Dystroglycan glycosylation, and therefore does not rule out the possibility that Neurexins play a role at CCK^+/CB_1R^+ synapses. It is also possible that a yet undescribed Dystroglycan interacting protein is required for initial synapse recognition, and Nrxn-Dag1 interactions are required for subsequent synapse maturation and maintenance only. Indeed, the majority of studies indicate that Neurexins are not required for the initial formation of synapses, but rather regulate the maturation and structural maintenance of synapses after they have formed (Chen et al., 2017; Dudanova et al., 2007; Lin et al.,

2023; Missler et al., 2003; Trotter et al., 2023). Interestingly, while Dystroglycan localizes to both PV^+ and CCK^+/CB_1R^+ inhibitory basket synapses in CA1, only the CCK^+/CB_1R^+ IN population was affected in the dystroglycanopathy models (Früh et al., 2016). Presumably, PV^+ INs have a distinct developmental program independent of Dystroglycan and likely require a different postsynaptic recognition partner.

A role for the Dystrophin-Glycoprotein Complex in CCK^+/CB_1R^+ interneuron development

In brain and muscle tissue, Dystroglycan forms a complex with Dystrophin and several other proteins, collectively known as the Dystrophin Glycoprotein Complex (DGC). Like Dystroglycan, Dystrophin is also expressed throughout the forebrain and is associated with inhibitory synapses in multiple brain regions (Knuesel et al., 1999). Patients with mutations in *Dystrophin* develop Duchenne Muscular Dystrophy (DMD), and frequently exhibit cognitive impairments in the absence of brain malformations, suggesting a general role for the DGC in synapse development and function (Jagadha and Becker, 1988; Moizard et al., 2000; Naidoo and Anthony, 2020). A mouse model of DMD lacking all neuronal Dystrophin isoforms (*mdx*) exhibits defects in CCK^+/CB_1R^+ IN synapse development and abnormal innervation in the hippocampus, resembling the innervation pattern we observed in $Emx1^{Cre};Dag1^{cKO}$ and $Emx1^{Cre};Pomt2^{cKO}$ mice in this study (Krasowska et al., 2014). Since Dystroglycan interacts with Dystrophin through its intracellular domain, we expected to observe similar phenotypes in mice lacking the intracellular domain of Dystroglycan ($Dag1^{cyto/-}$). However, $Dag1^{cyto/-}$ showed a milder axon targeting defect than $Emx1^{Cre};Dag1^{cKO}$ or *mdx* mice. In addition, IIH6 puncta were normally localized to the somatodendritic compartment in $Dag1^{cyto/-}$ mutants, suggesting that Dystroglycan does not require interactions with Dystrophin for is localization to somatodendritic synapses. However, Dystroglycan's synaptic localization has not been

examined in the *mdx* mutants. Clearly, additional work is required to better understand the relationship between Dystroglycan and Dystrophin at synapses in the brain.

While the density of CCK^+/CB_1R^+ IN synaptic puncta was normal in *Dag1*$^{cyto/-}$ mice, synaptic function was impaired to the same level as *Emx1*^{Cre}*;Dag*^{cKO} and *Emx1*^{Cre}*;Pomt2*^{cKO} mice, and seizure latency was reduced. Given that *Dag1*$^{cyto/-}$ and *B4gat1*$^{M155T/M155T}$ mutants show a similar reduction in Dystroglycan glycosylation (**Figure 2.1 B-C**), our observation that the functional synaptic phenotype is restricted to the *Dag1*$^{cyto/-}$ mutant reinforces the notion that the intracellular domain of Dystroglycan plays an active role in organizing essential postsynaptic signaling elements. One possibility is that the intracellular domain of Dystroglycan is required to recruit additional postsynaptic scaffolding elements and receptors necessary for CCK^+/CB_1R^+ basket synapse function (Uezu et al., 2019). Importantly, *Dag1*$^{cyto/-}$ mice did not show a cortical migration phenotype (**Figure 2.2 A-D**), indicating that the functional synaptic deficits and reduced seizure latency occurred independent of cortical malformation.

Altered inhibitory synapse development and function may contribute to neurological symptoms in dystroglycanopathy

In addition to muscular atrophy and hypotonia, dystroglycanopathy patients often present with central nervous system symptoms. Patients with the most severe forms of dystroglycanopathy (FCMD, Muscle-Eye-Brain disease, and Walker-Warburg Syndrome) exhibit structural changes including hypoplasia of the retina, brainstem and spinal cord, cerebellar cysts, hydrocephalus, Type II lissencephaly, and microcephaly, associated with seizures and cognitive disability (Meilleur et al., 2014; Mercuri et al., 2009). Patients with milder forms of dystroglycanopathy may show cognitive disability and/or seizures without gross brain malformations, suggesting that there may be synaptic deficits independent of early neurodevelopmental processes (e.g. neuronal migration, axon

guidance) (Mercuri et al., 2009; Yang et al., 2022). The mouse models used in this study recapitulate the full spectrum of brain malformations seen in human patients. *Emx1*^{Cre}*;Dag*^{cKO} and *Emx1*^{Cre}*;Pomt2*^{cKO} mice show Type II lissencephaly consistent with severe dystroglycanopathy, whereas *B4gat1*$^{M155T/M155T}$ and *Fkrp*$^{P448L/P448L}$ mutants have relatively normal cortical development consistent with mild dystroglycanopathy. Mutations in any of the genes involved in the glycosylation of Dystroglycan can result in dystroglycanopathy with seizures, but the incidence and severity of seizures is higher in patients with brain malformations (Mercuri et al., 2009; Wang et al., 2017; Yang et al., 2022).

Mice have been used to model dystroglycanopathy for decades, however to our knowledge the present study is the first to investigate seizure susceptibility in mouse models of dystroglycanopathy. It is probable that the CCK^+/CB_1R^+ interneuron axon targeting and synapse phenotypes in the mouse models described in the present study contribute to their seizure susceptibility and open the possibility that defective inhibitory synaptic signaling mechanisms may underlie seizures in dystroglycanopathy patients. Although severe neuronal migration phenotypes In *Emx1*^{Cre}*;Dag1*^{cKO} and *Emx1*^{Cre}*;Pomt2*^{cKO} mice may contribute to seizure activity, our observation that *Dag1*$^{cyto/-}$ mutants showed both abnormal CCK^+/CB_1R^+synaptic function and reduced seizure latency, with intact cortical migration, indicates that the seizure phenotype is likely associated with synaptic defects. Supporting these results, CCK^+/CB_1R^+ interneurons in the hippocampus are selectively lost in models of temporal lobe epilepsy with recurrent seizures induced by pilocarpine. CCK^+/CB_1R^+ axons in CA1-3 begin to degenerate within hours of status epilepticus, whereas PV^+ INs are unaffected in this model (Whitebirch et al., 2023; Wyeth et al., 2010).

While our *B4gat1*$^{M155T/M155T}$ mutants showed only a slightly reduced seizure latency, the mutants experienced more severe seizures than the other mouse models,

resulting in death in 50% of cases (4/8 mutants compared to 0/6 fatalities among littermate controls) (**Supplementary Figure 2.13 A**). Flurothyl-induced seizures are typically generalized forebrain seizures; however in seizure-prone mouse models or in mice exposed to higher concentrations of flurothyl, mice can experience a suppression of brainstem oscillations followed by sudden death (Gu et al., 2022; Kadiyala et al., 2016). The *B4gat1*$^{M155T/M155T}$ mutation was originally identified based on a hindbrain axon guidance phenotype, suggesting they may have currently unknown defects in brainstem development or circuitry that could render them more susceptible to fatal brainstem seizures (Wright et al., 2012). *Fkrp*$^{P448L/P448L}$ mutants did not show this same hindbrain axon guidance phenotype (**Supplementary Figure 2.14**), perhaps explaining why they were not similarly affected. Because the *Dag1* and *Pomt2* mutants are forebrain-specific conditional knockouts, (**Supplementary Figure 2.1 A**), we would not anticipate abnormal axon guidance in the brainstem or hindbrain of these mutants. Further research on the nature and progression of seizures observed in mouse models may have a profound impact on our understanding of dystroglycanopathy and potential therapeutic interventions.

Potential therapeutics for the restoration of synapse function in patients with dystroglycanopathy

Most patients with dystroglycanopathy present with mutations in one of the 19 genes required for the glycosylation of Dystroglycan, resulting in hypoglycosylated Dystroglycan. We have demonstrated that a mild reduction in the glycosylation of Dystroglycan, as seen in *Fkrp*$^{P448L/P448L}$ and *B4gat1*$^{M155T/M155T}$ mutants, does not significantly disrupt synapse function. This suggests that glycosylation may not need to be restored to wild-type levels in order to achieve normal synapse function. Gene replacement therapy may be well suited to treat certain forms of dystroglycanopathy by

rescuing glycosylation. AAV-mediated delivery of fully functional glycosyltransferases has been shown to significantly improve muscle pathology and function in dystrophic mice, however synaptic phenotypes have not been examined (Kanagawa, 2021). Supplementation with (CDP)-ribitol, which is synthesized by *Crppa* (previously known as *ISPD*), can restore functional Dystroglycan glycosylation and improve muscle function in mouse models with hypomorphic mutations in *Crppa* or *Fkrp* (Cataldi et al., 2018). In mice lacking functional *Crppa* or *Fkrp* in skeletal muscle, (CDP)-ribitol can further enhance the therapeutic impact of gene restoration (Cataldi et al., 2020). However, whether (CDP)-ribitol treatment can improve Dystroglycan function in other models of dystroglycanopathy, or is capable of restoring Dystroglycan glycosylation and synaptic function in the nervous system, remains untested.

Conclusion

We demonstrate that Dystroglycan is critical for the postnatal development of CCK^+/CB_1R^+ interneuron axon targeting and synapse formation/function in the hippocampus of severe mouse models of dystroglycanopathy. Extracellular glycosylation of Dystroglycan and intracellular interactions involving the cytoplasmic domain are both essential for Dystroglycan's synaptic organizing role. Mice with a partial reduction in glycosylation have relatively normal CCK^+/CB_1R^+ interneuron axon targeting and synapse function, suggesting that even a partial restoration of glycosylation may have some therapeutic benefit. These findings suggest that CCK^+/CB_1R^+ interneuron axon targeting defects may contribute to cognitive impairments and seizure susceptibility in dystroglycanopathy.

Materials and Methods

Animal husbandry

All animals were housed and cared for by the Department of Comparative Medicine (DCM) at Oregon Health and Science University (OHSU), an AAALAC-accredited institution. Animal procedures were approved by OHSU Institutional Animal Care and Use Committee (Protocol # IS00000539), adhered to the NIH *Guide for the care and use of laboratory animals*, and provided with 24-hour veterinary care. Animal facilities are regulated for temperature and humidity and maintained on a 12-hour light-dark cycle and were provided food and water *ad libitum*. Animals older than postnatal day 6 (P6) were euthanized by administration of CO_2, animals <P6 were euthanized by rapid decapitation.

Mouse strains and genotyping

The day of birth was designated postnatal day 0 (P0). Ages of mice used for each analysis are indicated in the figure and figure legends. Mouse strains used in this study have been previously described and were obtained from Jackson Labs, unless otherwise indicated (**Table 2.1**) (Chan et al., 2010; Cohn et al., 2002; Goebbels et al., 2006; Gorski et al., 2002; Hu et al., 2011; Peron et al., 2015; Satz et al., 2009; Tronche et al., 1999; Wright et al., 2012). *Dag1*$^{+/-}$ mice were generated by crossing the *Dag1*$^{flox/flox}$ line to a *Sox2*^{Cre} line to generate germline *Dag1*$^{\Delta/+}$ mice hereafter referred to as *Dag1*$^{+/-}$ as the resultant transcript is nonfunctional. These mice were thereafter maintained as heterozygotes. Breeding schemas are as described in **Table 2.2**. Where possible, mice were maintained on a C57BL/6 background. *Dag1*$^{cyto/-}$ mice occurred at a frequency lower than Mendelian, suggesting that a proportion of progeny die embryonically. To increase viability of pups, the *Dag1*^{cyto} line was outcrossed to a CD-1 background for one generation. The *B4gat1* line has a mixed genetic background: it was founded on a

C3H/He background and then crossed on to C57BL/6 for future generations. Genomic DNA extracted from toe or tail samples (Quanta BioSciences) was used to genotype animals. Primers for genotyping can be found on the JAX webpage or originating article. *Dag1*$^{+/-}$ mice were genotyped with the following primers: CGAACACTGAGTTCATCC (forward) and CAACTGCTGCATCTCTAC (reverse). For each mouse strain, littermate controls were used for comparison with mutant mice. For all experiments, unless otherwise noted, mice of both sexes were used indiscriminately.

Table 2.1 Mouse strains

Common name	Strain name	Reference	Stock #
Dag1^{flox}	*B6.129(Cg)-Dag1*$^{tm2.1Kcam}$*/J*	(Cohn et al., 2002)	009652
Dag1^{cyto}	N/A	(Satz et al., 2009)	N/A
Pomt2^{flox}	*POMT2tm1.1Hhu/J*	(Hu et al., 2011)	017880
B4gat1^{M155T}	*B6(C3)-B4GAT1*^{m1Ddg}*/J*	(Wright et al., 2012)	022018
Fkrp^{P448L}	*C57BL/6NJ-Fkrp*^{em1Lgmd}*/J*	(Chan et al., 2010)	034659
R26$^{LSL-H2B-mCherry}$	*B6.Gt(ROSA)26Sor*$^{tm1.1Ksvo}$	(Peron et al., 2015)	023139
Emx1^{Cre}	*B6.129S2-Emx1*$^{tm1(cre)Krj}$*/J*	(Gorski et al., 2002)	005628
Nestin^{Cre}	*B6.Cg-Tg(Nes-cre)*^{1Kln}*/J*	(Tronche et al., 1999)	003771
NEX^{Cre}	*NeuroD6*$^{tm1(cre)Kan}$	(Goebbels et al., 2006)	MGI:4429523
Sox2^{Cre}	*B6N.Cg-Edil*$^{3Tg(Sox2-cre)1Amc}$*/J*	(Hayashi et al., 2002)	014094

Table 2.2 Breeding schemes

Breeding Scheme	Control Genotype	Mutant Genotype
Emx1$^{Cre/+}$*;Dag1*$^{+/-}$ *x Dag1*$^{flox/flox}$	*Emx1*$^{Cre/+}$*;Dag1*$^{flox/+}$	*Emx1*$^{Cre/+}$*;Dag1*$^{flox/-}$
Nestin$^{Cre/+}$*;Dag1*$^{+/-}$ *x Dag1*$^{flox/flox}$	*Nestin*$^{Cre/+}$*;Dag1*$^{flox/+}$	*Nestin*$^{Cre/+}$*;Dag1*$^{flox/-}$
NEX$^{Cre/+}$*;Dag1*$^{+/-}$ *x Dag1*$^{flox/flox}$	*NEX*$^{Cre/+}$*;Dag1*$^{flox/+}$	*NEX*$^{Cre/+}$*;Dag1*$^{flox/-}$
Emx1$^{Cre/+}$*;Pomt2*$^{flox/+}$ *x Pomt2*$^{flox/flox}$	*Emx1*$^{Cre/+}$*;Pomt2*$^{flox/+}$	*Emx1*$^{Cre/+}$*;Pomt2*$^{flox/flox}$
Dag1$^{cyto/+}$ *x Dag1*$^{+/-}$	*WT*	*Dag1*$^{cyto/-}$
B4gat1$^{M155T/+}$ *x B4gat1*$^{M155T/+}$	*WT*	*B4gat1*$^{M155T/M155T}$
Fkrp$^{P448L/+}$ *x Fkrp*$^{P448L/+}$	*WT*	*Fkrp*$^{P448L/P448L}$

Perfusions and tissue preparation

Brains from mice younger than P15 were dissected and drop fixed in 5 mLs of 4% paraformaldehyde (PFA) in phosphate buffered saline (PBS) overnight for 18-24 hours at 4°C. Mice P15 and older were deeply anesthetized using CO2 and

transcardially perfused with ice cold 0.1M PBS for two minutes to clear blood from the brain, followed by 15 mLs of ice cold 4% PFA in PBS. After perfusion, brains were dissected and post-fixed in 4% PFA for 30 minutes at room temperature. Brains were rinsed with PBS, embedded in 4% low-melt agarose (Fisher cat. no. 16520100), and sectioned at 50µm using a vibratome (VT1200S, Leica Microsystems Inc., Buffalo Grove, IL) into 24-well plates containing 1 mL of 0.1M PBS with Sodium Azide.

Immunohistochemistry

Single and multiple immunofluorescence detection of antigens was performed as follows: free-floating vibratome sections (50µm) were briefly rinsed with PBS, then blocked for 1 hour in PBS containing 0.2% Triton-X (PBST) plus 10% normal goat or donkey serum. Sections were incubated with primary antibodies (**Table 2.3**) diluted in blocking solution at 4°C for 48-72 hours. For staining of Dystroglycan synaptic puncta, an antigen retrieval step was performed prior to incubation in primary antibody. Briefly, sections were incubated in sodium citrate solution for 15 min at 95 degrees in a water bath. Following incubation in primary antibody, sections were rinsed with PBS then washed with PBST three times for 20 min each. Sections were then incubated with a cocktail of secondary antibodies (1:500, Alexa Fluor 488, 546, 647) in blocking solution overnight at room temperature. Sections were washed with PBS three times for 20 min each and counterstained with Hoechst 33342 (1:10,000, Life Technologies, Cat# H3570) for 20 min to visualize nuclei. Finally, sections were mounted on slides using Fluoromount-G (SouthernBiotech) and sealed using nail polish.

Table 2.3 Primary antibodies used for immunohistochemistry

Target	Host	Dilution	Source	Catalog #	RRID
α-Dystroglycan (IIH6C4)	Mouse	1:250	Millipore	05-593	AB_309828
β-Dystroglycan	Mouse	1:50	Leica Biosystems	NCL-b-DG	AB_442043
CB_1R	Guinea pig	1:1000	Synaptic Systems	258-104	AB_2661870
Cux1	Rabbit	1:500	Santa Cruz Biotech	sc-13024	AB_2261231
Laminin	Rabbit	1:1000	Sigma	L9393	AB_477163
NECAB1	Rabbit	1:500	Sigma	HPA023629	AB1848014
NECAB2	Rabbit	1:500	Proteintech	12257-1-AP	AB_2877841
NeuN	Mouse	1:250	Millipore	MAB377	AB_2298772
Parvalbumin	Rabbit	1:1000	Swant	PV27	AB_2631173
Parvalbumin	Mouse	1:50	Swant	235	AB_10000343
Somatostatin	Rabbit	1:2000	Peninsula Labs	T-4103	AB_518614
Tbr1	Rabbit	1:500	Millipore	AB10554	AB_10806888
VGAT	Rabbit	1:500	Synaptic Systems	131-003	AB_887869
VGAT	Guinea Pig	1:500	Synaptic Systems	131-005	AB_1106810
VGlut3	Rabbit	1:1000	Synaptic Systems	135-203	AB_887886
VIP	Rabbit	1:1000	ImmunoStar	20077	AB_572270

Microscopy

Imaging was performed on either a Zeiss Axio Imager M2 fluorescence upright microscope equipped with an Apotome.2 module or a Zeiss LSM 980 laser scanning confocal build around a motorized Zeiss Axio Observer Z1 inverted microscope with a Piezo stage. The Axio Imager M2 uses a metal halide light source (HXP 200 C), Axiocam 506 mono camera, and 10X/0.3 NA EC Plan-Neofluar, 20X/0.8 NA Plan-Apochromat objectives. The LSM 980 confocal light path has two multi-alkali PMTs and two GaAsP PMTs for four track imaging. Confocal images were acquired using a 63X/1.4 NA Plan-Apochromat Oil DIC M27 objective. Z-stack images were acquired and analyzed offline in ImageJ/FIJI (Schindelin et al., 2012) or Imaris 9.8 (Oxford Instruments). Images used for quantification between genotypes were acquired using the same exposure times. Brightness and contrast were adjusted in FIJI to improve

visibility of images for publication. Figures were composed in Adobe Illustrator 2023 (Adobe Systems).

Image Quantification

For imaging experiments, 4-8 images were acquired from 2-4 coronal sections per animal, and at least three animals per genotype were used for analysis.

Cortical Lamination

Images of somatosensory cortex were acquired using a 10X objective on a Zeiss Axio Imager M2. 4μm z-stacks covering 16μm were acquired and multiple tiles were stitched together. Maximum projections were used for analysis. In FIJI, the straight line tool with a 300μm line width was used to measure the fluorescence profile from corpus callosum to pial surface. Background fluorescence was determined as the average fluorescence of the 20 darkest pixels; background was then subtracted from all points. The cortical distance was broken into 10 bins and average fluorescence within each bin was compared between genotypes.

Hippocampal CA1 CB_1R and PV Distribution

Images of dorsal hippocampal CA1 were acquired using a 20X objective on a Zeiss Axio Imager M2. Maximum projection images of 0.6μm z-stacks covering 9μm were analyzed in FIJI. The straight line tool with a 300μm line width was used to measure the fluorescence profile within SO, SP, and SR of CA1, avoiding Parvalbumin$^+$ cell bodies. Background fluorescence was determined as the average fluorescence of the 50 darkest pixels; background was then subtracted from all points. The thickness of SP was determined using Hoechst fluorescence. Average fluorescence within SO/SP/SR was compared between genotypes.

Interneuron Cell Counts in CA1

Images of dorsal hippocampal CA1 were acquired using a 10X objective on a Zeiss Axio Imager M2. Maximum projection images of 4µm z-stacks covering 40µm were analyzed in FIJI. Immunolabeled NECAB1/NECAB2/PV cell bodies were counted if they were within 100µm of *stratum pyramidale*. The freehand line tool was used to measure the length of *stratum pyramidale*. Cell number was normalized to the length of *stratum pyramidale* present in the analyzed region.

Hippocampal CB_1R/PV/VGAT Density and Co-localization

Images of dorsal hippocampal CA1 were acquired using a 63X objective on a Zeiss LSM 980. 0.2µm z-stacks covering 3µm were analyzed in Imaris. Hoechst fluorescence was used to determine the bounds of SP. The Imaris Spots function was used to determine the location of synaptic puncta in 3-dimensional space. Synaptic puncta were deemed to be co-localized if they were within 1µm of each other.

Western Blot

Cortex or hippocampus was dissected and solubilized in 1 mL of lysis buffer containing 100mM NaCl, 50nM Tris, 2.5mM $CaCl_2$, 1% Triton X-100, 1% n-Octyl-β-D-glucopyranoside, and protease inhibitors. Lysate was incubated at 4°C for 1 hour and then spun at 12,500g for 25 minutes. Supernatant containing 3,000µg (cortex) or 2,000µg (hippocampus) of protein (as determined by Pierce BCA Protein Assay) was applied to agarose-bound Wheat Germ Agglutinin (WGA) (Vector Labs) overnight at 4°C. Beads were washed 3X in TBS and boiled in 1X LDS sample buffer with 2-Mercaptoethanol (1:100) for 5 minutes. Samples were run on a 4-15% gradient polyacrylamide gel at 100V for 75 minutes and then transferred to a PVDF membrane (100V for 100 minutes). For immunoblotting, membranes were blocked in 5% milk TBST and then incubated overnight at 4°C in 5% milk TBST containing primary antibody. Antibodies used: α-Dystroglycan (IIH6C4) (Millipore cat. no. 05-593, RRID: AB_309828,

mouse IgM, 1:500), MANDAG2 (DSHB cat. no. 7D11, RRID: AB_2211772, mouse IgG1, 1:500), β3-tubulin (Cell Signaling Technology cat. no. 5568, RRID: AB_10694505, rabbit, 1:2000). Membranes were washed 3X in TBST and incubated on fluorescent IRDye secondary antibody (1:10,000, LI-COR) in 5% milk TBST for 1 hour at room temperature. Membranes were imaged using a LI-COR Odyssey CLx 0918 imager and signal analyzed using LI-COR Image Studio Lite version 5.2.

Electrophysiology

For acute slice preparation, mice were deeply anesthetized in 4% isoflurane and subsequently injected with a lethal dose of 2% 2, 2, 2-Tribromoethanol in sterile water followed by transcardial perfusion with 10 mL ice cold cutting solution containing the following (in mM): 93 NMDG, 2.5 KCl, 1.2 NaH_2PO_4, 30 $NaHCO_3$, 20 HEPES, 24 glucose, 5 Na Ascorbate, 2 Thiourea, 3 Na Pyruvate, 13 N-Acetyl Cysteine, 1 Kynurenic acid, 10 $MgSO_4$, 0.5 $CaCl_2$; pH 7.3, 300-340mmol/kg. After rapid decapitation, the brain was briefly submerged in ice cold cut solution bubbled with carbogen (95% oxygen, 5% CO2) and then sectioned into 300μm sagittal sections (Leica VT1200S vibratome) in bubbled ice-cold cut solution. Slices were recovered in 37°C cut solution, bubbled, for 15 minutes followed by 1 hour in room temperature recording ACSF (containing, in mM: 125 NaCl, 25 $NaHCO_3$, 1.25 NaH_2PO_4, 3 KCl, 25 D-Glucose, 2 $CaCl_2$, 1 $MgCl_2$) with an osmolarity of 310-320mmol/kg and supplemented with 1.5mM Na Ascorbate, bubbled.

CA1 pyramidal cells were patched in whole cell configuration using 3-5MΩ borosilicate glass pipettes filled with high chloride internal solution containing the following (in mM): 125 CsCl, 2.5 $MgCl_2$, 0.5 EGTA, 10 HEPES, 2 Mg-ATP, 0.3 Na-GTP, 5 QX-314; pH 7.2, 300mmol/kg. Pipettes were wrapped in parafilm to reduce capacitive currents. Cells were voltage clamped at -70mV and continuously superfused with 2-3 mL/min bubbled recording ACSF (310-320mmol/kg) containing 10μM NBQX to block

excitatory transmission. Recordings were performed at 34°C. After 5 minutes of spontaneous IPSC (sIPSC) recording, 10μM Carbachol was added to the perfusate and another 5 minutes of sIPSC were recorded. Slices were discarded after exposure to Carbachol. Signals were amplified with an AxoPatch 200B amplifier (Molecular Devices), low-pass filtered at 5 kHz, and digitized and sampled at 10 kHz with a NIDAQ analog-to-digital board (National Instruments). Data were acquired and analyzed using a custom script in Igor Pro 8 (Wavemetrics) (Jahncke, 2023). A hyperpolarizing step of -10mV was applied before each sweep to monitor input resistance, series resistance, and measure cell capacitance. Series resistance was not compensated and was maintained below 20MΩ. Cells were excluded if series resistance changed by more than 25%.

To calculate the proportion of cells that responded to Carbachol, cells were sorted into “responsive” and “non-responsive” categories. Cells were categorized as responsive if sIPSC frequency increased by 20% or more with the addition of Carbachol. If sIPSC frequency in a cell changed by less than 20% or less than 0.5Hz it was deemed non-responsive.

Flurothyl Seizure Induction

Mice aged P40-P55 were used for the flurothyl-induced seizure susceptibility assay to determine seizure threshold. Briefly, mice were placed in an enclosed glass chamber equipped with a vaporization chamber out of reach of the mouse. Volatile liquid 10% Bis (2,2,2-Trifluorotheyl) Ether (Millipore Sigma cat. no 287571) in 95% EtOH was delivered to the vaporization chamber at a rate of 6 mL/hour. Seizure latency was determined as the amount of time until generalized tonic-clonic seizure (TCS). Upon exhibiting TCS, animals were immediately removed from the chamber and returned to their home cage, whereupon seizures ceased rapidly. Sample size was determined using power analysis as described below. The *Emx1^{Cre};Dag1* experimental groups were powered sufficiently

to determine sex differences. Because no sex difference was found (**Supplementary Figure 2.13 C**), sexes were pooled for the remaining experiments. For statistical tests, outliers were excluded. Outliers were calculated as follows: first, the interquartile range (IQR) was calculated and multiplied by 1.5. This 1.5*IQR value was subtracted from the 25% quartile (Q1) and added to the 75% quartile (Q3). Points outside of the range Q1 - 1.5*IQR < x < Q3 + 1.5*IQR were categorized as outliers and indicated as such on all graphs. This was done to remove bias from extreme outliers observed in this experiment.

Whole Mount Immunohistochemistry

Embryonic day (E) 12.5 embryos were delivered by cesarian section at after mild CO_2-induced anesthesia and rapid cervical dislocation. After removal from the uterus and amniotic sac, a small portion of tail was removed for genotyping and the embryo was drop fixed in 4% PFA overnight at 4°C and then washed in PBS twice for 10 minutes each. Embryos were then dehydrated in a methanol series at room temperature (50% for 1 hour, 80% for 2 hours, 100% overnight) and then bleached overnight in 3% H_2O_2, 70% methanol, 20% DMSO. Embryos were washed in TNT pH 7.8 (10mM Tris, 150mM NaCl, 1% Triton X-100) 5 times for 45 minutes each and moved into primary antibody solution (4% Nonfat powdered milk, 2% Goat serum, 5% DMSO, 2% Sodium Azide in TNT) with 1:500 rabbit anti-β3-tubulin (Cell Signaling Technology cat. no. 5568, RRID: AB_10694505) for 2-3 days at room temperature. Embryos were washed in TNT 5 times for 45 minutes each and moved into secondary antibody solution (4% BSA, 2% Goat serum, 5% DMSO, 2% Sodium Azide in TNT) with goat anti-rabbit Alexa Fluor 546 (Thermo Fisher Scientific, Cat. No. A-11035) for 2-3 days at room temperature. Embryos were washed in TBS overnight and dehydrated through the same methanol series as

previously before clearing in BABB (1:2 Benzyl alcohol:Benzyl benzoate). Samples were stored in BABB until imaging on a fluorescent dissecting scope.

Statistical analysis

Phenotypic analyses were conducted using tissue collected from at least three mice per genotype from at least two independent litters. Samples from each mouse were only used for one technical replicate. Power analysis using pilot data was used to determine samples sizes with $\alpha = 0.05$ and $\beta = 0.80$. Phenotypes were indistinguishable between male and female mice and were analyzed together. Although experimenters were blind to genotype during analysis, in many cases highly penetrant phenotypes revealed the genotypes of the mice and no blinding could be faithfully performed. Unless otherwise stated, no data was excluded from analysis. For comparisons between two groups, significance was determined using a two-tailed Students t-test. For comparisons between more than two groups, significance was determined using a 2-way ANOVA with Tukey HSD post-hoc analysis. Statistical significance was set at $\alpha = 0.05$ ($p < 0.05$) and data presented as means ± SEM. Statistical analyses and data visualization were performed in R (version 4.0.2).

Supplementary Figures

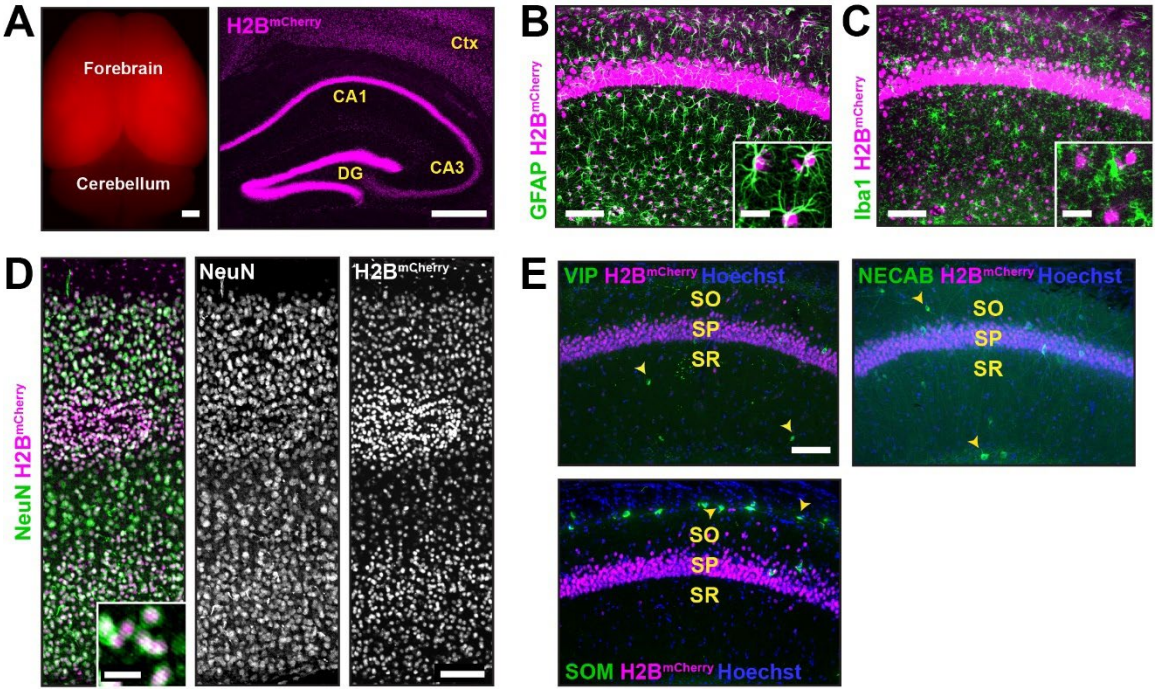

Supplementary Figure 2.1 *Emx1*^{Cre} drives recombination in forebrain excitatory neurons and astrocytes, but not interneurons or microglia.

(A) Left; endogenous red fluorescence in the forebrain of P60 *Emx1*^{Cre};*R26*$^{LSL\text{-}H2B\text{-}mCherry}$ reporter mice (scale bar = 1mm). Right; coronal section of the forebrain from *Emx1*^{Cre};*R26*$^{LSL\text{-}H2B\text{-}mCherry}$ mice showing robust nuclear mCherry signal (magenta) in the cortex and hippocampus (scale bar = 500μm). **(B-E)** mCherry^{+} nuclei shown with markers of multiple cell types in the brain including astrocytes (GFAP, green) **(B)**, microglia (Iba1, green) **(C)**, and neurons (NeuN, green) **(D)** (scale bar = 100μm). Insets show enlarged images of mCherry^{+} nuclei with cell type markers (scale bar = 20μm). **(E)** mCherry^{+} nuclei with markers for different interneuron subtype markers (yellow arrowheads) (scale bar = 100μm) (VIP = Vasoactive intestinal peptide, NECAB = Neuronal calcium-binding protein 1, SOM = Somatostatin). *CA1 layers: SO, stratum oriens; SP, stratum pyramidale; SR, stratum radiatum.*

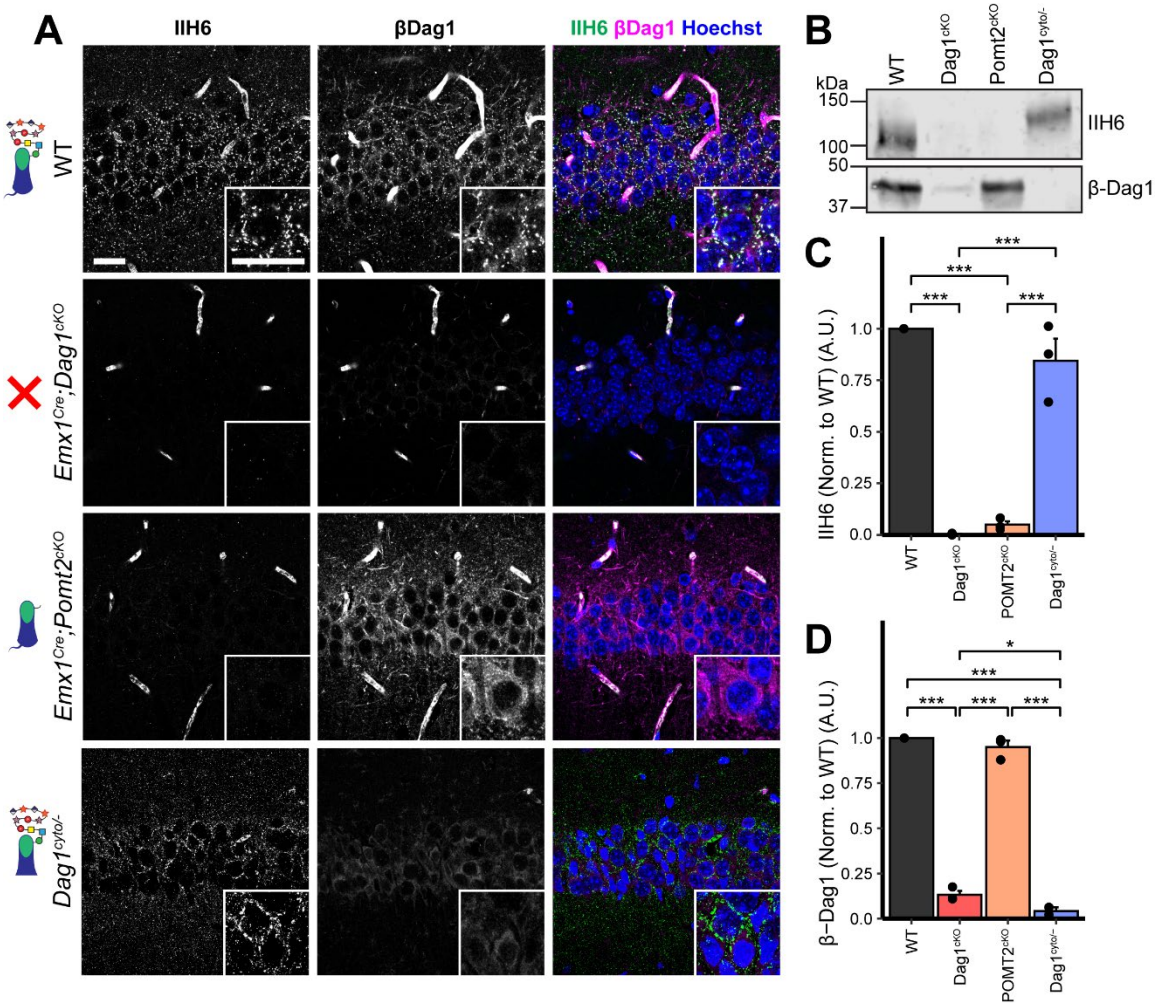

Supplementary Figure 2.2 Dystroglycan glycosylation is required for synaptic localization.

(A) Immunostaining for matriglycan (IIH6, green) and β-Dag1 (magenta) in CA1 pyramidal cells of WT controls, *Emx1*^{Cre}*;Dag1*^{cKOs}, *Emx1*^{Cre}*;Pomt2*^{cKOs}, and *Dag1*$^{cyto/-}$ mutants. Scale bars = 25μm. **(B)** WGA-enriched lysates from P21-P30 hippocampus were immunoblotted for IIH6 and β-Dag1. **(C-D)** Quantification of immunoblot in **(B)**. Error bars show mean + SEM.

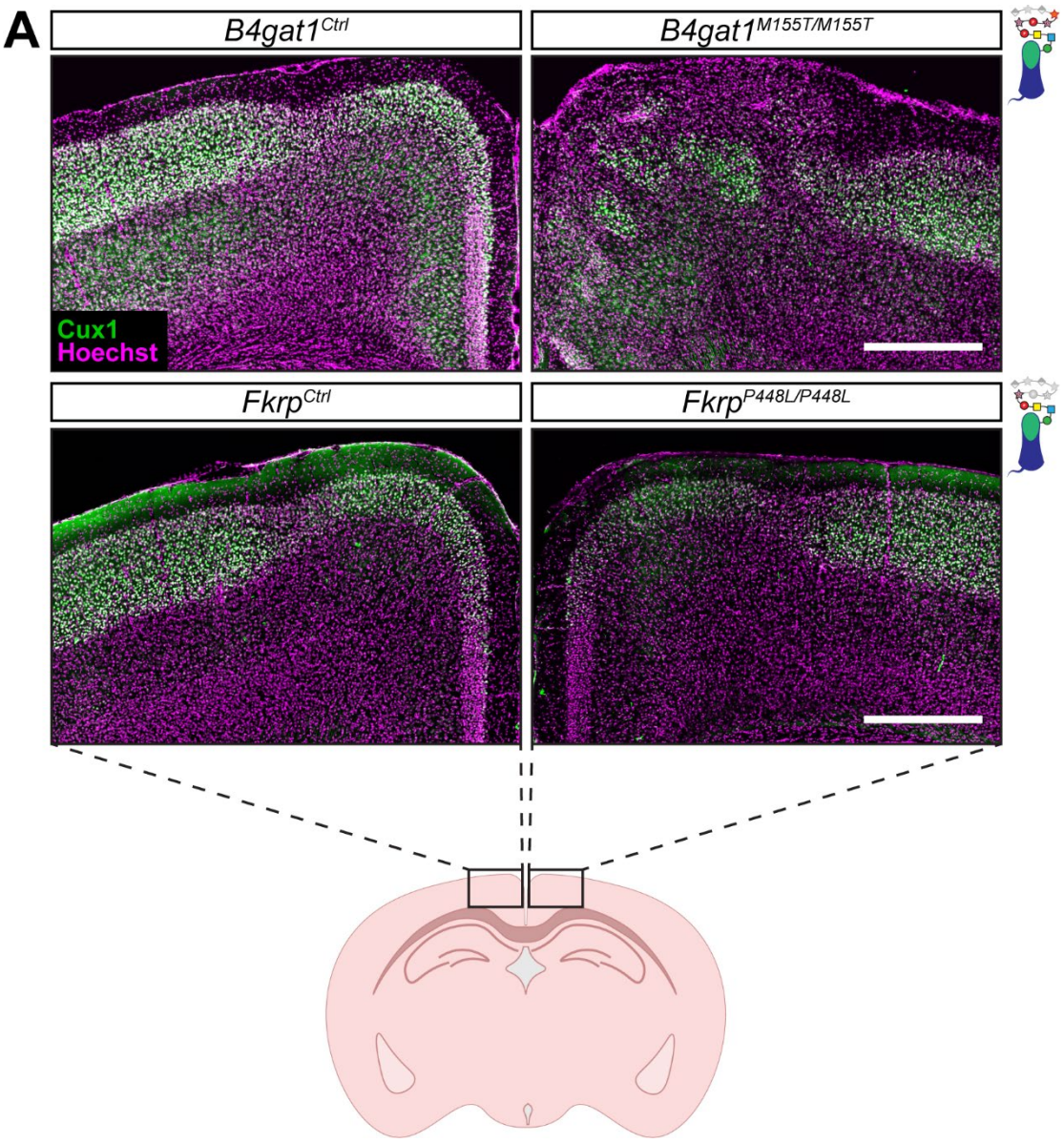

Supplementary Figure 2.3 Cortical migration is disrupted at midline of *B4gat1*$^{M155T/M155T}$ but not *Fkrp*$^{P448L/P448L}$ mutants.

(A) Immunostaining for cortical layer marker Cux1 (layers 2-4) in P30 somatosensory cortex (scale bar = 500μm). Cux1 is shown in green. Nuclear marker Hoechst is shown in magenta. Cortical migration is normal in both *B4gat1* and *Fkrp* point mutants except at midline, where the *B4gat1* mutants show a migration phenotype not seen in the *Fkrp* point mutants. This phenotype was observed with 100% penetrance in the *B4gat1* mutants and 0% in the *Fkrp* mutants.

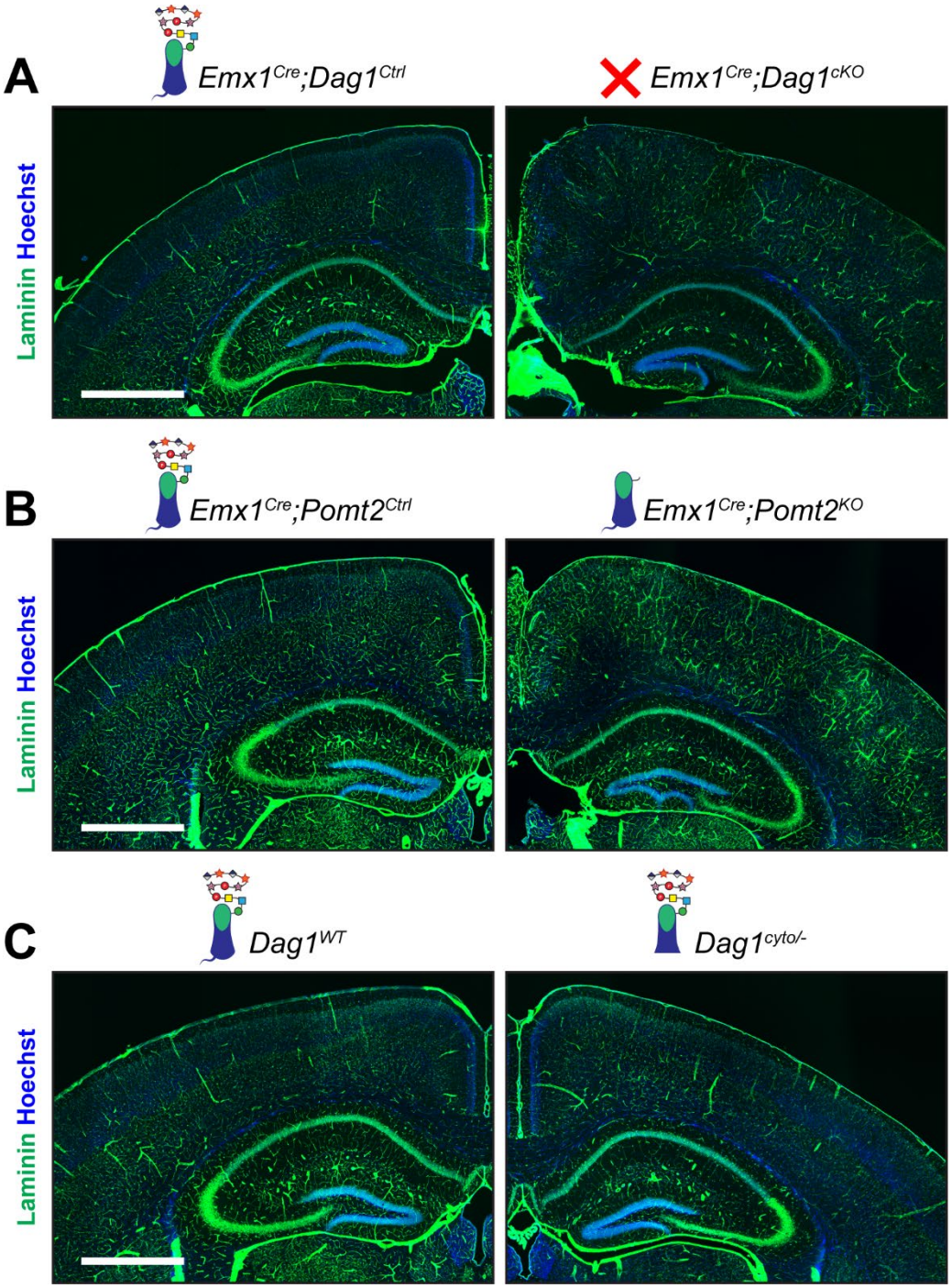

Supplementary Figure 2.4 Laminin immunoreactivity in adult neocortex appears discontinuous in *Dag1* mutants.

(A-C) Immunostaining for ECM protein Laminin (green). Nuclear marker Hoechst is shown in blue. Scale bar = 1000μm.

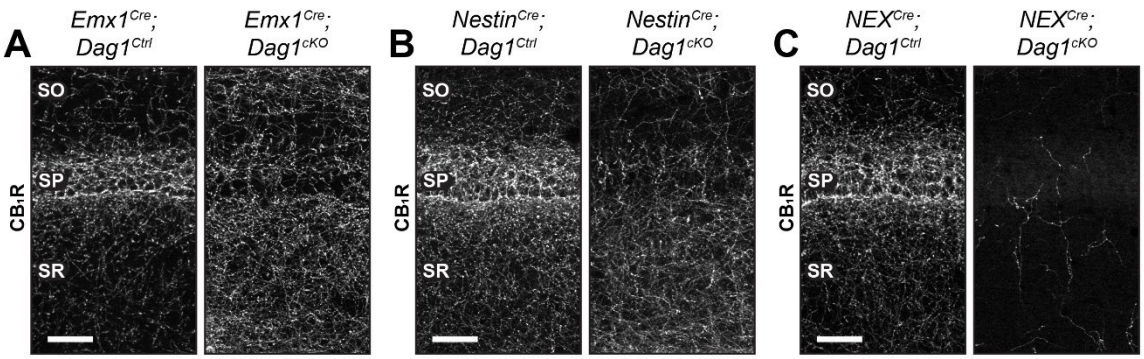

Supplementary Figure 2.5 CCK^+/CB_1R^+ IN axon targeting phenotypes in hippocampal CA1 of various *$Dag1^{cKOs}$*.

CB_1R immunostaining in hippocampal CA1 of control mice (left panels) and *$Dag1^{cKOs}$* (right panels) generated using *$Emx1^{Cre}$* (forebrain progenitors, E10.5) **(A)**, *$Nestin^{Cre}$* (neural stem cells in the central and peripheral nervous systems, E11.5) **(B)**, and *NEX^{Cre}* (forebrain postmitotic excitatory neurons, E12.5) **(C)**. Scale bar = 50μm. *Abbreviations: SO, stratum oriens; SP, stratum pyramidale; SR, stratum radiatum.*

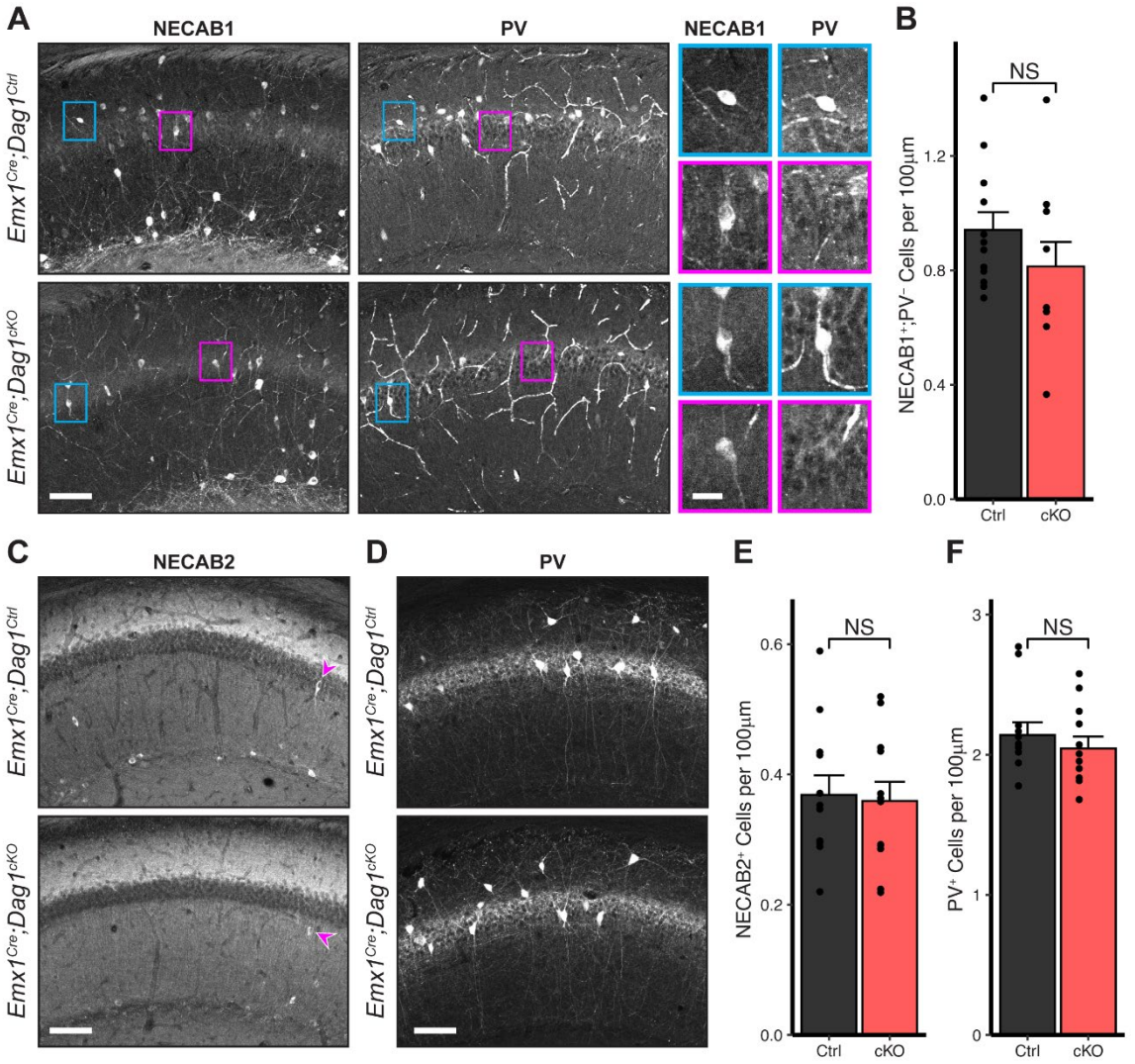

Supplementary Figure 2.6 CCK$^+$/CB$_1$R$^+$ IN cell numbers are unchanged in *Emx1^{Cre};Dag1^{cKOs}*.

(A) Immunostaining in hippocampal CA1 for NECAB1 (left) and PV (right) in *Emx1^{Cre};Dag1^{Ctrl}* and *Emx1^{Cre};Dag1^{cKO}* mice. NECAB1 labeling is evident in PV$^+$ cells (example shown in blue inset) and in an additional PV$^-$ population that contains the CCK$^+$/CB$_1$R$^+$ population (example shown in magenta inset). The average number of NECAB1$^+$;PV$^-$ cells per 100µm of SP is quantified in **(B)**. Immunostaining for NECAB2 **(C)** and PV **(D)** with cell number quantification in **(E)** and **(F)**. Scale bar = 100µm. Error bars show mean + SEM. Significance: * = $p < 0.05$, ** = $p < 0.01$, *** = $p < 0.001$, NS = $p \geq 0.05$. *Abbreviations: SP, stratum pyramidale; PV, Parvalbumin.*

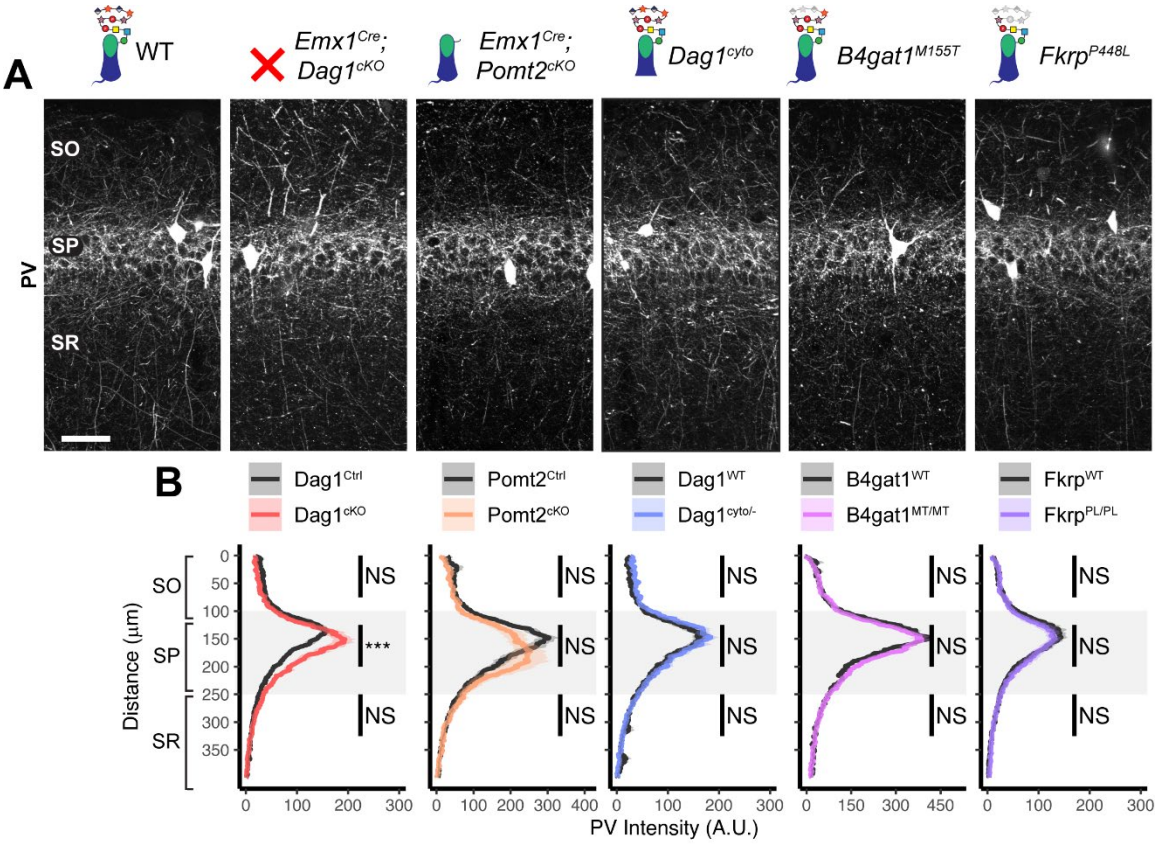

Supplementary Figure 2.7 Parvalbumin⁺ basket INs do not require *Dag1* for proper axon targeting in hippocampal CA1.

(A) Parvalbumin (PV) immunostaining in P30 hippocampal CA1 shows that PV⁺ basket interneurons exhibit normal distribution in CA1 for all genetic models except for an increase in PV intensity within *stratum pyramidale* of *Emx1^{Cre};Dag1^{cKOs}* (scale bar = 50µm). **(B)** Quantification of CA1 PV fluorescence intensity profile. Shaded regions of intensity profile illustrate ± SEM. Gray region highlights SP. Significance: * = $p < 0.05$, ** = $p < 0.01$, *** = $p < 0.001$, NS = $p \geq 0.05$. *Abbreviations: A.U., arbitrary units; SO, stratum oriens; SP, stratum pyramidale; SR, stratum radiatum.*

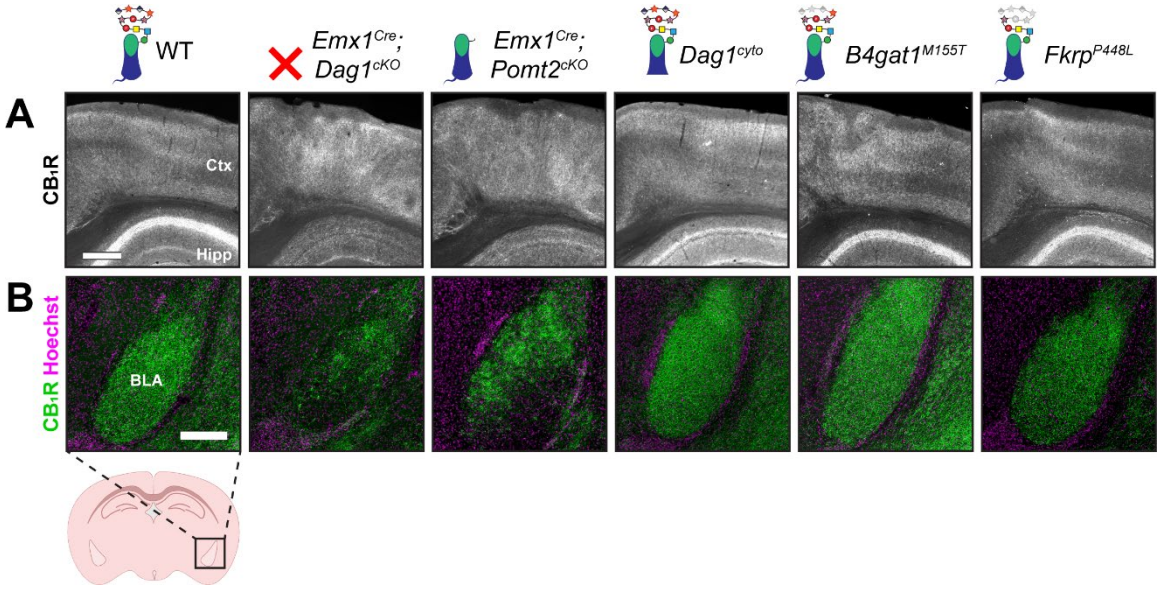

Supplementary Figure 2.8 Altered CB_1R expression in cortex and basolateral amygdala of *Dag1* and *POMT2* mutants.

(A) CB_1R immunostaining in P30 coronal sections showing somatosensory cortex (Ctx) and CA1 of hippocampus (Hipp) (scale bar = 400μm). **(B)** CB_1R immunostaining (green) shown with nuclear marker Hoechst (magenta) in basolateral amygdala (BLA) (scale bar = 250μm).

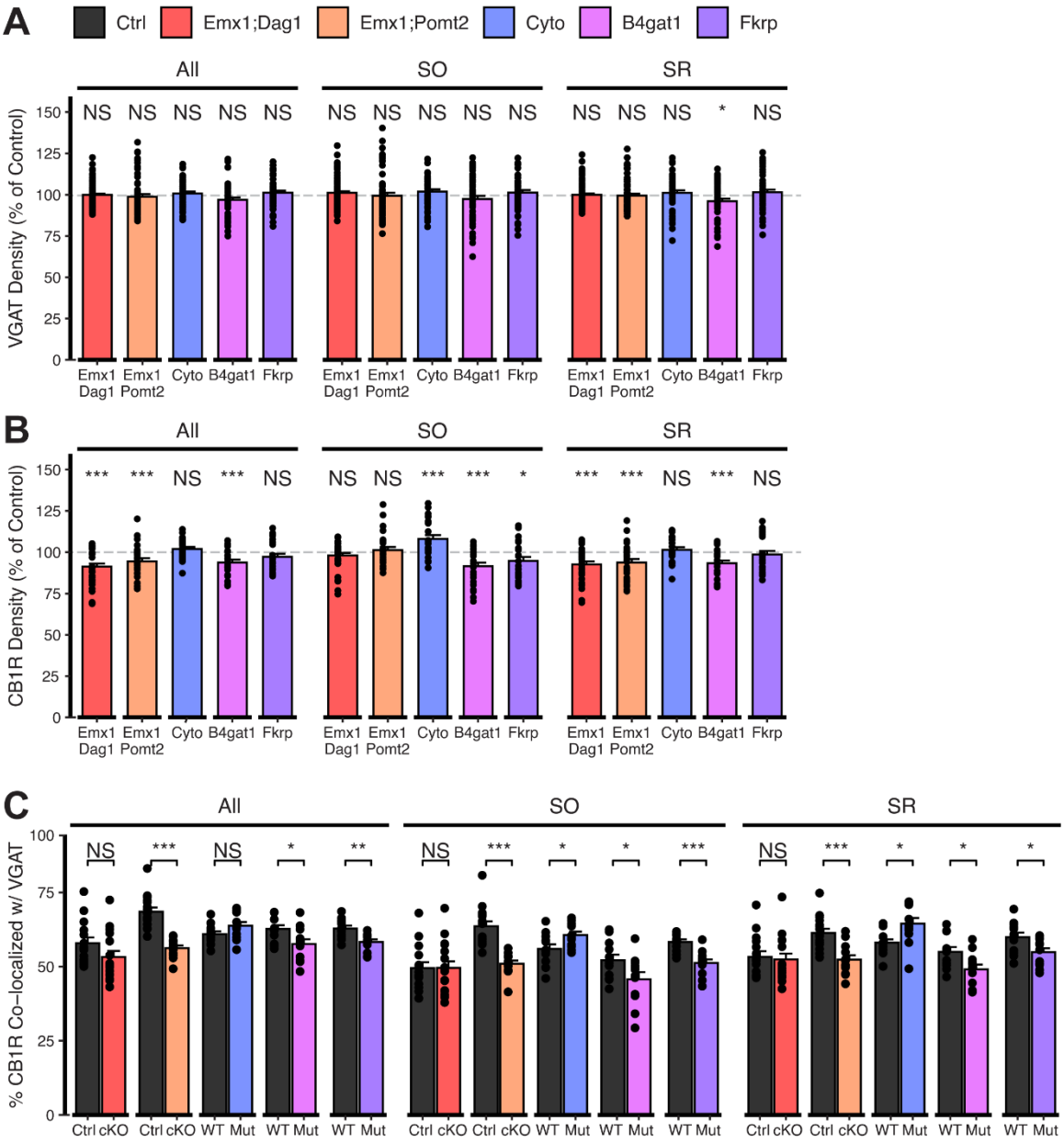

Supplementary Figure 2.9 Extended quantification of images in Figure 2.5 A-C. Quantification within hippocampal CA1 SO and SR regions and all regions pooled together.

(A) Quantification of VGAT puncta density expressed as a percent of control. **(B)** Quantification of CB_1R puncta density expressed as a percent of control. **(C)** Quantification of co-localization between VGAT and CB_1R to estimate putative CB_1R^+ basket cell synapse formation. Error bars show mean + SEM. (To see quantification of puncta densities and co-localization in SP see **Figure 2.5 D-F**.) See Significance: * = $p < 0.05$, ** = $p < 0.01$, *** = $p < 0.001$, NS = $p \geq 0.05$. *Abbreviations: SO, stratum oriens; SP, stratum pyramidale; SR, stratum radiatum.*

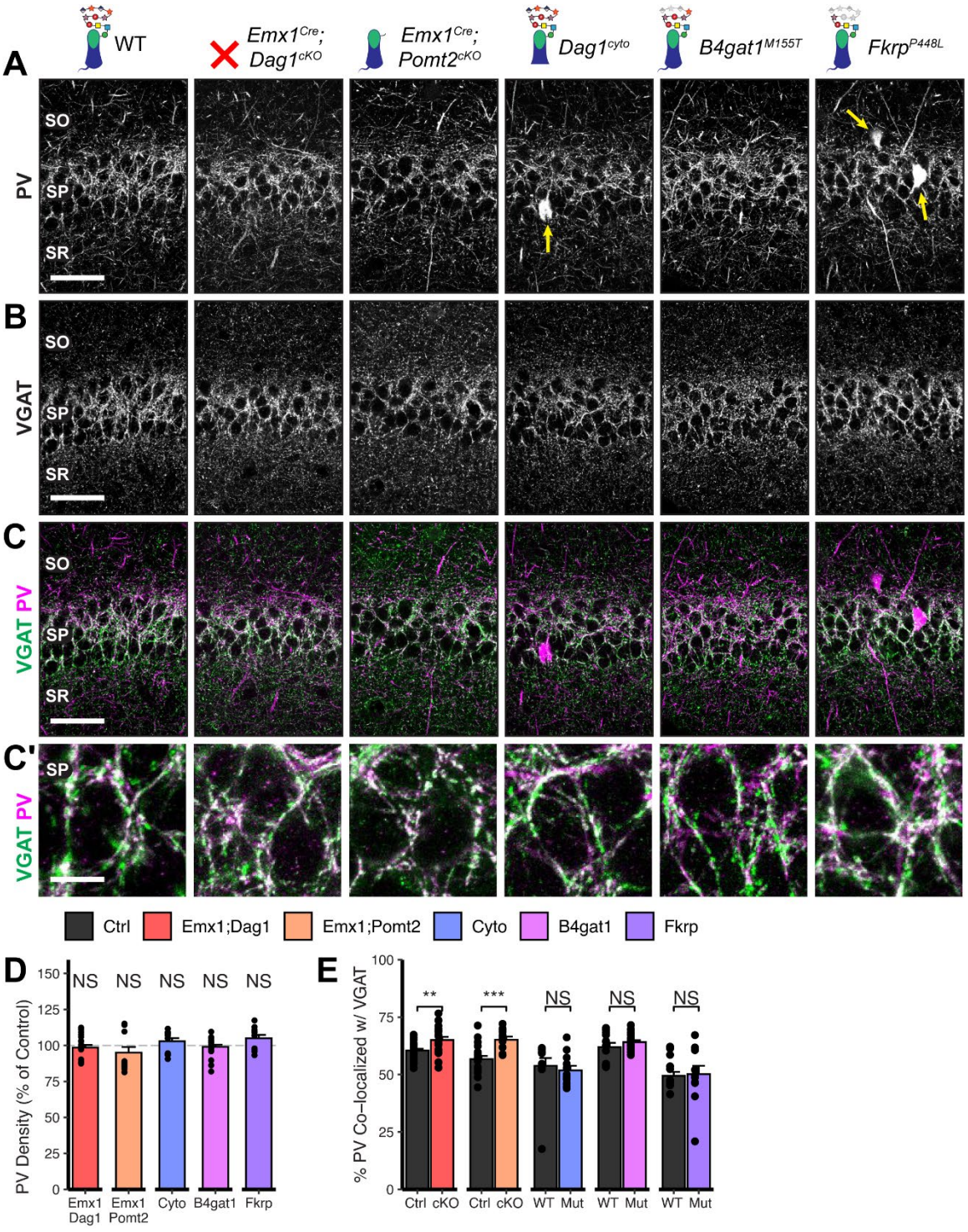

Supplementary Figure 2.10 *Dag1* and *Pomt2* cKOs exhibit increased PV⁺ basket synapse formation in *stratum pyramidale* of hippocampal CA1.

P30 coronal sections immunostained for **(A)** PV and **(B)** VGAT in hippocampal CA1; merged image in **(C)** shows PV in magenta and VGAT in green. Yellow arrows indicate PV⁺ interneuron cell bodies. (A-C) Scale bar = 50μm. (Higher magnification view of SP in **(C')**; scale bar = 10μm.) **(D)** Quantification of PV puncta density in SP expressed as a

percent of control. **(E)** Quantification of co-localization between VGAT and PV in SP to estimate putative PV^+ basket synapse formation. Error bars show mean + SEM. (To see quantification of puncta densities and co-localization in SO and SR see **Supplementary Figure 2.11**.) Significance: * = $p < 0.05$, ** = $p < 0.01$, *** = $p < 0.001$, NS = $p \geq 0.05$. *Abbreviations: PV, Parvalbumin; SO, stratum oriens; SP, stratum pyramidale; SR, stratum radiatum.*

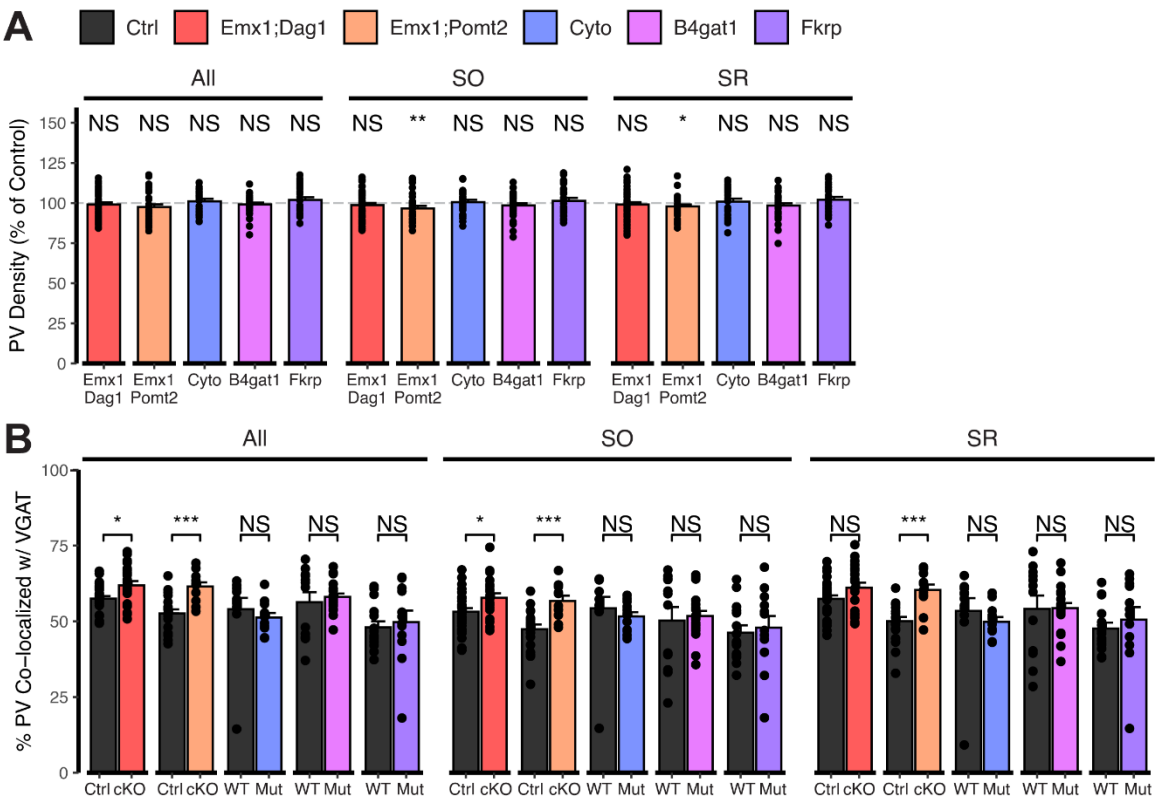

Supplementary Figure 2.11 Extended quantification of images in Supplementary Figure 2.10 A-C.

Quantification within hippocampal CA1 SO and SR regions and all regions pooled together. **(A)** Quantification of PV puncta density expressed as a percent of control. **(B)** Quantification of co-localization between VGAT and PV to estimate putative PV^{+} basket cell synapse formation. Error bars show mean + SEM. (To see quantification of puncta densities and co-localization in SP see **Supplementary Figure 2.10 D-E**.) Significance: * = $p < 0.05$, ** = $p < 0.01$, *** = $p < 0.001$, NS = $p \geq 0.05$. *Abbreviations: PV, Parvalbumin; SO, stratum oriens; SP, stratum pyramidale; SR, stratum radiatum.*

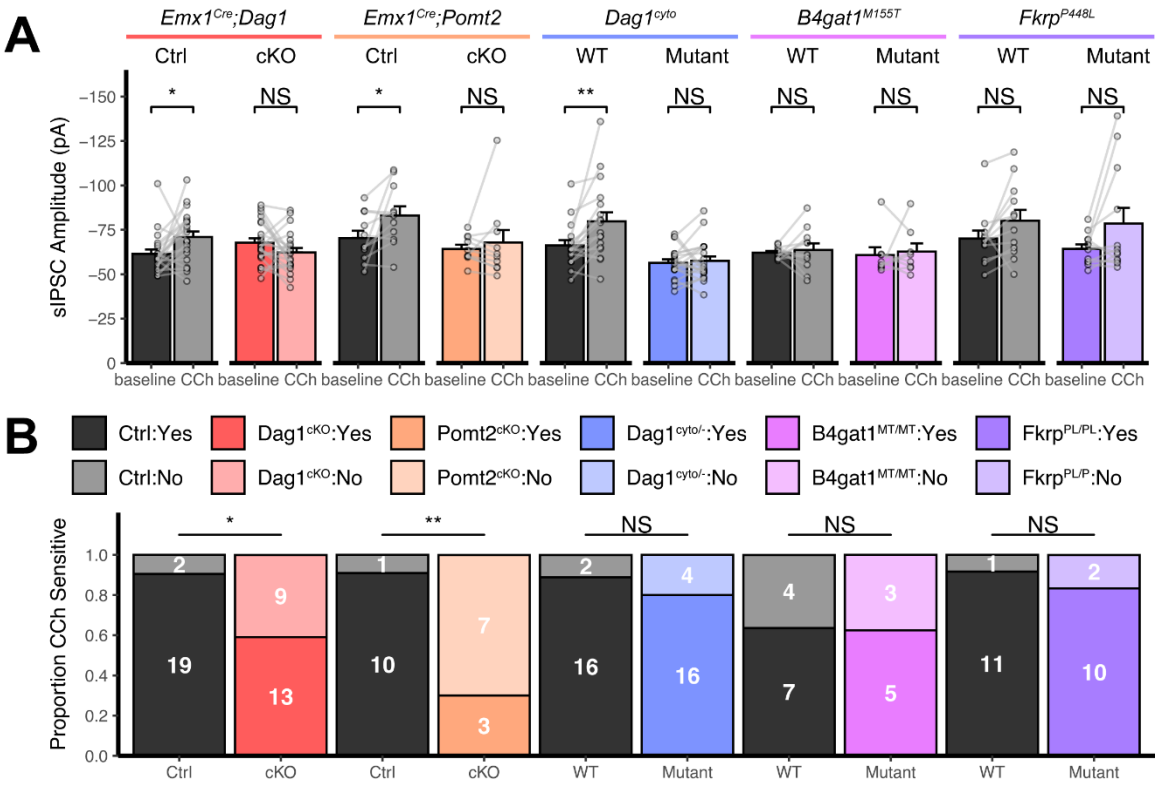

Supplementary Figure 2.12 Additional quantification of sIPSC recordings.

(A) Quantification of average sIPSC amplitude at baseline and after the addition of carbachol. Error bars show mean + SEM. **(B)** Quantification of the proportion of carbachol-sensitive cells within each genotype. Non-responsive cells are shown in lighter color, responsive cells are shown in darker color. Significance: * = $p < 0.05$, ** = $p < 0.01$, *** = $p < 0.001$, NS = $p \geq 0.05$. *Abbreviations: sIPSC, spontaneous inhibitory postsynaptic current; CCh, carbachol.*

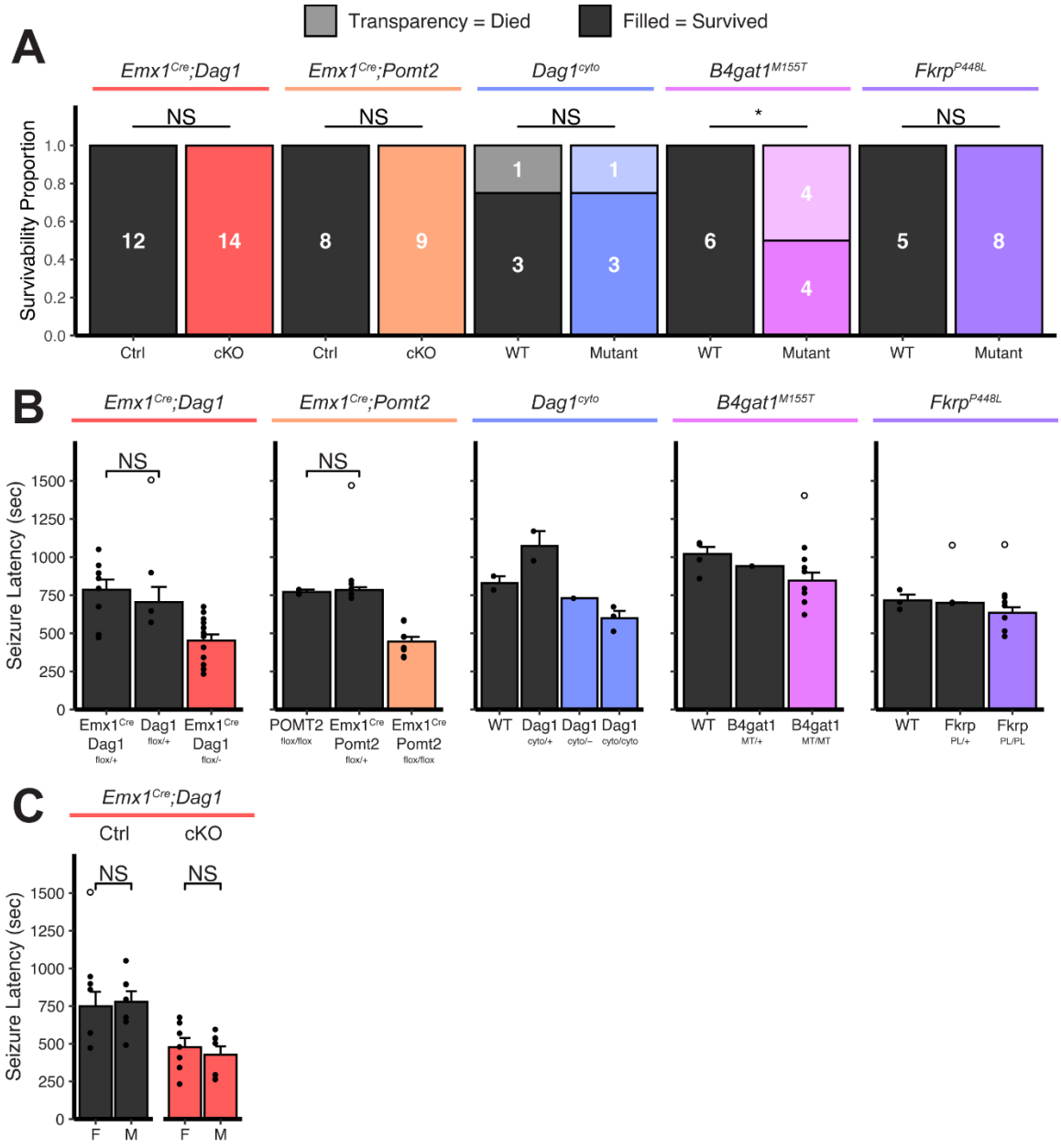

Supplementary Figure 2.13 Extended seizure induction threshold data.

(A) Proportion of mice that died as a direct result of a flurothyl-induced seizure. Survivors are depicted in darker colors, fatalities in lighter colors. **(B)** To minimize the number of animals needed for this experiment, certain genotypes were pooled together. Here we show that pooled genotypes are not different. Statistical tests were run where Ns were sufficient to provide meaningful comparison. **(C)** Seizure latencies split by sex. Note: only the *Emx1^{Cre};Dag1* group is powered sufficiently to statistically compare sexes. Open points denote statistical outliers. Error bars show mean + SEM.

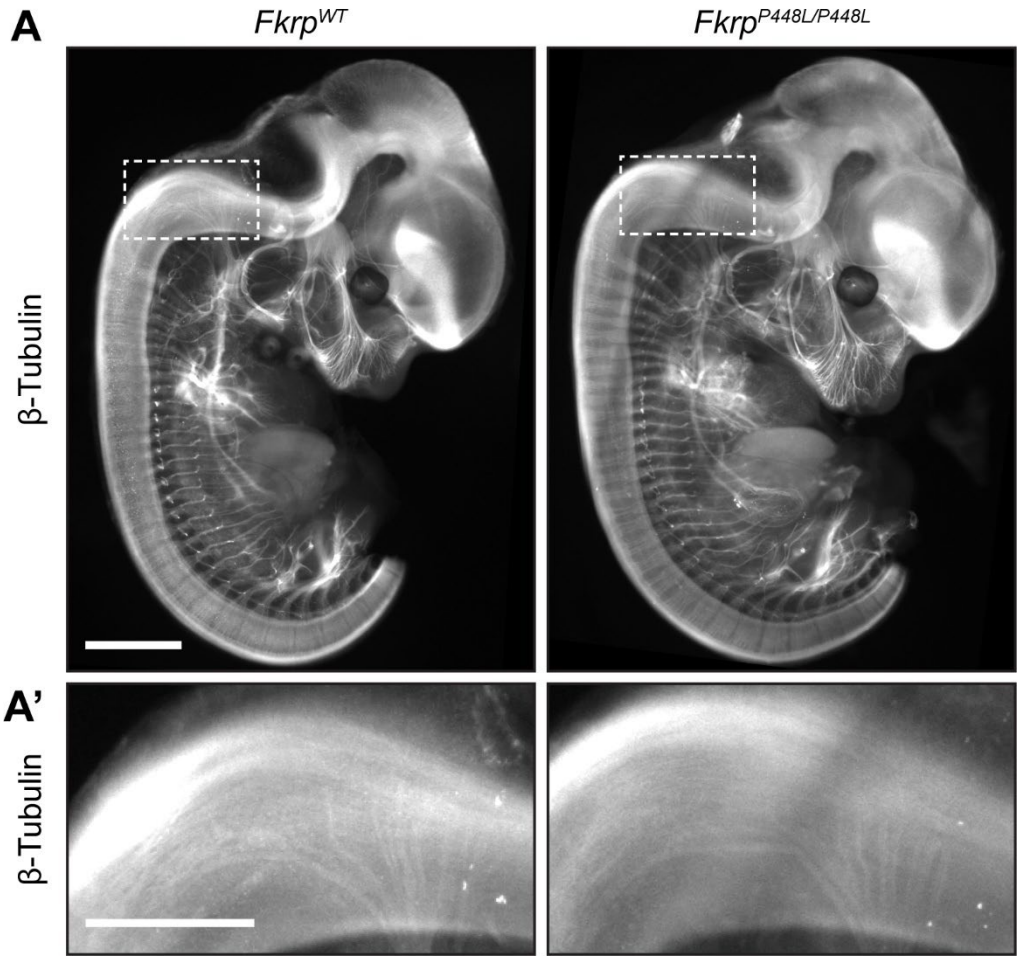

Supplementary Figure 2.14 Hindbrain axon targeting is normal in *Fkrp*$^{PL/PL}$ mutants.

(A) Whole mount immunohistochemical labeling of neuronal populations (β-Tubulin) in embryonic (E) 12.5 *Fkrp*^{WT} and *Fkrp*$^{PL/PL}$ littermates shows hindbrain axon targeting. Dashed box indicates region shown in **(A')**. Scale bar = 1000μm **(A)**, 500μm **(A')**.

Chapter 3: Tools for *Cre*-mediated conditional deletion of floxed alleles from developing cerebellar Purkinje cells

Jennifer N. Jahncke[1,] and Kevin M. Wright[2]

[1] Neuroscience Graduate Program, Oregon Health & Science University, Portland, OR 97239, USA

[2] Vollum Institute, Oregon Health & Science University, Portland, OR 97239, USA

Abstract

The Cre-lox system has become an indispensable tool in neuroscience research for targeting gene deletions to specific cellular populations. Here we assess the utility of several *Cre* lines and a viral approach for targeting cerebellar Purkinje cells. Using a combination of a fluorescent reporter line (*Ai14*) to indicate *Cre*-mediated recombination and a floxed Dystroglycan line (*Dag1*^{flox}) we show that the timing of reporter expression does not always align precisely with loss of protein. The commonly used *Pcp2*^{Cre} line exhibits a gradual mosaic pattern of *Cre* recombination in Purkinje cells from P7-P14, while loss of Dag1 protein is not complete until P30. *Ptf1a*^{Cre} drives recombination in precursor cells that give rise to GABAergic neurons in the embryonic cerebellum, including Purkinje cells and molecular layer interneurons. However, due to its transient expression, *Ptf1a*^{Cre} results in stochastic loss of Dag1 protein in these neurons. *Nestin*^{Cre}, which is often used as a "pan-neuronal" *Cre* line for the central nervous system does not drive any *Cre* mediated recombination in Purkinje cells. We identify a *Calb1*^{Cre} line that drives efficient and complete recombination in embryonic Purkinje cells, resulting in loss of Dag1 protein before the period of synaptogenesis. AAV8-mediated delivery of *Cre* at P0 results in transduction of Purkinje cells from P10-P18, with loss of Dag1 protein not reaching appreciable levels until P35. These results characterize several tools for targeting conditional deletions in cerebellar Purkinje cells at different development stages and illustrate the importance of validating the loss of protein following recombination.

Introduction

Over the past thirty-five years, researchers have used genetically modified mouse models to define the molecular pathways involved in nervous system development and function. This began with the generation of the first gene knockout mouse lines in 1989 (Joyner et al., 1989; Koller et al., 1989; Navabpour et al., 2020; Schwartzberg et al., 1989; Zijlstra et al., 1989). While the use of knockout mice has led to many fundamental discoveries, the constitutive nature of gene deletion can have inherent limitations. These can include early developmental phenotypes that prevent analysis of a gene's function at later stages, as well as phenotypes that arise from cellular populations other than the ones being directly studied.

Mouse genetic tools have continually evolved, with the development of conditional knockouts in the early-mid 1990s enabling control over when and where a specific gene is manipulated (Gu et al., 1994; Luo et al., 2020; Joe Z Tsien et al., 1996; Joe Z. Tsien et al., 1996). This spatiotemporal control of gene deletion requires two components: (1) a "floxed" allele of the target gene that incorporates 34 base pair *loxP* recognition sites flanking a critical genomic region of the target gene, and (2) a driver line that expresses *Cre* recombinase under the control of regulatory elements that confer cellular and/or temporal specificity. When *Cre* is expressed in the same animal that is homozygous for the floxed allele, *Cre* will drive recombination of the *loxP* sites, deleting the intervening genomic region. Importantly, this deletion only occurs in cells expressing *Cre*, leaving the floxed allele intact in Cre negative cells. For example, one of the original *Cre*-driver lines used the regulatory elements of *CamKIIα* to drive recombination that is restricted to specific excitatory neuron populations beginning in the third postnatal week (Joe Z Tsien et al., 1996). This allowed for the investigation of the role of NMDAR1 (GluN1) in hippocampal plasticity and spatial learning when crossed to a *NMDAR1* floxed line, which is lethal when deleted constitutively (Li et al., 1994; Joe Z. Tsien et al.,

1996). Additional conditional genetics systems similar to Cre-lox have been developed including Flp-FRT (Dymecki & Tomasiewicz, 1998; Park et al., 2011) and Dre-rox (Anastassiadis et al., 2009). All three systems (Cre-lox, Flp-FRT, and Dre-rox) use the same basic mechanism, differing in recombinase (Cre, Flp, Dre) and recognition site (loxP, FRT, rox). Access to additional recombination systems allows for the use of multiple conditional genetic manipulations concurrently and has led to the development of intersectional approaches that require the co-expression of multiple recombinases to affect gene expression, giving rise to increased cellular specificity.

An important consideration when using conditional deletion strategies is the fidelity of the expected recombination and efficiency of deletion. The accuracy of Cre recombination is often validated by crossing the *Cre* line to a *Cre*-dependent reporter line. These reporter lines typically express a fluorescent (*tdTomato*, *EGFP*) or enzymatic (*LacZ*, *Alkaline Phosphatase*) gene from “safe harbor” loci in the genome that are accessible to Cre-mediated recombination. The reporter sequence is preceded by a “lox-stop-lox” (LSL) cassette that prevents constitutive expression in the absence of *Cre*. However, recombination of these cassettes can be highly sensitive to low levels or transient expression of *Cre* and therefore can be an insufficient proxy for the deletion of a target floxed allele (Luo et al., 2020). It is therefore imperative to validate the expected deletion of the target allele directly by assaying mRNA to show loss of the expected transcript in Cre positive cells. However, loss of mRNA may not precisely recapitulate the timing of functional protein loss due to differences in the rate of protein turnover. Therefore, the gold standard for verifying a conditional deletion should involve examining loss of protein.

One particular challenge in using conditional deletion strategies for studying developmental events like synapse formation is identifying lines that express *Cre* early in development in a cell-type specific manner. For example, Parvalbumin (PV) positive

interneurons in the hippocampus provide strong inhibition onto pyramidal neurons in CA1-CA3 (Nörenberg et al., 2010). While these cells are widely studied and commonly targeted by several PV^{Cre} lines (Hippenmeyer et al., 2005; Madisen et al., 2010), *Cre* expression does not initiate in these cells until P10-P12 (Lecea et al., 1995), which is after they begin the process of synaptogenesis around P6 (Doischer et al., 2008). Therefore, the PV^{Cre} line can be used to examine the role of specific genes in synaptic maintenance and/or function, but not initial synapse formation. There are lines that express *Cre* early in development in the cells that ultimately give rise to the hippocampal PV^{+} interneuron population ($Dlx5/6^{Cre}$, $GAD67^{Cre}$, $Nkx2.1^{Cre}$, $Tac1^{Cre}$), but these use regulatory elements from transcription factors that are expressed in multiple interneuron populations, reducing the cell-type specificity of deletion (Potter et al., 2009; Taniguchi et al., 2011).

In this study, we examine the efficiency of several *Cre* lines in driving deletion of the synaptic cell adhesion protein Dystroglycan (Dag1) from cerebellar Purkinje cells. We show that the widely used $Pcp2^{Cre}$ line is insufficient for driving loss of Dag1 before the period of synaptogenesis. We show that $Ptf1a^{Cre}$, which drives recombination of a *tdTomato* reporter allele in all embryonic GABAergic neurons in the cerebellum, results in stochastic loss of Dag1 protein from Purkinje cells. We identify a *Calb1-IRES-Cre-D* ($Calb1^{Cre}$) line that drives specific and robust recombination in Purkinje cells by P0, resulting in loss of Dag1 protein prior to synaptogenesis. Finally, we show that AAV mediated delivery of *Cre* results in gradual transduction of cells with a lag between reporter expression and loss of Dag1 protein on the order of weeks.

Results

$Pcp2^{Cre}$ drives gradual *Cre*-mediated recombination in Purkinje cells

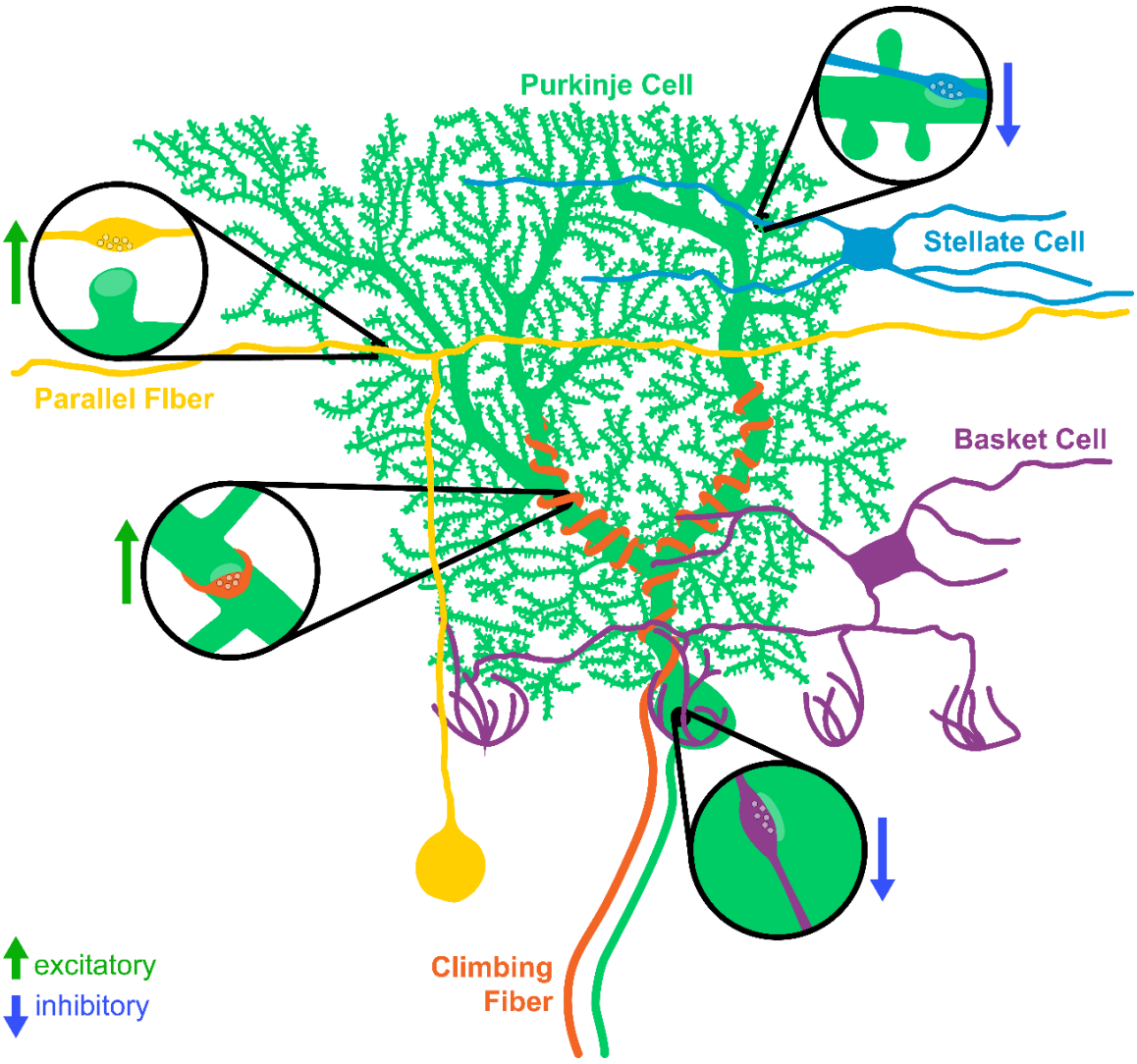

Figure 3.1 Major synaptic inputs onto Purkinje cells in cerebellar cortex.
Purkinje cells (green) receive excitatory inputs from two populations: parallel fibers originating from granule cells (yellow) and climbing fibers originating from the inferior olive (orange). The molecular layer interneurons (basket cells, purple and stellate cells, blue) provide inhibitory input onto Purkinje cells.

The simple, well-defined, and stereotyped circuitry of the cerebellum makes it an ideal model system for studying synapse development and maintenance (**Figure 3.1**). At the center of the circuit are Purkinje cells (PCs), the primary output neurons of the cerebellum which project their axons to the deep cerebellar nuclei (DCN) and the vestibular nuclei in the brainstem. Purkinje cells receive excitatory inputs from two different sources. Parallel fibers originate from cerebellar granule cells, the most

numerous neuron type in the brain, and provide a large number of weak excitatory inputs to the dendrites of Purkinje cells (Itō, 1984; Palay and Chan-Palay, 2012). Climbing fibers originate from excitatory neurons in the inferior olive, and their axons wrap around the primary dendritic branches of Purkinje cells, forming strong excitatory contacts (Itō, 1984; Palay and Chan-Palay, 2012). Purkinje cells initially receive inputs from multiple climbing fibers, which undergo activity-depending pruning during the first 3 weeks of postnatal development until achieving a 1:1 ratio (Bosman et al., 2008; Bosman and Konnerth, 2009; Crepel et al., 1976). These inputs represent one of the best-studied examples of synaptic competition in the central nervous system (CNS). Purkinje cells receive the majority of their inhibitory inputs from two types of Molecular Layer Interneurons (MLIs): Basket Cells (BCs) and Stellate Cells (SCs) (Itō, 1984; Palay and Chan-Palay, 2012). BCs form inhibitory contacts on the soma and proximal dendrites of Purkinje cells, whereas SCs innervate the distal dendrites. Each BC/SC contacts multiple Purkinje cells in the same plane. There are also recurrent inhibitory connections between Purkinje cells (Altman, 1972; Bernard and Axelrad, 1993; Witter et al., 2016).

Purkinje cells in the mouse are born between embryonic days 11-13 and elaborate their dendrites over the first four postnatal weeks (Altman, 1972; Miale and Sidman, 1961; Yuasa et al., 1991). They begin to receive excitatory and inhibitory inputs after the first postnatal week and the development of the circuit is largely complete by postnatal day 28 (P28) (Altman, 1972; Kapfhammer, 2004). The most commonly used *Cre* lines for targeting Purkinje cells are the $Pcp2^{Cre}$ (Zhang et al., 2004) and $L7^{Cre}$ (Barski et al., 2000) lines. *Pcp2* (previously referred to as *L7*), or *Purkinje cell protein 2*, is exclusively expressed by Purkinje cells in the brain, making the *Pcp2* promoter a logical driver for Purkinje cell *Cre* expression. Both the $Pcp2^{Cre}$ and $L7^{Cre}$ transgenic lines generated with similar bacterial artificial chromosome (BAC) constructs (Barski et al., 2000; Lewis et al., 2004; Zhang et al., 2004). One key limitation of these lines is that

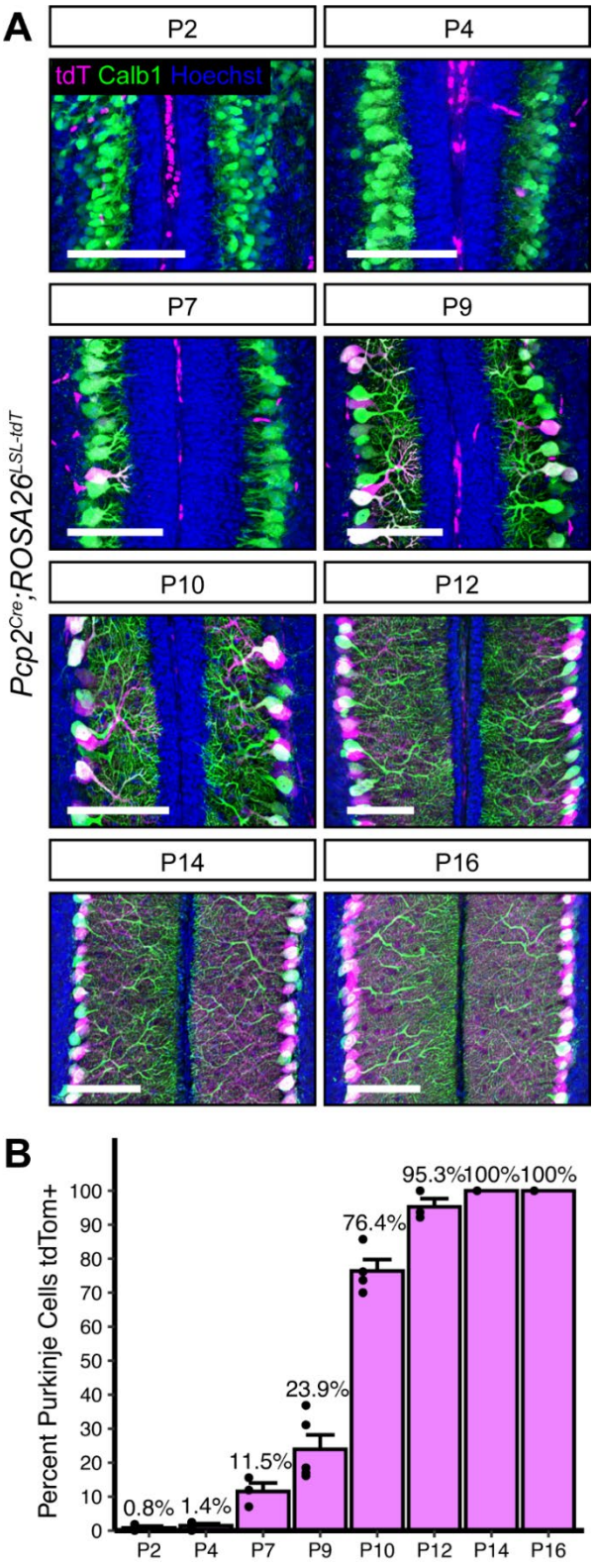

Figure 3.2 *Pcp2*^{Cre} drives *Cre* recombination gradually in the second postnatal week.

(A) *Pcp2*^{Cre} was crossed to a tdTomato reporter to observe the time course of *Cre* recombination. Cerebella were analyzed at time points from P2-P16. *Cre* recombined cells are labeled with tdTomato (magenta). Purkinje cells are visualized with Calbindin immunostaining (green). Nuclei (blue) are most evident in granule cells. Scale bars = 100μm. **(B)** The percent of all Purkinje cells that were tdTomato positive was quantified at each time point.

they turn on gradually during the period of Purkinje cell development. To rigorously and precisely define the period of *Cre*-mediated recombination in Purkinje cells, we analyzed cerebellar lobule 5/6 from *Pcp2^{Cre};Ai14* brains, which carry a *Cre*-dependent tdTomato reporter knocked in to the *ROSA26* locus (hereafter referred to as *Pcp2^{Cre};ROSA26$^{LSL\text{-}tdTomato}$*). The first tdTomato^{+} Purkinje cells were visible at P7 (11.5% of all Purkinje cells), and this increased to 23.9% positive at P9. There was an appreciable increase at P10, with 76.4% of Purkinje cells labeled by tdTomato, and recombination of *tdTomato* was complete by P14 (**Figure 3.2 A, B**). As previously reported, this line shows high specificity for Purkinje cells, as we saw no other tdTomato^{+} neuron types in the cerebellum.

A key consideration when using *Cre* lines is the timing of protein loss following deletion of floxed alleles. The presence of fluorescent reporters like tdTomato are frequently used as a proxy for *Cre*-mediated recombination, particularly in situations where antibodies for the targeted proteins are lacking. However, this does not account for the timing of mRNA and protein turnover following deletion of the targeted allele, which can vary widely. This is exemplified by Dystroglycan (Dag1), a cell adhesion molecule present postsynaptically at PC:MLI synapses. Dag1 is a stable protein, with a half-life of ~25 days in skeletal muscle (Novak et al., 2021). Recent work has shown that Dag1 is required for PC:MLI synapse maintenance (Briatore et al., 2020). However, this study was unable to examine its role in synapse formation due to the gradual recombination driven by the *L7^{Cre}* line.

Although *Pcp2^{Cre}* recombines with similar timing to *L7^{Cre}*, because of the increased specificity for Purkinje cells in the *Pcp2^{Cre}* line we chose to examine whether deleting *Dag1* with *Pcp2^{Cre}* could be used to resolve Dag1 function in PC:MLI synapse development (Barski et al., 2000; Zhang et al., 2004). We examined *Pcp2^{Cre};Dag1$^{flox/-}$* mice (hereafter referred to as *Pcp2^{Cre};Dag1^{cKO}*), to see whether starting with one allele of

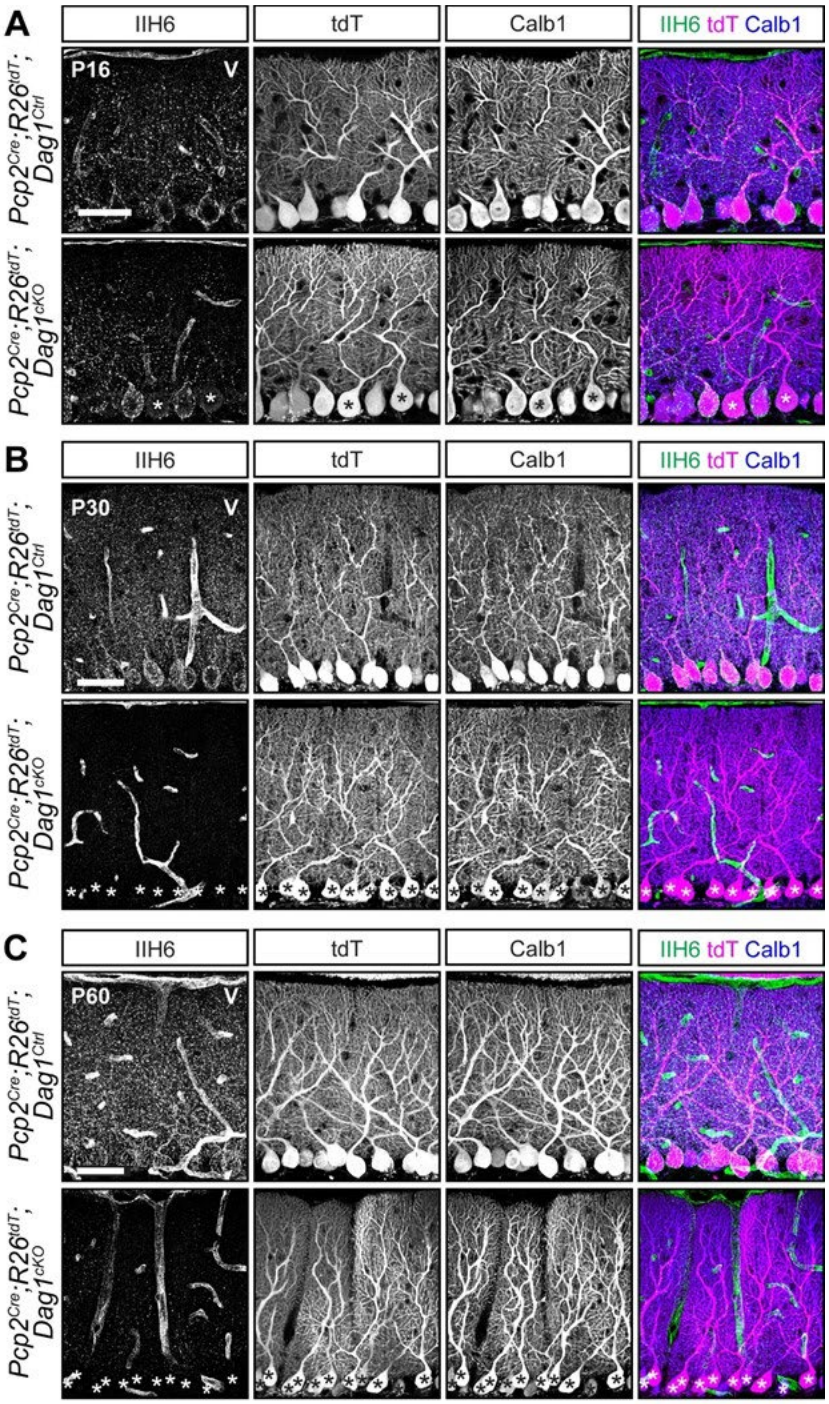

Figure 3.3 Dystroglycan protein loss lags behind *Pcp2^{Cre}* recombination of fluorescent tdTomato reporter.

(A-C) Lobule V Purkinje cells of *Pcp2^{Cre};ROSA26$^{LSL\text{-}tdTomato}$;Dag1^{cKOs}* and littermate controls immunostained for α-Dystroglycan (IIH6, green) to visualize Dag1 protein and Calbindin (Calb1, blue) to label Purkinje cells. *Cre* recombination was assessed by native fluorescence of the tdTomato reporter (tdT, magenta). Expression was evaluated at **(A)** P16, **(B)** P30, and **(C)** P60. Asterisks denote Purkinje cells with no detectable IIH6 signal. Scale bars = 50μm.

Dag1 already deleted would result in more rapid protein loss. We started by examining P16, a timepoint at which all Purkinje cells are tdTomato positive in *Pcp2*^{Cre} mice (**Figure 3.2**). However, punctate Dag1 staining consistent with its synaptic localization was still evident in the majority of *Pcp2*^{Cre}*;Dag1*^{cKO} Purkinje cells at this timepoint (**Figure 3.3 A**). Analysis at P30, a period after developmental synaptogenesis is complete, showed a loss of Dag1 protein in *Pcp2*^{Cre}*;Dag1*^{cKO} Purkinje cells by immunohistochemistry, which appeared identical at P60 (**Figure 3.3 B**). The incomplete loss of Dag1 protein in *Pcp2*^{Cre}*;Dag1*^{cKO} Purkinje cells at P16 highlights a limitation of using a *Cre* line that turns on after gene expression initiates when the protein is particularly stable, as many synaptic molecules are.

Widespread *Nestin*^{Cre} recombination does not extend to Purkinje cells

We sought to identify a *Cre* line that would express in Purkinje cells prior to synaptogenesis. We first examined *Nestin*^{Cre}, which has widespread expression in the CNS beginning at E10.5 (Graus-Porta et al., 2001; Tronche et al., 1999). Examination of brains from *Nestin*^{Cre}*;ROSA26*$^{LSL\text{-}tdTomato}$ mice at P8 showed extensive recombination in the forebrain, but minimal recombination in the cerebellum (**Figure 3.4 A**). Higher magnification images confirmed that there was no recombination in Purkinje cells, MLIs, or cerebellar granule neurons at P8 (**Figure 3.4 B**). Consistent with previous reports, there are mild perturbations in cerebellar granule neuron migration in *Nestin*^{Cre}*;Dag1*^{cKO} mice due to Dystroglycan's function Bergmann glia (**Figure 3.4 C**) (Nguyen et al., 2014). It important to note the particular *Nestin*^{Cre} line that we used, B6.Cg-Tg(Nes-cre)1Kln/J (Tronche et al., 1999, RRID: IMSR_JAX:003771), as there are a number of different *Nestin*^{Cre} lines that have been generated, some of which have been used to delete genes from Purkinje cells with success (Sun et al., 2014; Takeo et al., 2021).

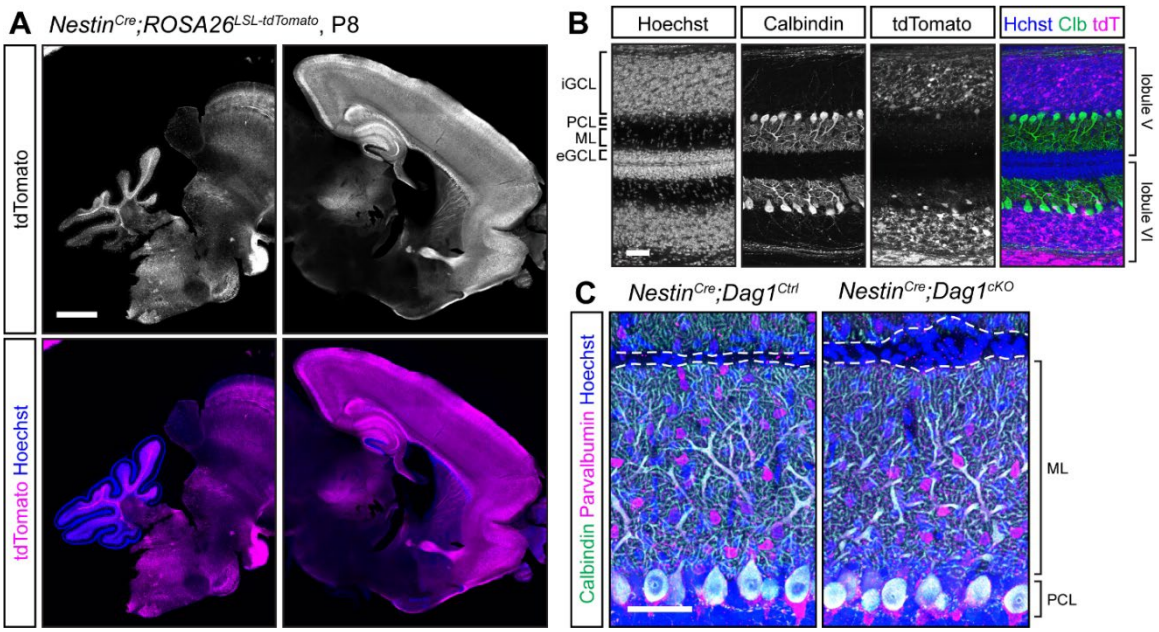

Figure 3.4 *Nestin*^{Cre} does not drive *Cre* recombination in cerebellar Purkinje cells.

(A) Fluorescent tdTomato reporter (magenta) in a sagittal brain slice of a P8 *Nestin*^{Cre}*;ROSA*$^{LSL\text{-}tdTomato}$ mouse. Nuclei are stained in blue. Right and left panels are of the same image but adjusted differently as fluorescence in the forebrain is much brighter than the rest of the brain. Scale bar = 1000μm. **(B)** Higher magnification view of tdTomato expression pattern in cerebellar lobules V and VI at P8 (magenta). Purkinje cells are immunolabeled with anti-Calbindin (green). Scale bar = 50μm. (eGCL = external granule cell layer, iGCL = internal granule cell layer, PCL = Purkinje cell layer, ML = molecular layer.) **(C)** P25 *Nestin*^{Cre}*;Dag1*^{cKO} and littermate control Purkinje cells in cerebellar lobule V. Calbindin (green) labels Purkinje cells, Parvalbumin (magenta) labels Purkinje cells and molecular layer interneurons, Hoechst (blue) labels nuclei. Dashed line shows the edge of Purkinje cell dendrites at the pial surface. Scale bar = 50μm.

Embryonic expression of *Ptf1a*^{Cre} in GABAergic precursors results in stochastic deletion of *Dag1* from Purkinje cells despite ubiquitous reporter expression

We next tested a *Ptf1a*^{Cre} line, which expresses *Cre* from the endogenous *Ptf1a* locus. *Ptf1a* is a transcription factor that is required for GABAergic neuronal fate in cerebellum (Hoshino et al., 2005). Examination of *Ptf1a*^{Cre}*;ROSA26*$^{LSL\text{-}tdTomato}$ brains at P0 showed strong tdTomato fluorescence in the nascent cerebellum which co-localized

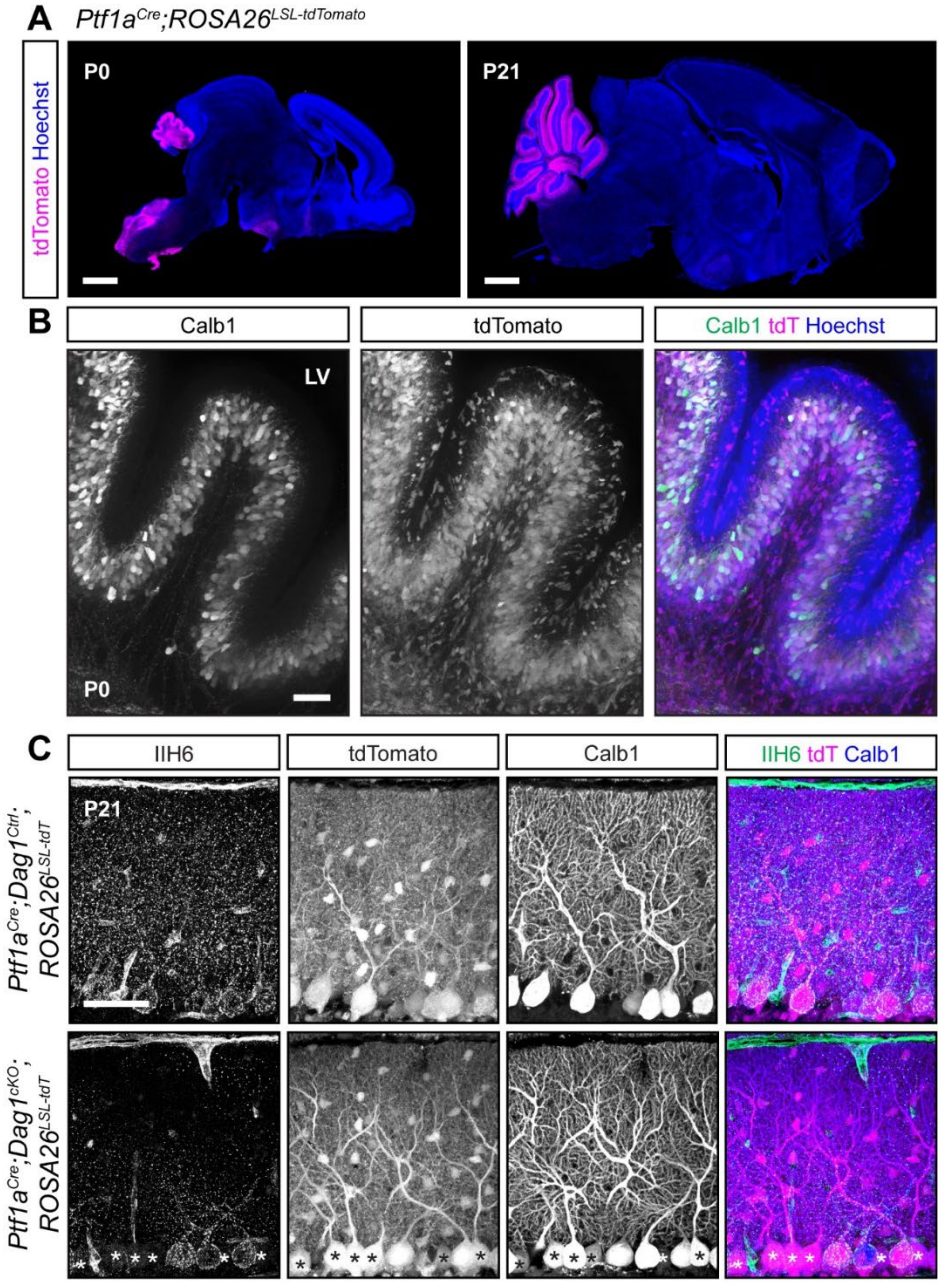

Figure 3.5 Early *Cre* recombination in developing Purkinje cells and MLIs with *Ptf1a*^{Cre} results in a mosaic loss of Dystroglycan protein despite uniform reporter expression.

(A) *Ptf1a*^{Cre}*;ROSA26*$^{LSL\text{-}tdTomato}$ shows that *Cre* recombination, as reported by tdTomato (magenta), is evident at P0 and restricted to the cerebellum. Scale bars = 1000μm. **(B)** Higher magnification view of cerebellar lobule V at P0. Purkinje cells are labeled with Calbindin (Calb1, green) and *Cre* recombination is reported by native fluorescence of tdTomato (tdT, magenta). Nuclei are visualized with Hoechst (blue). Scale bar = 50μm. **(C)** Immunostaining in lobule V of P21 cerebella from *Ptf1a*^{Cre}*;ROSA26*$^{LSL\text{-}tdTomato}$*;Dag1*^{cKO} and littermate controls for α-Dystroglycan (IIH6, green) to visualize Dag1 protein and Calbindin (Calb1, blue) to label Purkinje cells. *Cre* recombination was assessed by native fluorescence of the tdTomato reporter (tdT, magenta). Asterisks denote Purkinje cells with no detectable IIH6 signal. Scale bar = 50μm.

with Calbindin, a marker for Purkinje cells (**Figure 3.5 A, B**). Examination of adult brains showed tdTomato in all Purkinje cells and MLIs (**Figure 3.5 A, C**). The early expression of tdTomato suggested that this line may be useful for developmental deletion of synaptogenic genes in Purkinje cells, although with reduced cellular specificity. However, when we examined Dag1 protein localization at P21, we found that despite all Purkinje cells being tdTomato positive, *Ptf1a*^{Cre}*;Dag1*^{cKO} Purkinje cells showed mosaic loss of Dag1 protein (**Figure 3.5 C**). This result was surprising, as we anticipated that the early expression of *Cre* in Purkinje cells would delete the *Dag1* allele before it is expressed at appreciable levels. This difference between robust tdTomato expression and mosaic *Dag1* deletion may be due to the transient expression of *Ptf1a* in GABAergic precursors in conjunction with the known sensitivity of the particular *ROSA26*$^{LSL\text{-}tdTomato}$ floxed locus in the *Ai14* line to *Cre*-mediated recombination (Jin and Xiang, 2019; Luo et al., 2020). In this situation, the transient Cre activity can drive recombination of the reporter allele without driving recombination of the Dag1 floxed allele. This makes the *Ptf1a*^{Cre} line of limited utility for studying deletion of proteins in GABAergic cerebellar neurons, as the presence tdTomato is not predictive of loss of the targeted allele.

Calb1^{Cre} drives stable *Cre* expression and *Dag1* deletion in all Purkinje cells prior to synaptogenesis

In the course of characterizing the *Ptf1a*^{Cre} line, we observed abundant Calbindin staining in Purkinje cells at P0 (**Figure 3.5**), and previous work has shown *Calb1* expression in the cerebellum as early as E14.5 (Morales and Hatten, 2006). While Calbindin is widely expressed in multiple neuronal subtypes in the majority of the CNS, its expression is highly selective for Purkinje cells in the cerebellum. We therefore obtained a recently generated *Calb1-IRES-Cre-D* line (hereafter referred to as *Calb1*^{Cre}) that expresses *Cre* from the endogenous *Calb1* locus while retaining *Calb1* expression

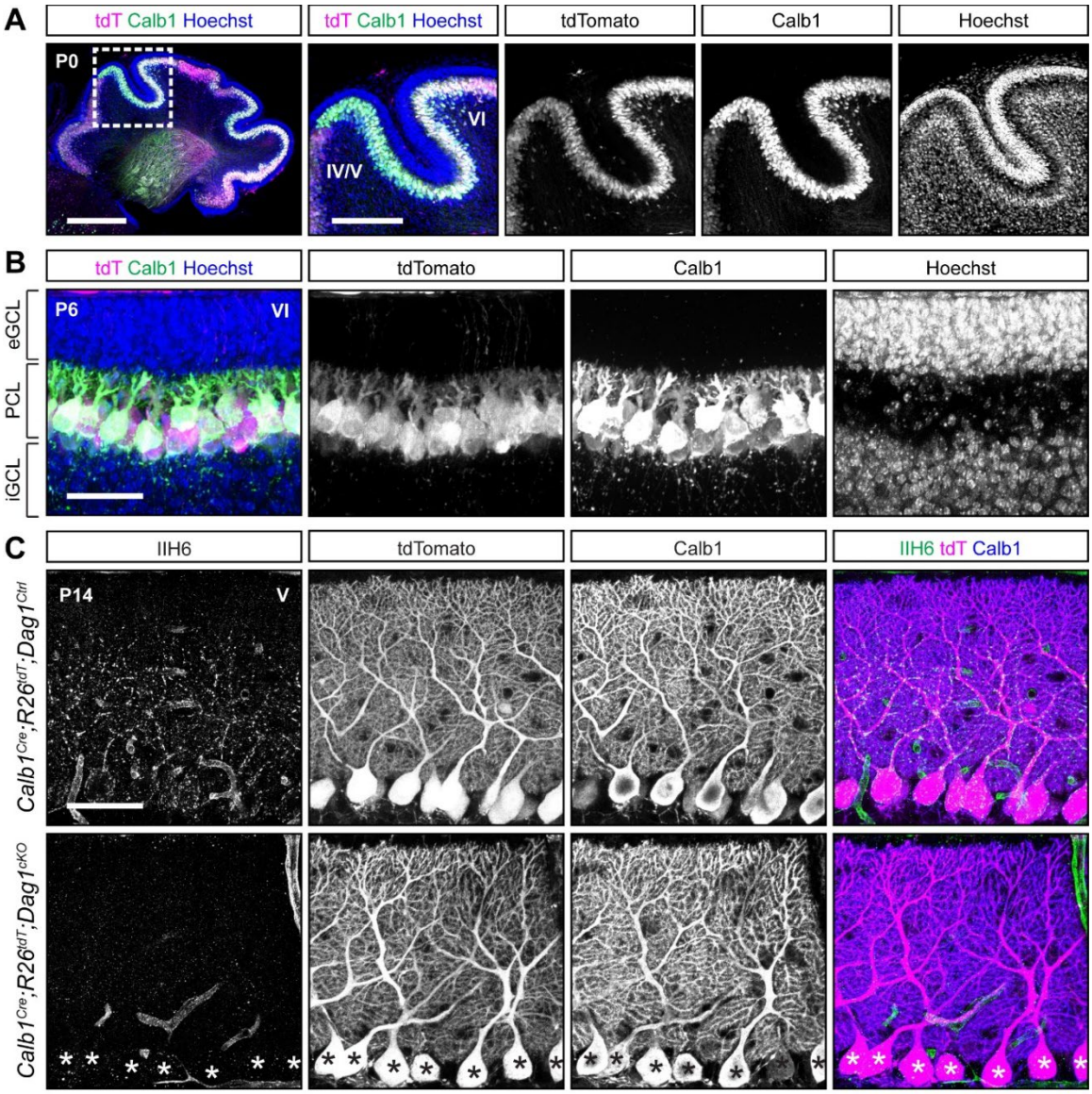

Figure 3.6 *Calb1*^{Cre} drives *Cre* recombination early in development resulting in complete loss of synaptic Purkinje cell Dystroglycan protein.

(A-B) Cerebellum of **(A)** P0 (insets show lobules IV/V and VI) and **(B)** P6 (lobule VI) *Calb1*^{Cre}*;ROSA26*$^{LSL\text{-}tdTomato}$ mouse immunolabeled with Calbindin (Calb1, green) to label Purkinje cells and Hoechst (blue) to label nuclei. *Cre* recombination is reported by native tdTomato fluorescence (tdT, magenta). (eGCL = external granule cell layer, iGCL = internal granule cell layer, PCL = Purkinje cell layer.) Scale bars = **(A)** 500μm, 250μm (inset), **(B)** 50μm. **(C)** Immunostaining in lobule V of P14 cerebella from *Calb1*^{Cre}*;ROSA26*$^{LSL\text{-}tdTomato}$*;Dag1*^{cKO} and littermate controls for α-Dystroglycan (IIH6, green) to visualize Dag1 protein and Calbindin (Calb1, blue) to label Purkinje cells. *Cre* recombination was assessed by native fluorescence of the tdTomato reporter (tdT, magenta). Asterisks denote Purkinje cells with no detectable IIH6 signal. Scale bar = 50μm.

(Daigle et al., 2018). Analysis of *Calb1*^{Cre}*;ROSA26*$^{LSL\text{-}tdTomato}$ brains showed tdTomato

signal in all Purkinje cells at P0 (**Figure 3.6 A**). Further analysis of staining at P6 and P14 continued to show that recombination is specific to Purkinje cells (**Figure 3.6 B, C**). We next examined *Dag1* deletion in *Calb1^{Cre};Dag1^{cKO}* mice at P14 during the period of active synaptogenesis in Purkinje cells. In contrast to the *Pcp2^{Cre};Dag1^{cKO}* mice which retained Dag1 at P16, we saw a complete loss of punctate Dag1 signal in Purkinje cells at P14 in *Calb1^{Cre};Dag1^{cKO}* cerebella. These results highlight the utility of the *Calb1^{Cre}* line for studying synaptogenesis or other developmental processes in Purkinje cells.

AAV delivery of *Cre* to Purkinje cells results in gradual *Cre* expression over the course of three weeks

In addition to *Cre* lines, viral-mediated delivery of *Cre* is commonly used to delete synaptogenic proteins throughout the brain. One advantage of viral-mediated deletion is the ability to test cell-autonomous deletion of target alleles in a mosaic fashion by titrating the amount of virus. However, this approach is limited by the timing of viral transduction, subsequent *Cre* expression, and recombination. To better define this time course in Purkinje cells, we examined recombination of tdTomato in *ROSA26$^{LSL\text{-}tdTomato}$* mice injected in the lateral ventricles at P0 with dilute *AAV8-CMV-Cre*. The first tdTomato positive Purkinje cells were observed around P7-P10, with the number of positive cells increasing to maximal levels by P18 (**Figure 3.7 A, B**). This timing is similar to the recombination driven by *Pcp2^{Cre}*, limiting its utility to examining synapse maintenance. Examination of Dag1 protein in *Dag$^{flox/-}$;ROSA26$^{LSL\text{-}tdTomato}$* mice injected with *AAV8-CMV-Cre* at P0 showed that loss of Dag1 lagged behind tdTomato expression, similar to what was observed in the *Pcp2^{Cre};Dag1^{cKO}* Purkinje cells **Figure 3.7 C-F**). All tdTomato expressing Purkinje cells were immunoreactive for Dag1 protein at P18 and most (90.8 ± 6.5%) remained Dag1 immunoreactive at P21 (**Figure 3.7 C-D, F**). By P35 the majority of tdTomato expressing Purkinje cells lacked Dag1

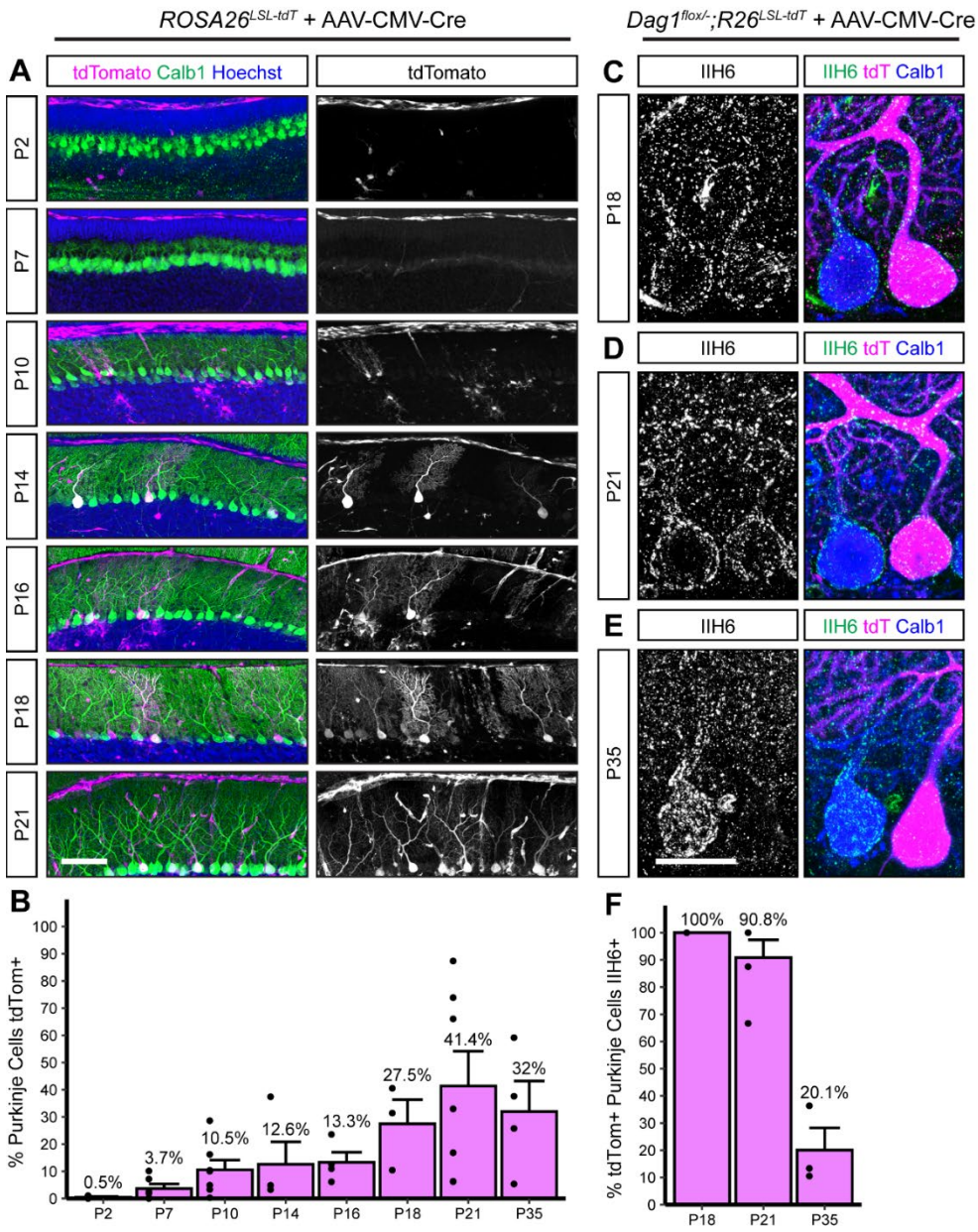

Figure 3.7 Viral delivery of *Cre* under the ubiquitous CMV promoter takes several weeks to recombine the *Dag1* floxed locus in Purkinje cells.

(A) Dilute AAV8-CMV-Cre (1.00E+12) was injected into the lateral ventricles of P0 *ROSA26*$^{LSL\text{-}tdTomato}$ reporter mice. Cerebella were collected at timepoints from P2 to P35 to observe tdTomato expression. Sagittal sections were immunolabeled with Calbindin (Calb1, green) to label Purkinje cells and Hoechst (blue) to label nuclei. *Cre* recombination was assessed by native fluorescence of the tdTomato reporter (magenta). Scale bar = 100μm. **(B)** Quantification of the percent of Purkinje cells that express tdTomato in **(A)**. **(C-E)** *Dag1*$^{flox/-}$;*ROSA26*$^{LSL\text{-}tdTomato}$ mice were injected with dilute AAV8-CMV-Cre at P0 and brains collected at **(C)** P18, **(D)** P21, and **(E)** P35. Cerebellar sections were counterstained with Calbindin (Calb1, blue) to label Purkinje cells and IIH6 (green) to label Dag1 protein. *Cre* expressing Purkinje cells were visualized with native tdTomato expression (magenta). Scale bar = 25μm. **(F)** Quantification of the percent of tdTomato expressing Purkinje cells that are IIH6 immunoreactive in **(C-E)**.

immunoreactivity (**Figure 3.7 E, F**). This lag between tdTomato expression and loss of Dag1 protein implies that it can take two or more weeks for Dag1 synaptic protein to turn over.

Discussion

The Cre-lox system has proven to be an invaluable tool for studying the role of genes in a population-specific manner as *Cre*-mediated gene deletion is often required to avoid lethality of constitutive deletion. However, as more of these tools are developed it is important to perform rigorous validation to ensure that a *Cre* line behaves as expected. While the timing of *Cre* expression in a given line should be consistent across different conditional lines, the recombination efficiency of the floxed allele and the stability of the existing protein that needs to be turned over before a cell can be deemed a knockout can vary. For these reasons, it is important to use both a *Cre*-dependent reporter and a method for evaluating loss of protein (or RNA) to validate a conditional knockout.

New *Cre*-dependent reporter lines continue to be developed, each with different advantages and limitations. The *ROSA26* and *TIGRE* loci are popular sites for insertion of *Cre*-dependent fluorescent reporters due to their genomic accessibility. However, even reporters within the same loci (ie: *ROSA26*) can show differences in recombination efficiency, which could lead to confusion about patterns of *Cre* expression (Daigle et al., 2018; Madisen et al., 2010). There have also been cases reported in which a *Cre* line may become lethal or cause health complications when crossed to certain fluorescent reporter lines but not others (Daigle et al., 2018). Here we used the popular *Ai14* line which expresses a *LSL-tdTomato* in the *ROSA26* locus. The *Ai14* line is particularly sensitive to recombination, likely due to the proximity of the two loxP sites. This could

lead to off-target reporter expression and requires especially rigorous validation of any knockout when paired with inducible *Cre* lines which require administration of tamoxifen to activate the Cre protein (Álvarez-Aznar et al., 2020; Luo et al., 2020).

Inducible *Cre* lines (e.g. *CreER^{T2})* are often used to either control the timing of Cre activity or to restrict Cre activity to a subset of a cellular population. However, because of the transient nature, inducible *Cre* lines require especially careful validation. *CreER^{T2}* consists of *Cre* fused to the hormone binding domain of the estrogen receptor (Feil et al., 1997, 2009). Under baseline conditions, CreER^{T2} localization is excluded from the nucleus. Once tamoxifen is administered it is metabolized into 4-hydroxytamoxifen, a synthetic ligand of the estrogen receptor that binds to CreER^{T2} and permits localization to the nucleus. After tamoxifen has been cleared from the system, CreER^{T2} is once again excluded from the nucleus, restricting CreER^{T2} activity to roughly 24 hours after tamoxifen administration (Feil et al., 1997). Since the effect of tamoxifen is both transient and dose-dependent it is prudent that a *Cre*-dependent reporter is used to identify which cells experienced Cre-mediated recombination. However, due to differences in sensitivity to recombination between floxed alleles, reporter expression cannot be used alone to predict loss of protein (Álvarez-Aznar et al., 2020; Feil et al., 2009; Luo et al., 2020).

Based on expression of tdTomato driven by *Pcp2^{Cre}* in our hands, we found that *Pcp2^{Cre}* drives *Cre* expression selectively in Purkinje cells, however expression turns on slowly beginning at P7 and reaching all Purkinje cells by P14 (**Figure 3.2**). This time course is similar to what has been reported for the related *L7^{Cre}* line (Barski et al., 2000; Lewis et al., 2004). However, when *L7^{Cre}* was used to delete *Dag1* from Purkinje cells, loss of protein wasn't complete until P90 (Briatore et al., 2020), whereas we observed loss of Dag1 protein by P30 (**Figure 3.3**). We hypothesize that this difference in the loss of protein is due to differing breeding strategies. Briatore and colleagues report crossing

L7^{Cre}*;Dag1*$^{flox/flox}$ mice with *Dag1*$^{flox/flox}$ mice to generate *L7*^{Cre}*;Dag1*$^{flox/flox}$ mutants and *Dag1*$^{flox/flox}$ littermate controls. While this is an efficient breeding strategy allowing for the use of all progeny in a litter, the use of flox/flox mutants may not be ideal for studying *Dag1* specifically. Dag1 is a stable protein, and in this case *Cre* must recombine both alleles of *Dag1* before protein loss can begin. We crossed *Pcp2*^{Cre}*;Dag1*$^{+/-}$ mice to *Dag1*$^{flox/flox}$ mice to generate *Pcp2*^{Cre}*;Dag1*$^{flox/-}$ mutants and *Pcp2*^{Cre}*;Dag1*$^{flox/+}$ littermate controls. Not only does this approach control for potential off-target effects of *Cre* expression by ensuring that both controls and mutants are *Pcp2*^{Cre} expressing, *Cre* only needs to recombine one floxed allele of *Dag1*. This alone could account for the faster loss of protein. However, this approach requires ensuring that heterozygous mice lack a phenotype. While *L7*^{Cre} and *Pcp2*^{Cre} remain useful tools for studying the effect of losing protein later in development, an inducible *Cre* such as *Pcp2*^{CreERT2} with tamoxifen administration at or after P14 might be more useful for standardizing the timing of gene deletion across Purkinje cells, avoiding gradual *Cre* expression seen in the *Pcp2*^{Cre} line. However, as described above, tamoxifen administration represents a new variable with additional optimization and validation required.

The time course of *Cre* expression with viral delivery of *Cre* using AAV8-CMV-Cre injected into the lateral ventricles of P0 mice was similar to that observed with *Pcp2*^{Cre} (**Figure 3.1**, **Figure 3.7**). One advantage of viral delivery is the ability to achieve sparse or mosaic *Cre* expression. This can also be achieved using inducible *CreER*^{T2} lines with low dose tamoxifen, however virally-expressed *Cre* remains expressed in the cell after transduction whereas Cre activity with *CreER*^{T2} is temporally limited to approximately 24 hours after tamoxifen administration (Feil et al., 1997). This increased stability from virally-expressed *Cre* is therefore less likely to result in expression of a *Cre*-dependent reporter without recombination of target floxed alleles, which can occur following transient CreER^{T2} activity induced by low doses of tamoxifen. The timing of

AAV8 viral transduction limits the utility of this approach to later developmental processes. The use of AAVs for gene transduction has become standard in the field, and new viral capsids to expand the utility of the approach are under rapid development. Different capsids can exhibit differences in tropism, efficiency, and transduction timeline (Haery et al., 2019). While the most widely used capsids show a delay in transduction of several days to a couple weeks, newer developments can speed up that timeline considerably. A recent study found that AAV-SCH9 can transduce neurons in 24-48 hours , making it useful for studying developmental processes (Zheng et al., 2023).

Development of genetic tools for targeting inhibitory populations has lagged behind those available for targeting excitatory populations of neurons. The cerebellum is a unique case in which Purkinje neurons (the primary output of the cerebellum) and MLIs (local interneurons) are both inhibitory neurons, making it challenging to separate the two based on common markers for inhibitory populations (ex. *VGAT*^{Cre}*, GAD2*^{Cre}). Both populations also express Parvalbumin, meaning *PV*^{Cre} will cause recombination in both PCs and MLIs. *Dlx5/6*^{Cre} is becoming increasingly popular to target forebrain interneuron populations, however *Dlx5/*6 is not expressed in the cerebellum. Here we have described a suite of tools for targeting Purkinje cells for either genetic labeling or gene deletion at various developmental stages: *Calb1*^{Cre} for embryonic deletion (**Figure 3.6**), *Pcp2*^{Cre} for post-developmental deletion (**Figure 3.1**, **Figure 3.2**), and AAV-Cre for deletion during or after development (**Figure 3.7**). We also highlight important considerations when identifying and validating new tools for conditional genetic deletion applicable to any population of cells.

Materials and Methods

Animal Husbandry

All animals were housed and cared for by the Department of Comparative Medicine (DCM) at Oregon Health and Science University (OHSU), an AAALAC-accredited institution. Animal procedures were approved by OHSU Institutional Animal Care and Use Committee (Protocol # IS00000539) and adhered to the NIH *Guide for the care and use of laboratory animals*. Animal facilities are regulated for temperature and humidity and maintained on a 12-hour light-dark cycle; animals are provided with 24-hour veterinary care and food and water *ad libitum*. Animals were group housed whenever possible and provided with environmental enrichment in the form of extra crinkle paper and a red plastic shelter. Experiments were performed between Zeitgeber Time (ZT) 0 and ZT12. Animals older than postnatal day 6 (P6) were euthanized by administration of CO_2, animals <P6 were euthanized by rapid decapitation. Mice of both sexes were used for all experiments.

Mouse Strains and Genotyping

The day of birth was designated postnatal day 0 (P0). Ages of mice used for each analysis are indicated in the figure and figure legends. Mice were maintained on a C57BL/6 background. $Dag1^{+/-}$ mice were generated by crossing a male $Dag1^{flox/flox}$ mouse to a female $Sox2^{Cre}$ mouse to generate germline $Dag1^{\Delta/+}$ mice, hereafter referred to as $Dag1^{+/-}$ mice; $Dag1^{+/-}$ offspring lacking the $Sox2^{Cre}$ allele were thereafter maintained as heterozygotes. For all *Dag1* conditional crosses, a *Cre* positive $Dag1^{+/-}$ breeder was crossed to a $Dag1^{flox/flox;tdT/tdT}$ breeder to generate *Cre* positive $Dag1^{flox/+;tdT/+}$ controls and *Cre* positive $Dag1^{flox/-;tdT/+}$ conditional knockouts. Genomic DNA extracted from toe or tail samples using the HotSHOT method (Truett et al., 2000) was used to genotype animals.

Primers for genotyping can be found on the Jackson Labs webpage or originating article. *Dag1*$^{+/-}$ mice were genotyped with the following primers: CGAACACTGAGTTCATCC (forward) and CAACTGCTGCATCTCTAC (reverse). For each mouse strain, littermate controls were used for comparison with mutant mice.

Table 3.1 Mouse strains

Common name	Strain name	Reference	Stock #
BAC-Pcp2-IRES-Cre	B6.Cg-*Tg(Pcp2-cre)3555Jdhu/J*	(Zhang et al., 2004)	010536
Ai14(RCL-tdT)-D	B6.Cg-*Gt(ROSA)26Sor*$^{tm14(CAG-tdTomato)Hze}$*/J*	(Madisen et al., 2010)	007914
Dag1^{flox}	B6.129(Cg)-*Dag1*$^{tm2.1Kcam}$*/J*	(Cohn et al., 2002)	009652
Nestin-Cre	B6.Cg-*Tg(Nes-cre)1Kln/J*	(Tronche et al., 1999)	003771
p48-Cre	*Ptf1a*$^{tm1(cre)Hnak}$*/RschJ*	(Nakhai et al., 2007)	023329
Calb1-IRES2-Cre-D	B6;129S-*Calb1*$^{tm2.1(cre)Hze}$*/J*	(Daigle et al., 2018)	028532
B6NJ.Sox2-Cre	B6N.Cg-*Edil*$^{3Tg(Sox2-cre)1Amc}$*/J*	(Hayashi et al., 2002)	014094

Intracerebroventricular virus injection

Borosilicate capillary glass (World Precision Instruments, Cat. No. 1B150F-4) was pulled into a fine tip and then beveled to an angled point. The capillary was then filled with AAV8-CMV.III.eGFP-Cre.WPRE.SV40 with a titer of 1.00E+13 (Penn Vector Core, University of Pennsylvania) diluted 1:10 in PBS with Fast Green FCF (Fisher Scientific, Cat. No. BP123-10) for visualization. P0 mice were deeply anesthetized through indirect exposure to ice until unresponsive to light touch. An ethanol wipe was used to sterilize the skin of each pup prior to injection. The capillary tip was manually guided into the lateral ventricle and a Toohey Spritzer Pressure System IIe (Toohey Company, Fairfield, NJ, USA) delivered a 30 psi pulse for 30 msec. The process was repeated in the other hemisphere. Pups then recovered on a warm pad until mobile and returned to their home cage.

Perfusions and tissue preparation

Brains from mice younger than P21 were dissected and drop fixed in 5 mL of 4% paraformaldehyde (PFA) in phosphate buffered saline (PBS) overnight for 18-24 hours at 4°C. Mice P21 and older were deeply anesthetized using CO_2 and transcardially perfused with ice cold 0.1M PBS followed by 15 mL of ice cold 4% PFA in PBS. After perfusion, brains were post-fixed in 4% PFA for 30 minutes at room temperature. Brains were rinsed with PBS, embedded in 4% low-melt agarose (Fisher cat. no. 16520100), and sectioned at 70μm using a vibratome (VT1200S, Leica Microsystems Inc., Buffalo Grove, IL) into 24-well plates containing 1 mL of 0.1M PBS with 0.02% Sodium Azide.

Immunohistochemistry

Free-floating vibratome sections (70μm) were briefly rinsed with PBS, then blocked for 1 hour in PBS containing 0.2% Triton-X (PBST) plus 2% normal goat or donkey serum. For staining of Dystroglycan synaptic puncta, an antigen retrieval step was performed prior to the blocking step: sections were incubated in sodium citrate solution (10mM Sodium Citrate, 0.05% Tween-20, pH 6.0) for 12 min at 95°C in a water bath followed by 12 min at room temperature. Free-floating sections were incubated with primary antibodies (**Table 3.2**) diluted in blocking solution at 4°C for 48-72 hours. Sections were then washed with PBS three times for 20 min each. Sections were then incubated with a cocktail of secondary antibodies (1:500, Alexa Fluor 488, 546, 647) in blocking solution containing Hoechst 33342 (1:10,000, Life Technologies, Cat. No. H3570) overnight at room temperature followed by three final washes with PBS. Finally, sections were mounted on Fisher Superfrost Plus microscope slides (Fisher, Cat. No. 12-550-15) using Fluoromount-G (SouthernBiotech, Cat. No. 0100-01), covered with #1 coverslip glass (Fisher, Cat. No. 12-541-025), and sealed using nail polish.

Table 3.2 Primary antibodies used for immunohistochemistry

Target	Host	Dilution	Source	Catalog #	RRID
α-Dystroglycan (IIH6C4)	Mouse	1:250	Millipore Sigma	05-593	AB_309828
tdTomato	Goat	1:1000	Biorbyt	orb182397	AB_2687917
Calbindin	Chicken	1:1000	Boster Bio	M03047-2	AB_2936235
Calbindin	Rabbit	1:1000	Swant	CB38a	AB_10000340
Parvalbumin	Goat	1:1000	Swant	PVG213	AB_2721207

Microscopy

Imaging was performed on either a Zeiss Axio Imager M2 fluorescence upright microscope equipped with an Apotome.2 module or a Zeiss LSM 980 laser scanning confocal build around a motorized Zeiss Axio Observer Z1 inverted microscope with a Piezo stage. The Axio Imager M2 uses a metal halide light source (HXP 200 C), Axiocam 506 mono camera, and 10X/0.3 NA EC Plan-Neofluar, 20X/0.8 NA Plan-Apochromat objectives. The LSM 980 confocal light path has two multi-alkali PMTs and two GaAsP PMTs for four track imaging. Confocal images were acquired using a 63X/1.4 NA Plan-Apochromat Oil DIC M27 objective. For some experiments utilizing the LSM 980 confocal, a linear Wiener filter deconvolution step (Zeiss LSM Plus) was used at the end of image acquisition with 1.2X Nyquist sampling (**Figure 3.3 B-C**, **Figure 3.7 C-E**). Z-stack images were acquired and analyzed offline in ImageJ/FIJI (Schindelin et al., 2012). Images within each experiment were acquired using the same exposure times. Brightness and contrast were adjusted in FIJI to improve visibility of images for publication. Figures were composed in Adobe Illustrator 2023 (Adobe Systems), with graphs assembled in R (Version 4.2.3).

Chapter 4: Functional domains of Dystroglycan in synapse formation and maintenance at inhibitory synapses in cerebellar cortex

Jennifer N. Jahncke[1,], Eric Schnell[2,3], and Kevin M. Wright[4]

[1] Neuroscience Graduate Program, Oregon Health & Science University, Portland, OR 97239, USA

[2] Operative Care Division, Portland VA Health Care System

[3] Anesthesiology and Perioperative Medicine, Oregon Health & Science University, Portland, OR 97239, USA

[4] Vollum Institute, Oregon Health & Science University, Portland, OR 97239, USA

Abstract

Dystroglycan is a cell adhesion molecule that is expressed at multiple synaptic populations throughout the brain. While Dystroglycan is required to maintain inhibitory synapses from cerebellar molecular layer interneurons (MLIs) onto Purkinje cells (PCs), it is unknown whether early developmental synaptogenesis requires Dystroglycan. We used mice of both sexes to show that conditional deletion of *Dystroglycan* from Purkinje cells prior to synaptogenesis impairs MLI:PC synapse function due to both a reduction in presynaptic inputs and abnormal postsynaptic $GABA_A$ receptor clustering. Using genetic manipulations that disrupt glycosylation of Dystroglycan or truncate its intracellular domain, we show that Dystroglycan's role in synapse formation and function is dependent on both extracellular and intracellular interactions. Together, these findings provide molecular insight into the mechanism of inhibitory synapse formation and maintenance in cerebellar cortex.

Introduction

Throughout development, synapses are formed, refined, and eliminated. Synapse formation begins when a presynaptic axon recognizes potential postsynaptic sites through molecular cues. After contact between the pre- and post-synaptic neurons is established, a wide range of transmembrane and secreted molecules are recruited to the nascent synapse to regulate its maturation and refinement in response to activity (Südhof, 2018). The wide diversity in cell adhesion molecules (CAMs) present at synapses implies that they can form a “code” for determining synapse type and specificity. Although several CAMs have been shown to be involved in the maintenance of synapses, less is known about the molecular players involved in early synaptogenesis.

Dystroglycan is a CAM expressed throughout the nervous system early in development in a variety of cellular populations including neurons, astrocytes, oligodendrocytes, vascular endothelial cells, and neuroepithelial cells (Colognato et al., 2007; Nguyen et al., 2014; Nickolls and Bönnemann, 2018; Tian et al., 1996; Zaccaria et al., 2001). Dystroglycan is encoded by a single gene (*Dag1*) and undergoes post-translational autoproteolytic cleavage to produce two subunits: α- and β-Dystroglycan (Holt et al., 2000; Ibraghimov-Beskrovnaya et al., 1992). The extracellular alpha subunit is extensively glycosylated through a process involving at least 19 different genes, and employs a specific glycan motif referred to as "matriglycan" to bind several extracellular proteins that contain Laminin-G (LG) domains (Jahncke and Wright, 2023). The transmembrane beta subunit of Dystroglycan noncovalently binds the alpha subunit in the extracellular environment, and contains a short C-terminal intracellular domain that binds multiple scaffolding and signaling proteins (Moore and Winder, 2010). Dystroglycan is the transmembrane component of the Dystrophin Glycoprotein Complex

(DGC), which functions to connect the actin cytoskeleton to the extracellular matrix. Dystroglycan and Dystrophin, which interacts with Dystroglycan's intracellular domain, are both central to the DGC, whereas other components of the complex can vary depending on the cellular type.

Early in nervous system development, Dystroglycan plays important roles in neuronal migration, axon targeting, and maintenance of the blood-brain barrier (Menezes et al., 2014; Myshrall et al., 2012; Wright et al., 2012). Later in development, as synapses begin to form, Dystroglycan expression increases in several neuronal populations throughout the brain, where it localizes specifically at inhibitory synapses (Briatore et al., 2020, 2010; Brünig et al., 2002; Lévi et al., 2002; Patrizi et al., 2008). Dystroglycan is required for the formation and function of subsets of inhibitory synapses onto hippocampal and cortical pyramidal neurons, where it is thought to be the postsynaptic recognition cue for CCK^+/CB_1R^+ basket interneuron axons (Früh et al., 2016; Jahncke et al., 2024; Miller and Wright, 2021). In pyramidal neurons, Dystroglycan expression continues past the period of synapse formation, and is required to maintain CCK^+/CB_1R^+ basket synapses (Früh et al., 2016). However, whether Dystroglycan plays these same roles at other synapses has not yet been explored in detail. In the cerebellum, Dystroglycan is present at inhibitory somatic and dendritic synapses onto Purkinje cells and deletion of *Dag1* from Purkinje cells after synapse formation results in a gradual reduction of inhibitory synapse number and impairment of synaptic function, (Briatore et al., 2020, 2010; Patrizi et al., 2008). Constitutive loss of *Dystrophin* results in similar alterations in inhibitory inputs onto Purkinje cells, confirming an important role for the DGC at these synapses (Kueh et al., 2008; Wu et al., 2022).

Until recently, tools for the conditional deletion of genes in cerebellar Purkinje cells prior to the period of synaptogenesis have been lacking (**Chapter 3**). We identified $Calb1^{Cre}$ as a line that drives recombination in embryonic Purkinje cells, specifically in

the cerebellum, allowing us to conditionally delete *Dag1* from Purkinje cells prior to the onset of synapse formation. We show that Dystroglycan is required for inhibitory synapse formation, and also confirm its role in synapse maintenance by conditionally deleting Dystroglycan after synaptogenesis using *Pcp2*^{Cre}. Furthermore, we provide mechanistic insight by showing that both extracellular glycosylation of α-Dystroglycan and intracellular interactions through β-Dystroglycan are required for normal synaptic function.

Results

Dystroglycan is localized to inhibitory but not excitatory synaptic populations in cerebellar cortex

While Dystroglycan is associated with populations of inhibitory synapses throughout the brain (Briatore et al., 2010, 2020; Jahncke et al., 2024; Trotter et al., 2023), its localization at specific synaptic populations in cerebellar cortex has not yet been defined. We therefore analyzed co-localization of Dystroglycan immunoreactivity with established markers of synaptic populations. Inhibitory synapses in cerebellar cortex reflect synapses from (1) molecular layer interneurons (MLIs) onto Purkinje cells (PCs), (2) MLIs onto other MLIs, and (3) PC collaterals onto other PCs. While currently available markers are unable to distinguish between these three populations of synapses, Dystroglycan-positive synapses are presumed to be from MLIs onto PCs (Briatore et al., 2010) and potentially reflect a population that is at least partially distinct from the Gephyrin-containing population of synapses (Lévi et al., 2002; Uezu et al., 2019). We therefore used two presynaptic inhibitory markers (VGAT and GAD67) to analyze inhibitory MLI:PC synapses. The IIH6 antibody, which specifically recognizes matriglycan disaccharide repeats on α-Dystroglycan, significantly co-localized with both

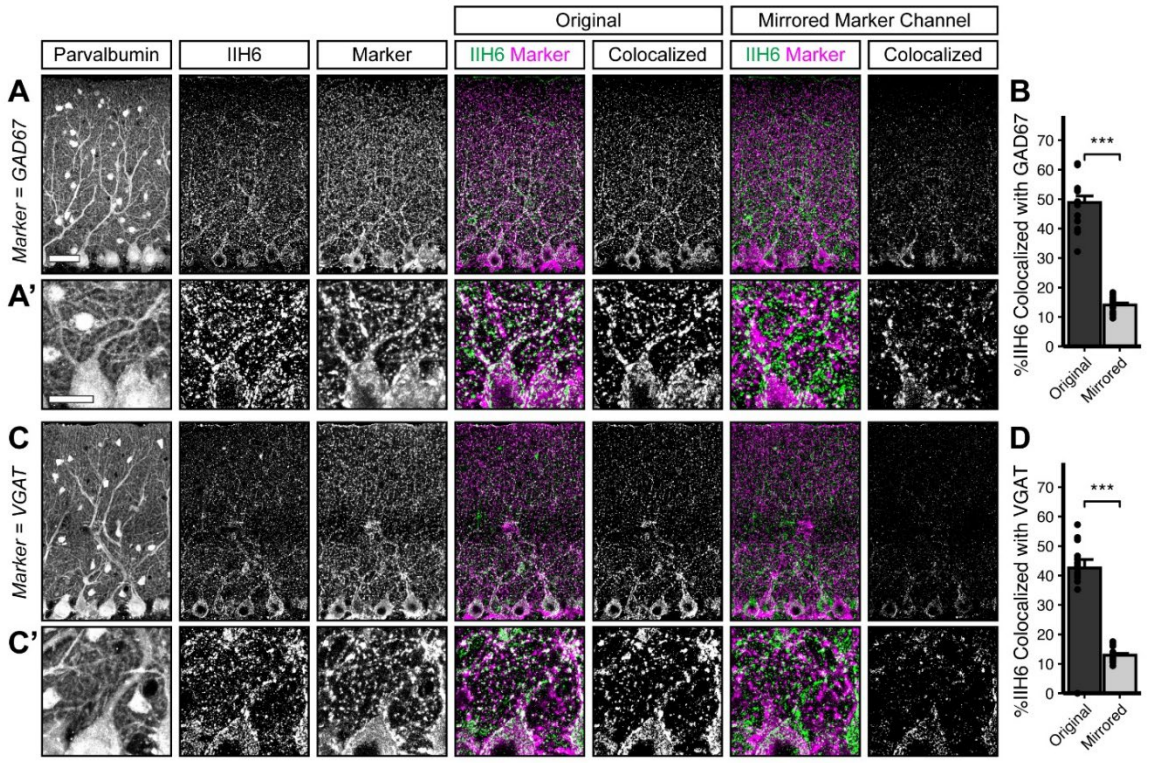

Figure 4.1 Dystroglycan co-localizes with markers of inhibitory synapses.
Cerebellar cortex of lobules V-VI were immunostained with Parvalbumin to show Purkinje cell and MLI morphology and counterstained with IIH6 (glycosylated Dystroglycan) and GAD67 (**A**) or VGAT (**C**). Both the merged channels (IIH6, green; GAD67/VGAT, magenta) and colocalized pixels are shown for the original image and for original IIH6 with the mirrored GAD67/VGAT channel. Images are maximum projections. (**B, D**) Quantification of the percent of IIH6 puncta that are colocalized with GAD67/VGAT puncta. Scale bar for (**A**, **C**) is 50µm; scale bar for insets (**A'**, **C'**) is 25µm. GAD67 N = 16 images, 3 animals. VGAT N = 18 images, 4 animals.

VGAT and GAD67, with nearly 50% of IIH6 puncta positive for VGAT or GAD67 (**Figure 4.1 A**, **C**). As a control, we flipped the synaptic marker channel along the vertical axis (VGAT or GAD67) to generate a mirror image of the original channel and calculated co-localization between the original IIH6 channel and the mirrored synaptic marker channel. IIH6 co-localized with the original channel significantly more than the mirrored channel for both VGAT and GAD67 (**Figure 4.1 A-D**), confirming that Dystroglycan is localized to inhibitory synapses in cerebellar cortex.

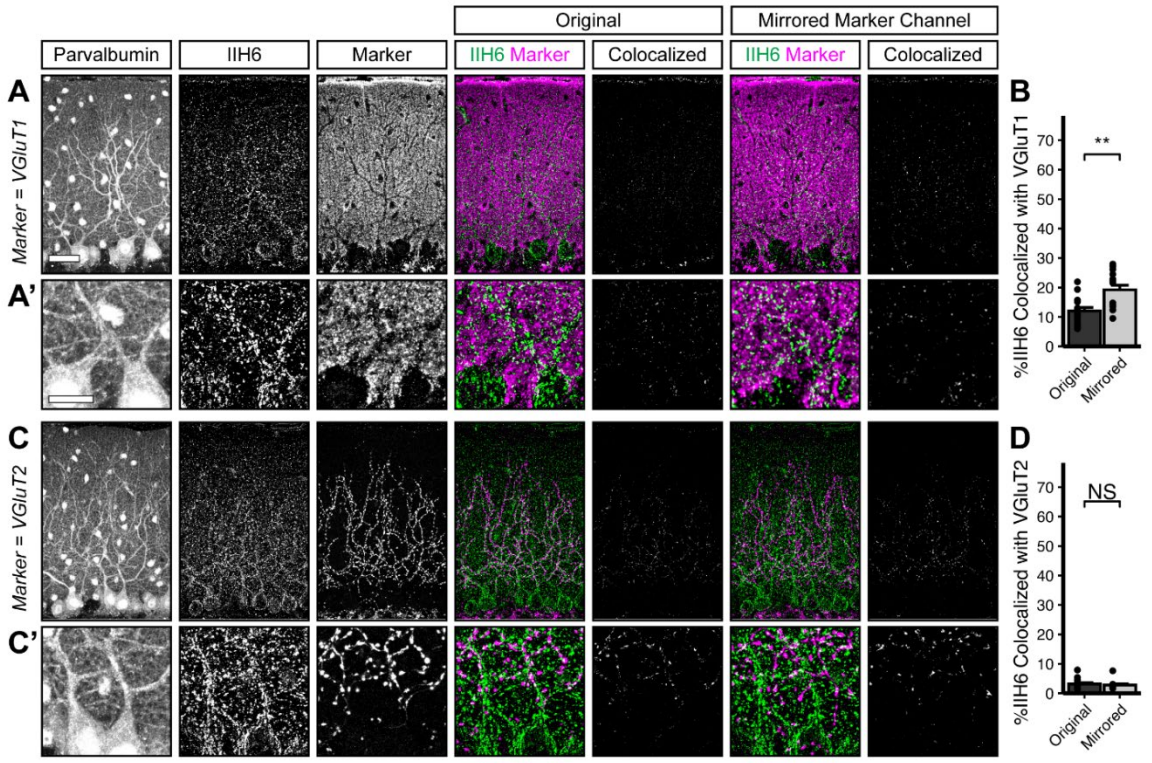

Figure 4.2 Dystroglycan does not co-localize with markers of excitatory synapses. Cerebellar cortex of lobules V-VI were immunostained with Parvalbumin to show Purkinje cell and MLI morphology and counterstained with IIH6 (glycosylated Dystroglycan) and VGluT1 (parallel fibers) (**A**) or VGluT2 (climbing fibers) (**C**). Both the merged channels (IIH6, green; VGluT1/VGluT2, magenta) and colocalized pixels are shown for the original image and for original IIH6 with the mirrored VGluT1/VGluT2 channel. Images are maximum projections. (**B, D**) Quantification of the percent of IIH6 puncta that are colocalized with VGluT1/VGluT2 puncta. Scale bar for (**A**, **C**) is 50μm; scale bar for insets (**A'**, **C'**) is 25μm. VGluT1 N = 15 images, 3 animals. VGluT2 N = 15 images, 3 animals.

There are two populations of excitatory synapses onto Purkinje cells: (1) VGluT1$^+$ parallel fiber inputs from granule cells within the cerebellar cortex and (2) VGluT2$^+$ climbing fiber inputs originating from neurons of the inferior olivary nucleus. Despite the high density of VGluT1$^+$ parallel fibers, Dystroglycan immunoreactivity showed minimal overlap with VGluT1, and mirroring the VGluT1 channel actually increased the incidence of Dystroglycan:VGluT1 overlap due to its high density (**Figure 4.2 A-B**). Co-localization between IIH6 and VGluT2 was minimal, and was not affected by mirroring the VGluT2 channel, indicating that Dystroglycan does not localize to climbing fiber synapses

(**Figure 4.2 C-D**). Together, this illustrates that Dystroglycan expression is exclusively localized to inhibitory synapses but not excitatory synapses in cerebellar cortex.

Dystroglycan is required for the formation and function of inhibitory synapses onto Purkinje cells

While recent work has shown that Dystroglycan is required for the formation and function of basket interneuron synapses onto pyramidal neurons in the hippocampus and cortex, our understanding of Dystroglycan's role at inhibitory cerebellar synapses remains incomplete due to the limited genetic tools available to manipulate cell populations prior to synapse formation in the cerebellum (Briatore et al., 2020; Früh et al., 2016; Jahncke et al., 2024). We recently identified *Calb1*^{Cre} as a tool for conditional deletion of *Dag1* from embryonic Purkinje cells prior to synaptogenesis, allowing us to investigate Dystroglycan's role in the initial formation of inhibitory synapses onto Purkinje

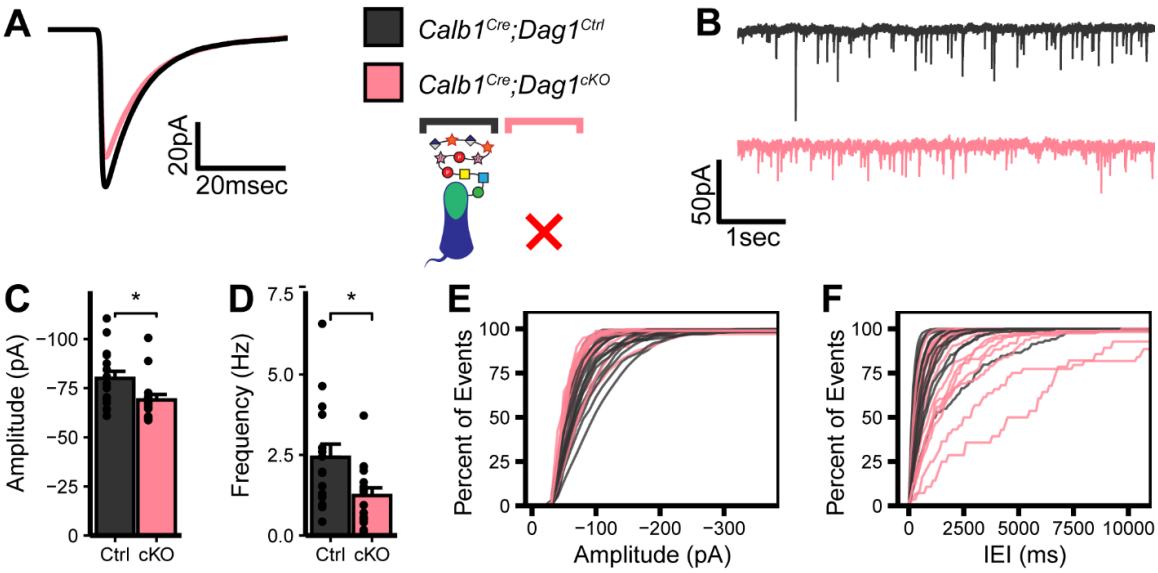

Figure 4.3 Impaired inhibitory synapse function in *Calb1*^{Cre}*;Dag1*^{cKO} Purkinje cells. **(A)** Average mIPSC event. **(B)** Representative 15 second trace of mIPSCs. **(C-D)** mIPSC amplitude **(C)** and frequency **(D)**; error bars are presented as mean + SEM. **(E-F)** Cumulative frequency histogram for individual mIPSC amplitudes **(E)** and inter-event intervals (IEI) **(F)**. *Calb1*^{Cre}*;Dag1*^{Ctrl} N = 16 cells, 6 animals. *Calb1*^{Cre}*;Dag1*^{cKO} N = 16 cells, 6 animals.

cells (**Chapter 3**). We crossed *Calb1*^{Cre}*;Dag1*$^{+/-}$ mice with a Dystroglycan conditional line (*Dag1*$^{flox/flox}$) to generate *Calb1*^{Cre}*;Dag1*$^{flox/-}$ conditional knockouts (*Calb1*^{Cre}*;Dag1*^{cKO}) and littermate *Calb1*^{Cre}*;Dag1*$^{flox/+}$ controls (*Calb1*^{Cre}*;Dag1*^{Ctrl}). Due to the restricted expression of *Cre* to Purkinje cells in the cerebellum, this approach allowed us to investigate the role of Dystroglycan at MLI:PC synapses in a cell-autonomous manner.

In order to assess inhibitory synapse function in *Calb1*^{Cre}*;Dag1*^{Ctrl} and *Calb1*^{Cre}*;Dag1*^{cKO} cerebella, we recorded mini inhibitory postsynaptic currents (mIPSCs) from Purkinje cells at P25. On average, *Calb1*^{Cre}*;Dag1*^{cKO} Purkinje cells exhibited reduced mIPSC amplitude and frequency compared to littermate controls (**Figure 4.3 A-F**). There was no observed difference in either mIPSC rise or decay time between control and conditional knockout Purkinje cells (**Table 4.1**), suggesting no substantial changes in GABAa receptor subtypes between genotypes. Reduced mini frequency is generally an indicator of a reduction in the number of synapses. Reduced mIPSC amplitude most likely reflects either (1) changes to postsynaptic receptor clustering, (2) altered subcellular distribution of synapses, or (3) reduced presynaptic quantal content. Recent work examining MLI:PC synapses in Dystrophin-deficient *mdx* mice, in which the intracellular component of the DGC is disrupted, found that quantal content was reduced at MLI:PC synapses in *mdx* mice, suggesting a presynaptic mechanism for altered

Table 4.1 mIPSC rise and decay kinetics.
Average mIPSC rise and decay times in milliseconds. Expressed as mean ± SEM. Ns are indicated in corresponding figure legends.

Experiment	$Rise_{Ctrl}$ (ms)	$Rise_{cKO}$ (ms)	$Rise_{p\text{-}val}$	$Decay_{Ctrl}$ (ms)	$Decay_{cKO}$ (ms)	$Decay_{p\text{-}val}$
Calb1^{Cre}*;Dag1*	0.73±0.05	0.79±0.05	0.4	7.87±0.39	8.77±0.62	0.23
Pcp2^{Cre}*;Dag1* (P25)	1.03±0.12	0.97±0.11	0.72	8.64±1.32	8.65±0.96	0.99
Pcp2^{Cre}*;Dag1* (P60)	0.93±0.1	0.96±0.07	0.82	7.59±0.55	7.78±0.55	0.81
Calb1^{Cre}*;Pomt2*	0.71±0.05	0.72±0.05	0.89	7.61±0.58	7.47±0.53	0.86
Calb1^{Cre}*;Dag1*$^{\Delta ICD}$	0.66±0.06	0.87±0.16	0.23	7.12±0.43	7.55±0.84	0.65

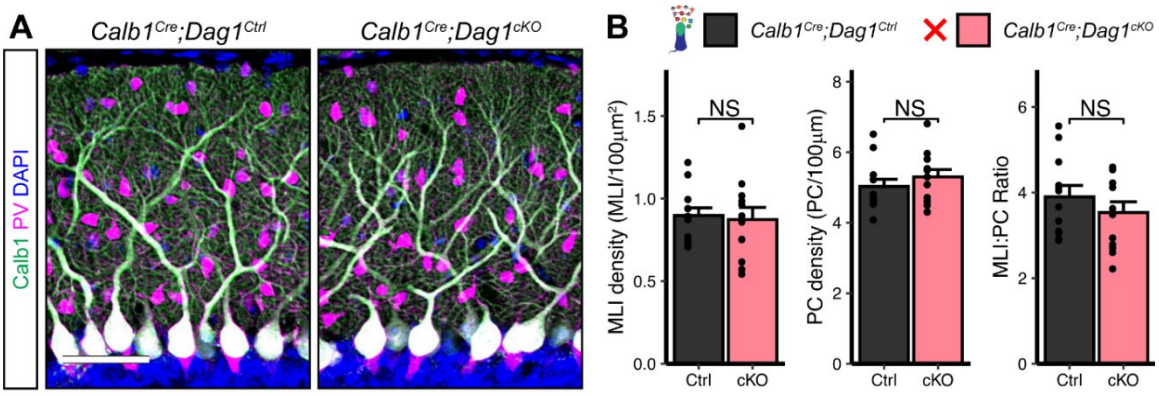

Figure 4.4 Purkinje and MLI cell counts are unchanged in *Calb1^{Cre};Dag1^{cKOs}*.
(A) *Calb1^{Cre};Dag1^{cKO}* and littermate controls immunostained for Calbindin (Purkinje cells, green) and Parvalbumin (Purkinje cells and MLIs, magenta). Nuclei are shown in blue. Images are maximum projections. Scale bar = 50µm. **(B)** Quantification of MLI density, Purkinje cell density, and the ratio of MLIs to Purkinje cells. Error bars represent mean + SEM. *Calb1^{Cre};Dag1^{Ctrl}* N = 12 ROIs, 6 images, 3 animals. *Calb1^{Cre};Dag1^{cKO}* N = 12 ROIs, 6 images, 3 animals.

mIPSC amplitude (Wu et al., 2022). However, postsynaptic receptor clustering was not examined in *mdx* mice and therefore remains a possible component of the reduced mIPSC amplitude.

To determine whether the observed synaptic deficits could be explained by fewer MLIs, we immunostained cerebellar tissue for Calbindin (Purkinje cells) and Parvalbumin (Purkinje cells and MLIs) and quantified Purkinje and MLI cell densities. There was no significant difference in Purkinje cell density, MLI density, or the ratio of MLIs to Purkinje cells (**Figure 4.4 A-B**), suggesting that the observed changes in synapse function were not due to defects in cellular proliferation or survival.

To evaluate potential structural correlates of the observed reduction in mIPSC frequency and amplitude, we immunostained for the presynaptic inhibitory synapse marker VGAT along with the inhibitory postsynaptic $GABA_A$ receptor subunit $GABA_A\alpha1$. Analysis of synaptic puncta in *Calb1^{Cre};Dag1^{cKO}* mice using conventional confocal microscopy with linear Wiener filter deconvolution revealed a small reduction in both VGAT and $GABA_A\alpha1$ puncta density compared to littermate controls (**Figure 4.5 A-C**),

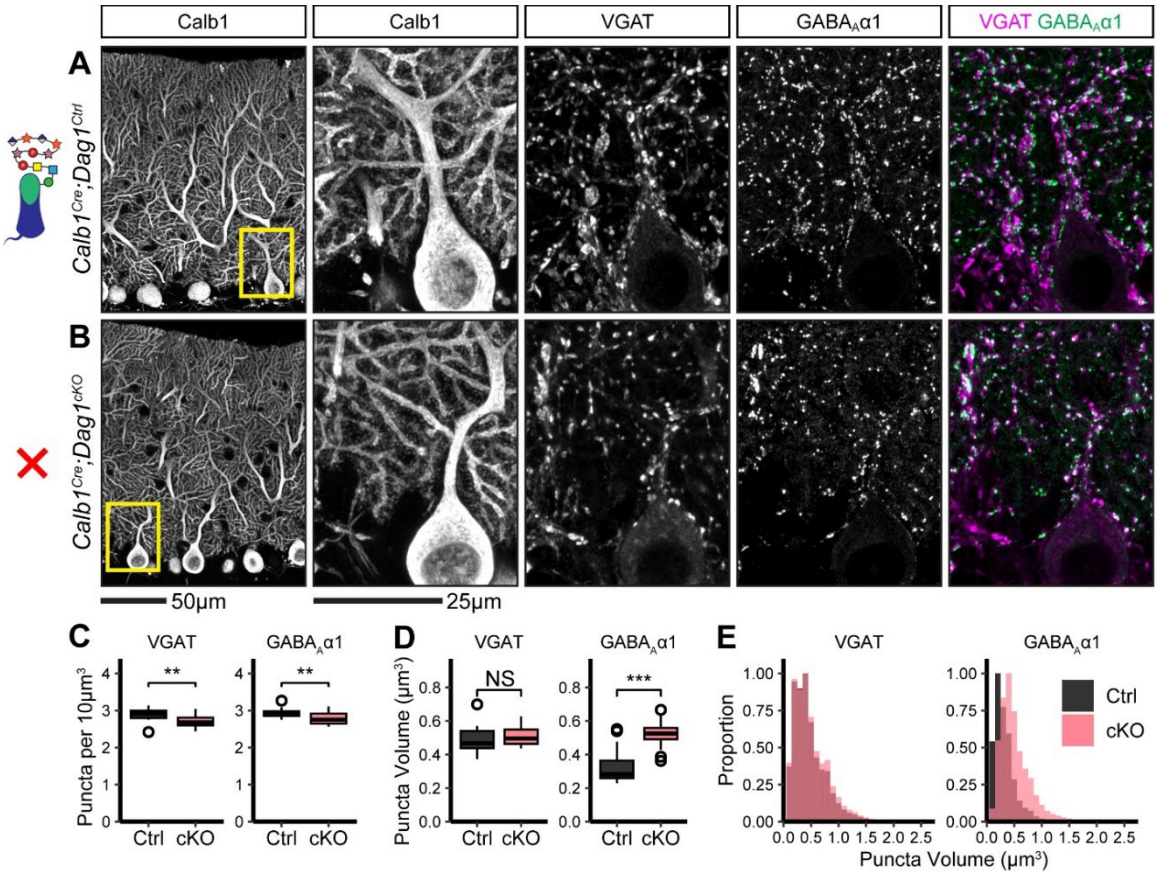

Figure 4.5 Inhibitory pre- and post-synaptic markers are altered in *Calb1^{Cre};Dag1^{cKO}* cerebellar cortex.

(A-B) Glyoxal perfused tissue from *Calb1^{Cre};Dag1^{cKOs}* **(B)** and littermate controls **(A)** was immunostained for Calbindin to visualize Purkinje cells along with the presynaptic marker VGAT (magenta) and postsynaptic $GABA_A$ receptor subunit $GABA_A\alpha1$ (green). The first panel shows a low-magnification view the Calbindin channel. Subsequent panels are magnified views of the yellow outlined region in the first panel. Images are maximum projections. **(C)** Quantification of VGAT (left) and $GABA_A\alpha1$ (right) puncta density (per 10µm^3). Open points indicate statistical outliers, however no datapoints were excluded from statistical analysis. **(D)** Quantification of VGAT (left) and $GABA_A\alpha1$ (right) puncta size (in µm^3). **(E)** Quantification of the distribution of VGAT (left) and $GABA_A\alpha1$ (right) puncta sizes (in µm^3), normalized to a maximum of 1. *Calb1^{Cre};Dag1^{Ctrl}* N = 20 images, 5 animals. *Calb1^{Cre};Dag1^{cKO}* N = 20 images, 5 animals.

supporting a reduction in synapse number. We also quantified synaptic puncta size and observed no change in VGAT puncta size but a significant increase in $GABA_A\alpha1$ puncta size (**Figure 4.5 D-E**), suggesting that Dystroglycan regulates the organization of the inhibitory postsynapse. The increase in puncta size may reflect a deficit in $GABA_A\alpha1$ receptor clustering, with $GABA_A$ receptors moving away from direct apposition to

subsynaptic release sites. This disruption in the alignment of synaptic microdomains could explain the observed reduction in mIPSC amplitude (Olah et al., 2023), however it does not rule out the contribution of pre-synaptic changes (Wu et al., 2022).

Dystroglycan is required for the long term maintenance of inhibitory MLI:PC synapses

The synaptic phenotypes observed following early deletion of *Dag1* from Purkinje cells using *Calb1*^{Cre} suggests that Dystroglycan is required for MLI axonal recognition of postsynaptic sites and subsequent synapse formation, similar to what we have reported for CCK^+/CB_1R^+ basket synapses in the hippocampus. Testing whether Dystroglycan is involved in the maintenance of synapses requires deleting *Dag1* after synapse formation. MLI:PC synapses begin forming around P7 and are largely formed by P14, with additional synaptogenesis extending past P21 (Morales and Hatten, 2006; Viltono et al., 2008; Wizeman et al., 2019). Recent work using *L7*^{Cre} to delete *Dag1* found that Dystroglycan was eliminated from Purkinje cells, with different rates across Purkinje cells, and wasn't fully absent from all Purkinje cells until P90. This prolonged localization of Dystroglycan at synapses in these mice likely reflects its high protein stability, which has a half-life of ~25 days in skeletal muscle (Novak et al., 2021). *L7*^{Cre}*;Dag1*^{cKOs} did exhibit impaired MLI:PC synapse function and a reduction in pre- and post-synaptic markers at P180, suggesting that Dystroglycan does indeed play a role in synapse maintenance (Briatore et al., 2020). To confirm this result, we used *Pcp2*^{Cre}, which expresses *Cre* in Purkinje cells gradually between P7-P14, to delete *Dag1* after synapse formation has initiated (**Chapter 3**). To reduce the amount of protein that has to be turned over, we generated compound mutants with one copy of *Dag1* constitutively deleted and the other copy flanked by LoxP sites for conditional deletion by *Cre*. *Pcp2*^{Cre}*;Dag1*$^{flox/-}$ conditional knockouts (*Pcp2*^{Cre}*;Dag1*^{cKO}) showed *Cre*-mediated

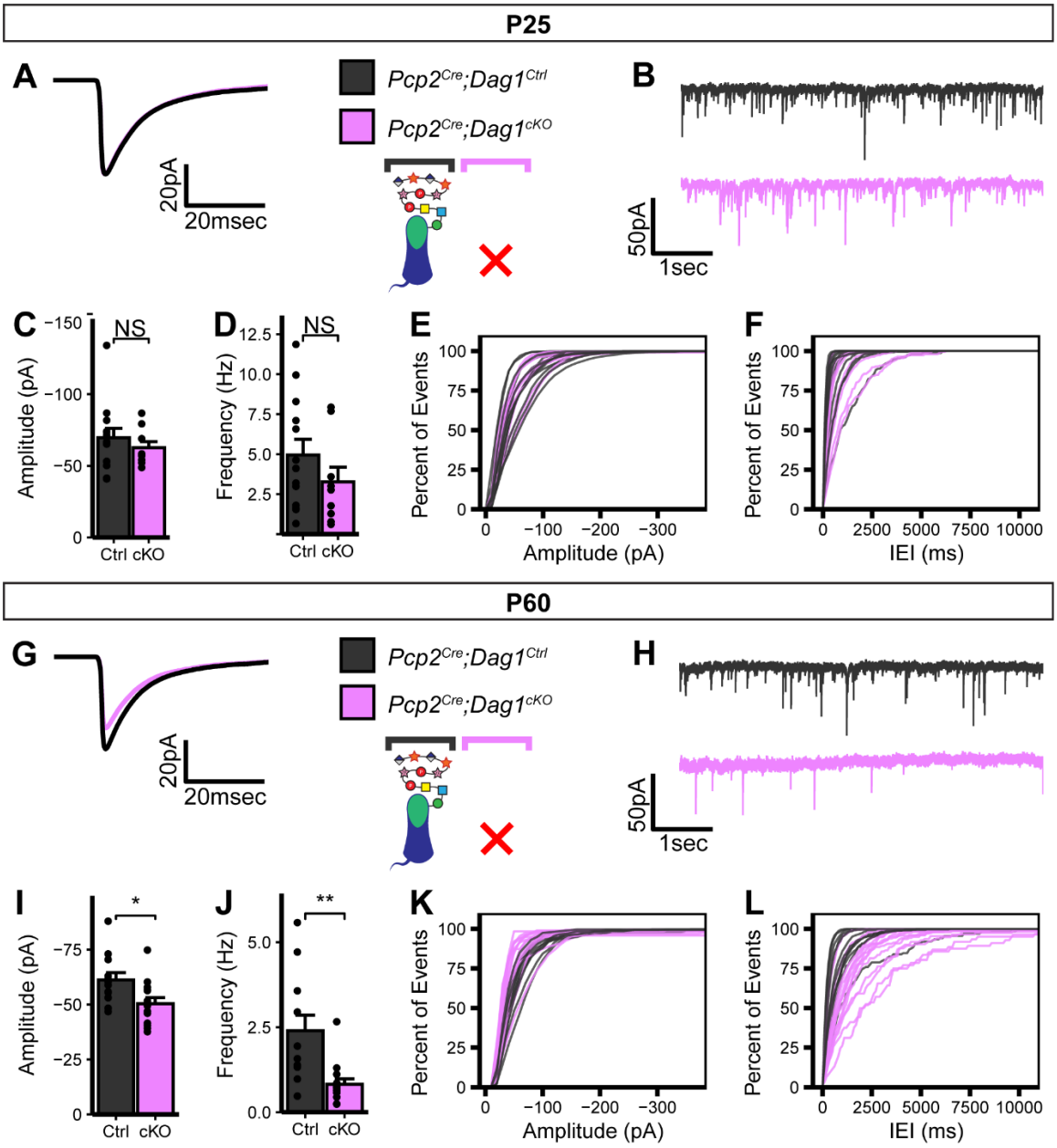

Figure 4.6 Impaired inhibitory synapse function in *Pcp2^{Cre};Dag1^{cKO}* Purkinje cells at P60 but not P25.

(A-F) mIPSC analysis in *Pcp2^{Cre};Dag1^{cKO}* and littermate control Purkinje cells at P25. **(A)** Average mIPSC event. **(B)** Representative 15 second trace of mIPSCs. **(C-D)** mIPSC amplitude **(C)** and frequency **(D)**; error bars are presented as mean + SEM. **(E-F)** Cumulative frequency histogram for individual mIPSC amplitudes **(E)** and inter-event intervals (IEI) **(F)**. **(G-L)** mIPSC analysis in *Pcp2^{Cre};Dag1^{cKO}* and littermate control Purkinje cells at P60. **(G)** Average mIPSC event. **(H)** Representative 15 second trace of mIPSCs. **(I-J)** mIPSC amplitude **(I)** and frequency **(J)**; error bars are presented as mean + SEM. **(K-L)** Cumulative frequency histogram for individual mIPSC amplitudes **(K)** and inter-event intervals (IEI) **(L)**. P25 *Pcp2^{Cre};Dag1^{Ctrl}* N = 13 cells, 5 animals. P25 *Pcp2^{Cre};Dag1^{cKO}* N = 9 cells , 5 animals. P60 *Pcp2^{Cre};Dag1^{Ctrl}* N = 12 cells, 5 animals. P60 *Pcp2^{Cre};Dag1^{cKO}* N = 14 cells , 4 animals.

recombination in all Purkinje cells at P14 and loss of Dystroglycan protein by P30 (**Chapter 3**).

The observed *Pcp2*^{Cre} recombination timeline is closely aligned with the synaptogenic period, and given the time course of protein turnover, is likely deleting *Dag1* soon after synapse formation. When we recorded mIPSCs from *Pcp2*^{Cre}*;Dag1*^{cKOs} at age P25, they showed no significant difference from littermate controls (**Figure 4.6 A-F**), suggesting that synapses remain functional without Dystroglycan in the short term. However, when we recorded mIPSCs from animals aged P60, we observed a reduction in mIPSC amplitude and frequency (**Figure 4.6 G-L**), indicating that Dystroglycan is indeed required for the long term maintenance of MLI:PC synapses.

Extracellular glycosylation of α-Dystroglycan is required for inhibitory synapse formation and function

The observed synaptic phenotypes in the absence of Dystroglycan are likely driven by a combination of (1) extracellular interactions mediated by the matriglycan chains on α-Dystroglycan interacting with binding partners in *cis* or *trans* and (2) intracellular protein-protein interactions or signaling cascades through the intracellular C-terminus of β-Dystroglycan. To distinguish which aspects of Dystroglycan's synaptic function is mediated by these distinct molecular mechanisms, we generated mice with Dystroglycan either (1) lacking extracellular glycosylation or (2) lacking the intracellular domain.

The extracellular alpha subunit of Dystroglycan contains *O*-mannosyl linked glycan chains with terminal -3Xylα1-3GlcAβ1- disaccharide repeats termed "matriglycan" that interacts with extracellular binding partners that contain LG domains (Goddeeris et al., 2013; Yoshida-Moriguchi and Campbell, 2015). In the hippocampal CA1, glycosylation of Dystroglycan is required for proper axon targeting and subsequent

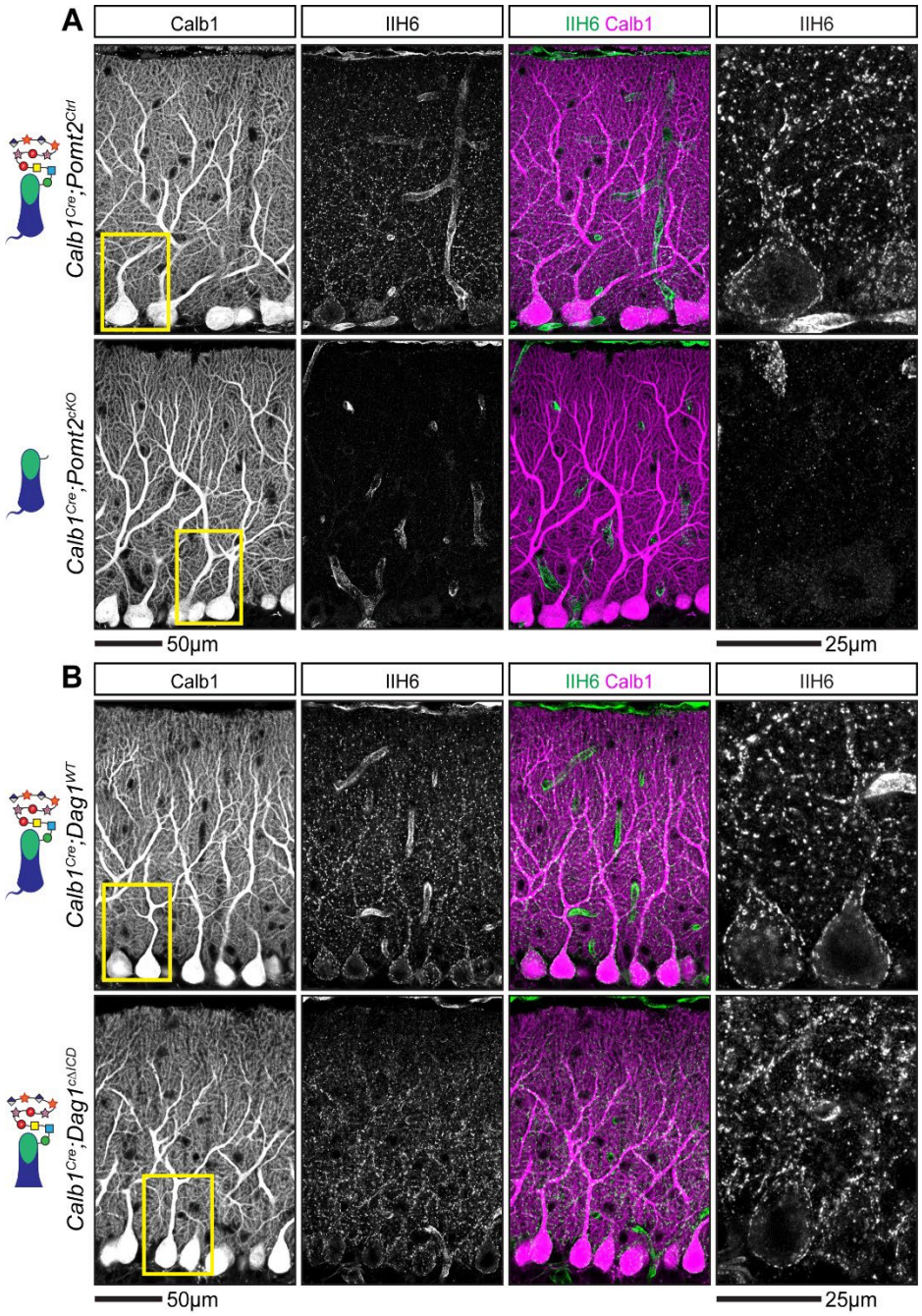

Figure 4.7 Localization of matriglycan chains on Dystroglycan in *Calb1^{Cre};Pomt2^{cKO}* and *Calb1^{Cre};Dag1^{cΔICD}* Purkinje cells.

(A-B) Cerebellar sections from *Calb1^{Cre};Pomt2^{cKOs}* and littermate controls **(A)** or *Calb1^{Cre};Dag1^{cΔICDs}* and littermate controls **(B)** were immunostained for Calbindin (magenta), to visualize Purkinje cells, along with IIH6 (green), to visualize matriglycan chains on Dystroglycan. The rightmost panel represents a magnified view of the area outlined in yellow in the leftmost low magnification panel. Images are maximum projections.

synapse function of CCK^+/CB_1R^+ basket interneurons, presumably through interactions with an unknown presynaptic cell adhesion molecule (Jahncke et al., 2024). We therefore wanted to investigate whether Purkinje cell Dystroglycan also requires interactions through its glycan chains for its synaptic function.

Pomt2, in a heterocomplex with Pomt1, is responsible for adding the initial *O*-mannose to Dystroglycan, and its deletion results in a complete loss of matriglycan chains (Manya et al., 2004). We used *Calb1*^{Cre} to conditionally delete the glycosyltransferase *Pomt2* (*Protein O-mannosyltransferase 2*) from Purkinje cells, generating *Calb1*^{Cre}*;Pomt2*$^{flox/flox}$ conditional knockouts (*Calb1*^{Cre}*;Pomt2*^{cKO}) and *Calb1*^{Cre}*;Pomt2*$^{flox/+}$ littermate controls (*Calb1*^{Cre}*;Pomt2*^{Ctrl}). Loss of Dag1 glycosylation was confirmed by immunostaining with the IIH6 antibody, which recognizes matriglycan. In contrast to the punctate synaptic staining pattern seen in *Calb1*^{Cre}*;Pomt2*^{Ctrl} Purkinje cells, *Calb1*^{Cre}*;Pomt2*^{cKO} Purkinje cells did not show any IIH6 immunoreactivity (**Figure 4.7 A**). We tested several potential antibodies against Dystroglycan core protein epitopes to confirm that loss of the glycan chains did not affect Dystroglycan's synaptic localization but were unable to see specific labeling on control experiments.

To assess MLI:PC synapse function in the absence of matriglycan chains on Dystroglycan, we conducted mIPSC recordings in P25 *Calb1*^{Cre}*;Pomt2*^{cKOs} Purkinje cells and littermate controls (**Figure 4.8 A-F**). Similar to the *Dag1* conditional knockouts, *Calb1*^{Cre}*;Pomt2*^{cKOs} exhibited a reduced mIPSC frequency compared to controls (**Figure 4.8 A-B**, **D**, **F**). However, mIPSC amplitude was normal (**Figure 4.8 C**, **E**). This suggests that extracellular glycosylation drives the frequency phenotype, at least in part, but is dispensable for the mIPSC amplitude phenotype observed in **Figure 4.3**.

Based on the reduced mIPSC frequency, we hypothesized that we would observe a reduction in inhibitory synapse density in *Calb1*^{Cre}*;Pomt2*^{cKOs} similar to that observed in *Calb1*^{Cre}*;Dag1*^{cKOs}. Indeed, both VGAT and $GABA_A\alpha1$ puncta density was

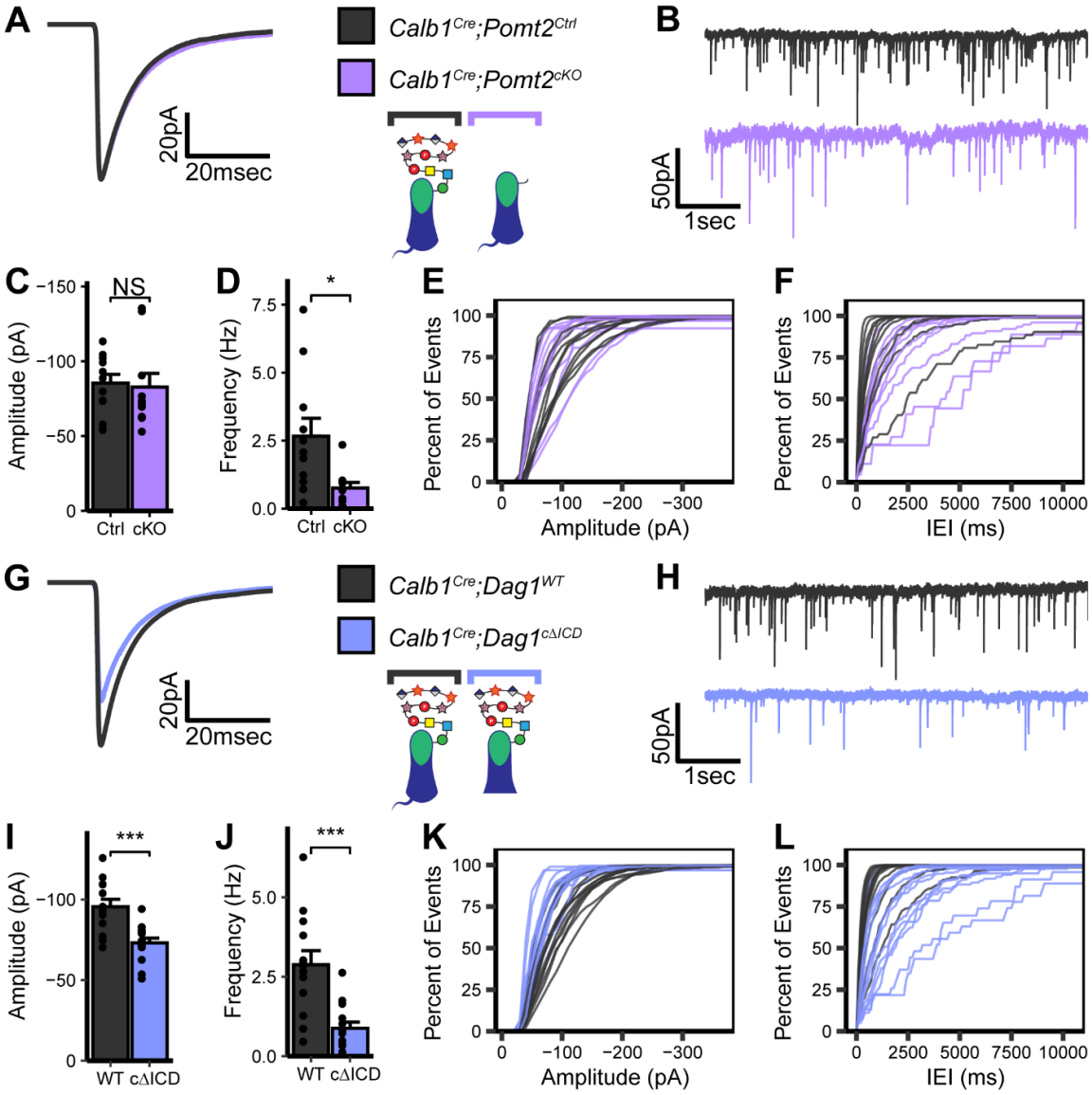

Figure 4.8 Impaired inhibitory synapse function in *Calb1^{Cre};Pomt2^{cKO}* and *Calb1^{Cre};Dag1^{cΔICD}* Purkinje cells.

(A-F) mIPSC analysis in *Calb1^{Cre};Pomt2^{cKO}* and littermate control Purkinje cells at P25. **(A)** Average mIPSC event. **(B)** Representative 15 second trace of mIPSCs. **(C-D)** mIPSC amplitude **(C)** and frequency **(D)**; error bars are presented as mean + SEM. **(E-F)** Cumulative frequency histogram for individual mIPSC amplitudes **(E)** and inter-event intervals (IEI) **(F)**. **(G-L)** mIPSC analysis in *Calb1^{Cre};Dag1^{cΔICD}* and littermate control Purkinje cells at P25. **(G)** Average mIPSC event. **(H)** Representative 15 second trace of mIPSCs. **(I-J)** mIPSC amplitude **(I)** and frequency **(J)**; error bars are presented as mean + SEM. **(K-L)** Cumulative frequency histogram for individual mIPSC amplitudes **(K)** and inter-event intervals (IEI) **(L)**. *Calb1^{Cre};Pomt2^{Ctrl}* N = 11 cells, 3 animals. *Calb1^{Cre};Pomt2^{cKO}* N = 10 cells , 4 animals. *Calb1^{Cre};Dag1^{WT}* N = 13 cells, 4 animals. *Calb1^{Cre};Dag1^{cΔICD}* N = 14 cells , 4 animals.

reduced in *Calb1*^{Cre}*;Pomt2*^{cKOs} compared to littermate controls (**Figure 4.9 A-C**). We also observed an increase in $GABA_A\alpha1$, but not VGAT, puncta size, similar to that observed in the *Dag1* conditional knockouts (**Figure 4.9 D-E**). As the *Pomt2* conditional knockouts did not exhibit a change in mIPSC amplitude (**Figure 4.8**), the increased $GABA_A\alpha1$ puncta size does not appear to be driving the amplitude reduction. Rather, the amplitude phenotype may be due to reduced presynaptic quantal size, similar to the mechanism in Dystrophin-deficient mice (Wu et al., 2022). However, it is clear that extracellular glycan-protein interactions are also important for regulating the size and organization of the inhibitory post-synapse.

The intracellular domain of β-Dystroglycan is required for inhibitory synapse function but not formation

The intracellular domain of Dystroglycan interacts directly with Dystrophin, which mediates interactions with the actin cytoskeleton and other scaffolding/signaling molecules. In a mouse model lacking brain isoforms of Dystrophin (*mdx*), recordings from Purkinje cells revealed reduced mIPSC frequency and amplitude, which are accompanied by reduced $GABA_A\alpha1$ receptor puncta density, and a reduction in the number of MLI:PC contacts, showing that Dystrophin is required for inhibitory Purkinje cell synapses in a manner similar to Dystroglycan (Anderson et al., 2003; Grady et al., 2006; Knuesel et al., 1999; Kueh et al., 2011, 2008; Wu et al., 2022). Mice lacking the cytoplasmic portion of Dystroglycan that interacts with Dystrophin develop muscular dystrophy but exhibit largely normal neural development (Satz et al., 2010). Recently, however, it was shown that cytoplasmic deletion mutants exhibit synaptic deficits at inhibitory hippocampal CCK^+/CB_1R^+ basket synapses (Jahncke et al., 2024). We therefore hypothesized that in addition to extracellular Dystroglycan glycosylation, the intracellular domain of Dystroglycan may also be required for MLI:PC synapse function.

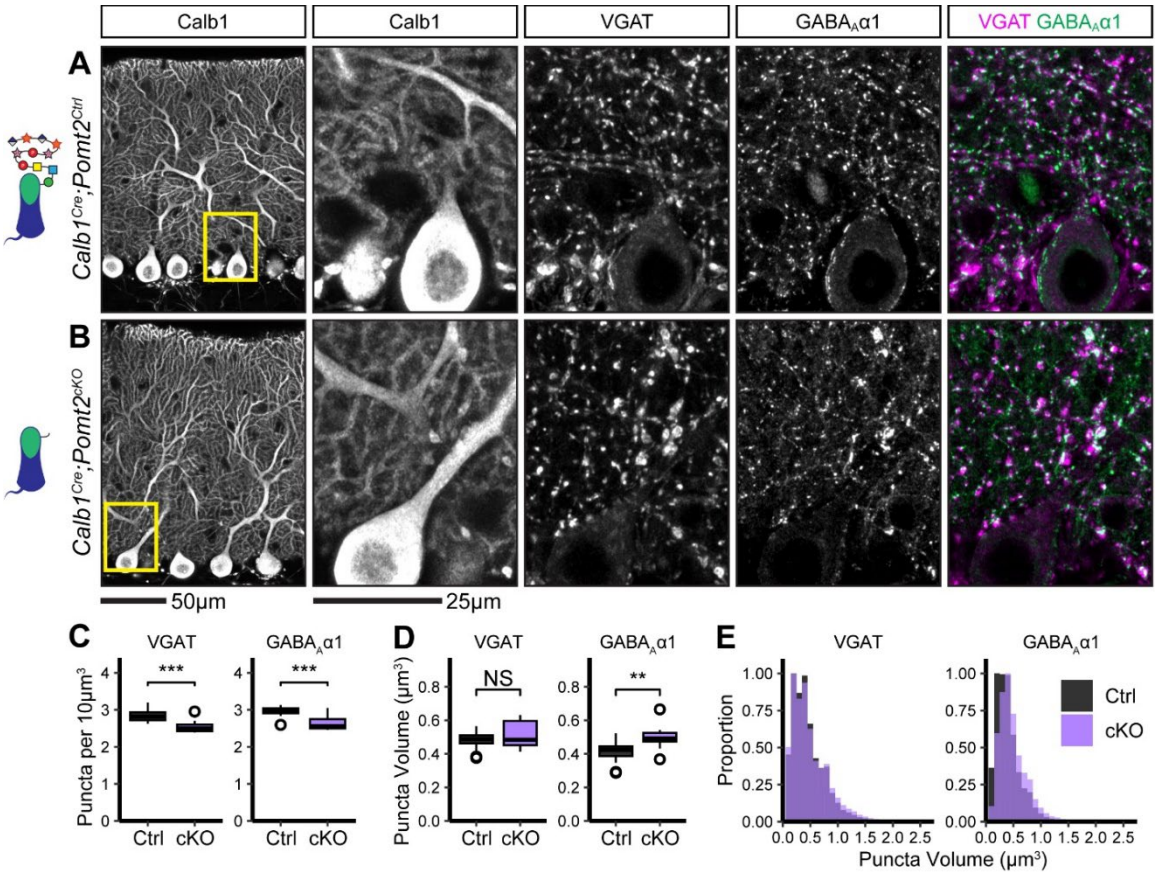

Figure 4.9 Inhibitory pre- and post-synaptic markers are altered in *Calb1^{Cre};Pomt2^{cKO}* cerebellar cortex.

(A-B) Glyoxal perfused tissue from *Calb1^{Cre};Pomt2^{cKOs}* **(B)** and littermate controls **(A)** was immunostained for Calbindin to visualize Purkinje cells along with the presynaptic marker VGAT (magenta) and postsynaptic GABA$_A$ receptor subunit GABA$_A$α1 (green). The first panel shows a low-magnification view of the Calbindin channel. Subsequent panels are magnified views of the yellow outlined region in the first panel. Images are maximum projections. **(C)** Quantification of VGAT (left) and GABA$_A$α1 (right) puncta density (per 10μm^3). Open points indicate statistical outliers, however no datapoints were excluded from statistical analysis. **(D)** Quantification of VGAT (left) and GABA$_A$α1 (right) puncta size (in μm^3). **(E)** Quantification of the distribution of VGAT (left) and GABA$_A$α1 (right) puncta sizes (in μm^3), normalized to a maximum of 1. *Calb1^{Cre};Pomt2^{Ctrl}* N = 16 images, 4 animals. *Calb1^{Cre};Pomt2^{cKO}* N = 12 images, 3 animals.

To investigate the role of the intracellular domain of Dystroglycan at MLI:PC synapses, we generated conditional cytoplasmic domain mutants by crossing *Calb1^{Cre};Dag1$^{flox/+}$* mice with mice expressing one copy of truncated Dystroglycan lacking the intracellular domain (*Dag1$^{ΔICD/+}$*) to generate *Calb1^{Cre};Dag1$^{flox/ΔICD}$* mutants (*Calb1^{Cre};Dag1^{cΔICD}*) and *Calb1^{Cre};Dag1$^{+/+}$* littermate controls (*Calb1^{Cre};Dag1^{WT}*). Immunohistochemistry with IIH6

showed that *Calb1^{Cre};Dag1^{cΔICD}* mutants maintained synaptic localization of glycosylated Purkinje cell Dystroglycan in the absence of the intracellular domain (**Figure 4.7 B**).

To measure the contribution of the intracellular domain of Dystroglycan to MLI:PC synapse function we conducted mIPSC recordings from P25 *Calb1^{Cre};Dag1^{cΔICD}* Purkinje cells and those of littermate controls (**Figure 4.8 G-L**). We found a phenotype that resembled that of *Calb1^{Cre};Dag1^{cKO}* Purkinje cell mIPSCs: a reduction in both mIPSC amplitude and frequency (**Figure 4.8 G-L**). We therefore conclude that the amplitude component of Dystroglycan-containing MLI:PC synapses is governed by intracellular interactions between Dystroglycan and other postsynatpic proteins (likely including Dystrophin) and/or intracellular signaling initiated by the C-terminus of β-Dystroglycan. The mIPSC frequency component in Purkinje cells, however, appears to be influenced by factors dictated by both extracellular glycan-protein interactions and intracellular interactions or signaling.

Due to the reduction in mIPSC frequency observed in *Calb1^{Cre};Dag1^{cΔICD}* Purkinje cells (**Figure 4.8 J**, **L**), we hypothesized that we would see a similar reduction in inhibitory synapse density in *Calb1^{Cre};Dag1^{cΔICD}* as that observed in *Calb1^{Cre};Dag1^{cKO}* (**Figure 4.5 C**) and *Calb1^{Cre};Pomt2^{cKO}* (**Figure 4.9 C**) Purkinje cells. To our surprise, we instead found no change in the density of presynaptic VGAT puncta and a slight increase in the density of postsynaptic $GABA_A$α1 puncta (**Figure 4.10 A-C**). Therefore, loss of the intracellular domain of Dystroglycan did not affect presynapse formation but did slightly perturb postsynapse formation. There was no change in the size of synaptic puncta in *Calb1^{Cre};Dag1^{cΔICD}* compared to littermate controls (**Figure 4.10 D-E**).

In the absence of a reduction in synapse density we are left to assume that the reduced mIPSC frequency we observed in *Calb1^{Cre};Dag1^{cΔICD}* Purkinje cells is due to alterations to the synapse other than simply synapse number. Previous work involving paired recordings between coupled MLI and Purkinje cell pairs in Dystrophin-deficient

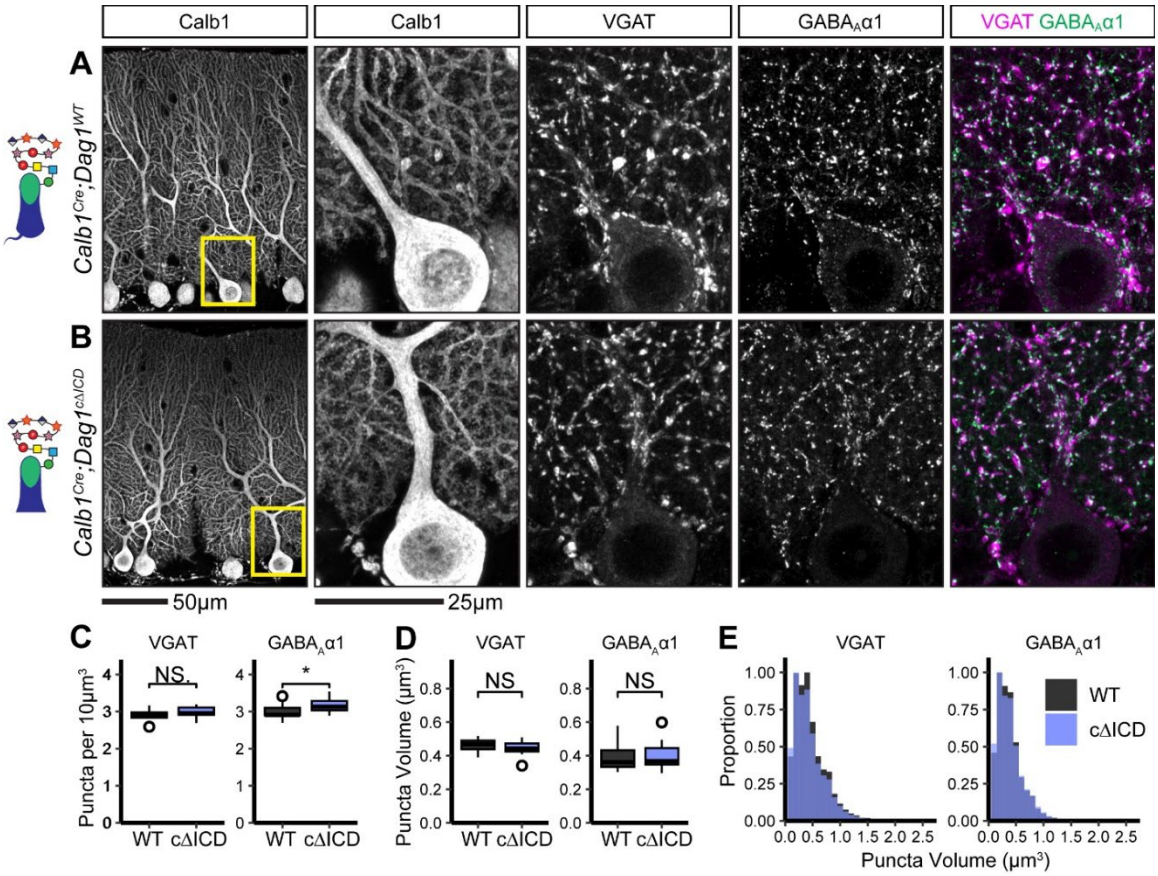

Figure 4.10 Inhibitory pre- and post-synaptic markers are relatively normal in *Calb1^{Cre};Dag1^{cΔICD}* cerebellar cortex.

(A-B) Glyoxal perfused tissue from *Calb1^{Cre};Dag1^{cΔICDs}* **(B)** and littermate controls **(A)** was immunostained for Calbindin to visualize Purkinje cells along with the presynaptic marker VGAT (magenta) and postsynaptic $GABA_A$ receptor subunit $GABA_Aα1$ (green). The first panel shows a low-magnification view of the Calbindin channel. Subsequent panels are magnified views of the yellow outlined region in the first panel. Images are maximum projections. **(C)** Quantification of VGAT (left) and $GABA_Aα1$ (right) puncta density (per 10μm^3). Open points indicate statistical outliers, however no datapoints were excluded from statistical analysis. **(D)** Quantification of VGAT (left) and $GABA_Aα1$ (right) puncta size (in μm^3). **(E)** Quantification of the distribution of VGAT (left) and $GABA_Aα1$ (right) puncta sizes (in μm^3), normalized to a maximum of 1. *Calb1^{Cre};Dag1^{WT}* N = 13 images, 3 animals. *Calb1^{Cre};Dag1^{cKO}* N = 13 images, 3 animals.

mdx mice has revealed an increase in the number of failures in Purkinje cell responses to MLI firing (Wu et al., 2022). A similar mechanism could explain the reduced mIPSC frequency in *Calb1^{Cre};Dag1^{cΔICD}* Purkinje cells (**Figure 4.8 J**, **F**). The intracellular domain of Dystroglycan interacts directly with Dystrophin, so a common mechanism between the *mdx* and *Calb1^{Cre};Dag1^{cΔICD}* models is plausible (Jung et al., 1995). While it is clear that

additional work will be necessary to determine the details underlying the observed phenotypes, these data show for the first time that the intracellular domain of Dystroglycan plays a crucial role in MLI:PC synapse function but not formation.

Discussion

Prior to this study, it was unknown whether Dystroglycan was required for synaptogenesis at MLI:PC synapses. Previous work used the *L7^{Cre}* line to delete *Dag1* from Purkinje cells, which did not achieve complete loss of Dystroglycan protein until P90, limiting the study to the role of Dystroglycan in long-term synapse maintenance (**Chapter 3**) (Briatore et al., 2020). Nevertheless, it was determined that Dystroglycan is indeed required for synapse maintenance, as the *L7^{Cre};Dag1$^{flox/flox}$* Purkinje cells showed a decreased inhibitory synapse density and decreased mIPSC frequency and amplitude (Briatore et al., 2020). We confirmed these results using *Pcp2^{Cre}* mated with mice in which only one copy of *Dag1* needed to be excised (*Dag1$^{flox/-}$*), achieving complete loss of Dystroglycan by P30 (**Chapter 3**). We observed similarly impaired synapse function in *Pcp2^{Cre};Dag1$^{flox/-}$* (*Pcp2^{Cre};Dag1^{cKO}*) Purkinje cells (**Figure 4.6 G-L**), confirming Dystroglycan's role in MLI:PC synapse maintenance.

Curiously, mIPSC recordings in *Pcp2^{Cre};Dag1^{cKO}* Purkinje cells at P25, in which *Dag1* is deleted from most cells and most protein turned over, showed no significant impact on MLI:PC function (**Figure 4.6 A-F**). There are two potential explanations for this result: (1) synapses remain stable for some period of time (most likely on the order of days to a couple weeks) after Dystroglycan protein is eliminated, or (2) the amount of Dystroglycan protein remaining at P30 is below the detection threshold for immunohistochemistry, but sufficient to maintain synapse function.

With the identification of *Calb1^{Cre}* as a tool for the deletion of genes from Purkinje cells early in development, we have now been able to test for the first time whether

Dystroglycan is required for synapse formation at MLI:PC synapses (Daigle et al., 2018) **Chapter 3**. We indeed found that MLI:PC function is impaired in *Calb1*^{Cre}*;Dag1*^{cKO} (**Figure 4.3 A-F**) at P25, which was accompanied by a reduction in inhibitory synapse density (**Figure 4.5 A-C**), illustrating that synapses are not able to form normally in the absence of Dystroglycan. Furthermore, we identified that extracellular glycosylation of Dystroglycan is required for its role in both synapse formation and function (**Figure 4.8 A-F, Figure 4.9**) while the intracellular domain is required only for synapse function but not formation (**Figure 4.8 G-L**, **Figure 4.10**) – an important first step towards understanding the mechanism through which Dystroglycan acts at MLI:PC synapses.

A Dag1:Nrxn:Nlgn molecular complex to shape MLI:PC synapse function

Dystroglycan is known to biochemically interact with presynaptic Neurexins in a glycosylation-dependent manner, and Dystroglycan:Neurexin-3 interactions regulate inhibitory synapse function in the olfactory bulb and medial prefrontal cortex (Reissner et al., 2014; Sugita et al., 2001; Trotter et al., 2023). However whether this occurs at MLI:PC synapses has not yet been examined. Neurexins also interact with postsynaptic Neuroligins, and Neuroligin-2 (Nlgn2) localization is reduced at somatic MLI:PC synapses in Purkinje cell *Dag1* conditional knockouts (Briatore et al., 2020; Nguyen and Südhof, 1997). In turn Neuroligin is thought to be linked to the intracellular domain of β-Dystroglycan through S-SCAM/MAGI-2 (Sumita et al., 2007). Thus, Dystroglycan can interact directly and indirectly with Neurexins and Neuroligins in a network of pre- and post-synaptic cell adhesion complexes.

Synapse formation occurs in multiple phases: a presynaptic axon must first recognize its postsynaptic target through some sort of recognition cue, after which pre- and post-synaptic molecules are recruited to the nascent synapse. The precise content of molecules can change over the lifetime of a synapse in response to activity. Some

molecules may be required only for the recruitment of synaptic components, some only for maintaining molecules at the synapse, and some for both. Presynaptic Neurexins are undoubtedly critical for the maintenance of functional synapses and the interaction between Neurexin and Nlgn2 is likely a prominent component of maintaining function at MLI:PC synapses. Similar to our observations (**Figure 4.3**, **Figure 4.5**), triple conditional knockout of *Neuroligin1/2/3* has been shown to increase in inhibitory MLI:PC synaptic puncta size and reduce Purkinje cell mIPSC frequency and amplitude (Zhang et al., 2015). This effect was not observed in *Nlgn1/Nlgn3* double knockout but was seen in *Ngln2/Nlgn3* double knockout. A *Nlgn2* constitutive knockout, however, only partially recapitulated these results, suggesting that Nlgn2 is the primary driver of this phenotype, but that some degree of molecular compensation can occur in its absence (Zhang et al., 2015).

Neither Neurexin nor Neuroligin are generally thought to be required for synaptogenesis. Although Neurexin or Neuroligin manipulations can lead to many different synaptic phenotypes, typically a constitutive or developmentally early knockout of either protein results in impaired synapse function without a decrease in synapse number, suggesting that postsynaptic partner recognition and synaptogenesis does not rely on Neurexin or Neuroligin (Liang et al., 2015; Missler et al., 2003; Trotter et al., 2023; Varoqueaux et al., 2006; Zhang et al., 2015). Dystroglycan, on the other hand, appears to be required for both the initial formation of a synapse and its maintenance. Developmentally early deletion of *Dag1* results in a loss of synapses and reduced synaptic function (**Figure 4.3**, **Figure 4.5**) (Früh et al., 2016; Jahncke et al., 2024). Similarly, later deletion of *Dag1* also impacts synapse function, showing it is also required for synapse maintenance (**Figure 4.6**) (Briatore et al., 2020).

Together with evidence from other Dystroglycan-expressing synaptic systems (Früh et al., 2016; Jahncke et al., 2024; Miller and Wright, 2021; Trotter et al., 2023), our

data suggests that Dystroglycan acts as a synaptic recognition molecule for axon targeting of the postsynaptic compartment at MLI:PC synapses, after which the role of Dystroglycan switches to one of postsynaptic molecule recruitment and stabilization. While the glycan-protein interaction between Dystroglycan and Neurexin is likely instructive of the stabilization of the synapse, the presynaptic ligand of Dystroglycan during axon targeting of the postsynapse remains unknown.

Refining the mechanism of Dystroglycan's contributions to synapse function

Our finding that extracellular glycosylation of α-Dystroglycan is required for Dystroglycan's role in both synaptogenesis and synapse function (**Figure 4.8**, **Figure 4.9**) is in agreement with our previous work that illustrated that a forebrain deletion of *Pomt2* shows similar deficits in hippocampal CCK^+/CB_1R^+ basket synapse formation and function as forebrain deletion of *Dag1* (Jahncke et al., 2024). While removal of *Pomt2* results in loss of all *O*-mannosyl linked glycosylation on Dystroglycan (**Figure 4.7 A**) (Manya et al., 2004), the critical domain that mediates all known extracellular interactions is the terminal portion of the glycan chain in which the glycosyltransferase *LARGE1 e*longates repeats of a -3Xylα1-3GlcAβ1- disaccharide referred to as matriglycan (Briggs et al., 2016; Inamori et al., 2012). Because matriglycan is extended in long repeated chains, Dystroglycan is capable of binding multiple proteins simultaneously, allowing for large complexes to form (Goddeeris et al., 2013; Sheikh et al., 2022). Purkinje cell matriglycan migrates at a higher molecular weight than other populations of matriglycan, suggesting that Purkinje cell Dystroglycan contains longer matriglycan chains with increased binding capacity (Satz et al., 2010).

The presumed presynaptic partner at MLI:PC synapses is Neurexin, though exactly which isoform will need to be determined as all three Neurexins are expressed by MLIs (Kozareva et al., 2021; Saunders et al., 2018). There could also be additional

undescribed synaptic proteins that bind Dystroglycan in *trans* or *cis* as part of the inhibitory synaptic complex. Extracellular glycan-protein interactions with Dystroglycan have been between matriglycan and a Laminin G (LG) domain-containing protein. Neurexins each contain multiple LG domains and bind to Dystroglycan in a glycosylation-dependent manner in biochemical assays. However, there are upwards of 20 other LG domain-containing proteins expressed in cerebellar cellular populations that are candidate extracellular binding partners of Dystroglycan. Isolation of Dystroglycan-containing complexes to identify its potential synaptic partners is complicated by the ubiquitous expression of Dystroglycan among many cell types in the brain, with neuronal Dystroglycan representing the minority of total Dystroglycan. A conditional tagged Dystroglycan transgenic mouse could alleviate current limitations, though identifying a candidate site for tag insertion on Dystroglycan represents its own challenge as the extracellular domain is essential for glycosylation and the intracellular domain is essential for intracellular interaction with Dystrophin and both features are required for normal synapse function.

The intracellular domain of Dystroglycan was long thought to be dispensable for neuronal functions as mice lacking the intracellular domain of Dystroglycan exhibit normal cellular migration and axon targeting (Jahncke et al., 2024; Lindenmaier et al., 2019; Satz et al., 2010). However, we recently found that hippocampal CCK^+/CB_1R^+ basket cells have slightly impaired perisomatic axon targeting and exhibit impaired synapse function despite normal synapse formation when the intracellular domain is deleted (Jahncke et al., 2024). In the present study we similarly found impaired synapse function (**Figure 4.8 G-L**) despite relatively normal MLI:PC synapse formation (**Figure 4.10**) in our $Calb1^{Cre};Dag1^{c\Delta ICD}$ mice. Not only do these new findings confirm the role of the cytoplasmic domain in synapse function, it illustrates the cell autonomous nature of

the mechanism as the *Calb1*^{Cre} mutation is restricted to Purkinje cells within the cerebellum whereas previous work utilized constitutive intracellular domain mutations.

While intracellular interactions with Dystroglycan remain poorly described, the prevailing interaction contributing to MLI:PC synapse function is likely between Dystroglycan and Dystrophin (Dmd). Dystroglycan and Dystrophin interact directly through the intracellular domain of Dystroglycan (Rosa et al., 1996; Suzuki et al., 1994). There is extensive literature supporting a role for Dystrophin at MLI:PC synapses (Anderson et al., 2003; Briatore et al., 2020; Gao and McNally, 2015; Knuesel et al., 1999; Kueh et al., 2011, 2008; Wu et al., 2022). Similar to our data in *Calb1*^{Cre}*;Dag1*$^{c\Delta ICD}$ Purkinje cells (**Figure 4.8 G-L**), the Dystrophin-deficient *mdx* mouse exhibits impaired mIPSC frequency and amplitude (Anderson et al., 2003; Kueh et al., 2011, 2008; Wu et al., 2022).

The similarity in functional defects observed in *Calb1*^{Cre}*;Dag1*$^{c\Delta ICD}$ and *mdx* Purkinje cells supports a model wherein a Dag1:Dmd interaction is critical for MLI:PC synapse function. Paired recordings between MLIs and PCs in *mdx* mice revealed an increase in the failure rate, in which an action potential elicited in an MLI did not elicit a detectable IPSC in the postsynaptic Purkinje cell at a rate higher than observed in wild-type controls (Wu et al., 2022). An increased failure rate could account for the reduced mIPSC frequency that we observed in *Calb1*^{Cre}*;Dag1*$^{c\Delta ICD}$ Purkinje cells in the absence of a change in synapse numbers (**Figure 4.8 G-L**, **Figure 4.10**). Wu et al. did not observe a change in paired pulse ratio (PPR) in *mdx* Purkinje cells, suggesting that release probability does not explain the increased failure rate. Instead, it was determined that the size of the readily releasable pool (RRP) and the quantal content were both reduced (Wu et al., 2022). Future studies using MLI:PC paired recordings in *Calb1*^{Cre}*;Dag1*$^{c\Delta ICD}$ mice will inform whether the same mechanism is at play.

Molecular diversity among MLI:PC synapses

Classically, MLI:PC synapses are thought to comprise basket and stellate cell synapses with the basket cells synapsing onto the Purkinje cell soma and proximal dendrites and stellate cell synapsing onto the distal dendrites. However, the molecular composition and functional roles of these two classes of synapses remain largely uncharacterized and there are likely more than just two classes of synapses that arise from the two morphological classes of MLIs (Kozareva et al., 2021; Lackey et al., 2023; Park et al., 2023; Wang and Lefebvre, 2022). Recent work has started to try to classify MLI:PC synapses with more precision. IIH6 immunoreactivity shows Dystroglycan localized at synaptic puncta on Purkinje cell somata and throughout the entirety of the molecular layer, suggesting it is likely present at multiple classes of MLI synapses (**Figure 4.1**, **Figure 4.2**).

While we observed a reduction in both VGAT and $GABA_A\alpha1$ puncta in $Calb1^{Cre};Dag1^{cKOs}$ throughout the Purkinje cell layer and molecular layer, the reduction on the surface of the Purkinje cell soma was particularly striking, especially so for the postsynaptic $GABA_A\alpha1$ receptor subunit ($Calb1^{Cre};Dag1^{Ctrl}$ = 2.69 ± 0.053 puncta/10 μm^3, $Calb1^{Cre};Dag1^{cKO}$ = 2.12 ± 0.097 puncta/10 μm^3, p = 0.000016) (**Figure 4.5 A-B**). One unique molecular feature of somatic MLI:PC synapses is that they lack the inhibitory postsynaptic scaffolding molecule Gephyrin (Viltono et al., 2008). Therefore, Dystroglycan may function as the primary postsynaptic scaffolding molecule at somatic MLI:PC synapses, where it is responsible for recruiting and/or stabilizing $GABA_A$ receptors apposed to presynaptic sites.

Interestingly, $Calb1^{Cre};Pomt2^{cKOs}$ showed a reduction in somatic $GABA_A\alpha1$ receptor subunits ($Calb1^{Cre};Pomt2^{Ctrl}$ = 2.45 ± 0.072 puncta/10 μm^3, $Calb1^{Cre};Pomt2^{cKO}$ = 2.14 ± 0.096 puncta/10 μm^3, p = 0.017) (**Figure 4.9 A-B**) while $Calb1^{Cre};Dag1^{c\Delta ICDs}$ did not ($Calb1^{Cre};Dag1^{WT}$ = 2.59 ± 0.122 puncta/10 μm^3, $Calb1^{Cre};Dag1^{c\Delta ICD}$ = 2.44 ± 0.148

puncta/10 μm^3, p = 0.43) (**Figure 4.10 A-B**). This suggests that a trans-synaptic mechanism regulates somatic $GABA_A$ receptor synaptic localization. While $GABA_A$ receptors are typically thought to be anchored to the post-synapse through Gephyrin, at the Gephyrin-lacking somatic MLI:PC synapses there may be an undescribed secondary interaction linking Dystroglycan, along with the Nrxn:Nlgn complex, to $GABA_A$ receptors. It has been reported that Neurexin can interact directly with $GABA_A$ receptors, providing one possible alternative avenue (Zhang et al., 2010).

While somatic MLI:PC synapses are a striking example of Gephyrin-independent Dystroglycan-containing synapses, Gephyrin is not thought to be present at all Dystroglycan-containing synapses. Unfortunately there have been very few studies that have examined Dystroglycan and Gephyrin localization together and, to our knowledge, this has not been examined at PC:MLI synapses (Lévi et al., 2002; Trotter et al., 2023). However, recent work showed that *L7^{Cre};Dag1$^{flox/flox}$* mice exhibit a reduction in Gephyrin puncta density at MLI:PC synapses, suggesting that there may be more of a relationship between Gephyrin and Dystroglycan than previously believed (Briatore et al., 2020). Together, this suggests that that there is more molecular diversity among MLI:PC synapses than currently appreciated and leaves much work to be done.

Conclusion

We show that Dystroglycan is localized to inhibitory MLI:PC synapses but not excitatory parallel fiber or climbing fiber synapses. At MLI:PC synapses, Dystroglycan is required for both synapse formation and maintenance, and is necessary for synapse function, reaffirming Dystroglycan's role as a critical synaptic organizer. Extracellular glycosylation is required for both synapse formation and function, whereas the intracellular domain of Dystroglycan is required for synapse function but not formation.

Together, these results illustrate for the first time that Dystroglycan is required for the early formation of MLI:PC synapses in a cell autonomous manner and begin to inform the mechanism through which Dystroglycan performs this function.

Materials and Methods

Animal Husbandry

All animals were housed and cared for by the Department of Comparative Medicine (DCM) at Oregon Health and Science University (OHSU), an AAALAC-accredited institution. Animal procedures were approved by OHSU Institutional Animal Care and Use Committee (Protocol # IS00000539), adhered to the NIH *Guide for the care and use of laboratory animals*, and provided with 24-hour veterinary care. Animal facilities are regulated for temperature and humidity and maintained on a 12-hour light-dark cycle and were provided food and water *ad libitum*. Mice were used between ages P21-P60 (as indicated in the text or figure legend). Mice were euthanized by administration of CO_2 followed by exsanguination.

Mouse Strains and Genotyping

The day of birth was designated postnatal day 0 (P0). Ages of mice used for each analysis are indicated in the figure and figure legends. Mouse strains used in this study have been previously described and were obtained from Jackson Labs, unless otherwise indicated (**Table 4.2**). Breeding schemas are as described in **Table 4.3**. Where possible, mice were maintained on a C57BL/6 background. The *Dag1*$^{\Delta ICD}$ line was outcrossed to a CD-1 background for one generation to increase the viability of mutant pups. The *Dag1*$^{\Delta ICD}$ line was then backcrossed to C57BL/6 breeders for 3 generations before performing experiments. *Dag1*$^{+/-}$ mice were generated by crossing

the *Dag1*$^{flox/flox}$ line to a *Sox2*^{Cre} line to generate germline *Dag1*$^{\Delta/+}$ mice hereafter referred to as *Dag1*$^{+/-}$ as the resultant transcript is nonfunctional. These mice were thereafter maintained as heterozygotes. Genomic DNA extracted from toe or tail samples using the HotSHOT method (Truett et al., 2000) was used to genotype animals. Primers for genotyping can be found on the JAX webpage or originating article. *Dag1*$^{+/-}$ mice were genotyped with the following primers: CGAACACTGAGTTCATCC (forward) and CAACTGCTGCATCTCTAC (reverse). For each mouse strain, littermate controls were used for comparison with mutant mice. For all experiments mice of both sexes were used indiscriminately.

Table 4.2 Mouse strains

Common name	Strain name	Reference	Stock #
Calb1-IRES2-Cre	B6;129S-Calb1tm2.1(cre)Hze/J	(Daigle et al., 2018)	028532
Pcp2-IRES-Cre	B6.Cg-Tg(Pcp2-cre)3555Jdhu/J	(Zhang et al., 2004)	010536
Dag1^{flox}	*B6.129(Cg)-Dag1*$^{tm2.1Kcam}$*/J*	(Cohn et al., 2002)	009652
Pomt2^{flox}	*POMT2tm1.1Hhu/J*	(Hu et al., 2011)	017880
Dag1$^{\Delta ICD}$	N/A	(Satz et al., 2009)	N/A
Sox2^{Cre}	*B6N.Cg-Edil*$^{3Tg(Sox2-cre)1Amc}$*/J*	(Hayashi et al., 2002)	014094

Table 4.3 Breeding schemes

Breeding Scheme	Control Genotype	Mutant Genotype
Calb1$^{Cre/+}$*;Dag1*$^{+/-}$ *x Dag1*$^{flox/flox}$	*Calb1*$^{Cre/+}$*;Dag1*$^{flox/+}$	*Calb1*$^{Cre/+}$*;Dag1*$^{flox/-}$
Pcp2$^{Cre/+}$*;Dag1*$^{+/-}$ *x Dag1*$^{flox/flox}$	*Pcp2*$^{Cre/+}$*;Dag1*$^{flox/+}$	*Pcp2*$^{Cre/+}$*;Dag1*$^{flox/-}$
Calb1$^{Cre/+}$*;Pomt2*$^{flox/+}$ *x POMT2*$^{flox/flox}$	*Calb1*$^{Cre/+}$*;Pomt2*$^{flox/+}$	*Calb1*$^{Cre/+}$*;Pomt2*$^{flox/flox}$
Dag1 $^{\Delta ICD/+}$ *x Calb1*$^{Cre/+}$*;Dag1*$^{flox/+}$	*Calb1*$^{Cre/+}$*;Dag1*$^{+/+}$	*Calb1*$^{Cre/+}$*;Dag1* $^{\Delta ICD/flox}$

Perfusions and tissue preparation

Mice were perfused with either 4% paraformaldehyde (PFA) in PBS, pH 7 or 9% Glyoxal/8% Acetic acid (GAA) in PBS, pH 4-5 (modified from Konno et al., 2023). PFA was prepared from powder (Thermo Scientific Chemicals, Cat. No. A1131336). Glyoxal was purchased as a 40% stock solution (Thermo Scientific Chemicals, Cat. No. 156225000) and Glacial Acetic Acid was purchased from Fisher (Cat. No. A38-500). PFA perfusion was used for all immunohistochemical experiments except for those

involving anti-$GABA_A\alpha1$, which was only compatible with GAA perfused tissue. P30 mice were deeply anesthetized using CO_2 and transcardially perfused with ice cold 0.1M PBS for two minutes to clear blood from the brain, followed by either (1) 15 mL of ice cold 4% PFA in PBS or (2) 20 mL of ice cold 9%/8% GAA in PBS, as indicated. After perfusion, brains were dissected and post-fixed in either (1) 4% PFA for 30 minutes at room temperature or (2) 9%/8% GAA overnight at 4°C. Brains were rinsed with PBS, embedded in 4% low-melt agarose (Fisher, Cat. No. 16520100), and sectioned at 70µm using a vibratome (VT1200S, Leica Microsystems Inc., Buffalo Grove, IL) into 24-well plates containing 1 mL of 0.1M PBS with 0.02% Sodium Azide.

Immunohistochemistry

Single and multiple immunofluorescence detection of antigens was performed as follows: free-floating vibratome sections (70µm) were briefly rinsed with PBS, then blocked for 1 hour in PBS containing 0.2% Triton-X (PBST) plus 2% normal goat serum. For staining of Dystroglycan synaptic puncta, an antigen retrieval step was performed prior to the blocking step: sections were incubated in sodium citrate solution (10mM Sodium Citrate, 0.05% Tween-20, pH 6.0) for 12 min at 95°C in a water bath followed by 12 min at room temperature. Sections were incubated with primary antibodies (**Table 4.4**) diluted in blocking solution at 4°C for 48-72 hours. Following incubation in primary antibody, sections were washed with PBS three times for 20 min each. Sections were then incubated with a cocktail of secondary antibodies (1:500, Alexa Fluor 488, 546, 647) in blocking solution containing Hoechst 33342 (1:10,000, Life Technologies, Cat. No. H3570) overnight at room temperature. Finally, sections were mounted on slides using Fluoromount-G (SouthernBiotech) and sealed using nail polish.

Table 4.4 Primary antibodies used for immunohistochemistry

Target	Host	Dilution	Source	Catalog #	RRID
α-Dystroglycan (IIH6C4)	Mouse	1:250	MilliporeSigma	05-593	AB_309828
α-Dystroglycan (IIH6C4)	Mouse	1:250	MilliporeSigma	05-593-I	AB_3083460
VGAT	Rabbit	1:500	Synaptic Systems	131-003	AB_887869
VGAT	Guinea Pig	1:500	Synaptic Systems	131-005	AB_1106810
GAD67	Mouse	1:500	MilliporeSigma	MAB5406	AB_2278725
VGLUT1	Guinea Pig	1:500	MilliporeSigma	AB5905	AB_2301751
VGLUT2	Guinea Pig	1:250	Synaptic Systems	135-404	AB_887884
$GABA_A$ α1	Mouse	1:500	NeuroMab	N95/35	AB_2108811
Parvalbumin	Rabbit	1:1000	Swant	PV27	AB_2631173
Parvalbumin	Goat	1:1000	Swant	PVG213	AB_2650496
Calbindin	Rabbit	1:1000	Swant	CB38	AB_10000340
Calbindin	Chicken	1:2000	Boster Bio	M03047-2	AB_2936235

Microscopy

Imaging was performed on either a Zeiss Axio Imager M2 fluorescence upright microscope equipped with an Apotome.2 module or a Zeiss LSM 980 laser scanning confocal build around a motorized Zeiss Axio Observer Z1 inverted microscope with a Piezo stage. As indicated below (**Table 4.5**), some experiments utilizing the LSM 980 confocal, a linear Wiener filter deconvolution step (Zeiss LSM Plus) was used at the end of image acquisition with 1.2X Nyquist sampling. The Axio Imager M2 uses a metal halide light source (HXP 200 C), Axiocam 506 mono camera, and 20X/0.8 NA Plan-Apochromat objectives. The LSM 980 confocal light path has two multi-alkali PMTs and two GaAsP PMTs for four track imaging. Confocal images were acquired using a 63X/1.4 NA Plan-Apochromat Oil DIC M27 objective. Z-stack images were acquired and analyzed offline in ImageJ/FIJI (Schindelin et al., 2012) or Imaris 10.0 (Oxford Instruments). Images used for quantification between genotypes were acquired using

the same exposure times or laser power. Brightness and contrast were adjusted in FIJI to improve visibility of images for publication. Figures were composed in Adobe Illustrator 2024 (Adobe Systems).

Table 4.5 Image acquisition setup microscopy experiments

Microscope	Objective	Figure(s)
Zeiss Axio Imager M2	20X/0.8 NA	Figure 4.4
Zeiss LSM 980	63X/1.4 NA	Figure 4.1, 4.2
Zeiss LSM 980 (with deconvolution)	63X/1.4 NA	Figure 4.5, 4.7, 4.9, 4.10

Image Quantification

For imaging experiments, 4-8 images were acquired from 3-4 sagittal sections per animal, and at least three animals per genotype were used for analysis. Sections were chosen from cerebellar vermis and images were acquired within cerebellar cortex of lobules V-VI.

Synaptic Puncta Density, Size, and Colocalization

0.2µm z-stacks covering 5µm were acquired using a 63X objective on a Zeiss LSM 980 (as described above). Analysis of image stacks was performed in Imaris 10.0 (Oxford Instruments). The Surfaces function was used to reconstruct the Purkinje cells using the Parvalbumin (**Figure 4.1**, **Figure 4.2**) or Calbindin (**Figure 4.5**, **Figure 4.9**, **Figure 4.10**) channel. To enrich for Purkinje cell signal, the synaptic marker channels were masked to only include information at the surface or inside of the Purkinje cell surface. The Spots function was used to determine the location of synaptic puncta in 3-dimensional space using local contrast to identify puncta. Spots with a volume less than 0.1µm^3 were excluded. Puncta density (puncta per 10µm^3) was calculated by dividing 10 by the Average Distance To 5 Nearest Neighbours. Spots were determined to be colocalized if they were within 1µm. As a control for random colocalization, one synaptic marker channel was mirrored and colocalization was recalculated.

Purkinje Cell and MLI Cell Densities

0.5μm z-stacks covering 20μm were acquired using a 20X objective on a Zeiss Axio Imager M2. Maximum projections were used for analysis in FIJI (Schindelin et al., 2012). Cells were counted using the Multi-Point Tool. The length of the region of cerebellar cortex analyzed was measured using the Freehand Line tool; this value was used to normalize the cell counts to unit length.

Electrophysiology

For acute slice preparation, mice were deeply anesthetized in 4% isoflurane and subsequently injected with a lethal dose of 2% 2, 2, 2-Tribromoethanol in sterile water followed by transcardial perfusion with 10mL ice cold cutting solution containing the following (in mM): 100 Choline Chloride, 2.5 KCl, 1.2 NaH_2PO_4, 25 $NaHCO_3$, 3 3-myo-inositol, 25 glucose, 5 Na Ascorbate, 2 Na Pyruvate, 7 $MgSO_4$, 0.5 $CaCl_2$; pH 7.3, 300-340mmol/kg. After rapid decapitation, the brain was briefly submerged in ice cold cut solution bubbled with carbogen (95% oxygen, 5% CO2) and then sectioned into 300μm sagittal sections (Leica VT1200S vibratome) in bubbled ice-cold cut solution. Slices were recovered in 37°C recording ACSF, bubbled, for 15 minutes followed by 1 hour in room temperature recording ACSF (in mM: 125 NaCl, 25 $NaHCO_3$, 1.25 NaH_2PO_4, 3 KCl, 25 D-Glucose, 2 $CaCl_2$, 1 $MgCl_2$) with an osmolarity of 310-325mmol/kg and supplemented with 1.5mM Na Ascorbate, bubbled.

Purkinje cells were patched in whole cell configuration using 1.2-2MΩ borosilicate glass pipettes filled with high chloride internal solution containing the following (in mM): 125 CsCl, 2.5 $MgCl_2$, 0.5 EGTA, 10 HEPES, 2 Mg-ATP, 0.3 Na-GTP, 5 QX-314; pH 7.2, 300mmol/kg. Pipettes were wrapped in parafilm to reduce capacitive currents. Cells were voltage clamped at -70mV and continuously superfused with 2-3 mL/min bubbled recording ACSF (310-325mmol/kg) containing 10μM NBQX to block excitatory transmission and 500nM TTX to block action potentials. After reaching a

stable baseline, 5 minutes of mIPSCs were recorded. Signals were amplified with an AxoPatch 200B amplifier (Molecular Devices), low-pass filtered at 5 kHz, and digitized and sampled at 10 kHz with a NIDAQ analog-to-digital board (National Instruments). Data were acquired and analyzed using a custom script in Igor Pro 8 (Wavemetrics). A hyperpolarizing step of -10mV was applied before each sweep to monitor input resistance, series resistance, and measure cell capacitance. Series resistance was not compensated and was maintained below 20MΩ. Cells were excluded if series resistance changed by more than 25%.

Rise and decay kinetics were calculated on each detected event for a given cell and averaged to a single value for that cell. Rise time was defined as the amount of time between 10% and 90% of the maximum amplitude of a given event. Decay was calculated as the time constant when the decay phase of the event was fit to an exponential curve.

Statistical analysis

Phenotypic analyses were conducted using tissue collected from at least three mice per genotype from at least two independent litters. The number of mice and replicates used for each analysis ("N") are indicated in the text or figure legends. Power analysis was used to determine samples sizes with $\alpha = 0.05$ and $\beta = 0.80$ and effect size determined using pilot data. Phenotypes were indistinguishable between male and female mice and were analyzed together. Analyses were performed blind to genotype. For comparisons between two groups, significance was determined using a two-tailed Students t-test. For comparisons between more than two groups, significance was determined using a 2-way ANOVA with Tukey HSD post-hoc analysis. Statistical significance was set at $\alpha = 0.05$ ($p < 0.05$). Statistical analyses and data visualization were performed in R (version 4.2.3).

Chapter 5: Identification of Cntnap1 as a novel interacting partner of Dystroglycan in multiple brain regions

Jennifer N. Jahncke[1,] and Kevin M. Wright[2]

[1] Neuroscience Graduate Program, Oregon Health & Science University, Portland, OR 97239, USA

[2] Vollum Institute, Oregon Health & Science University, Portland, OR 97239, USA

Abstract

The glycoprotein Dystroglycan (Dag1) represents the transmembrane component of the Dystrophin Glycoprotein Complex (DGC), which functions to connect the extracellular matrix to the actin cytoskeleton. *Dystroglycan* is expressed throughout the body including in muscle and the central and peripheral nervous systems. In the nervous system, Dystroglycan is required for a number of neurodevelopmental processes and more recently was shown to be involved in the function of a subset of inhibitory synapses. While many interacting proteins of Dystroglycan have been identified, a systematic analysis of potential synaptic binding partners has not yet been performed. Using an unbiased proteomics screen to identify novel interacting partners of Dystroglycan in whole brain tissue we identified Cntnap1, a member of the Neurexin superfamily of transmembrane proteins, as a binding partner with higher abundance than any other previously described interaction. The interaction between Dag1 and Cntnap1 increases developmentally concurrent with the period of synaptogenesis. The Dag1:Cntnap1 interaction occurs in cortex, hippocampus, and cerebellum. However, because *Dag1* and *Cntnap1* are both expressed in multiple cell types in the brain, there remain many open questions regarding the nature of this novel interaction and its relevance to synapse development and/or function.

Introduction

Dystroglycan (Dag1) is expressed throughout the body and is involved in many biological processes during development and into adulthood. In muscle, Dystroglycan is required for muscle integrity and mutations affecting Dystroglycan or its glycosylation results in a class of muscular dystrophy termed dystroglycanopathy. The muscular features of Dystroglycanopathies are accompanied by neurological defects including cortical malformations, hydrocephalus, retinal dysplasia, cerebellar cysts, intellectual disability, and seizures (Barresi and Campbell, 2006; Muntoni et al., 2011; Taniguchi-Ikeda et al., 2016). Dystroglycan is expressed by neuroepithelial cells, astrocytes, oligodendrocytes, vascular endothelial cells, and several populations of neurons and has been shown to be involved in neurodevelopmental processes including axon targeting, cellular migration, myelination, and synaptic function (Briatore et al., 2020; Clements et al., 2017; Colognato et al., 2007; Früh et al., 2016; Lindenmaier et al., 2019; Reist et al., 1992; Saito et al., 2003; Satz et al., 2010; Wright et al., 2012).

Dystroglycan's role in synaptic function was first described at the neuromuscular junction (NMJ) where it is required for clustering acetylcholine receptors in response to Agrin binding to Dystroglycan's glycan chains (Reist et al., 1992). More recently, it was shown that Dystroglycan in postsynaptic hippocampal pyramidal neurons is required for CCK^+/CB_1R^+ basket interneuron synapse formation and function in a manner dependent on the glycosylation of Dystroglycan (Früh et al., 2016; **Chapter 2**). Similarly, Dystroglycan in cerebellar Purkinje cells is necessary for the formation of functional molecular layer interneuron synapses, possibly through the clustering of postsynaptic components including Neuroligin and $GABA_A$ receptors (Briatore et al., 2020; **Chapter 4**)

The central component of each of Dystroglycan's many functions is its role as a cell adhesion molecule, allowing it to localize other proteins to specific compartments through *cis*- and *trans*-cellular interactions at the cell surface. While only a handful of

intracellular interactions have been described, many extracellular binding partners have been identified, nearly all of which bind to the glycan chains on the extracellular alpha subunit of Dystroglycan. These proteins all contain Laminin G (LG) domains, which are capable of binding to the matriglycan GlcA-Xyl disaccharide repeats of the Core M3 glycan chains on Dystroglycan (Briggs et al., 2016; Dempsey et al., 2019). It remains unknown which presynaptic protein (or proteins) Dystroglycan interacts with at central synapses to accomplish its role as a trans-synaptic adhesion molecule, however we can assume that this interacting partner will similarly contain LG domains.

Neurexins (*Nrxns*) are a family of presynaptic cell-adhesion molecules, each of which contain multiple LG domains. Biochemical analysis has shown that Neurexins bind Dystroglycan in a glycosylation-dependent manner (Boucard et al., 2005; Fuccillo et al., 2015; Reissner et al., 2014; Sugita et al., 2001). It is quite likely that Dystroglycan's role in synapse function is at least in part mediated by interaction with Neurexins. *Neurexin-3* conditional knockout and CRISPR-mediated *Dag1* knockout both result in similar synaptic defects in the olfactory bulb and prefrontal cortex (Trotter et al., 2023). Furthermore, synaptic phenotypes in *Neurexin-3* conditional knockouts can be rescued only by *Neurexin-3* constructs that are capable of binding Dystroglycan (lacking an insert at either splice sites 2 or 4 but not both) (Trotter et al., 2023). However, whether Neurexins mediate the synaptic function of Dystroglycan at hippocampal or cerebellar synapses is unknown. Neurexins are not typically thought to play a role in synapse formation but they are critical for presynaptic maturation and maintenance (Chen et al., 2017; Dudanova et al., 2007; Lin et al., 2023; Missler et al., 2003; Trotter et al., 2023). Given Dystroglycan's role in synapse formation in addition to maintenance, it is possible that a Dag1:Nrxn interaction mediates the maintenance phase of synapse development while interactions with other presynaptic partners mediate the synapse formation phase.

Here I perform an unbiased proteomics screen to identify novel interacting partners of Dystroglycan in the brain. Many LG domain-containing proteins known to interact with Dystroglycan came out in our screen, validating our approach. In addition to these known interacting partners, I identified Cntnap1 (also known as Caspr, Neurexin-4, or Paranodin) as a novel interaction, with greater abundance than any other LG domain-containing interacting partner. Cntnap1 is classically known as a key component of Nodes of Ranvier, where it is localized to the paranode (Einheber et al., 1997). Evidence for Cntnap1 participation in synaptic contexts is limited (Santos et al., 2012). I describe Cntnap1 localization in the hippocampus and cerebellum and attempt to understand where the Dag1:Cntnap1 interaction occurs in the brain.

Results

Identifying potential LG domain-containing Dystroglycan binding partners *in silico*

There have been a number of extracellular binding partners of Dystroglycan previously identified, all binding in a manner dependent on the glycosylation on Dystroglycan and all containing at least one LG domain (Boucard et al., 2005; Briggs et al., 2016; Dempsey et al., 2019; Fuccillo et al., 2015; Reissner et al., 2014; Sugita et al., 2001). Consistent with this, we have previously shown that Dystroglycan's functional role at central synapses is dependent on glycosylation, as mice expressing unglycosylated Dystroglycan exhibit the same synaptic phenotypes observed in Dystroglycan conditional knockouts (**Chapter 2**, **Chapter 4**). In order to identify novel synaptic interactions, I first examined RNA expression of each known LG domain-containing protein in principal neuron and interneuron populations in the cerebellum and hippocampus using the publicly available DropViz dataset (Saunders et al., 2018). The public Pfam database of protein families reported 85 LG domain-containing proteins, 39

of which were unannotated, leaving 46 candidate proteins (Mistry et al., 2021). Examination of RNA expression of these 46 candidates in the DropViz dataset showed similar expression patterns of most genes in both cerebellum and hippocampus (**Figure 5.1 A**). Particularly high expression was noted for several genes including *Agrn*, *Gas6*, several *Celsr, Cntnap,* and *Fat* family members, along with all three *Slits* and all three *Neurexins*.

To confirm the expression of the DropViz hits, and provide expression data where no DropViz data was available, I performed reverse transcriptase PCR (RT-PCR) using adult cerebellum or hippocampus cDNA as template. For each gene examined I designed 2-3 primer sets spanning multiple exons, designed to capture multiple isoforms if they exist. Primer sets are available in **Appendix I: Table 0.2**. The RT-PCR results confirmed the DropViz data in all cases. DropViz data was unavailable for *BC069074*, *Cntnap3*, *Col24a1*, *Crb1*, and *Lama3* in the cerebellum as well as *Tspear* and *Ush2a* in both cerebellum and hippocampus. RT-PCR indicated *BC069074*, *Cntnap3*, *Crb1* expression in the cerebellum as well as a lack of expression of *Tspear* and *Ush2a* in both regions (**Figure 5.1 B**). (*Lama3* was not examined by RT-PCR based on *in situ* hybridization data from the Allen Brain Atlas (Lein et al., 2007) indicating low expression in cell populations of interest.) In total, of the 31 genes screened by RT-PCR, 28 were confirmed to be expressed in the cerebellum and 28 in the hippocampus.

An unbiased proteomics screen for novel interactions indicates an abundant Dag1:Cntnap1 interaction in whole brain tissue

In silico analysis and RT-PCR identified a large number of potential Dystroglycan interacting proteins based on expression patterns, however expression pattern alone is not predictive of physical interaction, particularly since not all LG domains are capable of binding Dystroglycan (Briggs et al., 2016). Individual biochemical confirmation of each

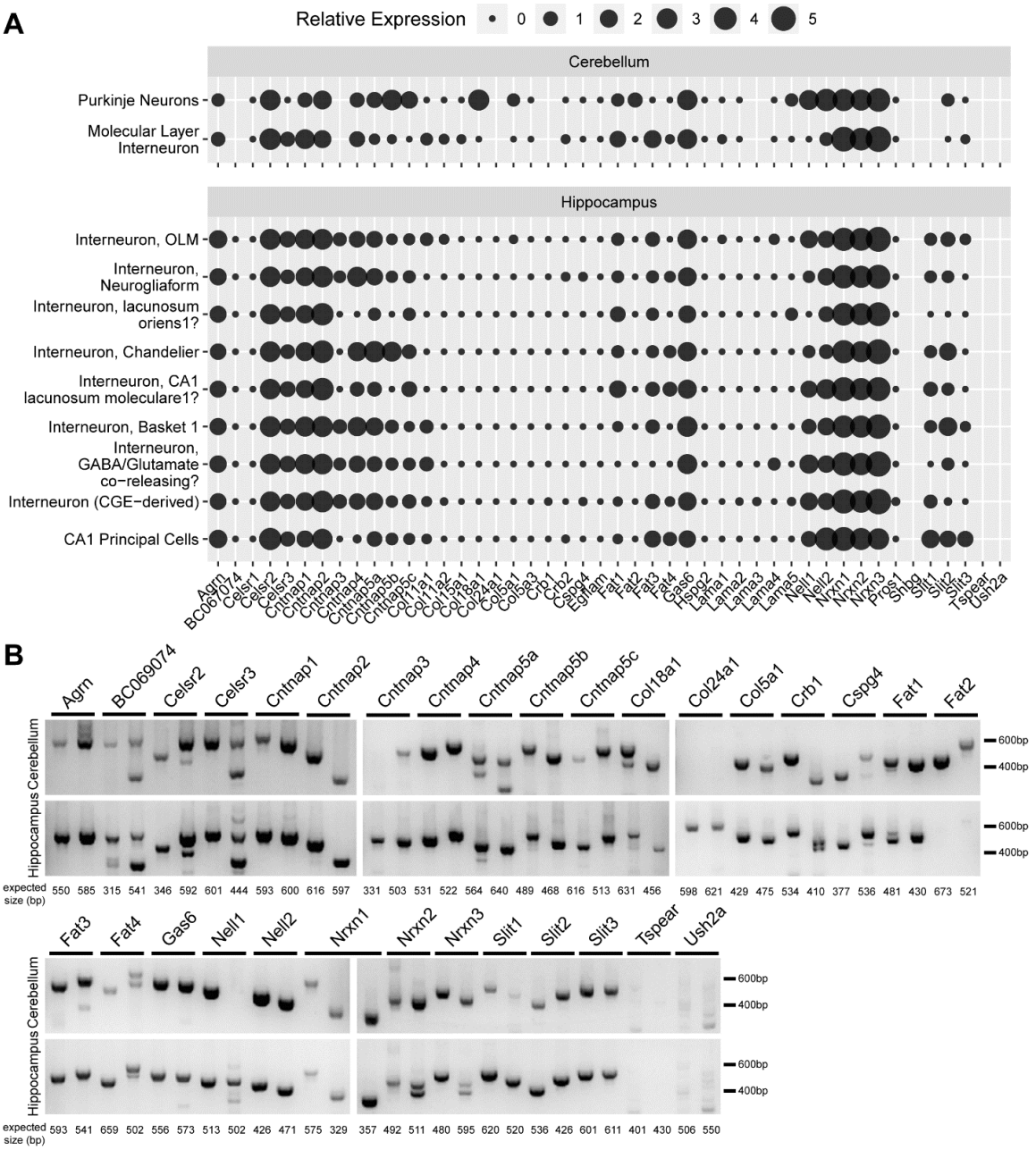

Figure 5.1 Identification of LG domain-containing proteins in hippocampal and cerebellar neuronal populations.

(A) Relative expression of all known LG domain-containing proteins in hippocampal and cerebellar principal neuron and interneuron populations as reported in the DropViz dataset. **(B)** Expression of a selected subset of LG domain-containing proteins as determined by RT-PCR. For a table of primer sets see **Appendix I: Table 0.2**.

of these possible interactions would be unnecessarily onerous. I instead chose to identify physical interactions by unbiased mass spectrometric analysis to produce a narrowed down list of interactions that could then be confirmed in cell populations of interest. I performed a Dystroglycan immunoprecipitation (IP) using wild-type (WT) adult mouse whole brain lysate as input and separated proteins by weight using SDS-PAGE. Proteins above ~100kDa were sent for analysis by mass spectroscopy for identification (**Figure 5.2 A**). For a complete table of results see **Appendix J: Table 0.3**. Of the proteins identified in our sample, there were 9 LG domain-containing proteins, 8 of which have previously been identified as Dystroglycan binding partners (**Figure 5.2 B**). The one novel interacting protein, Cntnap1, was the top hit in our mass spectroscopy dataset with more counts than any other LG domain-containing protein when normalized for molecular weight. In fact, Cntnap1 was one of the most abundant proteins in our entire sample, with more counts than Dystroglycan itself (Cntnap1:1210, Dag1:629). This suggests an abundant interaction between Dag1 and Cntnap1 in the brain. I therefore focused on identifying the nature of this novel interaction.

To confirm the interaction, I performed a Dystroglycan IP using either whole brain, cortex, hippocampus, or cerebellum tissue lysate as starting material and immunoblotted for Cntnap1 protein, finding the interaction to occur in all regions analyzed (**Figure 5.3 A-B**). I also analyzed the developmental time course of the interaction using whole brain tissue lysate prepared from mice aged postnatal day zero (P0) to P50. Dystroglycan levels remained stable across the time course, but the amount of Cntnap1 pulled out in the IP varied with development. Cntnap1 protein was undetectable at P0 and increased from P7 to P30 before dropping slightly at P50 (**Figure 5.3 C**). This pattern of expression scales with the period of synaptogenesis and subsequent synapse maturation, suggesting that the Dag1:Cntnap1 interaction could occur at synaptic sites throughout the brain.

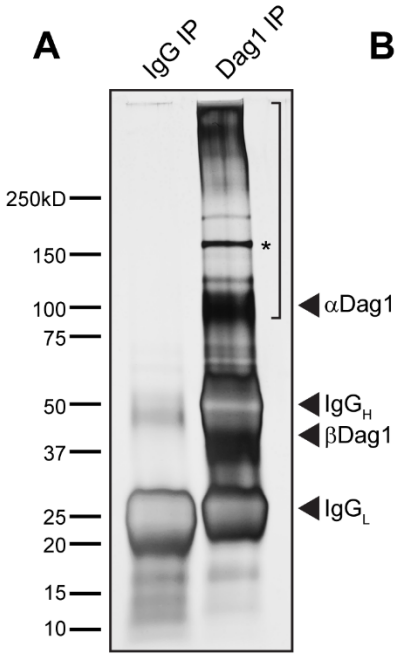

B

Gene	Counts	MW (kDa)	PMID
Cntnap1	1210	156.31	Novel
Agrn	255	207.54	8205616, 8205617
Lama2	207	343.81	8996823
Hspg2	198	398.29	10022829
Lama1	76	338.14	1741056
Lama4	61	201.82	10934193
Egflam	38	110.73	18641643
Nrxn3	30	173.43	11470830
Nrxn1	26	166.17	11470830

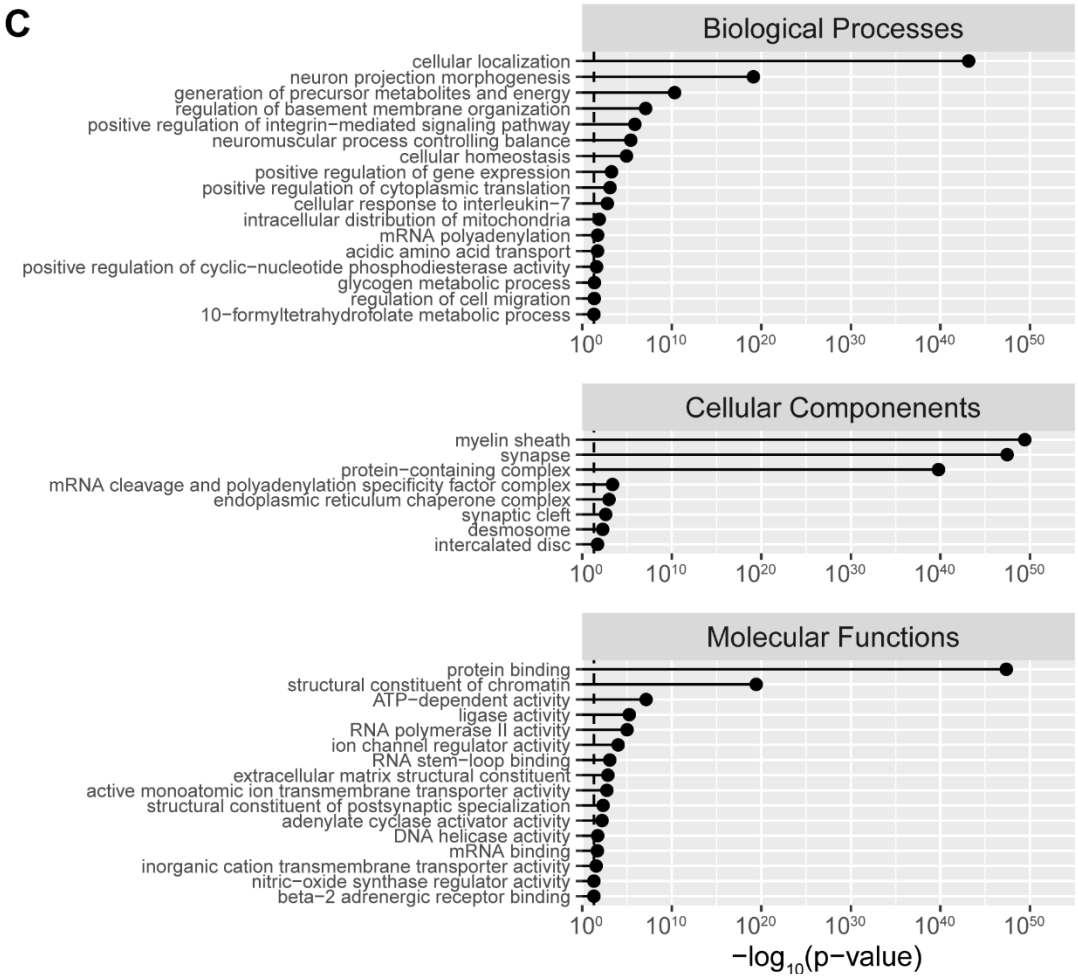

Figure 5.2 Dystroglycan immunoprecipitation and mass spectrometry identifies a novel Dag1:Cntnap1 interaction.

(A) Silver stain showing proteins co-precipitated with Dystroglycan in a Dystroglycan immunoprecipitation. The bracketed portion represents the portion of the gel analyzed by mass spectrometry. The asterisk shows the putative Cntnap1 band. (IgG_H = Heavy Chain, IgG_L = Light Chain.) **(B)** Co-precipitated LG domain-containing proteins identified by mass spectrometry. The counts represent the number of times a peptide matching the gene was identified in the sample. PMID = the PubMed ID for the paper that first identified the interaction with Dystroglycan. **(C)** Gene ontology analysis of the protein interactome. Dashed line indicates $p = 0.05$. Values further to the right are more enriched.

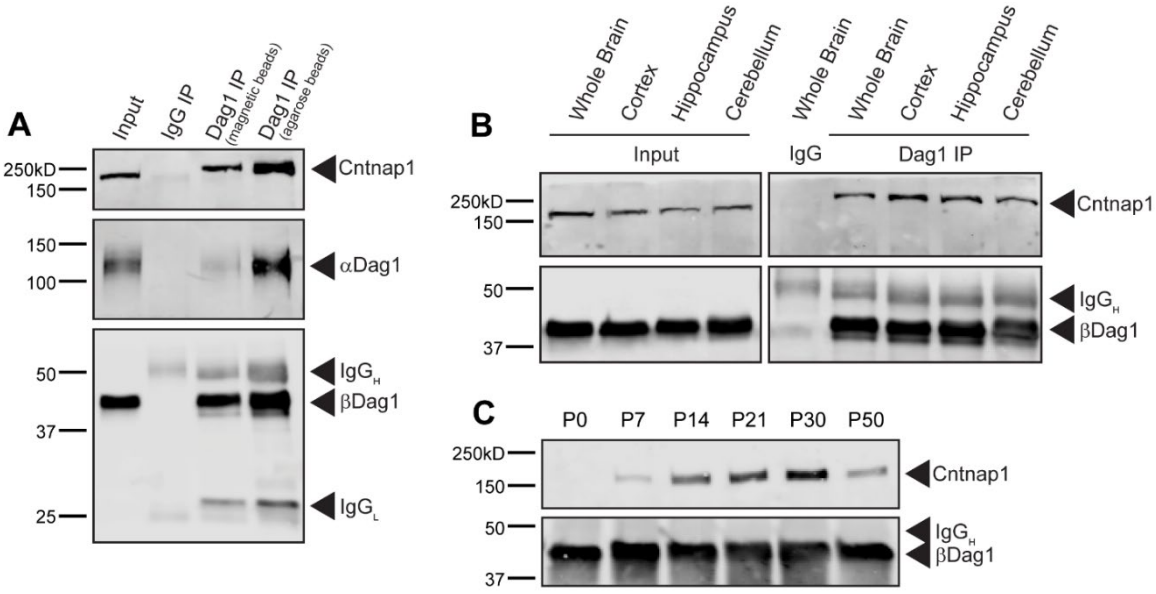

Figure 5.3 Biochemical confirmation of the Dag1:Cntnap1 interaction.

(A) Whole brain lysate was used as starting material for Dystroglycan immunoprecipitation. Immunoblot for Dystroglycan and Cntnap1 confirms the co-precipitation of Cntnap1 with Dystroglycan. **(B)** Dystroglycan immunoprecipitation in different brain regions (Whole Brain, Cortex, Hippocampus, Cerebellum) followed by immunoblot for Dystroglycan and Cntnap1. **(C)** Dystroglycan immunoprecipitation in cortex at timepoints from P0-P50 followed by immunoblot for Dystroglycan and Cntnap1. (IgG_H = Heavy Chain, IgG_L = Light Chain.)

Cntnap1 immunofluorescence does not colocalize with Dystroglycan at synaptic populations in cerebellar cortex or hippocampal CA1

Dystroglycan is expressed by many cell types in the brain including neurons, astrocytes, oligodendrocytes, and vascular endothelial cells (Colognato et al., 2007; Nguyen et al., 2014; Nickolls and Bönnemann, 2018; Tian et al., 1996; Zaccaria et al., 2001). *Cntnap1* has similarly broad expression; RNA sequencing data suggests that

Cntnap1 is expressed by projection neurons, interneurons, astrocytes, endothelial cells, microglia, and oligodendrocytes (Saunders et al., 2018). To better understand where Dystroglycan interacts with Cntnap1, I performed immunohistochemistry to label both proteins in cerebellar cortex and hippocampal CA1. In cerebellar cortex, Dystroglycan is localized to blood vessels as well as synaptic puncta on the Purkinje cell somas and dendrites (**Figure 5.4 A**). These puncta are sites of inhibitory synapses from molecular layer interneurons onto Purkinje cells (**Chapter 4**). While Cntnap1 expression in cerebellar cortex also appears punctate in a manner consistent with synaptic localization, it has a localization pattern more consistent with excitatory parallel fiber synapses (**Figure 5.4 A**). In the granule cell layer, where Dystroglycan immunofluorescence is not detected, Cntnap1 is localized in doublets consistent with its known role at axonal paranodes (Einheber et al., 1997). In hippocampal CA1, Dystroglycan is present at the postsynaptic side of inhibitory CCK^+/CB_1R^+ and PV^+ basket interneuron synapses onto pyramidal cell somas and proximal dendrites (**Figure 5.4 B**) (Früh et al., 2016; **Chapter 2**). Cntnap1 immunofluorescence, on the other hand, was only detectable at paranodal sites, not showing any evident colocalization with synaptic Dystroglycan (**Figure 5.4 B**). Given the abundance of the biochemical interaction in both the cerebellum and hippocampus, it is puzzling that I was unable to identify sites of colocalization between Dystroglycan and Cntnap1 by immunohistochemistry. This is the first of many unanswered questions about this interaction.

Hippocampal Cntnap1 appears largely unaffected by the knockout of *Dystroglycan*

Given the interaction between Cntnap1 and Dystroglycan, I next wanted to examine how Cntnap1 localization was affected in a *Dystroglycan* conditional knockout. I

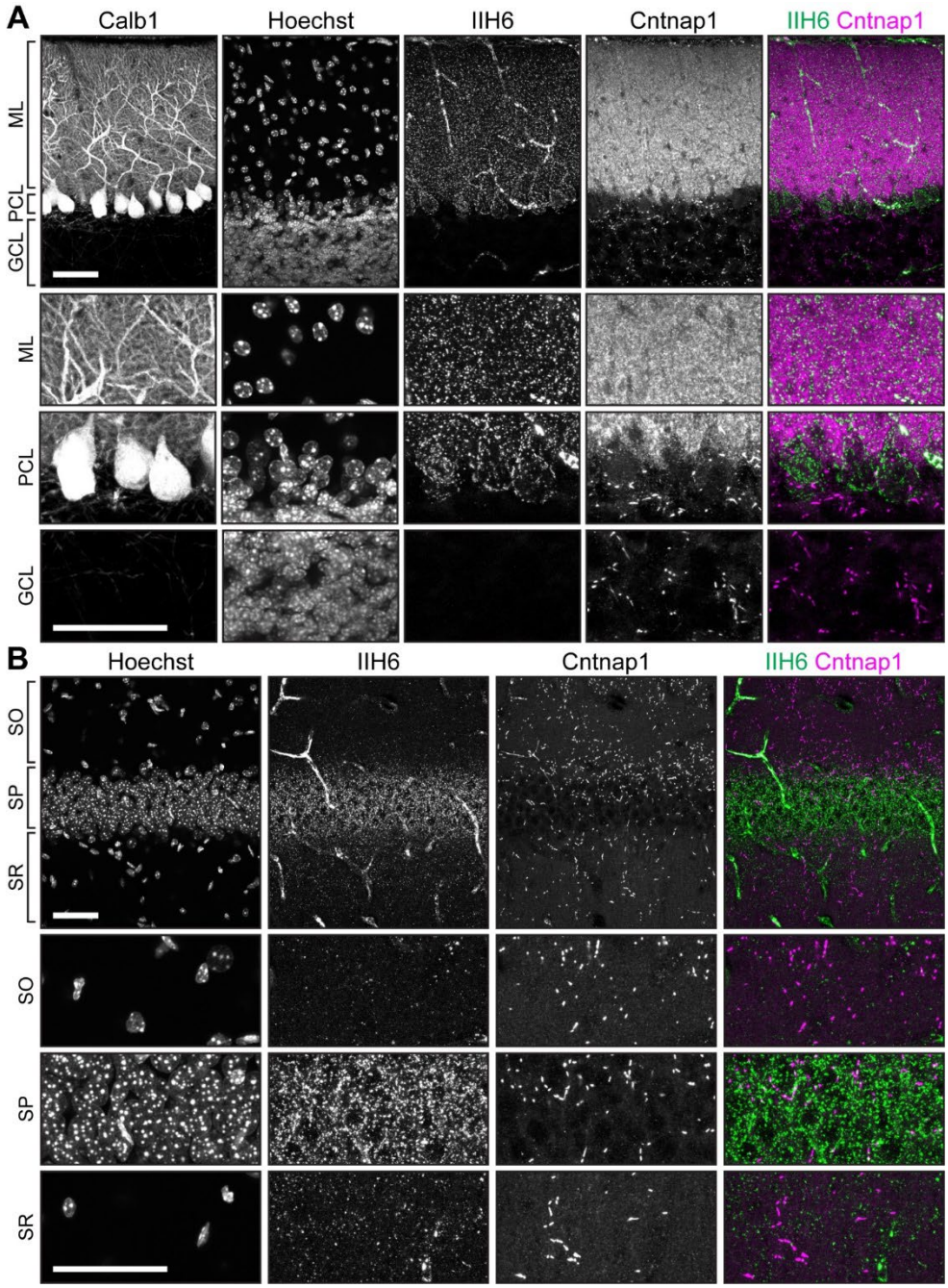

Figure 5.4 Non-overlapping Dystroglycan and Cntntap1 localization in cerebellar cortex and hippocampal CA1.

(A) Cerebellar cortex with multiplex immunohistochemical labeling of Calb1 (Purkinje cells), Hoechst (nuclei), IIH6 (Dystroglycan), and Cntnap1. Scale bars = 50μm. (ML = molecular layer, PCL = Purkinje cell layer, GCL = granule cell layer.) **(B)** Hippocampal CA1 with multiplex immunohistochemical labeling of Hoechst (nuclei), IIH6 (Dystroglycan), and Cntnap1. Scale bars = 50μm. (SO = *stratum oriens*, SP = *stratum pyramidale*, SR = *stratum radiatum*.)

generated *Emx1^{Cre};Dag1^{cKO}* mice, deleting *Dystroglycan* from forebrain progenitors. The knockout was confirmed by western blot in both the hippocampus and cortex (**Figure 5.5 A-B**) and immunohistochemistry in hippocampal CA1 (**Figure 5.5 C**). Despite the *Dystroglycan* knockout, Cntnap1 levels appeared only slightly reduced by western blot (**Figure 5.5 A-B**) and Cntnap1 localization was normal, still showing paranodal expression (**Figure 5.5 C**).

Using an antibody that recognizes the beta subunit of Dystroglycan, I performed an IP for Dystroglycan in *Emx1^{Cre};Dag1^{cKO}* mice to confirm the specificity of the Dag1:Cntnap1 biochemical interaction. To our surprise, Cntnap1 was still present in the co-immunoprecipitated fraction in both hippocampus and cortex (**Figure 5.5 A-B**). This is particularly surprising given that there was essentially no Dystroglycan detected in the IP, begging the question: how is Cntnap1 immunoprecipitated when there is no Dystroglycan to bind to the antibody? I did a number of control experiments with more stringent washes and still saw Cntnap1 co-precipitation (data not shown). Separately, I observed that Cntnap1 in WT rat brain lysate was detected by our Cntnap1 antibody, but Cntnap1 did not co-precipitate with Dystroglycan in rat lysate, suggesting that our Dystroglycan antibody is not nonspecifically binding Cntnap1 (data not shown). Furthermore, immunoblot for the membrane protein TrkB showed that no TrkB was present in the IP sample, indicating that the IP is not non-specifically pulling down membrane proteins (data not shown).

I generated *Emx1^{Cre};Pomt2^{cKO}* mice in which the glycosyltransferase *Pomt2* (*Protein O-mannosyltransferase 2*) is deleted and therefore unable to initiate glycosylation. In this context Dystroglycan is essentially unglycosylated on Core M3, the glycan chain that mediates Dystroglycan's interaction with extracellular proteins (Reeuwijk et al., 2005). Here Dystroglycan is no longer synaptically localized but the overall cell surface levels of β-Dystroglycan protein is unchanged (**Chapter 2**).

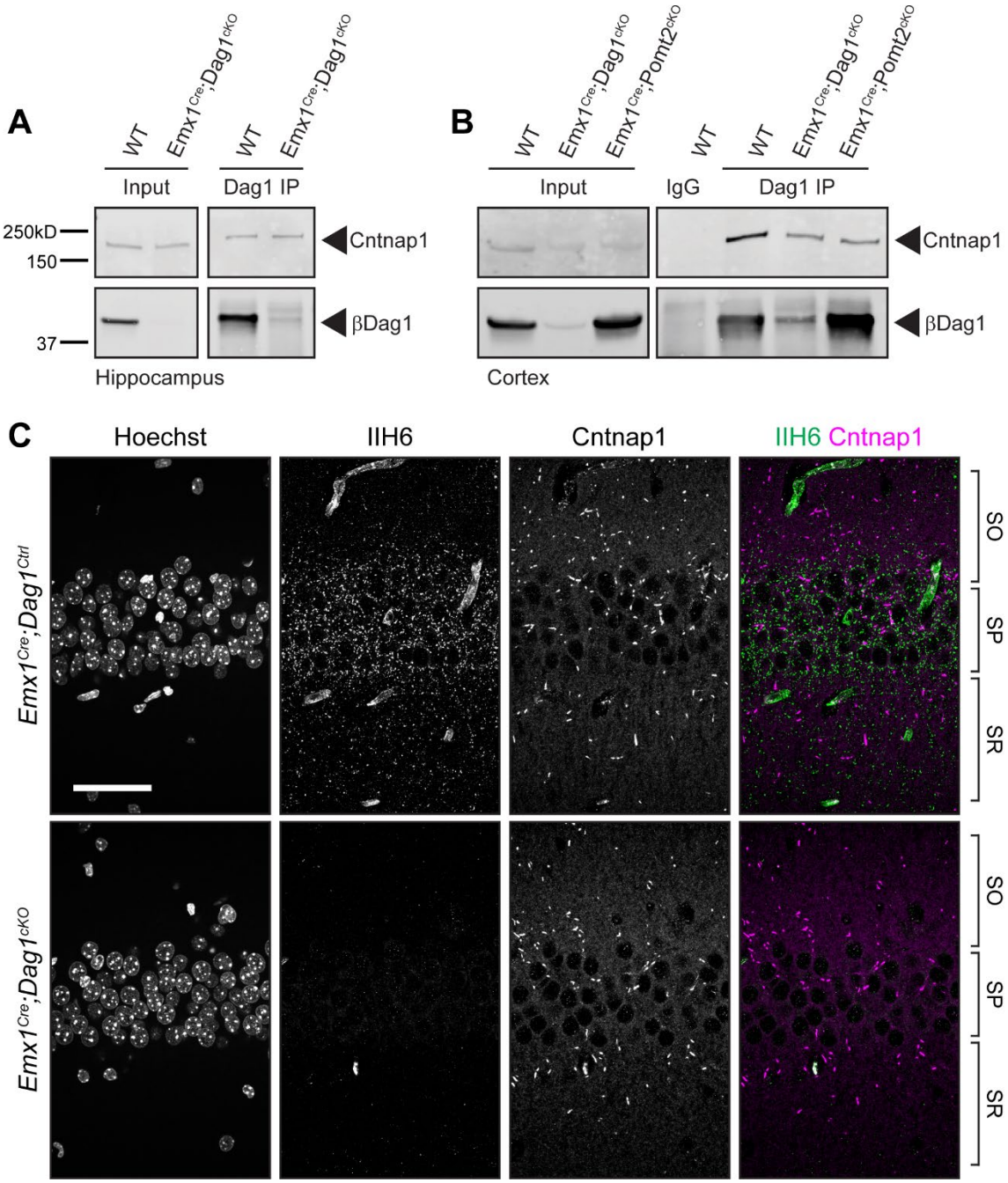

Figure 5.5 Cntnap1 expression is largely unperturbed in Dystroglycan conditional knockout mice.

(A) Dystroglycan immunoprecipitation in hippocampus of WT control and *Dag1*^{cKO} mice and immunoblot for Dystroglycan and Cntnap1. **(B)** Dystroglycan immunoprecipitation in cortex of WT control, *Dag1*^{cKO}, and *Pomt2*^{cKO} mice and immunoblot for Dystroglycan and Cntnap1. **(C)** Immunolabeling of Hoechst (nuclei), IIH6 (Dystroglycan), and Cntnap1 in hippocampal CA1 of *Dag1*^{cKO} mice and littermate controls. Scale bar = 50μm. (SO = *stratum oriens*, SP = *stratum pyramidale*, SR = *stratum radiatum*.)

In mouse cortical lysate Cntnap1 levels were slightly reduced in *Emx1^{Cre};Pomt2^{cKO}* mice to a similar level detected in *Emx1^{Cre};Dag1^{cKOs}* (**Figure 5.5 B**). Dystroglycan IP in *Emx1^{Cre};Pomt2^{cKO}* mice also showed slightly less Cntnap1 co-precipitate compared to WT controls, again a reduction similar to that observed in *Emx1^{Cre};Dag1^{cKOs}* (**Figure 5.5 B**). This increases our confidence that Cntnap1 expression is at least partially linked to Dystroglycan expression, albeit in a manner independent of the synaptic localization of Dystroglycan. However, I still have not identified where the interaction between Dystroglycan and Cntnap1 occurs.

The *Emx1^{Cre}* driver line does not drive *Cre* recombination in interneurons, microglia, blood vessels, or astrocytes leading us to believe that the Dag1:Cntnap1 interaction occurs with Dystroglycan expressed in one of these (**Chapter 2**). To test whether the interaction occurs with astrocytic Dystroglycan I generated *GFAP^{Cre};Dag1^{cKOs}*. The amount of Cntnap1 co-precipitate in the Dystroglycan IP was comparable to that of WT controls, suggesting that the astrocytic contribution to the interaction is minimal (**Supplementary Figure 5.1 A**). Supporting this, Cntnap1 localization appeared normal in *GFAP^{Cre};Dag1^{cKO}* hippocampal CA1 (**Supplementary Figure 5.1 B**).

Knockout of Cntnap family member Cntnap2 does not phenocopy Dystroglycan knockout

The Cntnap family of proteins has five major members, each of which contain multiple LG domains. Despite our mass spectrometry data only implicating Cntnap1 as a potential interacting partner of Dystroglycan, it is predicted that all of the Cntnap family members would be capable of binding Dystroglycan. Cntnap2 has been studied in depth as an autism-related gene and is present at excitatory and inhibitory synapses (Jurgensen and Castillo, 2015; Lu et al., 2016; Xing et al., 2019). I obtained *Cntnap2^{KO}*

mice and looked for known phenotypes of *Dag1* mutants. Dystroglycan localization was normal in hippocampal CA1 and cerebellar cortex (**Supplementary Figure 5.2 A, C**). Nevertheless, I looked at axon targeting in hippocampus and cerebellum in populations that are known to be disrupted in *Dag1* conditional knockouts (**Chapter 2**, **Appendix F: Figure 0.5**). Axon targeting appeared normal in both regions (**Supplementary Figure 5.2 B, D**). It therefore seems unlikely that Cntnap2 affects Dystroglycan localization at either of these synaptic populations.

Discussion

Dystroglycan has been shown to interact with a number of extracellular binding partners in a glycosylation-dependent manner. These proteins include Laminins, Agrin, Perlecan, Neurexins, Pikachurin, Slit2, and Celsr3/Adgrc3 (Campanelll et al., 1994; Gee et al., 1994; Ibraghimov-Beskrovnaya et al., 1992; Lindenmaier et al., 2019; Sato et al., 2008; Sugita et al., 2001; Sugiyama et al., 1994; Talts et al., 1999; Tian et al., 1996; Wright et al., 2012). The common feature of each of these interacting proteins is that each contains at least one LG domain, with most containing multiple LG domains. These LG domains bind to GlcA-Xyl disaccharide repeats (referred to as “matriglycan”) on the Core M3 glycan chains on the extracellular alpha subunit of Dystroglycan (Sheikh et al., 2022). Matriglycan is capable of extending into long chains capable of binding multiple proteins simultaneously (Goddeeris et al., 2013).

Dystroglycan is expressed at synapses in multiple regions including (1) the neuromuscular junction (NMJ) where it interacts with Laminin, Agrin, and Perlecan, (2) ribbon synapses in the retina where it interacts with Pikachurin, and (3) inhibitory central synapses in the hippocampus and cerebellum where it is presumed to interact with Neurexins. (Reviewed in Jahncke and Wright, 2023.) Although Dystroglycan has been

shown to interact with Neurexins in the brain biochemically, the precise synaptic populations at which this interaction occurs have not been identified (Sugita et al., 2001). The isoforms of Neurexin that are capable of binding to Dystroglycan are expressed by CCK^+/CB_1R^+ interneurons, a population known to require Dystroglycan for axon targeting and synapse function (Boucard et al., 2005; Früh et al., 2016; Miller and Wright, 2021; Ullrich et al., 1995; **Chapter 2**). It therefore follows that a Dag1:Nrxn interaction most likely occurs at these synapses. While the role of Neurexins in synapse maturation and maintenance has been well documented, they are not typically thought to be involved in axon targeting or synapse formation whereas Dystroglycan has indeed been shown to be involved in these early synaptogenic processes (Chen et al., 2017; Dudanova et al., 2007; Früh et al., 2016; Jahncke and Wright, 2023; Lin et al., 2023; Miller and Wright, 2021, 2021; Missler et al., 2003). This suggests that a yet undescribed presynaptic ligand might mediate postsynaptic recognition of Dystroglycan to support synapse formation.

The Cntnap family of proteins is closely related to the Neurexin family and represents a potential synaptic recognition ligand. Cntnaps each contain multiple LG domains and are expressed widely throughout the nervous system. Several Cntnap family members have been shown to be involved in synaptic processes (Ashrafi et al., 2014; Jurgensen and Castillo, 2015; Lu et al., 2016; Santos et al., 2012). Cntnap1, however, is canonically thought of as a paranodal protein, involved in mediating axonal-glial interactions in myelination and providing compartmentalization in order to physically separate nodal sodium channels from juxtaparanodal potassium channels (Einheber et al., 1997; Rios et al., 2003). Indeed, synaptic localization of Cntnap1 has not been described *in vivo*. In addition to its synaptic localization, Dystroglycan is localized to Nodes of Ranvier where it is involved in sodium channel clustering (Colognato et al., 2007). Dystroglycan is also expressed by oligodendrocytes in the CNS and Schwann

cells in the PNS where it is involved in myelin sheath formation and nodal structure (Saito et al., 2003). It is tempting to speculate that the Dag1:Cntnap1 interaction occurs at (1) nodes or (2) at the interface between neurons and oligodendrocytes. However, (1) Cntnap1 expression is limited to paranodes while Dystroglycan expression is limited to nodes with a very stark physical separation and (2) the *Emx1*^{Cre}-mediated conditional knockout of Dystroglycan deletes *Dag1* from oligodendrocytes and I saw no effect on the Dag1:Cntnap1 interaction in our *Emx1*^{Cre}*;Dag1*^{cKO} mice (**Figure 5.5**). However, another possible source of Dag1 is oligodendrocyte precursor cells (OPCs). While it is true that *Emx1*^{Cre} would deplete *Dag1* expression in one population of OPCs, different OPC populations are functionally redundant and known to travel long distances, making it difficult to study the role of OPCs in any one system (Kessaris et al., 2006). It is therefore possible that *Dag1*-expressing OPCs from other lineages are present in the forebrain of *Emx1*^{Cre}*;Dag1*^{cKO} mice.

Given that *Emx1*^{Cre} does not drive *Cre* recombination in interneurons, microglia, blood vessels, or astrocytes I am left to assume that Dystroglycan in one of these populations is mediating the interaction with Cntnap1. Interneuron or microglia expression of Dystroglycan has not been described but could certainly be feasible. Dystroglycan appears to be expressed by blood vessels, which was once a topic of debate, however research in this area is lacking (Haenggi and Fritschy, 2006; Tian et al., 1996; Zaccaria et al., 2001). Nevertheless, there is evidence that Dystroglycan in blood vessels is involved in angiogenesis (Hosokawa et al., 2002). In astrocytes, Dystroglycan is known to be localized to the endfeet of perivascular astrocytes at the blood-brain barrier and to radial glial endfeet abutting the pial surface (Ueda et al., 2000; Zaccaria et al., 2001). Although our *GFAP*^{Cre}*;Dag1*^{cKOs} did not show a reduction in Cntnap1 levels (**Supplementary Figure 5.1**), the *GFAP*^{Cre} recombination pattern is somewhat nonspecific and incomplete (**Appendix B: Figure 0.1**) and therefore does not rule out

the role of astrocytic Dystroglycan mediating the interaction with Cntnap1. Careful genetic dissection of each of these cellular populations will be necessary to identify the source of the Dag1:Cntnap1 interaction. Generation of a mouse expressing a tagged version of Dystroglycan under the control of *Cre* recombinase would allow for population-specific analysis of interactions with Dystroglycan.

Although the present study identified a novel glycan-protein interaction between Dystroglycan and Cntnap1, the subsequent data raised more questions than it answered. Is the Dag1:Cntnap1 interaction specific? Where is the Dag1:Cntnap1 interaction occurring? If not Cntnap1, what is the presynaptic ligand of Dystroglycan mediating axon targeting and synapse formation? Future biochemical and functional assays will be necessary to answer these prevailing questions.

Methods

Animal Husbandry

All animals were housed and cared for by the Department of Comparative Medicine (DCM) at Oregon Health and Science University (OHSU), an AAALAC-accredited institution. Animal procedures were approved by OHSU Institutional Animal Care and Use Committee (Protocol # IS00000539), adhered to the NIH *Guide for the care and use of laboratory animals*, and provided with 24-hour veterinary care. Animal facilities are regulated for temperature and humidity and maintained on a 12-hour light-dark cycle and were provided food and water *ad libitum*. Animals older than postnatal day 6 (P6) were euthanized by administration of CO_2, animals <P6 were euthanized by rapid decapitation.

Mouse Strains and Genotyping

The day of birth was designated postnatal day 0 (P0). Ages of mice used for each analysis are indicated in the figure and figure legends. Mouse strains used in this study have been previously described and were obtained from Jackson Labs, unless otherwise indicated (**Table 5.1**). *Dag1*$^{+/-}$ mice were generated by crossing the *Dag1*$^{flox/flox}$ line to a *Sox2*^{Cre} line to generate germline *Dag1*$^{\Delta/+}$ mice hereafter referred to as *Dag1*$^{+/-}$ as the resultant transcript is nonfunctional. These mice were thereafter maintained as heterozygotes. Breeding schemas are as described in **Table 5.2**. Mice were maintained on a C57BL/6 background. *Cntnap2*^{KO} mice were not bred in-house as they are maintained as knockouts at JAX. Genomic DNA extracted from toe or tail samples (Quanta BioSciences) was used to genotype animals. Primers for genotyping can be found on the JAX webpage or originating article. *Dag1*$^{+/-}$ mice were genotyped with the following primers: CGAACACTGAGTTCATCC (forward) and CAACTGCTGCATCTCTAC (reverse).

Table 5.1 Mouse Strains

Common name	Strain name	Reference	Stock #
WT	C57BL/6J		000664
Dag1^{flox}	B6.129(Cg)-*Dag1*$^{tm2.1Kcam}$/J	(Cohn et al., 2002)	009652
Pomt2^{flox}	*POMT2*$^{tm1.1Hhu}$/J	(Hu et al., 2011)	017880
Sox2^{Cre}	B6N.Cg-*Edil*$^{3Tg(Sox2-cre)1Amc}$/J	(Hayashi et al., 2002)	014094
Emx1^{Cre}	B6.129S2-*Emx1*$^{tm(cre)Krj}$/J	(Gorski et al., 2002)	005628
GFAP^{Cre}	B6.Cg-*Tg(Gfap-cre)77.6Mvs/2J*	(Gregorian et al., 2009)	024098
Cntnap2^{KO}	B6.129(Cg)-*Cntnap2*^{tm1Pele}/J	(Poliak et al., 2003)	017482

Table 5.2 Breeding Schemes

Breeding Scheme	Control Genotype	Mutant Genotype
Emx1^{Cre}*;Dag1*$^{+/-}$ *x Dag1*$^{flox/flox}$	*Emx1*^{Cre}*;Dag1*$^{flox/+}$	*Emx1*^{Cre}*;Dag1*$^{flox/-}$
Emx1^{Cre}*;Pomt2*$^{flox/+}$ *x Pomt2*$^{flox/flox}$	*Emx1*^{Cre}*;Pomt2*$^{flox/+}$	*Emx1*^{Cre}*;Pomt2*$^{flox/flox}$
GFAP^{Cre}*;Dag1*$^{+/-}$ *x Dag1*$^{flox/flox}$	*GFAP*^{Cre}*;Dag1*$^{flox/+}$	*GFAP*^{Cre}*;Dag1*$^{flox/-}$

RT-PCR

Using WT mouse hippocampus or cerebellum as starting material, RNA was extracted (RNeasy Midi Kit, Qiagen, Cat. No. 75144) and used to generate cDNA (SuperScript III Reverse Transcriptase, Invitrogen, Cat No. 18080044). A NanoDrop 2000 Spectrophotometer (Thermo Fisher Scientific) was used to measure cDNA concentration. Hippocampal cDNA was 562.1ng/µl and cerebellar cDNA was 631.9ng/µl. 1µl of cDNA was used as template to which 1µl of each 10µM primer (forward and reverse) was added along with 5µl 2X DreamTaq (Thermo Scientific, Cat. No. K1082) and 2µl dH_2O for a final reaction volume of 10µl. (See **Appendix I: Table 0.2** for a list of all primer sets.) All reactions were run with a standard program including a 60°C annealing step with a 1-minute extension, repeated for 37 cycles. RT-PCR product was run on a 2.5% agarose gel containing ethidium bromide for 25 minutes at 120V and imaged under UV illumination.

Large Scale Immunoprecipitation and Mass Spectrometry

5g of mouse whole brain material was lysed in 40mL of Buffer A (25mM HEPES pH 7.4, 200mM NaCl, 1mM EDTA, 2% Triton X-100) containing protease inhibitor (Roche cOmplete EDTA-free protease inhibitor cocktail, Millipore Sigma, Cat. No. COEDTAF-RO) in a glass dounce homogenizer. Homogenate was then rocked at 4°C for 2 hours after which homogenate was spun at 20,000g for 20 minutes two times, discarding the pellet each time. $CaCl_2$ and $MgCl_2$ were added to final concentrations of 2.5mM each. Lysate was pre-cleared on 200µl of Protein G beads for overnight at 4°C. 80µg of anti-β-Dystroglycan (MANDAG2) (DSHB, Cat. No. 7D11) antibody or IgM Fab (Jackson Immunoresearch, Cat. No. 115-007-020) was bound to 200µl Protein G beads in Buffer B (25mM HEPES pH 7.4, 250mM NaCl, 2.5mM $CaCl_2$, 2.5mM $MgCl_2$, 2% Triton

X-100) for 2 hours at 4°C, after which beads were washed 3X in Buffer B. Clearing beads were removed from lysate and the pre-cleared lysate was split into two equal volumes and added to antibody-bound beads (MANDAG2 or IgM) and incubated at 4°C overnight. At 4°C, two polystyrene columns were equilibrated with 1mL Buffer B. Lysate was spun down at 800g for 2 minutes to pellet beads after which supernatant was discarded. Beads were suspended in Buffer B and applied to equilibrated columns. Columns were washed with 50mL of Buffer B by gravity flow without disturbing the beads. Proteins were eluted off the beads with 2 x 500µl 100mM glycine. Proteins were precipitated with 20% Trichloroacetic acid (final volume) overnight. (All steps were performed at 4°C up to this point.) Tubes were spun for 15 minutes on a tabletop centrifuge to pellet protein precipitates and wash pellet 3X in ice cold acetone. Excess acetone was removed by placing the pellet on a 95°C heat block with tube lids open. The pellet was suspended in 100µl 1X LDS sample buffer with 1:100 2-Mercaptoethanol at 65°C for 2-3 hours with occasional agitation.

60µl of sample was run on a precast 4-15% gradient polyacrylamide gel (Bio-Rad, Cat. No. 4561084) at 120V for 80 minutes at room temperature. A Coomassie stain was used to visualize bands. The gel was fixed for 1 hour in 50% methanol, 10% acetic acid and stained for 20 minutes in 0.1% Coomassie Brilliant Blue R-250, 10% methanol, 10% acetic acid. Finally, the gel was destained in 40% methanol, 10% acetic acid for 1.5 hours with a kimwipe in the dish to absorb excess stain. Bands above 100kDa were cut out with a razor blade and digested with trypsin. Tryptic peptides were then prepared and analyzed by LC/MS using a Thermo Scientific Orbitrap Fusion mass spectrometer (Senko et al., 2013) and analyzed using the PAW pipeline (Wilmarth et al., 2009).

Silver Stain

10µl of sample from the large-scale immunoprecipitation was run on a precast 4-15% gradient gel (Bio-Rad, Cat. No. 4561084) at 120V for 80 minutes at room temperature. A silver stain kit (Pierce Silver Stain Kit, Thermo Scientific, Cat. No. 24612) was used to visualize bands with greater sensitivity than the Coomassie stain. The gel was imaged on a lightbox using a cell phone camera.

Gene Ontology Analysis

Gene ontology analysis was performed using the gprofiler2 R package (Kolberg et al., 2023, 2020; The Gene Ontology Consortium et al., 2023; Thomas et al., 2022). First, the g:Convert applet from g:Profiler was used to convert UniprotIDs to EntrezGene IDs. The EntrezGene IDs were provided to the gprofiler2 package in R to generate gene ontology terms. Driving terms were determined using the underlying topology of the annotations as described (Kolberg et al., 2023).

Small Scale Immunoprecipitation and WGA Membrane Enrichment

Lysate Preparation

Brain tissue was lysed in 1mL of lysis buffer (100mM NaCl, 20mM HEPES pH 7.4, 2mM $CaCl_2$, 2.5mM $MgCl_2$, 1% Triton X-100, 1% n-Octyl-β-D-glucopyranoside) containing protease inhibitor (Roche cOmplete EDTA-free protease inhibitor cocktail, Millipore Sigma, Cat. No. COEDTAF-RO) in a glass dounce homogenizer. Homogenate was rocked at 4°C for 2+ hours and then spun down at 12,500g for 20 minutes and the pellet discarded. Protein concentration in the lysate was measured using a Pierce BCA Assay Kit (Thermo Scientific, Cat. No 23225).

Small Scale Immunoprecipitation

2µg of anti-β-Dystroglycan (MANDAG2) (DSHB, Cat. No. 7D11) antibody was bound to 25µl Protein G beads for 2+ hours at 4°C after which beads were washed 3X in lysis buffer. 1000µg of lysate was applied to antibody-bound beads and incubated overnight at 4°C. Beads were washed 3X in PBS and suspended in 25µl of 1X LDS sample buffer with 1:100 2-Mercaptoethanol. Samples were boiled at 95°C for 5 minutes before proceeding to SDS-PAGE and western blotting.

WGA Membrane Enrichment

25µl of agarose-bound Wheat Germ Agglutinin (WGA) was washed 3X in lysis buffer. 1000µg of lysate was applied to WGA beads and incubated overnight at 4°C. Beads were washed 3X in PBS and suspended in 25µl of 1X LDS sample buffer with 1:100 2-Mercaptoethanol. Samples were boiled at 95°C for 5 minutes before proceeding to SDS-PAGE and western blotting.

SDS-PAGE and Western Blot

20µl of prepared sample was loaded into a 4-15% polyacrylamide gel (Bio-Rad, Cat. No. 4561085) and run at 100V for 100 minutes followed by transfer to PVDF membrane (100V for 100 minutes). Membranes were blocked in 5% milk TBST for 30+ minutes at room temperature and then incubated overnight in 5% milk TBST containing primary antibody. Antibodies used: α-Dystroglycan (IIH6C4) (Millipore, Cat. No. 05-593, mouse IgM, 1:500), β-Dystroglycan (MANDAG2) (DSHB, Cat. No. 7D11, mouse IgG1, 1:500), Cntnap1 (NeuroMab, Cat. No. K65/25, mouse IgG1, 1:500), β3-tubulin (Cell Signaling Technology, Cat. No. 5568, rabbit, 1:2000). Membranes were washed 3X in TBST and incubated on fluorescent IRDye secondary antibody (1:10,000, LI-COR) in 5% milk TBST for 1 hour at room temperature. Membranes were imaged using a LI-COR Odyssey CLx 0918 imager.

Immunohistochemistry

Mice were deeply anesthetized using CO_2 and transcardially perfused with ice cold 0.1M phosphate buffered saline (PBS) for two minutes to clear blood from the brain, followed by 15mL of ice cold 4% paraformaldehyde (PFA) in PBS. Brains were post-fixed in 4% PFA for 30 minutes at room temperature after which they were rinsed in PBS and embedded in 4% low-melt agarose (Fisher, Cat. No. 16520100) and sectioned at 50µm (hippocampus) or 70µm (cerebellum) using a vibratome (VT1200S, Leica Microsystems Inc., Buffalo Grove, IL) into 24-well plates containing 1mL of 0.1M PBS with 0.02% sodium azide.

Free-floating tissue sections were blocked in blocking solution (0.2% Triton X-100, 2% normal goat serum, 0.02% sodium azide in 0.1M PBS) for 1 hour at room temperature. Sections were then incubated with primary antibodies (**Table 5.3**) diluted in blocking solution for 48-72 hours at 4°C. For staining of Dystroglycan synaptic puncta, an antigen retrieval step was performed prior to incubation in primary antibody. Briefly, sections were incubated in sodium citrate solution for 15 min at 95 degrees in a water bath. Following incubation in primary antibody, sections washed with PBS three times for 20 min each. Sections were then incubated with a cocktail of secondary antibodies (1:500, Alexa Fluor 488, 546, 647) in blocking solution overnight at room temperature. Sections were washed with PBS three times for 20 min each and counterstained with Hoechst 33342 (1:10,000, Life Technologies, Cat# H3570) for 20 min to visualize nuclei. Finally, sections were mounted on slides using Fluoromount-G (SouthernBiotech) and sealed using nail polish.

Table 5.3 Primary Antibodies Used for Immunohistochemistry

Target	Host	Dilution	Source	Cat. No.	RRID
Calb1	Chicken	1:1000	Boster Bio	M03047-2	AB_2936235
IIH6	Mouse IgM	1:250	Millipore	05-539	AB_309828
Cntnap1	Mouse IgG1	1:500	NeuroMab	K65/35	AB_2083496
CB_1R	Guinea Pig	1:500	Synaptic Systems	258-104	AB_2661870
NF-M	Mouse IgG1	1:500	DSHB	2H3	AB_531793

Microscopy

Imaging was performed on either a Zeiss Axio Imager M2 fluorescence upright microscope equipped with an Apotome.2 module or a Zeiss LSM 980 laser scanning confocal build around a motorized Zeiss Axio Observer Z1 inverted microscope with a Piezo stage. The Axio Imager M2 uses a metal halide light source (HXP 200 C), Axiocam 506 mono camera, and 10X/0.3 NA EC Plan-Neofluar, 20X/0.8 NA Plan-Apochromat objectives. The LSM 980 confocal light path has two multi-alkali PMTs and two GaAsP PMTs for four track imaging. Confocal images were acquired using a 63X/1.4 NA Plan-Apochromat Oil DIC M27 objective. Z-stack images were acquired and analyzed offline in ImageJ/FIJI (Schindelin et al., 2012). Images used for comparison between genotypes were acquired using the same exposure times. Brightness and contrast were adjusted in FIJI to improve visibility of images for publication. Figures were composed in Adobe Illustrator 2023 (Adobe Systems).

Supplementary Figures

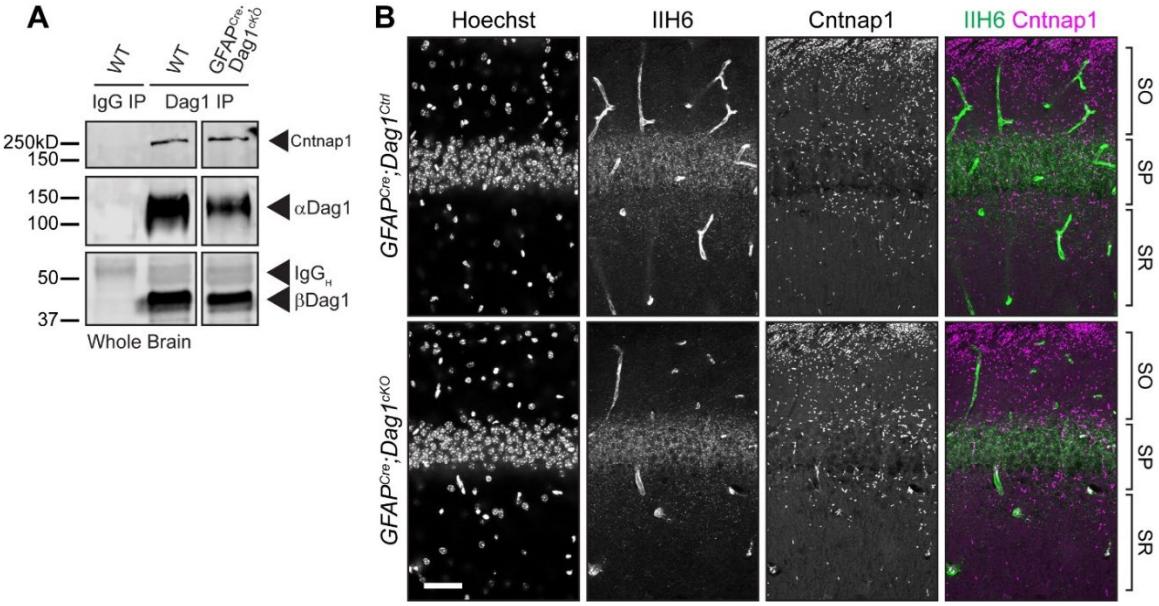

Supplementary Figure 5.1 Cntnap1 expression appears normal in mice with astrocytic knockout of Dystroglycan.

(A) Dystroglycan immunoprecipitation in whole brain from WT controls and *GFAP^{Cre};Dag1^{cKO}* mice. Immunoblot for Dystroglycan and Cntnap1. **(B)** Immunohistochemical labeling for Hoechst (nuclei), IIH6 (Dystroglycan), and Cntnap1 in hippocampal CA1 of *GFAP^{Cre};Dag1^{cKO}* mice and littermate controls. Scale bar = 50μm. (SO = *stratum oriens*, SP = *stratum pyramidale*, SR = *stratum radiatum*.)

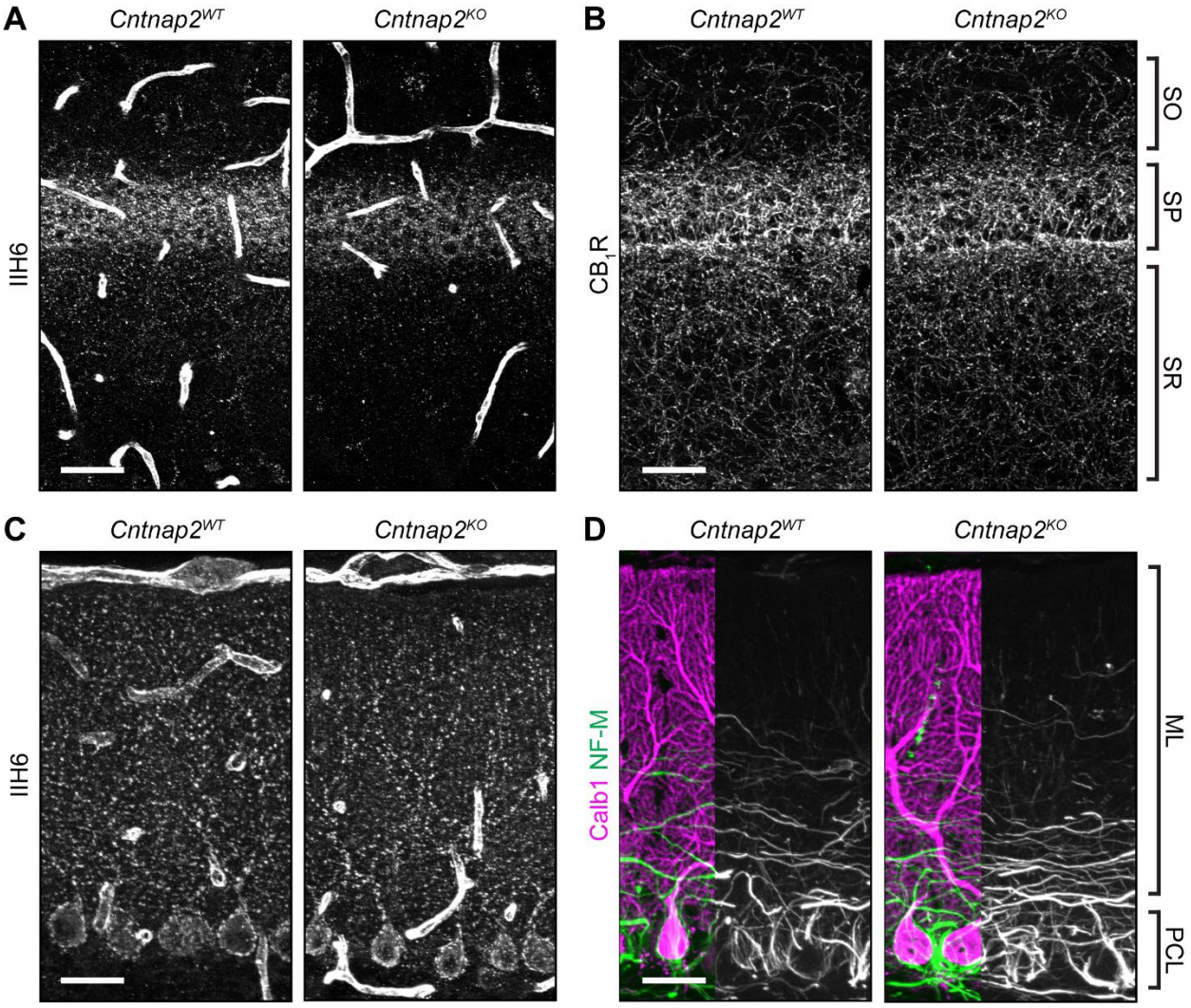

Supplementary Figure 5.2 Dystroglycan expression and axon targeting in *Cntnap2*^{KO} mice.

(A-B) Immunolabeling in hippocampal CA1 of WT and *Cntnap2*^{KO} mice for **(A)** Dystroglycan and **(B)** CB_1R, which labels CB_1R^+/CCK^+ interneuron axons. **(C-D)** Immunolabeling in cerebellar cortex of WT and *Cntnap2*^{KO} mice for **(C)** Dystroglycan and **(D)** NF-M, which labels basket interneuron axons. Scale bar = 50μm.

Chapter 6: Discussion

Summary of Results

Dystroglycan (Dag1) was first identified as the transmembrane component of the Dystrophin Glycoprotein Complex (DGC) in muscle where it functions to connect the actin cytoskeleton to the extracellular matrix (Ibraghimov-Beskrovnaya et al., 1992). In the 1990s it was discovered that Dystroglycan is necessary for the clustering of acetylcholine receptors at the neuromuscular junction (NMJ), illustrating a link between Dystroglycan and synaptic structure for the first time (Cohen et al., 1995; Montanaro et al., 1998). It was later discovered that Dystroglycan co-localizes with markers of inhibitory synapses in multiple systems (Briatore et al., 2010; Lévi et al., 2002), however its role at inhibitory synapses remained unclear. Initial reports *in vitro* acknowledged Dystroglycan's localization to inhibitory synapses but concluded that it was dispensable for synaptogenesis (Lévi et al., 2002). Over a decade later another *in vitro* study showed that Dystroglycan was involved in homeostatic synaptic scaling of GABAergic synapses, concluding that Dystroglycan played a role in $GABA_A$ receptor trafficking (Pribiag et al., 2014). The first evidence for a synaptic role for Dystroglycan *in vivo* wasn't until 2016, when Früh and colleagues reported that postsynaptic conditional deletion of *Dag1* from forebrain pyramidal neurons resulted in a near complete loss of hippocampal CCK^+/CB_1R^+ basket interneuron axons, accompanied by impaired inhibitory transmission from CCK^+/CB_1R^+ basket cells onto pyramidal cells (Früh et al., 2016). This led us to ask (1) what is the mechanism of Dystroglycan's function in inhibitory systems? (2) Do inhibitory synaptic defects in conditional knockouts result in aberrant seizure activity? And (3) is Dystroglycan required for synapse formation and/or function in other synaptic populations as well?

In Chapter 2 I showed that widespread deletion of *Dag1* from forebrain progenitors early in development (*Emx1*^{Cre}) did not result in a loss of hippocampal CCK^{+}/CB$_1$R^{+} axons, but rather a failure of these axons to appropriately target the somas of pyramidal neurons. This was accompanied by impaired synapse formation, impaired synapse function, and an increased susceptibility to seizures. These phenotypes were recapitulated in a mouse model in which Dystroglycan was not properly glycosylated, showing that each of these processes rely on extracellular glycan-protein interactions. Hypomorphic point mutations in two different glycosyltransferases (*Fkrp*^{P4448L}, *B4gat1*^{M155T}) showed slightly impaired synapse formation but normal synapse function, illustrating that the dependence on Dystroglycan's glycosylation for these processes is scalable and that a large reduction in glycosylation is necessary before detectable impairments manifest. Using a mouse model in which a truncated form of Dystroglycan lacking the intracellular domain was constitutively expressed, I showed that the intracellular domain is not required for synapse formation but it is required for synapse function.

In Chapter 3 I describe a suite of genetic tools available to drive conditional mutations in cerebellar Purkinje cells, applying their use to conditional knockout of *Dag1* with varying degrees of cellular and temporal specificity. *Pcp2*^{Cre} and AAV8 viral delivery of *Cre* had similar time courses of *Cre* expression with expression beginning around the second postnatal week and extending into the third. I found that the loss of synaptic Dystroglycan protein exhibited a significant lag behind the introduction of *Cre* expression when *Cre* is expressed after *Dag1* expression has already begun. This reflects the incredible stability and low turnover rate of Dystroglycan in the synapse and highlights that *Pcp2*^{Cre} and *AAV8-Cre* are only useful for studying the role of Dystroglycan in synapse maintenance. I identified and characterized *Calb1*^{Cre} as a line with embryonic expression of *Cre* in developing Purkinje cells, which resulted in early and complete loss

of Dystroglycan protein, allowing me to study the function of Dystroglycan in synaptogenesis.

The tools described in Chapter 3 allowed me to then study Dystroglycan's role in both the formation and maintenance of Purkinje cell synapses in Chapter 4. Early conditional knockout of *Dag1* from Purkinje cells using *Calb1*^{Cre} resulted in impaired formation and function of MLI:PC synapses. Later conditional knockout of *Dag1* from Purkinje cell using *Pcp2*^{Cre} resulted in a similar functional defect after P60, showing that Dystroglycan is required for both synapse formation and maintenance. Early removal of glycosylation on Dystroglycan resulted in similar defects in synapse formation and function, showing that Dystroglycan requires glycan-protein interactions to accomplish its function at MLI:PC synapses. Expression of a truncated version of Dystroglycan lacking the intracellular domain showed normal MLI:PC synapse formation but impaired synaptic function. These results suggest that Dystroglycan's function at MLI:PC synapses operates under a similar mechanism as described at hippocampal CCK^+/CB_1R^+ basket synapses onto pyramidal neurons (**Chapter 2**).

In Chapter 5 I present preliminary data showing a novel interaction between the Neurexin family member Cntnap1 and Dystroglycan in the brain. I first identified this interaction using a Dystroglycan immunoprecipitation coupled with mass spectrometry, and then confirmed the interaction *in vivo* biochemically. The interaction appears to occur in all regions analyzed (cortex, hippocampus, and cerebellum). However, the significance of this interaction at synapses remains unclear; the binding between Dystroglycan and Cntnap1 was not disrupted by widespread deletion of *Dag1* using *Emx1*^{Cre} and I was unable to identify regions where Cntnap1 and Dystroglycan protein colocalize using immunohistochemical labelling.

Together these results represent the very beginning of understanding the molecular mechanism of Dystroglycan's function at inhibitory synapses in the

hippocampus and cerebellum. It is interesting that Dystroglycan not only instructs axon targeting but is also required for synapse formation and synapse maintenance. It is likely that there are different interacting proteins at play for each of these different roles of Dystroglycan. We now understand the molecular domains that are involved, however the precise molecules that interact with Dystroglycan both pre- and post-synaptically will require further research.

Table 6.1 Summary of results.
Phenotype expression key: + = mild defect, ++ = moderate defect, +++ = severe defect, - = absence of phenotype. Note that expression timings refer to the onset of *Cre* expression in the targeted population, not the loss of Dystroglycan protein.

Genetic Model	Expression	Synaptic Population Studied	Axon Targeting Defect	Synapse Formation Defect	Synapse Function Defect
Emx1^{Cre};Dag1^{cKO}	E10.5 deletion of Dag1 from neurons and glia of the forebrain.	CCK:PyN	+++	+++	+++
Emx1^{Cre};Pomt2^{cKO}	Unglycosylated Dystroglycan (E10.5) in neurons and glia of the forebrain.	CCK:PyN	+++	+++	+++
Dag1$^{\Delta ICD}$	Truncated Dystroglycan lacking intracellular domain in all cells.	CCK:PyN	+	-	+++
Fkrp^{P448L}	Hypoglycosylated (mild) Dystroglycan in all cells.	CCK:PyN	+	++	-
B4gat1^{M155T}	Hypoglycosylated (mild-to-moderate) Dystroglycan in all cells.	CCK:PyN	+	++	-
Calb1^{Cre};Dag1^{cKO}	E14.5 deletion of Dag1 from Purkinje cells in the cerebellum.	MLI:PC	*Not examined*	++	+++
Pcp2^{Cre};Dag1^{cKO}	P7-P14 deletion of Dag1 from Purkinje cells in the cerebellum.	MLI:PC	*Not examined*	*Not examined*	+++
Calb1^{Cre};Pomt2^{cKO}	Unglycosylated Dystroglycan (E14.5) in Purkinje cells.	MLI:PC	*Not examined*	++	++
Calb1^{Cre};Dag1$^{c\Delta ICD}$	Truncated Dystroglycan (E14.5) lacking intracellular domain in Purkinje cells.	MLI:PC	*Not examined*	-	+++

Dag1 is a postsynaptic recognition target of basket cell axons

Postsynaptic deletion of *Dag1* from forebrain pyramidal cells (*NEX^{Cre};Dag1^{cKO}*) results in a dramatic CCK$^+$/CB$_1$R$^+$ basket interneuron targeting defect in which the axons are nearly completely absent in hippocampal CA1-3 (Früh et al., 2016; Miller and Wright, 2021). More widespread deletion of *Dag1* from forebrain progenitors (*Emx1^{Cre};Dag1^{cKO}*) or from neural stem cells (*Nestin^{Cre};Dag1^{cKO}*) results in a similar but somehow less severe basket targeting defect in which the axons are still present but fail to target the somatic compartment of pyramidal neurons (**Chapter 2**). Together, this suggests that Dystroglycan is acting as a crucial postsynaptic recognition receptor of presynaptic CCK$^+$/CB$_1$R$^+$ basket interneuron axons.

Dystroglycan's expression as an extensively glycosylated transmembrane cell adhesion molecule places it well suited to serve as an extracellular recognition cue. In other systems, Dystroglycan has similarly been shown to be required for axon targeting (Clements and Wright, 2018; Lindenmaier et al., 2019; Wright et al., 2012). These cases differ from the mechanism involved in CCK$^+$/CB$_1$R$^+$ axon targeting in that Dystroglycan's role in axon targeting in spinal cord commissural axons, retinal ganglion cells, descending corticothalamic projections, and ascending thalamocortical projections all reflect a role for neuroepithelial Dystroglycan whereas hippocampal CCK$^+$/CB$_1$R$^+$ basket interneuron axon targeting is mediated by neuronal Dystroglycan expressed by pyramidal cells (Clements & Wright, 2018; Früh et al., 2016; Lindenmaier et al., 2019; Miller & Wright, 2021; Wright et al., 2012; **Chapter 2**). The fact that *Emx1^{Cre};Pomt2^{cKO}* mice, in which the extracellular domain of Dystroglycan is severely hypoglycosylated, show the same CCK$^+$/CB$_1$R$^+$ basket axon targeting defect as *Emx1^{Cre};Dag1^{cKO}* mice provides compelling evidence that Dystroglycan itself, and not some interacting molecule, is the postsynaptic receptor of these basket axons and that the interface between the pre- and post-synaptic side occurs via the extracellular glycan chains of

Dystroglycan (**Chapter 2**). The presynaptic ligand, however, is still a mystery. Hippocampal Dystroglycan immunoprecipitation and mass spectrometry experiments at earlier developmental stages may provide candidate binding partners to explore.

An unexpected finding of this study was that other CCK^+/CB_1R^+ interneuron populations throughout the brain (olfactory bulb, basal amygdala, cortex) exhibited similarly mistargeted axons in *Emx1^{Cre};Dag1^{cKOs}* (**Chapter 2**). Perhaps this should have been expected, as these CB_1R^+ interneuron populations all belong to the same pool of progenitors as those that populate the hippocampus, originating from the caudal ganglionic eminence (CGE) before dispersing to their final destinations (Miczán et al., 2021; Nery et al., 2002; Touzot et al., 2016). This doesn't necessarily indicate a direct interaction between Dystroglycan and CB_1R as there are likely other commonly expressed genes between these populations, but any potential Dag1:CB_1R interaction could be easily confirmed biochemically. This finding does imply some sort of conserved role for Dystroglycan as an axon recognition cue for CCK^+/CB_1R^+ interneuron populations whereas other interneuron populations seem to form independently of Dystroglycan. There is likely a conserved transmembrane protein expressed uniquely by CCK^+/CB_1R^+ populations that interacts directly with Dystroglycan to initiate synapse formation. Alternatively, other interneuron populations have functional redundancy that the CCK^+/CB_1R^+ population does not.

In the cerebellum, we currently lack tools to rigorously assess MLI axon targeting of Purkinje cells. As such, I was unable to evaluate any axon targeting defect in my mutant models. The neurofilament medium chain (NF-M) protein appears to be selectively expressed by basket cells in cerebellar cortex, but a poorly understood subset of them (**Appendix F: Figure 0.5**). Furthermore, the particular Purkinje cell *Cre* driver lines that I used (*Calb1^{Cre}*, *Pcp2^{Cre}*) both only delete *Dag1* postsynaptically, from Purkinje cells (**Chapter 3**, **Chapter 4**). This is akin to the *NEX^{Cre}* model in which there is

a near complete loss of presynaptic axons, differing from the effect of a broad deletion of *Dag1* (Früh et al., 2016; Miller and Wright, 2021). Therefore, in addition to identifying a tool to label MLI axons, we must also identify a tool for driving a more widespread deletion of *Dag1* in the cerebellum to model more physiologically relevant loss of Dystroglycan. Patients with dystroglycanopathy commonly exhibit cerebellar hypoplasia, which has not been observed in mouse models, probably because of the mouse models used. An early "pan-cerebellar" mouse line would be a way to address this limitation. An obvious candidate would be *Nestin*^{Cre}, however we found that the particular *Nestin*^{Cre} line that we have in our colony does not target Purkinje cells (**Chapter 3**). While *Wnt1* is involved in hindbrain patterning, *Wnt1*^{Cre} showed variable *Cre* expression throughout the cerebellum in our hands (**Appendix D: Figure 0.3**). Another candidate *Cre* driver line is *En1*^{Cre}, though *En1* expression is known to vary between lobules and sagittal stripes, limiting its utility (Sillitoe et al., 2008). Thus, additional tools will need to be identified before we can assess Dystroglycan's role in cerebellar axon targeting.

Glycosylation of Dystroglycan is required for synapse formation and function

It has been known that the matriglycan repeats on the terminal portion of Dystroglycan's glycan chains represent the binding site between Dystroglycan and nearly all of its extracellular biding partners. The importance of these interactions is exemplified by clinical cases of dystroglycanopathy, a form of muscular dystrophy characterized by a reduction in the glycosylation of Dystroglycan. Dystroglycanopathies are characterized primarily by impaired muscle integrity but are often accompanied by neurological deficits. These neurological impairments led us to hypothesize that glycosylation of Dystroglycan is crucial for its role at synapses throughout the brain.

Over the course of this dissertation, I generated an array of hypoglycosylation mutants to assess the role of glycosylation in synapse formation and function in both the hippocampus, at CCK:PyN basket synapses (**Chapter 2**), and the cerebellum at MLI:PC synapses (**Chapter 4**). The results were synonymous between the two synaptic populations. In both regions I found that conditional deletion of the glycosyltransferase *Pomt2* resulted defects in both synapse formation and synapse function in a manner that largely phenocopied *Dag1* conditional knockout. This parallel between CCK:PyN and MLI:PC synapses implies a conserved mechanism of Dystroglycan's synaptic function.

My data show that extracellular glycosylation of Dystroglycan is acting as a binding site for some presynaptic interacting partner. However, the precise identity of this binding partner is unknown and may differ between synaptic populations. The most obvious candidate for both regions is some flavor of Neurexin isoform. There are three Neurexin family members (Nrxn1-3), each of which has many splice variants. Dystroglycan is biochemically capable of binding isoforms from all three Neurexins so long as they lack an insert at splice sites 2 or 4 (but not both) (Reissner et al., 2014; Sugita et al., 2001; Trotter et al., 2023). Single cell RNA sequencing suggests that CCK^{+}/CB_1R^{+} interneurons express Neurexin isoforms capable of binding Dystroglycan (Fuccillo et al., 2015). Whether the correct splice variants are expressed by presynaptic MLIs in the cerebellum needs to be examined.

Identifying the Neurexin isoform(s) at play at CCK:PyN and MLI:PC synapses is possible but nontrivial. Due to the ability of alternative isoforms to compensate for Neurexin mutations, a triple conditional knockout model with single isoform rescue must be employed to faithfully study the role of Neurexins. Presynaptic deletion of Neurexins from cerebellar MLIs can be accomplished using lines such as $Ascl1^{CreERT2}$, $cKit^{Cre}$, or $nNOS^{Cre}$, each of which drive *Cre* expression prior to synaptogenesis. Unfortunately, targeting triple knockout of Neurexins to CCK^{+}/CB_1R^{+} interneurons requires an

intersectional *Cre/Flp* approach that needs further refinement before it is useful (Grieco et al., 2023). *Sncg*^{FlpO} has been used to target the CCK^+/CB_1R^+ population with success, however while it is more specific than *CCK*^{Cre}, there is still some *Flp* expression in interneurons in *stratum oriens* and *stratum radiatum* (Dudok et al., 2021). These systems are particularly unattractive because such approaches would require three new conditional *Neurexin* lines with FRT sites to be designed for compatibility (or the generation of a *Sncg*^{Cre} line, for example). Furthermore, single isoform rescue is typically accomplished using AAV viral delivery, and the timing of AAV expression may prohibit the study of mechanisms underlying synapse formation (**Chapter 3**). New tools will permit faster transduction and open new avenues of research.

The cytoplasmic domain of Dystroglycan is required for synapse function but not formation

In 2009, a mouse model expressing a truncated version of Dystroglycan lacking an intracellular domain (*Dag1*$^{\Delta ICD}$) was first published (Satz et al., 2009). Though this mouse was reported to develop muscular dystrophy, it exhibited normal neural development (Satz et al., 2010, 2009). It was later reported that axon guidance in thalamocortical axons, corticothalamic axons, and axons in the spinal commissure of the floor plate was also normal in these mutants, as opposed to *Dag1* conditional knockouts which had perturbed axon targeting in each of these systems (Lindenmaier et al., 2019). This left the role of the cytoplasmic domain of Dystroglycan in the nervous system a mystery.

In this dissertation I present for the first time evidence that the cytoplasmic domain is required for neuronal Dystroglycan's role in synapse function, but not formation, in both the hippocampus and cerebellum. Synapse numbers for both

hippocampal CCK:PyN and cerebellar MLI:PC synapses appears normal in *Dag1*$^{\Delta ICD}$ mice, indicating normal synapse formation. Despite this, both populations of synapses exhibited functional impairments. In the hippocampus, *Dag1*$^{\Delta ICD}$ pyramidal cells had a reduced baseline sIPSC frequency and an attenuated response to the cholinergic agonist Carbachol, indicating impaired CCK^+/CB_1R^+ interneuron function. In the cerebellum, *Calb1*^{Cre}*;Dag1*$^{c\Delta ICD}$ Purkinje cells showed a reduced mIPSC frequency and amplitude. Thus, although synapse number is normal, there are functional impairments at multiple Dystroglycan positive synaptic populations in the *Dag1*$^{\Delta ICD}$ brains.

The mechanism through which the intracellular domain of Dystroglycan is informing synapse function remains unknown. It is possible that the intracellular domain of Dystroglycan is required to regulate the localization of Neuroligin in the inhibitory postsynapse. Neuroligin is linked to Dystroglycan intracellularly through S-SCAM and a reduction in cerebellar Neuroligin-2 puncta density has been observed in Dystroglycan conditional knockouts in which Dystroglycan is deleted from Purkinje cells after synaptogenesis (Briatore et al., 2020; Sumita et al., 2007). This remains to be examined in models of impaired synapse formation.

Due to Dystroglycan's role in ion channel clustering in other systems (see **Chapter 1**), it is tempting to hypothesize that Dystroglycan clusters $GABA_A$ receptors through intracellular interactions, however there is no evidence to suggest that Dystroglycan interacts with $GABA_A$Rs directly (see mass spec results from **Chapter 5**, **Appendix J: Table 0.3**) and $GABA_A\alpha1$ density was largely normal (slightly increased) in *Calb1*^{Cre}*;Dag1*$^{c\Delta ICD}$ cerebellar cortex (**Chapter 4**). While my mass spec results suggested a direct interaction between Dystroglycan and Gephyrin (**Chapter 5**), which would have to be intracellular and would surely influence $GABA_A$R clustering, I was unable to verify this interaction (**Appendix G: Figure 0.6**). That being said, Gephyrin interacts with

Neuroligin-2 (Nlgn2), which interacts with Dystroglycan through S-SCAM, suggesting a possible indirect interaction (Poulopoulos et al., 2009; Sumita et al., 2007), and I have preliminary data suggesting that Gephyrin puncta density and colocalization with Dystroglycan may be reduced in *Calb1*^{Cre}*;Dag1*$^{c\Delta ICD}$ cerebellar cortex (**Appendix G: Figure 0.6**). We still don't know whether $GABA_A$Rs are localized correctly, directly apposed to release sites in their synaptic nanodomains, in *Dag1*$^{\Delta ICD}$ mutants. Super resolution microscopy will be necessary to examine synapse structure in our mutant models.

Dystroglycan's role in synapse maintenance

While Neurexins and Neuroligins have been well established to be involved in synaptic maintenance, Dystroglycan's role in synapse maintenance remains poorly understood. Previous work using *L7*^{Cre} to delete *Dag1* from cerebellar Purkinje cells resulted in loss of Dystroglycan protein by P90. This late deletion of *Dag1* resulted in impaired MLI:PC synapse function and a loss of synaptic elements such as $GABA_A$Rs and Nlgn2, suggesting that Dystroglycan is required for the maintenance of MLI:PC synapses (Briatore et al., 2020). My work in Chapter 4 confirmed these findings using *Pcp2*^{Cre} to delete *Dag1* during the period of synaptogenesis, also resulting in impaired MLI:PC synapse function at P60. Interestingly, *Pcp2*^{Cre}*;Dag1*^{cKOs} showed a loss of Dystroglycan protein by P30 (**Chapter 3**), but mIPSC recordings at P25 showed no phenotype, whereas mIPSC recordings at P60 showed a reduction in mIPSC frequency and amplitude (**Chapter 4**). This implies that synapses are stable in the absence of Dystroglycan for some period of time before a detectable functional deficit manifests. Synapses aren't thought to be under physical strain, so what induces synapse disassembly after loss of Dystroglycan? While not quite currently feasible at this

population of synapses, long-term *in vivo* dual-channel imaging of tagged Dystroglycan with a tagged $GABA_AR$ or other synaptic component would help answer this question.

In the hippocampus, the role of Dystroglycan in synapse maintenance has not been well studied. Früh and colleagues (2016) injected *Dag1*$^{flox/flox}$ mice with AAV8-CaMKIIa-Cre at 8-10 weeks of age to drive the deletion of *Dag1* in pyramidal cells after synaptogenesis. As early as 4 weeks after viral injection, a loss of VGluT3 (a marker of CCK:PyN synapses) was observed, indicating that Dystroglycan is required for the maintenance of this population of synapses. Using a similar approach, Miller & Wright (2021) used a *CaMKIIa*^{CreERT2} mouse line with Tamoxifen administration at P23 to delete *Dag1* from excitatory cells after the establishment of mature synapses. Observation of CCK^+/CB_1R^+ axons in the hippocampus at P65 showed normal axonal organization, implying that Dystroglycan is not required for the maintenance of this circuit. However, loss of Dystroglycan protein was not confirmed, synapse function was never assessed, and synaptic components were not analyzed. Therefore, we cannot confidently confirm with current data whether or not Dystroglycan is required for the maintenance of hippocampal CCK:PyN synapses.

Functional domain involvement in surface trafficking and synaptic localization of Dystroglycan

Dystroglycan is first trafficked to the endoplasmic reticulum (ER) where it begins the early steps of glycosylation. It is then trafficked to the Golgi apparatus to complete its glycosylation before being trafficked to the surface (see **Chapter 1**). In Chapter 2 I found that Dystroglycan protein in *Emx1*^{Cre}*;Pomt2*^{cKO} pyramidal cells does not localize to punctate structures consistent with synaptic localization. Pomt2 is required for the very first steps of glycosylation in the ER. Does knockout of *Pomt2* therefore impair protein

trafficking and localization? Membrane-enriched WGA lysate indicated normal levels of Dystroglycan in the membrane, suggesting that trafficking is normal, but that trans-synaptic interactions are required to instruct synaptic localization.

IIH6 immunostaining to label glycosylated Dystroglycan in truncated *Dag1*$^{\Delta ICD}$ mutants indicated punctate localization in both hippocampal pyramidal cells (**Chapter 2**) and cerebellar Purkinje cells (**Chapter 4**). Immunohistochemical labeling with both IIH6 and anti-VGAT in *Calb1*^{Cre}*;Dag1*$^{\Delta ICD}$ suggests that Dystroglycan is localized to synapses, though the appearance of the IIH6 immunostaining seems less precisely organized in mutants compared to controls (**Chapter 4**, **Appendix H: Figure 0.7**). We were surprised to find that membrane-enriched WGA lysate indicated that Dystroglycan in *Dag1*$^{\Delta ICD}$ mutants is hypoglycosylated, suggesting that trafficking might be affected by the intracellular truncation (**Chapter 2**). Biochemical fractionation and/or surface expression assays in functional domain mutants (*Pomt2*^{cKO}, *Dag1*$^{\Delta ICD}$) will help to assess the requirements for Dystroglycan trafficking.

Overall working model of Dystroglycan's synaptic function

Much of what is known about synapse formation is known from studying excitatory glutamatergic synapses. Glutamatergic synapses tend to be formed between a presynaptic axonal terminal and a postsynaptic dendritic spine. The presence of a distinct postsynaptic structure makes the identification of postsynaptic sites possible without a synaptic marker and spine volume can be tracked across the lifespan of a synapse as a correlate of synapse maturity and strength. Inhibitory synapses, on the other hand, tend to be formed on the dendritic shaft and cannot be identified structurally. We are therefore more reliant on genetic tools and functional readouts. Even so, many of the processes that occur during excitatory synapse formation are likely to occur in

some capacity during inhibitory synapse formation as well. An axon must identify its postsynaptic target through some sort of cue or receptor. After contact is made between the pre- and postsynaptic sides, scaffolding molecules, receptors, and machinery are recruited as the synapse matures. The synapse then enters a maintenance phase, in which changes to synaptic content may be made in response to activity. Too much or too little activity may result in synapse elimination.

Conditional deletion of *Dag1* from the postsynaptic cell results in impaired axon targeting and synapse formation accompanied by diminished synapse function (Früh et al., 2016; Miller & Wright, 2021; **Chapter 2**, **Chapter 4**), indicating that Dystroglycan is involved in the earliest steps of synapse formation: axon recognition. This appears to be mediated through extracellular interaction via the glycan chains on α-Dystroglycan, as removal of glycosylation leads to these same axon targeting and synaptic formation impairments (**Chapter 2**, **Chapter 4**). When extracellular glycosylation is retained but the intracellular domain of β-Dystroglycan is removed, synapses appear to nucleate but synapse function is impaired, suggesting that the intracellular domain is required for synapse maturation and the recruitment of appropriate synaptic machinery (**Chapter 2**, **Chapter 4**). Finally, removal of *Dag1* later in development, after the period of synaptogenesis, results in impaired synapse function, implying that Dystroglycan is required for the maintenance of synapses as well (Briatore et al., 2020; **Chapter 4**).

This suggests that Dystroglycan is involved in just about every stage of synapse development. While we don't know the precise interactions that occur at each stage, we know much about the composition of the mature synapse from previous research and can make a hypothesis as to how Dystroglycan functions during synapse maturation and maintenance. Dystroglycan's interaction with presynaptic Neurexin is likely foundational to maintaining the structural apposition of the pre- and postsynapse (Sugita et al., 2001; Trotter et al., 2023). Postsynaptic Neuroligin is linked to Dystroglycan intracellularly

through S-SCAM and to presynaptic Neurexin across the synaptic cleft (Sumita et al., 2007). Dystroglycan and Neuroligin have been shown to compete to bind to Neurexin, so presynaptic Neurexins probably bind either Dystroglycan or Neuroligin (Reissner et al., 2014). This Nlgn:Dag1:Nrxn+Nrnx:Nlgn adhesion circuit could support the synapse structure. Neuroligin also interacts with the intracellular inhibitory scaffolding molecule Gephyrin, which is important for the localization of $GABA_A$Rs in the postsynapse (Poulopoulos et al., 2009). Together, this weaves a complex web of interactions to regulate the structure and content of inhibitory synapses.

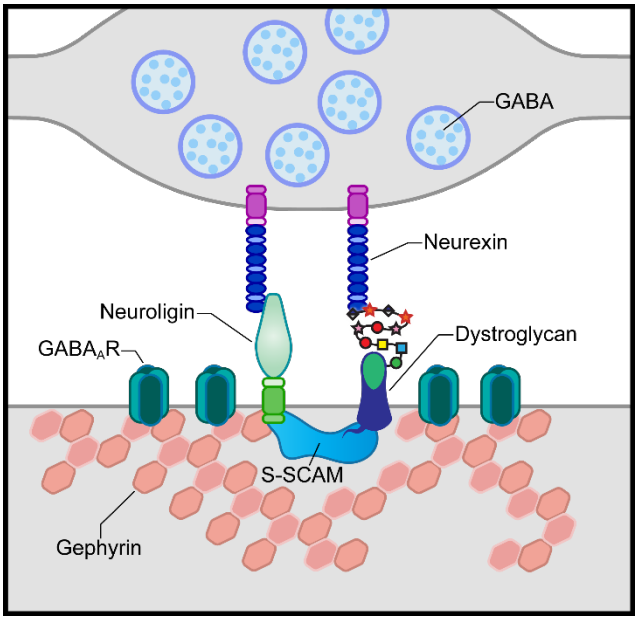

Figure 6.1 Working model of Dystroglycan's function at inhibitory synapses.
Postsynaptic Dystroglycan interacts with presynaptic Neurexin. A separate population of presynaptic Neurexin interacts with postsynaptic Neuroligin. Intracellularly, Neuroligin is linked to Dystroglycan through the MAGUK S-SCAM in the postsynapse. Neuroligin also interacts with the scaffolding molecule Gephyrin, which is required for the localization of postsynaptic $GABA_A$ receptors.

Translational implications

Treatment plans for patients with Dystroglycanopathies have long been focused on the muscular symptoms with little attention to neurological symptoms, but some patients experience intellectual disability and seizures with or without gross morphological abnormalities of the brain. Here I showed for the first time that mouse models of dystroglycanopathy exhibit a reduced seizure threshold. In addition to the seizure induction model, I observed that *Emx1*^{Cre}*;Pomt2*^{cKO} mice have spontaneous seizures that sometimes lead to death. Occasional spontaneous seizures in conditional

knockouts were observed during weaning and out of 7 spontaneous deaths of mice within my *Emx1^{Cre};Pomt2* colony over the course of a year, 6 were conditional knockouts. This allows us to also study epilepsy in this model in future studies. Now that we have a mouse model of seizure in dystroglycanopathy, we can explore therapies to alleviate possible synaptic deficits in patients.

Most cases of dystroglycanopathy are secondary dystroglycanopathies, in which the causative mutation is not in *Dag1* itself, but instead in one of the genes involved in the glycosylation of Dystroglycan. In Chapter 2 I presented three different models of secondary dystroglycanopathy (from severe to mild): *Emx1^{Cre};Pomt2^{cKO}*, *B4gat1$^{M155T/M155T}$*, *Fkrp$^{P448L/P448L}$*. Only the most severe model (*Pomt2*) showed a defect in synapse function by electrophysiology and only the most severe (*Pomt2*) and moderate (*B4gat1*) models showed increased seizure susceptibility. This leads us to believe that only a partial rescue of glycosylation will be required to alleviate neurological symptoms in dystroglycanopathy patients. Treatment via gene therapy is typically accomplished using viral delivery of DNA by AAV, but this is constrained by the packaging limit of AAV. While Dystroglycan is close to the packaging limit, most of the glycosyltransferases are smaller and can more easily be delivered by AAV for gene rescue. We can now test the efficacy of gene rescue for *Pomt2* and *B4gat1* in our mouse models, with seizure threshold as a readout of successful rescue.

In addition to seizure in dystroglycanopathy, Dystroglycan may be affected in temporal lobe epilepsy. Recent work showed that in a pilocarpine model of epilepsy, hippocampal CCK^+/CB_1R^+ interneuron axons become disorganized in a manner resembling the *Emx1^{Cre};Dag1^{cKO}* axon organization (Whitebirch et al., 2023). It would be interesting to evaluate whether Dystroglycan is downregulated in the pilocarpine model of epilepsy and whether overexpression of *Dag1* could rescue the interneuron axon phenotype. It is probable that Dystroglycan is only part of the puzzle here, as there is a

similar miswiring of PV^+ interneuron axons in the pilocarpine model, which is not observed in *Emx1^{Cre};Dag1^{cKOs}* (Whitebirch et al., 2023). While both CCK^+/CB_1R^+ and PV^+ populations of hippocampal basket synapses contain postsynaptic Dystroglycan, only the CCK^+/CB_1R^+ population is affected by *Dag1* knockout, suggesting that PV^+ axons do not require postsynaptic Dystroglycan for axon targeting (Früh et al., 2016; **Chapter 2**).

Future directions: Composition of the Dystroglycan-containing synaptic complex across development

Dystroglycan is the transmembrane component of the Dystrophin Glycoprotein Complex (DGC) and it thought to be co-expressed with other components of the DGC: wherever you find Dystroglycan, you should find the whole DGC. Many members of the DGC have been described, including Dystrophin, Utrophin, Sarcoglycans, Syntrophins, and Dystrobrevin (see **Chapter 1**). However, the precise composition of the DGC may vary from tissue to tissue and many of these members of the DGC were identified in muscle. Dystroglycan and Dystrophin colocalize at inhibitory synapses, but otherwise we don't know the composition of the synaptic DGC (Lévi et al., 2002). This has been difficult to examine due to Dystroglycan's broad expression throughout the brain. The ability to express a tagged version of Dystroglycan in a cell-type specific manner would permit the isolation of synaptic Dystroglycan which could then be examined via mass spectrometry to identify other members of the complex to be confirmed by immunohistochemistry.

Given Dystroglycan's involvement in synapse structure from axon recognition through the synapse maintenance period, it is likely that both the composition of the DGC and the presynaptic binding partner(s) of Dystroglycan shifts throughout development to accomplish each of these developmental roles. Dystroglycan probably

interacts with an axonal protein for axon recognition, then switches to a scaffolding molecule for synapse formation, maturation, and maintenance. While Neurexin is often thought to be involved in synapse maturation and maintenance, it is not typically involved in synapse formation, thus there is likely a separate interaction at play during synapse formation. Immunoprecipitation of cell-type specific Dystroglycan at different developmental timepoints, followed by analysis by mass spectrometry would allow us to identify candidate interactions at each life stage of a synapse. Once candidate interactions are identified, they can be confirmed biochemically, immunohistochemically, and then through genetic manipulation of candidate protein.

In Chapter 5, the identification of Cntnap1 as a novel interacting partner of Dystroglycan that is developmentally regulated represented an exciting candidate for a synaptic binding partner. However, the nature of this interaction is still unknown and may not occur at neuronal synapses. The difficulty I encountered in characterizing the Dag1:Cntnap1 interaction further illustrates the utility of a Cre-dependent tagged Dystroglycan mouse line as this would allow us to confirm or eliminate specific populations in which the interaction occurs, narrowing down the possible processes that the complex may be involved in.

Conclusion

In this dissertation I show that Dystroglycan is required for both synapse formation and maintenance at multiple populations of inhibitory synapses: hippocampal CCK:PyN basket synapses and cerebellar MLI:PC synapses. Extracellular glycosylation of Dystroglycan is required for synapse formation and function, whereas the intracellular domain of Dystroglycan is dispensable for synapse formation but required for synapse function. I also identify a novel interaction between Dystroglycan and Cntnap1, the

significance of which remains unclear. This represents important work towards understanding the neurological features of dystroglycanopathies.

References

Adams, J.C., Brancaccio, A., 2015. The evolution of the dystroglycan complex, a major mediator of muscle integrity. Biol. Open 4, 1163–1179. https://doi.org/10.1242/bio.012468

Akhavan, A., Crivelli, S.N., Singh, M., Lingappa, V.R., Muschler, J.L., 2008. SEA domain proteolysis determines the functional composition of dystroglycan. FASEB J. 22, 612–621. https://doi.org/10.1096/fj.07-8354com

Altman, J., 1972. Postnatal development of the cerebellar cortex in the rat. II. Phases in the maturation of Purkinje cells and of the molecular layer. J. Comp. Neurol. 145, 399–463. https://doi.org/10.1002/cne.901450402

Álvarez-Aznar, A., Martínez-Corral, I., Daubel, N., Betsholtz, C., Mäkinen, T., Gaengel, K., 2020. Tamoxifen-independent recombination of reporter genes limits lineage tracing and mosaic analysis using CreERT2 lines. Transgenic Res. 29, 53–68. https://doi.org/10.1007/s11248-019-00177-8

Anderson, C., Winder, S.J., Borycki, A.G., 2007. Dystroglycan protein distribution coincides with basement membranes and muscle differentiation during mouse embryogenesis. Dev. Dyn. 236, 2627–2635. https://doi.org/10.1002/dvdy.21259

Anderson, J.L., Head, S.I., Morley, J.W., 2003. Altered inhibitory input to Purkinje cells of dystrophin-deficient mice. Brain Res. 982, 280–283. https://doi.org/10.1016/S0006-8993(03)03018-X

Ashrafi, S., Betley, J.N., Comer, J.D., Brenner-Morton, S., Bar, V., Shimoda, Y., Watanabe, K., Peles, E., Jessell, T.M., Kaltschmidt, J.A., 2014. Neuronal Ig/Caspr Recognition Promotes the Formation of Axoaxonic Synapses in Mouse Spinal Cord. Neuron 81, 120–129. https://doi.org/10.1016/j.neuron.2013.10.060

Barresi, R., Campbell, K.P., 2006. Dystroglycan: From biosynthesis to pathogenesis of human disease. J. Cell Sci. 119, 199–207. https://doi.org/10.1242/jcs.02814

Barski, J.J., Dethleffsen, K., Meyer, M., 2000. Cre recombinase expression in cerebellar Purkinje cells. genesis 28, 93–98. https://doi.org/10.1002/1526-968X(200011/12)28:3/4<93::AID-GENE10>3.0.CO;2-W

Batchelor, C.L., Higginson, J.R., Chen, Y.J., Vanni, C., Eva, A., Winder, S.J., 2007. Recruitment of Dbl by ezrin and dystroglycan drives membrane proximal Cdc42 activation and filopodia formation. Cell Cycle 6, 353–363. https://doi.org/10.4161/cc.6.3.3819

Beedle, A.M., Turner, A.J., Saito, Y., Lueck, J.D., Foltz, S.J., Fortunato, M.J., Nienaber, P.M., Campbell, K.P., 2012. Mouse fukutin deletion impairs dystroglycan processing and recapitulates muscular dystrophy. J. Clin. Invest. 122, 3330–3342. https://doi.org/10.1172/JCI63004

Berghuis, P., Rajnicek, A.M., Morozov, Y.M., Ross, R.A., Mulder, J., Urbán, G.M., Monory, K., Marsicano, G., Matteoli, M., Canty, A., Irving, A.J., Katona, I., Yanagawa, Y., Rakic, P., Lutz, B., Mackie, K., Harkany, T., 2007. Hardwiring the brain: endocannabinoids shape neuronal connectivity. Science 316, 1212–1216. https://doi.org/10.1126/science.1137406

Bernard, C., Axelrad, H., 1993. Effects of recurrent collateral inhibition on Purkinje cell activity in the immature rat cerebellar cortex - an in vivo electrophysiological study. Brain Res. 626, 234–258. https://doi.org/10.1016/0006-8993(93)90584-A

Bigotti, M.G., Brancaccio, A., 2021. High degree of conservation of the enzymes synthesizing the laminin-binding glycoepitope of α-dystroglycan. Open Biol. 11. https://doi.org/10.1098/rsob.210104

Blaeser, A., Keramaris, E., Chan, Y.M., Sparks, S., Cowley, D., Xiao, X., Lu, Q.L., 2013. Mouse models of fukutin-related protein mutations show a wide range of disease phenotypes. Hum. Genet. 132, 923–934. https://doi.org/10.1007/s00439-013-1302-7

Bogdanik, L., Framery, B., Frölich, A., Franco, B., Mornet, D., Bockaert, J., Sigrist, S.J., Grau, Y., Parmentier, M.L., 2008. Muscle dystroglycan organizes the postysynapse and regulates presynaptic neurotransmitter release at the Drosophila neuromuscular junction. PLoS ONE 3. https://doi.org/10.1371/journal.pone.0002084

Bönnemann, C.G., Wang, C.H., Quijano-Roy, S., Deconinck, N., Bertini, E., Ferreiro, A., Muntoni, F., Sewry, C., Béroud, C., Mathews, K.D., Moore, S.A., Bellini, J., Rutkowski, A., North, K.N., 2014. Diagnostic approach to the congenital muscular dystrophies. Neuromuscul. Disord. 24, 289–311. https://doi.org/10.1016/j.nmd.2013.12.011

Booler, H.S., Williams, J.L., Hopkinson, M., Brown, S.C., 2016. Degree of Cajal–Retzius Cell Mislocalization Correlates with the Severity of Structural Brain Defects in Mouse Models of Dystroglycanopathy. Brain Pathol. 26, 465–478. https://doi.org/10.1111/bpa.12306

Bosman, L.W.J., Konnerth, A., 2009. Activity-dependent plasticity of developing climbing fiber–Purkinje cell synapses. Neuroscience, New Insights in Cerebellar Function 162, 612–623. https://doi.org/10.1016/j.neuroscience.2009.01.032

Bosman, L.W.J., Takechi, H., Hartmann, J., Eilers, J., Konnerth, A., 2008. Homosynaptic Long-Term Synaptic Potentiation of the “Winner” Climbing Fiber Synapse in Developing Purkinje Cells. J. Neurosci. 28, 798–807. https://doi.org/10.1523/JNEUROSCI.4074-07.2008

Boucard, A.A., Chubykin, A.A., Comoletti, D., Taylor, P., Südhof, T.C., 2005. A Splice Code for trans-Synaptic Cell Adhesion Mediated by Binding of Neuroligin 1 to α- and β-Neurexins. Neuron 48, 229–236. https://doi.org/10.1016/j.neuron.2005.08.026

Bowe, M.A., Mendis, D.B., Fallon, J.R., 2000. The small leucine-rich repeat proteoglycan biglycan binds to α-dystroglycan and is upregulated in dystrophic muscle. J. Cell Biol. 148, 801–810. https://doi.org/10.1083/jcb.148.4.801

Brancaccio, A., 2019. A molecular overview of the primary dystroglycanopathies. J. Cell. Mol. Med. 23, 3058–3062. https://doi.org/10.1111/jcmm.14218

Briatore, F., Patrizi, A., Viltono, L., Sassoe-Pognetto, M., Wulff, P., 2010. Quantitative organization of GABAergic synapses in the molecular layer of the mouse cerebellar cortex. PLoS ONE 5. https://doi.org/10.1371/journal.pone.0012119

Briatore, F., Pregno, G., Di Angelantonio, S., Frola, E., De Stefano, M.E., Vaillend, C., Sassoè-Pognetto, M., Patrizi, A., 2020. Dystroglycan Mediates Clustering of Essential GABAergic Components in Cerebellar Purkinje Cells. Front. Mol. Neurosci. 13, 164. https://doi.org/10.3389/fnmol.2020.00164

Briggs, D.C., Yoshida-Moriguchi, T., Zheng, T., Venzke, D., Anderson, M.E., Strazzulli, A., Moracci, M., Yu, L., Hohenester, E., Campbell, K.P., 2016. Structural basis of laminin binding to the LARGE glycans on dystroglycan. Nat. Chem. Biol. 12, 810–814. https://doi.org/10.1038/nchembio.2146

Brockington, M., Blake, D.J., Prandini, P., Brown, S.C., Torelli, S., Benson, M.A., Ponting, C.P., Estournet, B., Romero, N.B., Mercuri, E., Voit, T., Sewry, C.A., Guicheney, P., Muntoni, F., 2001. Mutations in the Fukutin-Related Protein Gene (FKRP) Cause a Form of Congenital Muscular Dystrophy with Secondary Laminin α2 Deficiency and Abnormal Glycosylation of α-Dystroglycan. Am. J. Hum. Genet. 69, 1198–1209. https://doi.org/10.1086/324412

Brose, K., Bland, K.S., Kuan, H.W., Arnott, D., Henzel, W., Goodman, C.S., Tessier-Lavigne, M., Kidd, T., 1999. Slit proteins bind robo receptors and have an evolutionarily conserved role in repulsive axon guidance. Cell 96, 795–806. https://doi.org/10.1016/S0092-8674(00)80590-5

Brun, B.N., Mockler, S.R.H., Laubscher, K.M., Stephan, C.M., Collison, J.A., Zimmerman, M.B., Mathews, K.D., 2017. Childhood Activity on Progression in Limb Girdle Muscular Dystrophy 2I. J. Child Neurol. 32, 204–209. https://doi.org/10.1177/0883073816677680

Brünig, I., Suter, A., Knuesel, I., Lüscher, B., Fritschy, J.M., 2002. GABAergic Terminals Are Required for Postsynaptic Clustering of Dystrophin but Not of GABAA Receptors and Gephyrin. J. Neurosci. 22, 4805–4813. https://doi.org/10.1523/jneurosci.22-12-04805.2002

Campanelll, J.T., Roberds, S.L., Campbell, K.P., Scheller, R.H., 1994. A role for dystrophin-associated glycoproteins and utrophin in agrin-induced AChR clustering. Cell 77, 663–674. https://doi.org/10.1016/0092-8674(94)90051-5

Carlson, C.G., Roshek, D.M., 2001. Adult dystrophic (mdx) endplates exhibit reduced quantal size and enhanced quantal variation. Pflugers Arch. 442, 369–375. https://doi.org/10.1007/s004240100561

Cataldi, M.P., Blaeser, A., Lu, P., Leroy, V., Lu, Q.L., 2020. ISPD Overexpression Enhances Ribitol-Induced Glycosylation of α-Dystroglycan in Dystrophic FKRP Mutant Mice. Mol. Ther. - Methods Clin. Dev. 17, 271–280. https://doi.org/10.1016/j.omtm.2019.12.005

Cataldi, M.P., Lu, P., Blaeser, A., Lu, Q.L., 2018. Ribitol restores functionally glycosylated α-dystroglycan and improves muscle function in dystrophic FKRP-mutant mice. Nat. Commun. 9, 3448. https://doi.org/10.1038/s41467-018-05990-z

Cavaldesi, M., Macchia, G., Barca, S., Defilippi, P., Tarone, G., Petrucci, T.C., 1999. Association of the dystroglycan complex isolated from bovine brain synaptosomes with proteins involved in signal transduction. J. Neurochem. 72, 1648–1655. https://doi.org/10.1046/j.1471-4159.1999.721648.x

C.górecki, D., Derry, J.M.J., Barnard, E.A., 1994. Dystroglycan: Brain localisation and chromosome mapping in the mouse. Hum. Mol. Genet. 3, 1589–1597. https://doi.org/10.1093/hmg/3.9.1589

Chan, Y.M., Keramaris-Vrantsis, E., Lidov, H.G., Norton, J.H., Zinchenko, N., Gruber, H.E., Thresher, R., Blake, D.J., Ashar, J., Rosenfeld, J., Lu, Q.L., 2010. Fukutin-related protein is essential for mouse muscle, brain and eye development and mutation recapitulates the wide clinical spectrums of dystroglycanopathies. Hum. Mol. Genet. 19, 3995–4006. https://doi.org/10.1093/hmg/ddq314

Chen, L.Y., Jiang, M., Zhang, B., Gokce, O., Südhof, T.C., 2017. Conditional Deletion of All Neurexins Defines Diversity of Essential Synaptic Organizer Functions for Neurexins. Neuron 94, 611-625.e4. https://doi.org/10.1016/j.neuron.2017.04.011

Chen, P.L., Clandinin, T.R., 2008. The Cadherin Flamingo Mediates Level-Dependent Interactions that Guide Photoreceptor Target Choice in Drosophila. Neuron 58, 26–33. https://doi.org/10.1016/j.neuron.2008.01.007

Chiba, A., Matsumura, K., Yamada, H., Inazu, T., Shimizu, T., Kusunoki, S., Kanazawa, I., Kobata, A., Endo, T., 1997. Structures of sialylated O-linked oligosaccharides of bovine peripheral nerve α-dystroglycan. The role of a novel O-mannosyl-type oligosaccharide in the binding of α-dystroglycan with laminin. J. Biol. Chem. 272, 2156–2162. https://doi.org/10.1074/jbc.272.4.2156

Clement, E., Mercuri, E., Godfrey, C., Smith, J., Robb, S., Kinali, M., Straub, V., Bushby, K., Manzur, A., Talim, B., Cowan, F., Quinlivan, R., Klein, A., Longman, C.,

McWilliam, R., Topaloglu, H., Mein, R., Abbs, S., North, K., Barkovich, A.J., Rutherford, M., Muntoni, F., 2008. Brain involvement in muscular dystrophies with defective dystroglycan glycosylation. Ann. Neurol. 64, 573–582. https://doi.org/10.1002/ana.21482
Clements, R., Turk, R., Campbell, K.P., Wright, K.M., 2017. Dystroglycan maintains inner limiting membrane integrity to coordinate retinal development. J. Neurosci. 37, 8559–8574. https://doi.org/10.1523/JNEUROSCI.0946-17.2017
Clements, R., Wright, K.M., 2018. Retinal ganglion cell axon sorting at the optic chiasm requires dystroglycan. Dev. Biol. 442, 210–219. https://doi.org/10.1016/j.ydbio.2018.08.010
Cohen, M.W., Jacobson, C., Godfrey, E.W., Campbell, K.P., Carbonetto, S., 1995. Distribution of α-dystroglycan during embryonic nerve-muscle synaptogenesis. J. Cell Biol. 129, 1093–1101. https://doi.org/10.1083/jcb.129.4.1093
Cohen, M.W., Jacobson, C., Yurchenco, P.D., Morris, G.E., Carbonetto, S., 1997. Laminin-induced clustering of dystroglycan on embryonic muscle cells: Comparison with agrin-induced clustering. J. Cell Biol. 136, 1047–1058. https://doi.org/10.1083/jcb.136.5.1047
Cohn, R.D., Henry, M.D., Michele, D.E., Barresi, R., Saito, F., Moore, S.A., Flanagan, J.D., Skwarchuk, M.W., Robbins, M.E., Mendell, J.R., Williamson, R.A., Campbell, K.P., 2002. Disruption of Dag1 in differentiated skeletal muscle reveals a role for dystroglycan in muscle regeneration. Cell 110, 639–648. https://doi.org/10.1016/S0092-8674(02)00907-8
Colognato, H., Galvin, J., Wang, Z., Relucio, J., Nguyen, T., Harrison, D., Yurchenco, P.D., Ffrench-Constant, C., 2007. Identification of dystroglycan as a second laminin receptor in oligodendrocytes, with a role in myelination. Development 134, 1723–1736. https://doi.org/10.1242/dev.02819
Colombelli, C., Palmisano, M., Eshed-Eisenbach, Y., Zambroni, D., Pavoni, E., Ferri, C., Saccucci, S., Nicole, S., Soininen, R., McKee, K.K., Yurchenco, P.D., Peles, E., Wrabetz, L., Feltri, M.L., 2015. Perlecan is recruited by dystroglycan to nodes of ranvier and binds the clustering molecule gliomedin. J. Cell Biol. 208, 313–329. https://doi.org/10.1083/jcb.201403111
Combs, A.C., Ervasti, J.M., 2005. Enhanced laminin binding by α-dystroglycan after enzymatic deglycosylation. Biochem. J. 390, 303–309. https://doi.org/10.1042/BJ20050375
Côté, P.D., Moukhles, H., Lindenbaum, M., Carbonetto, S., 1999. Chimaeric mice deficient in dystroglycans develop muscular dystrophy and have disrupted myoneural synapses. Nat. Genet. 23, 338–342. https://doi.org/10.1038/15519
Crepel, F., Mariani, J., Delhaye-Bouchaud, N., 1976. Evidence for a multiple innervation of purkinje cells by climbing fibers in the immature rat cerebellum. J. Neurobiol. 7, 567–578. https://doi.org/10.1002/neu.480070609
Daigle, T.L., Madisen, L., Hage, T.A., Valley, M.T., Knoblich, U., Larsen, R.S., Takeno, M.M., Huang, L., Gu, H., Larsen, R., Mills, M., Bosma-Moody, A., Siverts, L.A., Walker, M., Graybuck, L.T., Yao, Z., Fong, O., Nguyen, T.N., Garren, E., Lenz, G.H., Chavarha, M., Pendergraft, J., Harrington, J., Hirokawa, K.E., Harris, J.A., Nicovich, P.R., McGraw, M.J., Ollerenshaw, D.R., Smith, K.A., Baker, C.A., Ting, J.T., Sunkin, S.M., Lecoq, J., Lin, M.Z., Boyden, E.S., Murphy, G.J., da Costa, N.M., Waters, J., Li, L., Tasic, B., Zeng, H., 2018. A Suite of Transgenic Driver and Reporter Mouse Lines with Enhanced Brain-Cell-Type Targeting and Functionality. Cell 174, 465-480.e22. https://doi.org/10.1016/j.cell.2018.06.035
Dempsey, C.E., Bigotti, M.G., Adams, J.C., Brancaccio, A., 2019. Analysis of α-dystroglycan/LG domain binding modes: Investigating protein motifs that regulate

the affinity of isolated LG domains. Front. Mol. Biosci. 6. https://doi.org/10.3389/fmolb.2019.00018
Devisme, L., Bouchet, C., Gonzals, M., Alanio, E., Bazin, A., Bessires, B., Bigi, N., Blanchet, P., Bonneau, D., Bonnires, M., Bucourt, M., Carles, D., Clarisse, B., Delahaye, S., Fallet-Bianco, C., Figarella-Branger, D., Gaillard, D., Gasser, B., Delezoide, A.L., Guimiot, F., Joubert, M., Laurent, N., Laquerrire, A., Liprandi, A., Loget, P., Marcorelles, P., Martinovic, J., Menez, F., Patrier, S., Pelluard, F., Perez, M.J., Rouleau, C., Triau, S., Attié-Bitach, T., Vuillaumier-Barrot, S., Seta, N., Encha-Razavi, F., 2012. Cobblestone lissencephaly: Neuropathological subtypes and correlations with genes of dystroglycanopathies. Brain 135, 469–482. https://doi.org/10.1093/brain/awr357
Dhaibani, M.A.A., El-Hattab, A.W., Ismayl, O., Suleiman, J., 2018. B3GALNT2-Related Dystroglycanopathy: Expansion of the Phenotype with Novel Mutation Associated with Muscle-Eye-Brain Disease, Walker–Warburg Syndrome, Epileptic Encephalopathy-West Syndrome, and Sensorineural Hearing Loss. Neuropediatrics 49, 289–295. https://doi.org/10.1055/s-0038-1651519
Di Costanzo, S., Balasubramanian, A., Pond, H.L., Rozkalne, A., Pantaleoni, C., Saredi, S., Gupta, V.A., Sunu, C.M., Yu, T.W., Kang, P.B., Salih, M.A., Mora, M., Gussoni, E., Walsh, C.A., Manzini, M.C., 2014. POMK mutations disrupt muscle development leading to a spectrum of neuromuscular presentations. Hum. Mol. Genet. 23, 5781–5792. https://doi.org/10.1093/hmg/ddu296
Di Rosa, G., Messina, S., D'Amico, A., Bertini, E., Pustorino, G., Spanò, M., Tortorella, G., 2011. A new form of alpha-dystroglycanopathy associated with severe drug-resistant epilepsy and unusual EEG features. Epileptic. Disord. 13, 259–262. https://doi.org/10.1684/epd.2011.0461
Doischer, D., Hosp, J.A., Yanagawa, Y., Obata, K., Jonas, P., Vida, I., Bartos, M., 2008. Postnatal Differentiation of Basket Cells from Slow to Fast Signaling Devices. J. Neurosci. 28, 12956–12968. https://doi.org/10.1523/JNEUROSCI.2890-08.2008
Dudanova, I., Tabuchi, K., Rohlmann, A., Südhof, T.C., Missler, M., 2007. Deletion of α-neurexins does not cause a major impairment of axonal pathfinding or synapse formation. J. Comp. Neurol. 502, 261–274. https://doi.org/10.1002/cne.21305
Dudok, B., Klein, P.M., Hwaun, E., Lee, B.R., Yao, Z., Fong, O., Bowler, J.C., Terada, S., Sparks, F.T., Szabo, G.G., Farrell, J.S., Berg, J., Daigle, T.L., Tasic, B., Dimidschstein, J., Fishell, G., Losonczy, A., Zeng, H., Soltesz, I., 2021. Alternating sources of perisomatic inhibition during behavior. Neuron 109, 997-1012.e9. https://doi.org/10.1016/j.neuron.2021.01.003
Durbeej, M., Henry, M.D., Ferletta, M., Campbell, K.P., Ekblom, P., 1998. Distribution of dystroglycan in normal adult mouse tissues. J. Histochem. Cytochem. 46, 449–457. https://doi.org/10.1177/002215549804600404
Egawa, K., Nakakubo, S., Kimura, S., Goto, T., Manabe, A., Shiraishi, H., 2021. Flurothyl-induced seizure paradigm revealed higher seizure susceptibility in middle-aged Angelman syndrome mouse model. Brain Dev. 43, 515–520. https://doi.org/10.1016/j.braindev.2020.12.011
Eggan, S.M., Mizoguchi, Y., Stoyak, S.R., Lewis, D.A., 2010. Development of Cannabinoid 1 Receptor Protein and Messenger RNA in Monkey Dorsolateral Prefrontal Cortex. Cereb. Cortex 20, 1164–1174. https://doi.org/10.1093/cercor/bhp179
Einheber, S., Zanazzi, G., Ching, W., Scherer, S., Milner, T.A., Peles, E., Salzer, J.L., 1997. The Axonal Membrane Protein Caspr, a Homologue of Neurexin IV, Is a Component of the Septate-like Paranodal Junctions That Assemble during Myelination. J. Cell Biol. 139, 1495–1506. https://doi.org/10.1083/jcb.139.6.1495

Ervasti, J.M., Campbell, K.P., 1993. A role for the dystrophin-glycoprotein complex as a transmembrane linker between laminin and actin. J. Cell Biol. 122, 809–823. https://doi.org/10.1083/jcb.122.4.809
Ervasti, J.M., Campbell, K.P., 1991. Membrane organization of the dystrophin-glycoprotein complex. Cell 66, 1121–1131. https://doi.org/10.1016/0092-8674(91)90035-W
Esapa, C.T., Bentham, G.R.B., Schröder, J.E., Kröger, S., Blake, D.J., 2003. The effects of post-translational processing on dystroglycan synthesis and trafficking. FEBS Lett. 555, 209–216. https://doi.org/10.1016/S0014-5793(03)01230-4
Favuzzi, E., Deogracias, R., Marques-Smith, A., Maeso, P., Jezequel, J., Exposito-Alonso, D., Balia, M., Kroon, T., Hinojosa, A.J., F. Maraver, E., Rico, B., 2019. Distinct molecular programs regulate synapse specificity in cortical inhibitory circuits. Science 363, 413–417. https://doi.org/10.1126/science.aau8977
Feil, R., Wagner, J., Metzger, D., Chambon, P., 1997. Regulation of Cre Recombinase Activity by Mutated Estrogen Receptor Ligand-Binding Domains. Biochem. Biophys. Res. Commun. 237, 752–757. https://doi.org/10.1006/bbrc.1997.7124
Feil, S., Valtcheva, N., Feil, R., 2009. Inducible Cre Mice, in: Wurst, W., Kühn, R. (Eds.), Gene Knockout Protocols: Second Edition, Methods in Molecular Biology. Humana Press, Totowa, NJ, pp. 343–363. https://doi.org/10.1007/978-1-59745-471-1_18
Földy, C., Neu, A., Jones, M.V., Soltesz, I., 2006. Presynaptic, activity-dependent modulation of cannabinoid type 1 receptor-mediated inhibition of GABA release. J. Neurosci. Off. J. Soc. Neurosci. 26, 1465–1469. https://doi.org/10.1523/JNEUROSCI.4587-05.2006
Freund, T.F., Katona, I., 2007. Perisomatic inhibition. Neuron 56, 33–42. https://doi.org/10.1016/j.neuron.2007.09.012
Früh, S., Romanos, J., Panzanelli, P., Bürgisser, D., Tyagarajan, S.K., Campbell, K.P., Santello, M., Fritschy, J.M., 2016. Neuronal dystroglycan is necessary for formation and maintenance of functional CCK-positive basket cell terminals on pyramidal cells. J. Neurosci. 36, 10296–10313. https://doi.org/10.1523/JNEUROSCI.1823-16.2016
Fuccillo, M.V., Földy, C., Gökce, Ö., Rothwell, P.E., Sun, G.L., Malenka, R.C., Südhof, T.C., 2015. Single-Cell mRNA Profiling Reveals Cell-Type-Specific Expression of Neurexin Isoforms. Neuron 87, 326–340. https://doi.org/10.1016/j.neuron.2015.06.028
Gao, Q., McNally, E.M., 2015. The Dystrophin Complex: structure, function and implications for therapy. Compr. Physiol. 5, 1223–1239. https://doi.org/10.1002/cphy.c140048
Gee, S.H., Blacher, R.W., Douville, P.J., Provost, P.R., Yurchenco, P.D., Carbonetto, S., 1993. Laminin-binding protein 120 from brain is closely related to the dystrophin-associated glycoprotein, dystroglycan, and binds with high affinity to the major heparin binding domain of laminin. J. Biol. Chem. 268, 14972–14980. https://doi.org/10.1016/s0021-9258(18)82427-9
Gee, S.H., Montanaro, F., Lindenbaum, M.H., Carbonetto, S., 1994. Dystroglycan-α, a dystrophin-associated glycoprotein, is a functional agrin receptor. Cell 77, 675–686. https://doi.org/10.1016/0092-8674(94)90052-3
Gerin, I., Ury, B., Breloy, I., Bouchet-Seraphin, C., Bolsée, J., Halbout, M., Graff, J., Vertommen, D., Muccioli, G.G., Seta, N., Cuisset, J.-M., Dabaj, I., Quijano-Roy, S., Grahn, A., Van Schaftingen, E., Bommer, G.T., 2016. ISPD produces CDP-ribitol used by FKTN and FKRP to transfer ribitol phosphate onto α-dystroglycan. Nat. Commun. 7, 11534. https://doi.org/10.1038/ncomms11534

Goddeeris, M.M., Wu, B., Venzke, D., Yoshida-Moriguchi, T., Saito, F., Matsumura, K., Moore, S.A., Campbell, K.P., 2013. LARGE glycans on dystroglycan function as a tunable matrix scaffold to prevent dystrophy. Nature 503, 136–140. https://doi.org/10.1038/nature12605

Godfrey, C., Clement, E., Mein, R., Brockington, M., Smith, J., Talim, B., Straub, V., Robb, S., Quinlivan, R., Feng, L., Jimenez-Mallebrera, C., Mercuri, E., Manzur, A.Y., Kinali, M., Torelli, S., Brown, S.C., Sewry, C.A., Bushby, K., Topaloglu, H., North, K., Abbs, S., Muntoni, F., 2007. Refining genotype–phenotype correlations in muscular dystrophies with defective glycosylation of dystroglycan. Brain 130, 2725–2735. https://doi.org/10.1093/brain/awm212

Goebbels, S., Bormuth, I., Bode, U., Hermanson, O., Schwab, M.H., Nave, K.-A., 2006. Genetic targeting of principal neurons in neocortex and hippocampus of NEX-Cre mice. genesis 44, 611–621. https://doi.org/10.1002/dvg.20256

Gorski, J.A., Talley, T., Qiu, M., Puelles, L., Rubenstein, J.L.R., Jones, K.R., 2002. Cortical Excitatory Neurons and Glia, But Not GABAergic Neurons, Are Produced in the Emx1-Expressing Lineage. J. Neurosci. 22, 6309–6314. https://doi.org/10.1523/JNEUROSCI.22-15-06309.2002

Grady, R.M., Wozniak, D.F., Ohlemiller, K.K., Sanes, J.R., 2006. Cerebellar synaptic defects and abnormal motor behavior in mice lacking α- and β-dystrobrevin. J. Neurosci. 26, 2841–2851. https://doi.org/10.1523/JNEUROSCI.4823-05.2006

Grady, R.M., Zhou, H., Cunningham, J.M., Henry, M.D., Campbell, K.P., Sanes, J.R., 2000. Maturation and maintenance of the neuromuscular synapse: Genetic evidence for roles of the dystrophin-glycoprotein complex. Neuron 25, 279–293. https://doi.org/10.1016/S0896-6273(00)80894-6

Graus-Porta, D., Blaess, S., Senften, M., Littlewood-Evans, A., Damsky, C., Huang, Z., Orban, P., Klein, R., Schittny, J.C., Müller, U., 2001. β1-Class Integrins Regulate the Development of Laminae and Folia in the Cerebral and Cerebellar Cortex. Neuron 31, 367–379. https://doi.org/10.1016/S0896-6273(01)00374-9

Gregorian, C., Nakashima, J., Belle, J.L., Ohab, J., Kim, R., Liu, A., Smith, K.B., Groszer, M., Garcia, A.D., Sofroniew, M.V., Carmichael, S.T., Kornblum, H.I., Liu, X., Wu, H., 2009. Pten Deletion in Adult Neural Stem/Progenitor Cells Enhances Constitutive Neurogenesis. J. Neurosci. 29, 1874–1886. https://doi.org/10.1523/JNEUROSCI.3095-08.2009

Grieco, S.F., Johnston, K.G., Gao, P., Garduño, B.M., Tang, B., Yi, E., Sun, Y., Horwitz, G.D., Yu, Z., Holmes, T.C., Xu, X., 2023. Anatomical and molecular characterization of parvalbumin-cholecystokinin co-expressing inhibitory interneurons: implications for neuropsychiatric conditions. Mol. Psychiatry 1–16. https://doi.org/10.1038/s41380-023-02153-5

Gu, B., Levine, N.G., Xu, W., Lynch, R.M., Pardo-Manuel de Villena, F., Philpot, B.D., 2022. Ictal neural oscillatory alterations precede sudden unexpected death in epilepsy. Brain Commun. 4, fcac073. https://doi.org/10.1093/braincomms/fcac073

Gu, H., Marth, J.D., Orban, P.C., Mossmann, H., Rajewsky, K., 1994. Deletion of a DNA Polymerase β Gene Segment in T Cells Using Cell Type-Specific Gene Targeting. Science 265, 103–106. https://doi.org/10.1126/science.8016642

Haenggi, T., Fritschy, J.-M., 2006. Role of dystrophin and utrophin for assembly and function of the dystrophin glycoprotein complex in non-muscle tissue. Cell. Mol. Life Sci. CMLS 63, 1614–1631. https://doi.org/10.1007/s00018-005-5461-0

Haery, L., Deverman, B.E., Matho, K.S., Cetin, A., Woodard, K., Cepko, C., Guerin, K.I., Rego, M.A., Ersing, I., Bachle, S.M., Kamens, J., Fan, M., 2019. Adeno-

Associated Virus Technologies and Methods for Targeted Neuronal Manipulation. Front. Neuroanat. 13.
Hara, Y., Balci-Hayta, B., Yoshida-Moriguchi, T., Kanagawa, M., Beltrán-Valero de Bernabé, D., Gündeşli, H., Willer, T., Satz, J.S., Crawford, R.W., Burden, S.J., Kunz, S., Oldstone, M.B.A., Accardi, A., Talim, B., Muntoni, F., Topaloğlu, H., Dinçer, P., Campbell, K.P., 2011. A Dystroglycan Mutation Associated with Limb-Girdle Muscular Dystrophy. N. Engl. J. Med. 364, 939–946. https://doi.org/10.1056/nejmoa1006939
Hayashi, S., Lewis, P., Pevny, L., McMahon, A.P., 2002. Efficient gene modulation in mouse epiblast using a Sox2Cre transgenic mouse strain. Mech. Dev. 119, S97–S101. https://doi.org/10.1016/S0925-4773(03)00099-6
Henion, T.R., Qu, Q., Smith, F.I., 2003. Expression of dystroglycan, fukutin and POMGnT1 during mouse cerebellar development. Mol. Brain Res. 112, 177–181. https://doi.org/10.1016/S0169-328X(03)00055-X
Hinou, H., Kikuchi, S., Ochi, R., Igarashi, K., Takada, W., Nishimura, S.I., 2019. Synthetic glycopeptides reveal specific binding pattern and conformational change at O-mannosylated position of α-dystroglycan by POMGnT1 catalyzed GlcNAc modification. Bioorg. Med. Chem. 27, 2822–2831. https://doi.org/10.1016/j.bmc.2019.05.008
Hippenmeyer, S., Vrieseling, E., Sigrist, M., Portmann, T., Laengle, C., Ladle, D.R., Arber, S., 2005. A Developmental Switch in the Response of DRG Neurons to ETS Transcription Factor Signaling. PLOS Biol. 3, e159. https://doi.org/10.1371/journal.pbio.0030159
Hohenester, E., Tisi, D., Talts, J.F., Timpl, R., 1999. The crystal structure of a laminin G-like module reveals the molecular basis of α-dystroglycan binding to laminins, perlecan, and agrin. Mol. Cell 4, 783–792. https://doi.org/10.1016/S1097-2765(00)80388-3
Holt, K.H., Crosbie, R.H., Venzke, D.P., Campbell, K.P., 2000. Biosynthesis of dystroglycan: Processing of a precursor propeptide. FEBS Lett. 468, 79–83. https://doi.org/10.1016/S0014-5793(00)01195-9
Holzfeind, P.J., Grewal, P.K., Reitsamer, H.A., Kechvar, J., Lassmann, H., Hoeger, H., Hewitt, J.E., Bittner, R.E., 2002. Skeletal, cardiac and tongue muscle pathology, defective retinal transmission, and neuronal migration defects in the Largemyd mouse defines a natural model for glycosylation-deficient muscle – eye – brain disorders. Hum. Mol. Genet. 11, 2673–2687. https://doi.org/10.1093/hmg/11.21.2673
Hoshino, M., Nakamura, S., Mori, K., Kawauchi, T., Terao, M., Nishimura, Y.V., Fukuda, A., Fuse, T., Matsuo, N., Sone, M., Watanabe, M., Bito, H., Terashima, T., Wright, C.V.E., Kawaguchi, Y., Nakao, K., Nabeshima, Y., 2005. Ptf1a, a bHLH Transcriptional Gene, Defines GABAergic Neuronal Fates in Cerebellum. Neuron 47, 201–213. https://doi.org/10.1016/j.neuron.2005.06.007
Hosokawa, H., Ninomiya, H., Kitamura, Y., Fujiwara, K., Masaki, T., 2002. Vascular endothelial cells that express dystroglycan are involved in angiogenesis. J. Cell Sci. 115, 1487–1496. https://doi.org/10.1242/jcs.115.7.1487
Hu, H., Li, J., Gagen, C.S., Gray, N.W., Zhang, Z., Qi, Y., Zhang, P., 2011. Conditional knockout of protein O-mannosyltransferase 2 reveals tissue-specific roles of O-mannosyl glycosylation in brain development. J. Comp. Neurol. 519, 1320–1337. https://doi.org/10.1002/cne.22572
Hu, H., Liu, Y., Bampoe, K., He, Y., Yu, M., 2016. Postnatal Gene Therapy Improves Spatial Learning Despite the Presence of Neuronal Ectopia in a Model of

Neuronal Migration Disorder. Genes 7, 105. https://doi.org/10.3390/genes7120105
Ibraghimov-Beskrovnaya, O., Ervasti, J.M., Leveille, C.J., Slaughter, C.A., Sernett, S.W., Campbell, K.P., 1992. Primary structure of dystrophin-associated glycoproteins linking dystrophin to the extracellular matrix. Nature 355, 696–702. https://doi.org/10.1038/355696a0
Inamori, K.I., Yoshida-Moriguchi, T., Hara, Y., Anderson, M.E., Yu, L., Campbell, K.P., 2012. Dystroglycan function requires xylosyl- and glucuronyltransferase activities of LARGE. Science 335, 93–96. https://doi.org/10.1126/science.1214115
Itō, M., 1984. The Cerebellum and Neural Control. Raven Press.
Jacobson, C., Côté, P.D., Rossi, S.G., Rotundo, R.L., Carbonetto, S., 2001. The dystroglycan complex is necessary for stabilization of acetylcholine receptor clusters at neuromuscular junctions and formation of the synaptic basement membrane. J. Cell Biol. 153, 435–450. https://doi.org/10.1083/jcb.152.3.435
Jagadha, V., Becker, L.E., 1988. Brain morphology in Duchenne muscular dystrophy: A Golgi study. Pediatr. Neurol. 4, 87–92. https://doi.org/10.1016/0887-8994(88)90047-1
Jahncke, J.N., 2023. Mini Analysis Code.
Jahncke, J.N., Miller, D.S., Krush, M., Schnell, E., Wright, K.M., 2024. Inhibitory CCK+ basket synapse defects in mouse models of dystroglycanopathy. eLife 12, RP87965. https://doi.org/10.7554/eLife.87965
Jahncke, J.N., Wright, K.M., 2023. The many roles of dystroglycan in nervous system development and function. Dev. Dyn. 252, 61–80. https://doi.org/10.1002/dvdy.516
Jin, K., Xiang, M., 2019. Transcription factor Ptf1a in development, diseases and reprogramming. Cell. Mol. Life Sci. 76, 921–940. https://doi.org/10.1007/s00018-018-2972-z
Johnson, R.P., Kang, S.H., Kramer, J.M., 2006. C. elegans dystroglycan DGN-1 functions in epithelia and neurons, but not muscle, and independently of dystrophin. Development 133, 1911–1921. https://doi.org/10.1242/dev.02363
Johnson, R.P., Kramer, J.M., 2012. C. elegans dystroglycan coordinates responsiveness of follower axons to dorsal/ventral and anterior/posterior guidance cues. Dev. Neurobiol. 72, 1498–1515. https://doi.org/10.1002/dneu.22011
Joyner, A.L., Skarnes, W.C., Rossant, J., 1989. Production of a mutation in mouse En-2 gene by homologous recombination in embryonic stem cells. Nature 338, 153–156. https://doi.org/10.1038/338153a0
Jung, D., Yang, B., Meyer, J., Chamberlain, J.S., Campbell, K.P., 1995. Identification and Characterization of the Dystrophin Anchoring Site on β-Dystroglycan (*). J. Biol. Chem. 270, 27305–27310. https://doi.org/10.1074/jbc.270.45.27305
Jurgensen, S., Castillo, P.E., 2015. Selective Dysregulation of Hippocampal Inhibition in the Mouse Lacking Autism Candidate Gene CNTNAP2. J. Neurosci. 35, 14681–14687. https://doi.org/10.1523/JNEUROSCI.1666-15.2015
Kadiyala, S.B., Yannix, J.Q., Nalwalk, J.W., Papandrea, D., Beyer, B.S., Herron, B.J., Ferland, R.J., 2016. Eight Flurothyl-Induced Generalized Seizures Lead to the Rapid Evolution of Spontaneous Seizures in Mice: A Model of Epileptogenesis with Seizure Remission. J. Neurosci. 36, 7485–7496. https://doi.org/10.1523/JNEUROSCI.3232-14.2016
Kanagawa, M., 2021. Dystroglycanopathy: From Elucidation of Molecular and Pathological Mechanisms to Development of Treatment Methods. Int. J. Mol. Sci. 22, 13162. https://doi.org/10.3390/ijms222313162

Kanagawa, M., Toda, T., 2018. Ribitol-phosphate - A newly identified posttranslational glycosylation unit in mammals: Structure, modification enzymes and relationship to human diseases. J. Biochem. (Tokyo) 163, 359–369. https://doi.org/10.1093/jb/mvy020
Kanagawa, M., Toda, T., 2017. Muscular Dystrophy with Ribitol-Phosphate Deficiency: A Novel Post-Translational Mechanism in Dystroglycanopathy. J. Neuromuscul. Dis. 4, 259–267. https://doi.org/10.3233/JND-170255
Kapfhammer, J.P., 2004. Cellular and molecular control of dendritic growth and development of cerebellar Purkinje cells. Prog. Histochem. Cytochem. 39, 131–182. https://doi.org/10.1016/j.proghi.2004.07.002
Katona, I., Rancz, E.A., Acsady, L., Ledent, C., Mackie, K., Hajos, N., Freund, T.F., 2001. Distribution of CB1 cannabinoid receptors in the amygdala and their role in the control of GABAergic transmission. J. Neurosci. Off. J. Soc. Neurosci. 21, 9506–9518. https://doi.org/10.1523/JNEUROSCI.21-23-09506.2001
Kessaris, N., Fogarty, M., Iannarelli, P., Grist, M., Wegner, M., Richardson, W.D., 2006. Competing waves of oligodendrocytes in the forebrain and postnatal elimination of an embryonic lineage. Nat. Neurosci. 9, 173–179. https://doi.org/10.1038/nn1620
Knuesel, I., Mastrocola, M., Zuellig, R.A., Bornhauser, B., Schaub, M.C., Fritschy, J.M., 1999. Altered synaptic clustering of GABAA receptors in mice lacking dystrophin (mdx mice). Eur. J. Neurosci. 11, 4457–4462. https://doi.org/10.1046/j.1460-9568.1999.00887.x
Kolberg, L., Raudvere, U., Kuzmin, I., Adler, P., Vilo, J., Peterson, H., 2023. g:Profiler—interoperable web service for functional enrichment analysis and gene identifier mapping (2023 update). Nucleic Acids Res. 51, W207–W212. https://doi.org/10.1093/nar/gkad347
Kolberg, L., Raudvere, U., Kuzmin, I., Vilo, J., Peterson, H., 2020. gprofiler2 -- an R package for gene list functional enrichment analysis and namespace conversion toolset g:Profiler. F1000Research 9, ELIXIR-709. https://doi.org/10.12688/f1000research.24956.2
Koller, B.H., Hagemann, L.J., Doetschman, T., Hagaman, J.R., Huang, S., Williams, P.J., First, N.L., Maeda, N., Smithies, O., 1989. Germ-line transmission of a planned alteration made in a hypoxanthine phosphoribosyltransferase gene by homologous recombination in embryonic stem cells. Proc. Natl. Acad. Sci. 86, 8927–8931. https://doi.org/10.1073/pnas.86.22.8927
Konno, K., Yamasaki, M., Miyazaki, T., Watanabe, M., 2023. Glyoxal fixation: An approach to solve immunohistochemical problem in neuroscience research. Sci. Adv. 9, eadf7084. https://doi.org/10.1126/sciadv.adf7084
Kozareva, V., Martin, C., Osorno, T., Rudolph, S., Guo, C., Vanderburg, C., Nadaf, N., Regev, A., Regehr, W.G., Macosko, E., 2021. A transcriptomic atlas of mouse cerebellar cortex comprehensively defines cell types. Nature 598, 214–219. https://doi.org/10.1038/s41586-021-03220-z
Krasowska, E., Zabłocki, K., Górecki, D.C., Swinny, J.D., 2014. Aberrant location of inhibitory synaptic marker proteins in the hippocampus of dystrophin-deficient mice: Implications for cognitive impairment in Duchenne muscular dystrophy. PLoS ONE 9, e108364. https://doi.org/10.1371/journal.pone.0108364
Kueh, S.L.L., Dempster, J., Head, S.I., Morley, J.W., 2011. Reduced postsynaptic GABAA receptor number and enhanced gaboxadol induced change in holding currents in Purkinje cells of the dystrophin-deficient mdx mouse. Neurobiol. Dis. 43, 558–564. https://doi.org/10.1016/j.nbd.2011.05.002

Kueh, S.L.L., Head, S.I., Morley, J.W., 2008. GABAA receptor expression and inhibitory post-synaptic currents in cerebellar Purkinje cells in dystrophin-deficient mdx mice. Clin. Exp. Pharmacol. Physiol. 35, 207–210. https://doi.org/10.1111/j.1440-1681.2007.04816.x

Lackey, E.P., Moreira, L., Norton, A., Hemelt, M.E., Osorno, T., Nguyen, T.M., Macosko, E.Z., Lee, W.-C.A., Hull, C.A., Regehr, W.G., 2023. Cerebellar circuits for disinhibition and synchronous inhibition. https://doi.org/10.1101/2023.09.15.557934

Larsen, I.S.B., Narimatsu, Y., Joshi, H.J., Siukstaite, L., Harrison, O.J., Brasch, J., Goodman, K.M., Hansen, L., Shapiro, L., Honig, B., Vakhrushev, S.Y., Clausen, H., Halim, A., 2017a. Discovery of an O-mannosylation pathway selectively serving cadherins and protocadherins. Proc. Natl. Acad. Sci. U. S. A. 114, 11163–11168. https://doi.org/10.1073/pnas.1708319114

Larsen, I.S.B., Narimatsu, Y., Joshi, H.J., Yang, Z., Harrison, O.J., Brasch, J., Shapiro, L., Honig, B., Vakhrushev, S.Y., Clausen, H., Halim, A., 2017b. Mammalian O-mannosylation of cadherins and plexins is independent of protein O-mannosyltransferases 1 and 2. J. Biol. Chem. 292, 11586–11598. https://doi.org/10.1074/jbc.M117.794487

Lecea, L. de, del Ri´o, J., Soriano, E., 1995. Developmental expression of parvalbumin mRNA in the cerebral cortex and hippocampus of the rat. Mol. Brain Res. 32, 1–13. https://doi.org/10.1016/0169-328X(95)00056-X

Lee, R.C., Clandinin, T.R., Lee, C.H., Chen, P.L., Meinertzhagen, I.A., Zipursky, S.L., 2003. The protocadherin Flamingo is required for axon target selection in the Drosophila visual system. Nat. Neurosci. 6, 557–563. https://doi.org/10.1038/nn1063

Lein, E.S., Hawrylycz, M.J., Ao, N., Ayres, M., Bensinger, A., Bernard, A., Boe, A.F., Boguski, M.S., Brockway, K.S., Byrnes, E.J., Chen, Lin, Chen, Li, Chen, T.-M., Chi Chin, M., Chong, J., Crook, B.E., Czaplinska, A., Dang, C.N., Datta, S., Dee, N.R., Desaki, A.L., Desta, T., Diep, E., Dolbeare, T.A., Donelan, M.J., Dong, H.-W., Dougherty, J.G., Duncan, B.J., Ebbert, A.J., Eichele, G., Estin, L.K., Faber, C., Facer, B.A., Fields, R., Fischer, S.R., Fliss, T.P., Frensley, C., Gates, S.N., Glattfelder, K.J., Halverson, K.R., Hart, M.R., Hohmann, J.G., Howell, M.P., Jeung, D.P., Johnson, R.A., Karr, P.T., Kawal, R., Kidney, J.M., Knapik, R.H., Kuan, C.L., Lake, J.H., Laramee, A.R., Larsen, K.D., Lau, C., Lemon, T.A., Liang, A.J., Liu, Y., Luong, L.T., Michaels, J., Morgan, J.J., Morgan, R.J., Mortrud, M.T., Mosqueda, N.F., Ng, L.L., Ng, R., Orta, G.J., Overly, C.C., Pak, T.H., Parry, S.E., Pathak, S.D., Pearson, O.C., Puchalski, R.B., Riley, Z.L., Rockett, H.R., Rowland, S.A., Royall, J.J., Ruiz, M.J., Sarno, N.R., Schaffnit, K., Shapovalova, N.V., Sivisay, T., Slaughterbeck, C.R., Smith, S.C., Smith, K.A., Smith, B.I., Sodt, A.J., Stewart, N.N., Stumpf, K.-R., Sunkin, S.M., Sutram, M., Tam, A., Teemer, C.D., Thaller, C., Thompson, C.L., Varnam, L.R., Visel, A., Whitlock, R.M., Wohnoutka, P.E., Wolkey, C.K., Wong, V.Y., Wood, M., Yaylaoglu, M.B., Young, R.C., Youngstrom, B.L., Feng Yuan, X., Zhang, B., Zwingman, T.A., Jones, A.R., 2007. Genome-wide atlas of gene expression in the adult mouse brain. Nature 445, 168–176. https://doi.org/10.1038/nature05453

Lévi, S., Grady, R.M., Henry, M.D., Campbell, K.P., Sanes, J.R., Craig, A.M., 2002. Dystroglycan Is Selectively Associated with Inhibitory GABAergic Synapses but Is Dispensable for Their Differentiation. J. Neurosci. 22, 4274–4285. https://doi.org/10.1523/jneurosci.22-11-04274.2002

Lewis, A.E., Vasudevan, H.N., O'Neill, A.K., Soriano, P., Bush, J.O., 2013. The widely used Wnt1-Cre transgene causes developmental phenotypes by ectopic

activation of Wnt signaling. Dev. Biol. 379, 229–234. https://doi.org/10.1016/j.ydbio.2013.04.026
Lewis, P.M., Gritli-Linde, A., Smeyne, R., Kottmann, A., McMahon, A.P., 2004. Sonic hedgehog signaling is required for expansion of granule neuron precursors and patterning of the mouse cerebellum. Dev. Biol. 270, 393–410. https://doi.org/10.1016/j.ydbio.2004.03.007
Li, J., Yu, M., Feng, G., Hu, H., Li, X., 2011. Breaches of the pial basement membrane are associated with defective dentate gyrus development in mouse models of congenital muscular dystrophies. Neurosci. Lett. 505, 19–24. https://doi.org/10.1016/j.neulet.2011.09.040
Li, Y., Erzurumlu, R.S., Chen, C., Jhaveri, S., Tonegawa, S., 1994. Whisker-related neuronal patterns fail to develop in the trigeminal brainstem nuclei of NMDAR1 knockout mice. Cell 76, 427–437. https://doi.org/10.1016/0092-8674(94)90108-2
Liang, H., Hippenmeyer, S., Ghashghaei, H.T., 2012. A Nestin-cre transgenic mouse is insufficient for recombination in early embryonic neural progenitors. Biol. Open 1, 1200–1203. https://doi.org/10.1242/bio.20122287
Liang, J., Xu, W., Hsu, Y.-T., Yee, A.X., Chen, L., Südhof, T.C., 2015. Conditional neuroligin-2 knockout in adult medial prefrontal cortex links chronic changes in synaptic inhibition to cognitive impairments. Mol. Psychiatry 20, 850–859. https://doi.org/10.1038/mp.2015.31
Lin, P.-Y., Chen, L.Y., Jiang, M., Trotter, J.H., Seigneur, E., Südhof, T.C., 2023. Neurexin-2: An inhibitory neurexin that restricts excitatory synapse formation in the hippocampus. Sci. Adv. 9, eadd8856. https://doi.org/10.1126/sciadv.add8856
Lindenmaier, L.B., Parmentier, N., Guo, C., Tissir, F., Wright, K.M., 2019. Dystroglycan is a scaffold for extracellular axon guidance decisions. eLife 8. https://doi.org/10.7554/eLife.42143
Long, H., Sabatier, C., Ma, L., Plump, A., Yuan, W., Ornitz, D.M., Tamada, A., Murakami, F., Goodman, C.S., Tessier-Lavigne, M., 2004. Conserved roles for Slit and Robo proteins in midline commissural axon guidance. Neuron 42, 213–223. https://doi.org/10.1016/S0896-6273(04)00179-5
Lu, Z., Reddy, M.V.V.V.S., Liu, Jianfang, Kalichava, A., Liu, Jiankang, Zhang, L., Chen, F., Wang, Y., Holthauzen, L.M.F., White, M.A., Seshadrinathan, S., Zhong, X., Ren, G., Rudenko, G., 2016. Molecular Architecture of Contactin-associated Protein-like 2 (CNTNAP2) and Its Interaction with Contactin 2 (CNTN2) *. J. Biol. Chem. 291, 24133–24147. https://doi.org/10.1074/jbc.M116.748236
Luo, Lin, Ambrozkiewicz, M.C., Benseler, F., Chen, C., Dumontier, E., Falkner, S., Furlanis, E., Gomez, A.M., Hoshina, N., Huang, W.-H., Hutchison, M.A., Itoh-Maruoka, Y., Lavery, L.A., Li, W., Maruo, T., Motohashi, J., Pai, E.L.-L., Pelkey, K.A., Pereira, A., Philips, T., Sinclair, J.L., Stogsdill, J.A., Traunmüller, L., Wang, J., Wortel, J., You, W., Abumaria, N., Beier, K.T., Brose, N., Burgess, H.A., Cepko, C.L., Cloutier, J.-F., Eroglu, C., Goebbels, S., Kaeser, P.S., Kay, J.N., Lu, W., Luo, Liqun, Mandai, K., McBain, C.J., Nave, K.-A., Prado, M.A.M., Prado, V.F., Rothstein, J., Rubenstein, J.L.R., Saher, G., Sakimura, K., Sanes, J.R., Scheiffele, P., Takai, Y., Umemori, H., Verhage, M., Yuzaki, M., Zoghbi, H.Y., Kawabe, H., Craig, A.M., 2020. Optimizing Nervous System-Specific Gene Targeting with Cre Driver Lines: Prevalence of Germline Recombination and Influencing Factors. Neuron 106, 37-65.e5. https://doi.org/10.1016/j.neuron.2020.01.008
Lyons, P.R., Slater, C.R., 1991. Structure and function of the neuromuscular junction in young adult mdx mice. J. Neurocytol. 20, 969–981. https://doi.org/10.1007/BF01187915

Lyuksyutova, A.I., Lu, C.C., Milanesio, N., King, L.A., Guo, N., Wang, Y., Nathans, J., Tessier-Lavigne, M., Zou, Y., 2003. Anterior-Posterior Guidance of Commissural Axons by Wnt-Frizzled Signaling. Science 302, 1984–1988. https://doi.org/10.1126/science.1089610

Madisen, L., Zwingman, T.A., Sunkin, S.M., Oh, S.W., Zariwala, H.A., Gu, H., Ng, L.L., Palmiter, R.D., Hawrylycz, M.J., Jones, A.R., Lein, E.S., Zeng, H., 2010. A robust and high-throughput Cre reporting and characterization system for the whole mouse brain. Nat. Neurosci. 13, 133–140. https://doi.org/10.1038/nn.2467

Manya, H., Chiba, A., Yoshida, A., Wang, X., Chiba, Y., Jigami, Y., Margolis, R.U., Endo, T., 2004. Demonstration of mammalian protein O-mannosyltransferase activity: Coexpression of POMT1 and POMT2 required for enzymatic activity. Proc. Natl. Acad. Sci. 101, 500–505. https://doi.org/10.1073/pnas.0307228101

Meilleur, K.G., Zukosky, K., Medne, L., Fequiere, P., Powell-Hamilton, N., Winder, T.L., Alsaman, A., El-Hattab, A.W., Dastgir, J., Hu, Y., Donkervoort, S., Golden, J.A., Eagle, R., Finkel, R., Scavina, M., Hood, I.C., Rorke-Adams, L.B., Bönnemann, C.G., 2014. Clinical, pathologic, and mutational spectrum of dystroglycanopathy caused by LARGE mutations. J. Neuropathol. Exp. Neurol. 73, 425–441. https://doi.org/10.1097/NEN.0000000000000065

Menezes, M.J., McClenahan, F.K., Leiton, C.V., Aranmolate, A., Shan, X., Colognato, H., 2014. The extracellular matrix protein laminin α2 regulates the maturation and function of the blood–brain barrier. J. Neurosci. 34, 15260–15280. https://doi.org/10.1523/JNEUROSCI.3678-13.2014

Mercuri, E., Messina, S., Bruno, C., Mora, M., Pegoraro, E., Comi, G.P., D'Amico, A., Aiello, C., Biancheri, R., Berardinelli, A., Boffi, P., Cassandrini, D., Laverda, A., Moggio, M., Morandi, L., Moroni, I., Pane, M., Pezzani, R., Pichiecchio, A., Pini, A., Minetti, C., Mongini, T., Mottarelli, E., Ricci, E., Ruggieri, A., Saredi, S., Scuderi, C., Tessa, A., Toscano, A., Tortorella, G., Trevisan, C.P., Uggetti, C., Vasco, G., Santorelli, F.M., Bertini, E., 2009. Congenital muscular dystrophies with defective glycosylation of dystroglycan: A population study. Neurology 72, 1802–1809. https://doi.org/10.1212/01.wnl.0000346518.68110.60

Messina, S., Bruno, C., Moroni, I., Pegoraro, E., D'Amico, A., Biancheri, R., Berardinelli, A., Boffi, P., Cassandrini, D., Farina, L., Minetti, C., Moggio, M., Mongini, T., Mottarelli, E., Pane, M., Pantaleoni, C., Pichiecchio, A., Pini, A., Ricci, E., Saredi, S., Sframeli, M., Tortorella, G., Toscano, A., Trevisan, C.P., Uggetti, C., Vasco, G., Comi, G.P., Santorelli, F.M., Bertini, E., Mercuri, E., 2010. Congenital muscular dystrophies with cognitive impairment: A population study. Neurology 75, 898–903. https://doi.org/10.1212/WNL.0b013e3181f11dd5

Miale, I.L., Sidman, R.L., 1961. An autoradiographic analysis of histogenesis in the mouse cerebellum. Exp. Neurol. 4, 277–296. https://doi.org/10.1016/0014-4886(61)90055-3

Miczán, V., Kelemen, K., Glavinics, J.R., László, Z.I., Barti, B., Kenesei, K., Kisfali, M., Katona, I., 2021. NECAB1 and NECAB2 are Prevalent Calcium-Binding Proteins of CB1/CCK-Positive GABAergic Interneurons. Cereb. Cortex 31, 1786–1806. https://doi.org/10.1093/cercor/bhaa326

Miller, D.S., Wright, K.M., 2021. Neuronal Dystroglycan regulates postnatal development of CCK/cannabinoid receptor-1 interneurons. Neural Develop. 16. https://doi.org/10.1186/s13064-021-00153-1

Missler, M., Zhang, W., Rohlmann, A., Kattenstroth, G., Hammer, R.E., Gottmann, K., Südhof, T.C., 2003. α-Neurexins couple Ca2+ channels to synaptic vesicle exocytosis. Nature 423, 939–948. https://doi.org/10.1038/nature01755

Mistry, J., Chuguransky, S., Williams, L., Qureshi, M., Salazar, G.A., Sonnhammer, E.L.L., Tosatto, S.C.E., Paladin, L., Raj, S., Richardson, L.J., Finn, R.D., Bateman, A., 2021. Pfam: The protein families database in 2021. Nucleic Acids Res. 49, D412–D419. https://doi.org/10.1093/nar/gkaa913

Moizard, M.-P., Toutain, A., Fournier, D., Berret, F., Raynaud, M., Billard, C., Andres, C., Moraine, C., 2000. Severe cognitive impairment in DMD: obvious clinical evidence for Dp71 isoform point mutations screening. Eur. J. Hum. Genet. 8, 552–556. https://doi.org/10.1038/sj.ejhg.5200488

Monory, K., Polack, M., Remus, A., Lutz, B., Korte, M., 2015. Cannabinoid CB1 Receptor Calibrates Excitatory Synaptic Balance in the Mouse Hippocampus. J. Neurosci. 35, 3842–3850. https://doi.org/10.1523/JNEUROSCI.3167-14.2015

Montanaro, F., Gee, S.H., Jacobson, C., Lindenbaum, M.H., Froehner, S.C., Carbonetto, S., 1998. Laminin and α-dystroglycan mediate acetylcholine receptor aggregation via a MuSK-independent pathway. J. Neurosci. 18, 1250–1260. https://doi.org/10.1523/jneurosci.18-04-01250.1998

Moore, C.J., Winder, S.J., 2010. Dystroglycan versatility in cell adhesion: A tale of multiple motifs. Cell Commun. Signal. 8, 3. https://doi.org/10.1186/1478-811X-8-3

Moore, S.A., Saito, F., Chen, J., Michele, D.E., Henry, M.D., Messing, A., Cohn, R.D., Ross-Barta, S.E., Westra, S., Williamson, R.A., Hosl, T., Campbell, K.P., 2002. Deletion of brain dystroglycan recapitulates aspects of congenital muscular dystrophy. Nature 418, 422–425. https://doi.org/10.1038/nature00838

Morales, D., Hatten, M.E., 2006. Molecular Markers of Neuronal Progenitors in the Embryonic Cerebellar Anlage. J. Neurosci. 26, 12226–12236. https://doi.org/10.1523/JNEUROSCI.3493-06.2006

Morozov, Y. M, Freund, T.F., 2003. Postnatal development and migration of cholecystokinin-immunoreactive interneurons in rat hippocampus. Neuroscience 120, 923–939. https://doi.org/10.1016/S0306-4522(03)00409-3

Morozov, Yury M., Freund, T.F., 2003. Post-natal development of type 1 cannabinoid receptor immunoreactivity in the rat hippocampus. Eur. J. Neurosci. 18, 1213–1222. https://doi.org/10.1046/j.1460-9568.2003.02852.x

Morozov, Y.M., Torii, M., Rakic, P., 2009. Origin, Early Commitment, Migratory Routes, and Destination of Cannabinoid Type 1 Receptor-Containing Interneurons. Cereb. Cortex 19, i78–i89. https://doi.org/10.1093/cercor/bhp028

Mulder, J., Aguado, T., Keimpema, E., Barabás, K., Ballester Rosado, C.J., Nguyen, L., Monory, K., Marsicano, G., Di Marzo, V., Hurd, Y.L., Guillemot, F., Mackie, K., Lutz, B., Guzmán, M., Lu, H.-C., Galve-Roperh, I., Harkany, T., 2008. Endocannabinoid signaling controls pyramidal cell specification and long-range axon patterning. Proc. Natl. Acad. Sci. 105, 8760–8765. https://doi.org/10.1073/pnas.0803545105

Muntoni, F., Torelli, S., Wells, D.J., Brown, S.C., 2011. Muscular dystrophies due to glycosylation defects: diagnosis and therapeutic strategies. Curr. Opin. Neurol. 24, 437–442. https://doi.org/10.1097/WCO.0b013e32834a95e3

Myshrall, T.D., Moore, S.A., Ostendorf, A.P., Satz, J.S., Kowalczyk, T., Nguyen, H., Daza, R.A.M., Lau, C., Campbell, K.P., Hevner, R.F., 2012. Dystroglycan on radial glia end feet is required for pial basement membrane integrity and columnar organization of the developing cerebral cortex. J. Neuropathol. Exp. Neurol. 71, 1047–1063. https://doi.org/10.1097/NEN.0b013e318274a128

Nagae, M., Yamaguchi, Y., 2014. Three-dimensional structural aspects of protein-polysaccharide interactions. Int. J. Mol. Sci. 15, 3768–3783. https://doi.org/10.3390/ijms15033768

Nagel, A., Lehmann-Horn, F., Engel, A.G., 1990. Neuromuscular transmission in the mdx mouse. Muscle Nerve 13, 742–749. https://doi.org/10.1002/mus.880130813
Nagode, D.A., Tang, A.-H., Yang, K., Alger, B.E., 2014. Optogenetic identification of an intrinsic cholinergically driven inhibitory oscillator sensitive to cannabinoids and opioids in hippocampal CA1. J. Physiol. 592, 103–123. https://doi.org/10.1113/jphysiol.2013.257428
Naidoo, M., Anthony, K., 2020. Dystrophin Dp71 and the Neuropathophysiology of Duchenne Muscular Dystrophy. Mol. Neurobiol. 57, 1748–1767. https://doi.org/10.1007/s12035-019-01845-w
Nakhai, H., Sel, S., Favor, J., Mendoza-Torres, L., Paulsen, F., Duncker, G.I.W., Schmid, R.M., 2007. Ptf1a is essential for the differentiation of GABAergic and glycinergic amacrine cells and horizontal cells in the mouse retina. Development 134, 1151–1160. https://doi.org/10.1242/dev.02781
Navabpour, S., Kwapis, J.L., Jarome, T.J., 2020. A neuroscientist's guide to transgenic mice and other genetic tools. Neurosci. Biobehav. Rev. 108, 732–748. https://doi.org/10.1016/j.neubiorev.2019.12.013
Nery, S., Fishell, G., Corbin, J.G., 2002. The caudal ganglionic eminence is a source of distinct cortical and subcortical cell populations. Nat. Neurosci. 5, 1279–1287. https://doi.org/10.1038/nn971
Nguyen, H., Ostendorf, A.P., Satz, J.S., Westra, S., Ross-Barta, S.E., Campbell, K.P., Moore, S.A., 2014. Glial scaffold required for cerebellar granule cell migration is dependent on dystroglycan function as a receptor for basement membrane proteins. Acta Neuropathol. Commun. 2. https://doi.org/10.1186/2051-5960-1-58
Nguyen, T., Südhof, T.C., 1997. Binding Properties of Neuroligin 1 and Neurexin 1β Reveal Function as Heterophilic Cell Adhesion Molecules *. J. Biol. Chem. 272, 26032–26039. https://doi.org/10.1074/jbc.272.41.26032
Nickolls, A.R., Bönnemann, C.G., 2018. The roles of dystroglycan in the nervous system: Insights from animal models of muscular dystrophy. DMM Dis. Models Mech. 11, dmm035931. https://doi.org/10.1242/dmm.035931
Noell, S., Wolburg-Buchholz, K., Mack, A.F., Beedle, A.M., Satz, J.S., Campbell, K.P., Wolburg, H., Fallier-Becker, P., 2011. Evidence for a role of dystroglycan regulating the membrane architecture of astroglial endfeet. Eur. J. Neurosci. 33, 2179–2186. https://doi.org/10.1111/j.1460-9568.2011.07688.x
Nörenberg, A., Hu, H., Vida, I., Bartos, M., Jonas, P., 2010. Distinct nonuniform cable properties optimize rapid and efficient activation of fast-spiking GABAergic interneurons. Proc. Natl. Acad. Sci. 107, 894–899. https://doi.org/10.1073/pnas.0910716107
Novak, J.S., Spathis, R., Dang, U.J., Fiorillo, A.A., Hindupur, R., Tully, C.B., Mázala, D.A.G., Canessa, E., Brown, K.J., Partridge, T.A., Hathout, Y., Nagaraju, K., 2021. Interrogation of Dystrophin and Dystroglycan Complex Protein Turnover After Exon Skipping Therapy. J. Neuromuscul. Dis. 8, S383–S402. https://doi.org/10.3233/JND-210696
Olah, S.S., Kareemo, D.J., Buchta, W.C., Sinnen, B.L., Miller, C.N., Actor-Engel, H.S., Gookin, S.E., Winborn, C.S., Kleinjan, M.S., Crosby, K.C., Aoto, J., Smith, K.R., Kennedy, M.J., 2023. Acute reorganization of postsynaptic GABAA receptors reveals the functional impact of molecular nanoarchitecture at inhibitory synapses. Cell Rep. 42. https://doi.org/10.1016/j.celrep.2023.113331
Omori, Y., Araki, F., Chaya, T., Kajimura, N., Irie, S., Terada, K., Muranishi, Y., Tsujii, T., Ueno, S., Koyasu, T., Tamaki, Y., Kondo, M., Amano, S., Furukawa, T., 2012. Presynaptic dystroglycan-pikachurin complex regulates the proper synaptic

connection between retinal photoreceptor and bipolar cells. J. Neurosci. 32, 6126–6137. https://doi.org/10.1523/JNEUROSCI.0322-12.2012
Orban, P.C., Chui, D., Marth, J.D., 1992. Tissue- and site-specific DNA recombination in transgenic mice. Proc. Natl. Acad. Sci. U. S. A. 89, 6861–6865. https://doi.org/10.1073/pnas.89.15.6861
Orlandi, C., Omori, Y., Wang, Y., Cao, Y., Ueno, A., Roux, M.J., Condomitti, G., de Wit, J., Kanagawa, M., Furukawa, T., Martemyanov, K.A., 2018. Transsynaptic Binding of Orphan Receptor GPR179 to Dystroglycan-Pikachurin Complex Is Essential for the Synaptic Organization of Photoreceptors. Cell Rep. 25, 130-145.e5. https://doi.org/10.1016/j.celrep.2018.08.068
Palay, S.L., Chan-Palay, V., 2012. Cerebellar Cortex: Cytology and Organization. Springer Science & Business Media.
Park, C., Gim, J., Bahn, S., Kim, G.H., Im, Y., Lee, S.-H., Lee, K., Kim, M.-S., Lee, K.J., Kim, J.S., 2023. A cerebellar disinhibitory circuit supports synaptic plasticity. https://doi.org/10.1101/2023.09.15.557147
Parsons, M.J., Campos, I., Hirst, E.M.A., Stemple, D.L., 2002. Removal of dystroglycan causes severe muscular dystrophy in zebrafish embryos. Development 129, 3505–3512. https://doi.org/10.1242/dev.129.14.3505
Patrizi, A., Scelfo, B., Viltono, L., Briatore, F., Fukaya, M., Watanabe, M., Strata, P., Varoqueaux, F., Brose, N., Fritschy, J.-M., Sassoè-Pognetto, M., 2008. Synapse formation and clustering of neuroligin-2 in the absence of GABAA receptors. Proc. Natl. Acad. Sci. 105, 13151–13156. https://doi.org/10.1073/pnas.0802390105
Pawlisz, A.S., Feng, Y., 2011. Three-dimensional regulation of radial glial functions by lis1-nde1 and dystrophin glycoprotein complexes. PLoS Biol. 9. https://doi.org/10.1371/journal.pbio.1001172
Peng, H.B., Xie, H., Rossi, S.G., Rotundo, R.L., 1999. Acetylcholinesterase clustering at the neuromuscular junction involves perlecan and dystroglycan. J. Cell Biol. 145, 911–921. https://doi.org/10.1083/jcb.145.4.911
Peron, S.P., Freeman, J., Iyer, V., Guo, C., Svoboda, K., 2015. A Cellular Resolution Map of Barrel Cortex Activity during Tactile Behavior. Neuron 86, 783–799. https://doi.org/10.1016/j.neuron.2015.03.027
Petros, T.J., Rebsam, A., Mason, C.A., 2008. Retinal axon growth at the optic chiasm: To cross or not to cross. Annu. Rev. Neurosci. 31, 295–315. https://doi.org/10.1146/annurev.neuro.31.060407.125609
Poliak, S., Salomon, D., Elhanany, H., Sabanay, H., Kiernan, B., Pevny, L., Stewart, C.L., Xu, X., Chiu, S.-Y., Shrager, P., Furley, A.J.W., Peles, E., 2003. Juxtaparanodal clustering of Shaker-like K+ channels in myelinated axons depends on Caspr2 and TAG-1. J. Cell Biol. 162, 1149–1160. https://doi.org/10.1083/jcb.200305018
Potter, G.B., Petryniak, M.A., Shevchenko, E., McKinsey, G.L., Ekker, M., Rubenstein, J.L.R., 2009. Generation of Cre-transgenic mice using Dlx1/Dlx2 enhancers and their characterization in GABAergic interneurons. Mol. Cell. Neurosci. 40, 167–186. https://doi.org/10.1016/j.mcn.2008.10.003
Poulopoulos, A., Aramuni, G., Meyer, G., Soykan, T., Hoon, M., Papadopoulos, T., Zhang, M., Paarmann, I., Fuchs, C., Harvey, K., Jedlicka, P., Schwarzacher, S.W., Betz, H., Harvey, R.J., Brose, N., Zhang, W., Varoqueaux, F., 2009. Neuroligin 2 Drives Postsynaptic Assembly at Perisomatic Inhibitory Synapses through Gephyrin and Collybistin. Neuron 63, 628–642. https://doi.org/10.1016/j.neuron.2009.08.023

Pribiag, H., Peng, H., Shah, W.A., Stellwagen, D., Carbonetto, S., 2014. Dystroglycan mediates homeostatic synaptic plasticity at GABAergic synapses. Proc. Natl. Acad. Sci. U. S. A. 111, 6810–6815. https://doi.org/10.1073/pnas.1321774111
Raphael, A.R., Couthouis, J., Sakamuri, S., Siskind, C., Vogel, H., Day, J.W., Gitler, A.D., 2014. Congenital Muscular Dystrophy and Generalized Epilepsy Caused by GMPPB Mutations. Brain Res. 0, 66–71. https://doi.org/10.1016/j.brainres.2014.04.028
Reeuwijk, J. van, Janssen, M., Elzen, C. van den, Bernabé, D.B.-V. de, Sabatelli, P., Merlini, L., Boon, M., Scheffer, H., Brockington, M., Muntoni, F., Huynen, M.A., Verrips, A., Walsh, C.A., Barth, P.G., Brunner, H.G., Bokhoven, H. van, 2005. POMT2 mutations cause α-dystroglycan hypoglycosylation and Walker-Warburg syndrome. J. Med. Genet. 42, 907–912. https://doi.org/10.1136/jmg.2005.031963
Reissner, C., Stahn, J., Breuer, D., Klose, M., Pohlentz, G., Mormann, M., Missler, M., 2014. Dystroglycan binding to α-Neurexin competes with neurexophilin-1 and neuroligin in the brain. J. Biol. Chem. 289, 27585–27603. https://doi.org/10.1074/jbc.M114.595413
Reist, N.E., Werle, M.J., McMahan, U.J., 1992. Agrin released by motor neurons induces the aggregation of acetylcholine receptors at neuromuscular junctions. Neuron 8, 865–868. https://doi.org/10.1016/0896-6273(92)90200-W
Rios, J.C., Rubin, M., Martin, M.St., Downey, R.T., Einheber, S., Rosenbluth, J., Levinson, S.R., Bhat, M., Salzer, J.L., 2003. Paranodal Interactions Regulate Expression of Sodium Channel Subtypes and Provide a Diffusion Barrier for the Node of Ranvier. J. Neurosci. 23, 7001–7011. https://doi.org/10.1523/JNEUROSCI.23-18-07001.2003
Rosa, G., Ceccarini, M., Cavaldesi, M., Zini, M., Petrucci, T.C., 1996. Localization of the dystrophin binding site at the carboxyl terminus of β-dystroglycan. Biochem. Biophys. Res. Commun. 223, 272–277. https://doi.org/10.1006/bbrc.1996.0883
Rubio-Fernández, M., Uribe, M.L., Vicente-Tejedor, J., Germain, F., Susín-Lara, C., Quereda, C., Montoliu, L., de la Villa, P., Martín-Nieto, J., Cruces, J., 2018. Impairment of photoreceptor ribbon synapses in a novel Pomt1 conditional knockout mouse model of dystroglycanopathy. Sci. Rep. 8, 8543. https://doi.org/10.1038/s41598-018-26855-x
Saito, F., Moore, S.A., Barresi, R., Henry, M.D., Messing, A., Ross-Barta, S.E., Cohn, R.D., Williamson, R.A., Sluka, K.A., Sherman, D.L., Brophy, P.J., Schmelzer, J.D., Low, P.A., Wrabetz, L., Feltri, M.L., Campbell, K.P., 2003. Unique role of dystroglycan in peripheral nerve myelination, nodal structure, and sodium channel stabilization. Neuron 38, 747–758. https://doi.org/10.1016/S0896-6273(03)00301-5
Santos, S.D., Iuliano, O., Ribeiro, L., Veran, J., Ferreira, J.S., Rio, P., Mulle, C., Duarte, C.B., Carvalho, A.L., 2012. Contactin-associated Protein 1 (Caspr1) Regulates the Traffic and Synaptic Content of α-Amino-3-hydroxy-5-methyl-4-isoxazolepropionic Acid (AMPA)-type Glutamate Receptors *. J. Biol. Chem. 287, 6868–6877. https://doi.org/10.1074/jbc.M111.322909
Sasaki, T., Yamada, H., Matsumura, K., Shimizu, T., Kobata, A., Endo, T., 1998. Detection of O-mannosyl glycans in rabbit skeletal muscle α-dystroglycan. Biochim. Biophys. Acta - Gen. Subj. 1425, 599–606. https://doi.org/10.1016/S0304-4165(98)00114-7
Sato, S., Omori, Y., Katoh, K., Kondo, M., Kanagawa, M., Miyata, K., Funabiki, K., Koyasu, T., Kajimura, N., Miyoshi, T., Sawai, H., Kobayashi, K., Tani, A., Toda, T., Usukura, J., Tano, Y., Fujikado, T., Furukawa, T., 2008. Pikachurin, a

dystroglycan ligand, is essential for photoreceptor ribbon synapse formation. Nat. Neurosci. 11, 923–931. https://doi.org/10.1038/nn.2160
Satz, J.S., Barresi, R., Durbeej, M., Willer, T., Turner, A., Moore, S.A., Campbell, K.P., 2008. Brain and eye malformations resembling Walker-Warburg syndrome are recapitulated in mice by dystroglycan deletion in the epiblast. J. Neurosci. 28, 10567–10575. https://doi.org/10.1523/JNEUROSCI.2457-08.2008
Satz, J.S., Ostendorf, A.P., Hou, S., Turner, A., Kusano, H., Lee, J.C., Turk, R., Nguyen, H., Ross-Barta, S.E., Westra, S., Hoshi, T., Moore, S.A., Campbell, K.P., 2010. Distinct functions of glial and neuronal dystroglycan in the developing and adult mouse brain. J. Neurosci. 30, 14560–14572. https://doi.org/10.1523/JNEUROSCI.3247-10.2010
Satz, J.S., Philp, A.R., Nguyen, H., Kusano, H., Lee, J., Turk, R., Riker, M.J., Hernández, J., Weiss, R.M., Anderson, M.G., Mullins, R.F., Moore, S.A., Stone, E.M., Campbell, K.P., 2009. Visual impairment in the absence of dystroglycan. J. Neurosci. 29, 13136–13146. https://doi.org/10.1523/JNEUROSCI.0474-09.2009
Saunders, A., Macosko, E.Z., Wysoker, A., Goldman, M., Krienen, F.M., de Rivera, H., Bien, E., Baum, M., Bortolin, L., Wang, S., Goeva, A., Nemesh, J., Kamitaki, N., Brumbaugh, S., Kulp, D., McCarroll, S.A., 2018. Molecular Diversity and Specializations among the Cells of the Adult Mouse Brain. Cell 174, 1015-1030.e16. https://doi.org/10.1016/j.cell.2018.07.028
Schindelin, J., Arganda-Carreras, I., Frise, E., Kaynig, V., Longair, M., Pietzsch, T., Preibisch, S., Rueden, C., Saalfeld, S., Schmid, B., Tinevez, J.-Y., White, D.J., Hartenstein, V., Eliceiri, K., Tomancak, P., Cardona, A., 2012. Fiji: an open-source platform for biological-image analysis. Nat. Methods 9, 676–682. https://doi.org/10.1038/nmeth.2019
Schröder, J.E., Tegeler, M.R., Großhans, U., Porten, E., Blank, M., Lee, J., Esapa, C., Blake, D.J., Kröger, S., 2007. Dystroglycan regulates structure, proliferation and differentiation of neuroepithelial cells in the developing vertebrate CNS. Dev. Biol. 307, 62–78. https://doi.org/10.1016/j.ydbio.2007.04.020
Schwartzberg, P.L., Goff, S.P., Robertson, E.J., 1989. Germ-Line Transmission of a c-abl Mutation Produced by Targeted Gene Disruption in ES Cells. Science 246, 799–803. https://doi.org/10.1126/science.2554496
Senko, M.W., Remes, P.M., Canterbury, J.D., Mathur, R., Song, Q., Eliuk, S.M., Mullen, C., Earley, L., Hardman, M., Blethrow, J.D., Bui, H., Specht, A., Lange, O., Denisov, E., Makarov, A., Horning, S., Zabrouskov, V., 2013. Novel Parallelized Quadrupole/Linear Ion Trap/Orbitrap Tribrid Mass Spectrometer Improving Proteome Coverage and Peptide Identification Rates. Anal. Chem. 85, 11710–11714. https://doi.org/10.1021/ac403115c
Senti, K.A., Usui, T., Boucke, K., Greber, U., Uemura, T., Dickson, B.J., 2003. Flamingo regulates R8 axon-axon and axon-target interactions in the Drosophila visual system. Curr. Biol. 13, 828–832. https://doi.org/10.1016/S0960-9822(03)00291-4
Shafer, B., Onishi, K., Lo, C., Colakoglu, G., Zou, Y., 2011. Vangl2 Promotes Wnt/Planar Cell Polarity-like Signaling by Antagonizing Dvl1-Mediated Feedback Inhibition in Growth Cone Guidance. Dev. Cell 20, 177–191. https://doi.org/10.1016/j.devcel.2011.01.002
Shcherbata, H.R., Yatsenko, A.S., Patterson, L., Sood, V.D., Nudel, U., Yaffe, D., Baker, D., Ruohola-Baker, H., 2007. Dissecting muscle and neuronal disorders in a Drosophila model of muscular dystrophy. EMBO J. 26, 481–493. https://doi.org/10.1038/sj.emboj.7601503
Sheikh, M.O., Capicciotti, C.J., Liu, L., Praissman, J., Ding, D., Mead, D.G., Brindley, M.A., Willer, T., Campbell, K.P., Moremen, K.W., Wells, L., Boons, G.-J., 2022.

Cell surface glycan engineering reveals that matriglycan alone can recapitulate dystroglycan binding and function. Nat. Commun. 13, 3617. https://doi.org/10.1038/s41467-022-31205-7
Sheikh, M.O., Capicciotti, C.J., Liu, L., Praissman, J., Mead, D.G., Brindley, A., Willer, T., Campbell, K.P., Moremen, K.W., Wells, L., Hughes, H., Paul, S., Muscular, D.W., Specialized, D., 2021. Cell Surface Glycan Engineering Reveals that Matriglycan Alone can Recapitulate Dystroglycan Binding and Function. bioRxiv 2021.05.10.443358. https://doi.org/10.1101/2021.05.10.443358
Sillitoe, R.V., Stephen, D., Lao, Z., Joyner, A.L., 2008. Engrailed Homeobox Genes Determine the Organization of Purkinje Cell Sagittal Stripe Gene Expression in the Adult Cerebellum. J. Neurosci. 28, 12150–12162. https://doi.org/10.1523/JNEUROSCI.2059-08.2008
Smalheiser, N.R., Haslam, S.M., Sutton-Smith, M., Morris, H.R., Dell, A., 1998. Structural analysis of sequences O-linked to mannose reveals a novel Lewis X structure in cranin (dystroglycan) purified from sheep brain. J. Biol. Chem. 273, 23698–23703. https://doi.org/10.1074/jbc.273.37.23698
Specht, S., Straub, V., 2021. Intellectual disability in paediatric patients with genetic muscle diseases. Neuromuscul. Disord. 31, 988–997. https://doi.org/10.1016/j.nmd.2021.08.012
Spence, H.J., Chen, Y.J., Batchelor, C.L., Higginson, J.R., Suila, H., Carpen, O., Winder, S.J., 2004. Ezrin-dependent regulation of the actin cytoskeleton by β -dystroglycan. Hum. Mol. Genet. 13, 1657–1668. https://doi.org/10.1093/hmg/ddh170
Steimel, A., Wong, L., Najarro, E.H., Ackley, B.D., Garriga, G., Hutter, H., 2010. The Flamingo ortholog FMI-1 controls pioneer-dependent navigation of follower axons in C. elegans. Development 137, 3663–3673. https://doi.org/10.1242/dev.054320
Stetefeld, J., Alexandrescu, A.T., Maciejewski, M.W., Jenny, M., Rathgeb-Szabo, K., Schulthess, T., Landwehr, R., Frank, S., Ruegg, M.A., Kammerer, R.A., 2004. Modulation of agrin function by alternative splicing and Ca2+ binding. Structure 12, 503–515. https://doi.org/10.1016/j.str.2004.02.001
Südhof, T.C., 2018. Towards an Understanding of Synapse Formation. Neuron 100, 276–293. https://doi.org/10.1016/j.neuron.2018.09.040
Sugita, S., Saito, F., Tang, J., Satz, J., Campbell, K., Südhof, T.C., 2001. A stoichiometric complex of neurexins and dystroglycan in brain. J. Cell Biol. 154, 435–445. https://doi.org/10.1083/jcb.200105003
Sugiyama, J., Bowen, D.C., Hall, Z.W., 1994. Dystroglycan binds nerve and muscle agrin. Neuron 13, 103–115. https://doi.org/10.1016/0896-6273(94)90462-6
Sumita, K., Sato, Y., Iida, J., Kawata, A., Hamano, M., Hirabayashi, S., Ohno, K., Peles, E., Hata, Y., 2007. Synaptic scaffolding molecule (S-SCAM) membrane-associated guanylate kinase with inverted organization (MAGI)-2 is associated with cell adhesion molecules at inhibitory synapses in rat hippocampal neurons. J. Neurochem. 100, 154–166. https://doi.org/10.1111/j.1471-4159.2006.04170.x
Sun, M.-Y., Yetman, M.J., Lee, T.-C., Chen, Y., Jankowsky, J.L., 2014. Specificity and efficiency of reporter expression in adult neural progenitors vary substantially among nestin-CreERT2 lines. J. Comp. Neurol. 522, 1191–1208. https://doi.org/10.1002/cne.23497
Suzuki, A., Yoshida, M., Hayashi, K., Mizuno, Y., Hagiwara, Y., Ozawa, E., 1994. Molecular organization at the glycoprotein-complex-binding site of dystrophin: Three dystrophin-associated proteins bind directly to the carboxy-terminal portion of dystrophin. Eur. J. Biochem. 220, 283–292. https://doi.org/10.1111/j.1432-1033.1994.tb18624.x

Takeo, Y.H., Shuster, S.A., Jiang, L., Hu, M.C., Luginbuhl, D.J., Rülicke, T., Contreras, X., Hippenmeyer, S., Wagner, M.J., Ganguli, S., Luo, L., 2021. GluD2- and Cbln1-mediated competitive interactions shape the dendritic arbors of cerebellar Purkinje cells. Neuron 109, 629-644.e8. https://doi.org/10.1016/j.neuron.2020.11.028

Talts, J.F., Andac, Z., Göhring, W., Brancaccio, A., Timpl, R., 1999. Binding of the G domains of laminin α1 and α2 chains and perlecan to heparin, sulfatides, α-dystroglycan and several extracellular matrix proteins. EMBO J. 18, 863–870. https://doi.org/10.1093/emboj/18.4.863

Taniguchi, H., He, M., Wu, P., Kim, S., Paik, R., Sugino, K., Kvitsani, D., Fu, Y., Lu, J., Lin, Y., Miyoshi, G., Shima, Y., Fishell, G., Nelson, S.B., Huang, Z.J., 2011. A Resource of Cre Driver Lines for Genetic Targeting of GABAergic Neurons in Cerebral Cortex. Neuron 71, 995–1013. https://doi.org/10.1016/j.neuron.2011.07.026

Taniguchi-Ikeda, M., Morioka, I., Iijima, K., Toda, T., 2016. Mechanistic aspects of the formation of α-dystroglycan and therapeutic research for the treatment of α-dystroglycanopathy: A review. Mol. Aspects Med., Molecular Role of Glycoproteins in Disease 51, 115–124. https://doi.org/10.1016/j.mam.2016.07.003

Tayler, T.D., Robichaux, M.B., Garrity, P.A., 2004. Compartmentalization of visual centers in the Drosophila brain requires Slit and Robo proteins. Development 131, 5935–5945. https://doi.org/10.1242/dev.01465

The Gene Ontology Consortium, Aleksander, S.A., Balhoff, J., Carbon, S., Cherry, J.M., Drabkin, H.J., Ebert, D., Feuermann, M., Gaudet, P., Harris, N.L., Hill, D.P., Lee, R., Mi, H., Moxon, S., Mungall, C.J., Muruganugan, A., Mushayahama, T., Sternberg, P.W., Thomas, P.D., Van Auken, K., Ramsey, J., Siegele, D.A., Chisholm, R.L., Fey, P., Aspromonte, M.C., Nugnes, M.V., Quaglia, F., Tosatto, S., Giglio, M., Nadendla, S., Antonazzo, G., Attrill, H., dos Santos, G., Marygold, S., Strelets, V., Tabone, C.J., Thurmond, J., Zhou, P., Ahmed, S.H., Asanitthong, P., Luna Buitrago, D., Erdol, M.N., Gage, M.C., Ali Kadhum, M., Li, K.Y.C., Long, M., Michalak, A., Pesala, A., Pritazahra, A., Saverimuttu, S.C.C., Su, R., Thurlow, K.E., Lovering, R.C., Logie, C., Oliferenko, S., Blake, J., Christie, K., Corbani, L., Dolan, M.E., Drabkin, H.J., Hill, D.P., Ni, L., Sitnikov, D., Smith, C., Cuzick, A., Seager, J., Cooper, L., Elser, J., Jaiswal, P., Gupta, P., Jaiswal, P., Naithani, S., Lera-Ramirez, M., Rutherford, K., Wood, V., De Pons, J.L., Dwinell, M.R., Hayman, G.T., Kaldunski, M.L., Kwitek, A.E., Laulederkind, S.J.F., Tutaj, M.A., Vedi, M., Wang, S.-J., D'Eustachio, P., Aimo, L., Axelsen, K., Bridge, A., Hyka-Nouspikel, N., Morgat, A., Aleksander, S.A., Cherry, J.M., Engel, S.R., Karra, K., Miyasato, S.R., Nash, R.S., Skrzypek, M.S., Weng, S., Wong, E.D., Bakker, E., Berardini, T.Z., Reiser, L., Auchincloss, A., Axelsen, K., Argoud-Puy, G., Blatter, M.-C., Boutet, E., Breuza, L., Bridge, A., Casals-Casas, C., Coudert, E., Estreicher, A., Livia Famiglietti, M., Feuermann, M., Gos, A., Gruaz-Gumowski, N., Hulo, C., Hyka-Nouspikel, N., Jungo, F., Le Mercier, P., Lieberherr, D., Masson, P., Morgat, A., Pedruzzi, I., Pourcel, L., Poux, S., Rivoire, C., Sundaram, S., Bateman, A., Bowler-Barnett, E., Bye-A-Jee, H., Denny, P., Ignatchenko, A., Ishtiaq, R., Lock, A., Lussi, Y., Magrane, M., Martin, M.J., Orchard, S., Raposo, P., Speretta, E., Tyagi, N., Warner, K., Zaru, R., Diehl, A.D., Lee, R., Chan, J., Diamantakis, S., Raciti, D., Zarowiecki, M., Fisher, M., James-Zorn, C., Ponferrada, V., Zorn, A., Ramachandran, S., Ruzicka, L., Westerfield, M., 2023. The Gene Ontology knowledgebase in 2023. Genetics 224, iyad031. https://doi.org/10.1093/genetics/iyad031

Thomas, P.D., Ebert, D., Muruganujan, A., Mushayahama, T., Albou, L.-P., Mi, H., 2022. PANTHER: Making genome-scale phylogenetics accessible to all. Protein Sci. 31, 8–22. https://doi.org/10.1002/pro.4218

Tian, M., Jacobson, C., Gee, S.H., Campbell, K.P., Carbonetto, S., Jucker, M., 1996. Dystroglycan in the cerebellum is a laminin α2-chain binding protein at the glial-vascular interface and is expressed in Purkinje cells. Eur. J. Neurosci. 8, 2739–2747. https://doi.org/10.1111/j.1460-9568.1996.tb01568.x

Touzot, A., Ruiz-Reig, N., Vitalis, T., Studer, M., 2016. Molecular control of two novel migratory paths for CGE-derived interneurons in the developing mouse brain. Development 143, 1753–1765. https://doi.org/10.1242/dev.131102

Tronche, F., Kellendonk, C., Kretz, O., Gass, P., Anlag, K., Orban, P.C., Bock, R., Klein, R., Schütz, G., 1999. Disruption of the glucocorticoid receptor gene in the nervous system results in reduced anxiety. Nat. Genet. 23, 99–103. https://doi.org/10.1038/12703

Trotter, J.H., Wang, C.Y., Zhou, P., Nakahara, G., Südhof, T.C., 2023. A combinatorial code of neurexin-3 alternative splicing controls inhibitory synapses via a trans-synaptic dystroglycan signaling loop. Nat. Commun. 14, 1771. https://doi.org/10.1038/s41467-023-36872-8

Truett, G. e., Heeger, P., Mynatt, R. l., Truett, A. a., Walker, J. a., Warman, M. l., 2000. Preparation of PCR-Quality Mouse Genomic DNA with Hot Sodium Hydroxide and Tris (HotSHOT). BioTechniques 29, 52–54. https://doi.org/10.2144/00291bm09

Tsien, Joe Z, Chen, D.F., Gerber, D., Tom, C., Mercer, E.H., Anderson, D.J., Mayford, M., Kandel, E.R., Tonegawa, S., 1996. Subregion- and Cell Type–Restricted Gene Knockout in Mouse Brain. Cell 87, 1317–1326. https://doi.org/10.1016/S0092-8674(00)81826-7

Tsien, Joe Z., Huerta, P.T., Tonegawa, S., 1996. The Essential Role of Hippocampal CA1 NMDA Receptor–Dependent Synaptic Plasticity in Spatial Memory. Cell 87, 1327–1338. https://doi.org/10.1016/S0092-8674(00)81827-9

Ueda, H., Baba, T., Terada, N., Kato, Y., Fujii, Y., Takayama, I., Mei, X., Ohno, S., 2000. Immunolocalization of dystrobrevin in the astrocytic endfeet and endothelial cells in the rat cerebellum. Neurosci. Lett. 283, 121–124. https://doi.org/10.1016/S0304-3940(00)00925-3

Uezu, A., Hisey, E., Kobayashi, Y., Gao, Y., Bradshaw, T.W.A., Devlin, P., Rodriguiz, R., Tata, P.R., Soderling, S.H., 2019. Essential role for insyn1 in dystroglycan complex integrity and cognitive behaviors in mice. eLife 8. https://doi.org/10.7554/eLife.50712

Ullrich, B., Ushkaryov, Y.A., Südhof, T.C., 1995. Cartography of neurexins: More than 1000 isoforms generated by alternative splicing and expressed in distinct subsets of neurons. Neuron 14, 497–507. https://doi.org/10.1016/0896-6273(95)90306-2

van der Pijl, E.M., van Putten, M., Niks, E.H., Verschuuren, J.J.G.M., Aartsma-Rus, A., Plomp, J.J., 2016. Characterization of neuromuscular synapse function abnormalities in multiple Duchenne muscular dystrophy mouse models. Eur. J. Neurosci. 43, 1623–1635. https://doi.org/10.1111/ejn.13249

Varoqueaux, F., Aramuni, G., Rawson, R.L., Mohrmann, R., Missler, M., Gottmann, K., Zhang, W., Südhof, T.C., Brose, N., 2006. Neuroligins Determine Synapse Maturation and Function. Neuron 51, 741–754. https://doi.org/10.1016/j.neuron.2006.09.003

Viltono, L., Patrizi, A., Fritschy, J.-M., Sassoè-Pognetto, M., 2008. Synaptogenesis in the cerebellar cortex: differential regulation of gephyrin and GABAA receptors at

somatic and dendritic synapses of Purkinje cells. J. Comp. Neurol. 508, 579–591. https://doi.org/10.1002/cne.21713
Vitalis, T., Lainé, J., Simon, A., Roland, A., Leterrier, C., Lenkei, Z., 2008. The type 1 cannabinoid receptor is highly expressed in embryonic cortical projection neurons and negatively regulates neurite growth in vitro. Eur. J. Neurosci. 28, 1705–1718. https://doi.org/10.1111/j.1460-9568.2008.06484.x
Wang, J., Lin, Z.-J., Liu, L., Xu, H.-Q., Shi, Y.-W., Yi, Y.-H., He, N., Liao, W.-P., 2017. Epilepsy-associated genes. Seizure, 25th Anniversary Issue 44, 11–20. https://doi.org/10.1016/j.seizure.2016.11.030
Wang, W.X., Lefebvre, J.L., 2022. Morphological pseudotime ordering and fate mapping reveal diversification of cerebellar inhibitory interneurons. Nat. Commun. 13, 3433. https://doi.org/10.1038/s41467-022-30977-2
Whitebirch, A.C., Santoro, B., Barnett, A., Lisgaras, C.P., Scharfman, H.E., Siegelbaum, S.A., 2023. Reduced Cholecystokinin-Expressing Interneuron Input Contributes to Disinhibition of the Hippocampal CA2 Region in a Mouse Model of Temporal Lobe Epilepsy. J. Neurosci. 43, 6930–6949. https://doi.org/10.1523/JNEUROSCI.2091-22.2023
Willer, T., Inamori, K., Venzke, D., Harvey, C., Morgensen, G., Hara, Y., Beltrán Valero de Bernabé, D., Yu, L., Wright, K.M., Campbell, K.P., 2014. The glucuronyltransferase B4GAT1 is required for initiation of LARGE-mediated α-dystroglycan functional glycosylation. eLife 3, e03941. https://doi.org/10.7554/eLife.03941
Wilmarth, P.A., Riviere, M.A., David, L.L., 2009. Techniques for accurate protein identification in shotgun proteomic studies of human, mouse, bovine, and chicken lenses. J. Ocul. Biol. Dis. Infor. 2, 223–234. https://doi.org/10.1007/s12177-009-9042-6
Witter, L., Rudolph, S., Pressler, R.T., Lahlaf, S.I., Regehr, W.G., 2016. Purkinje Cell Collaterals Enable Output Signals from the Cerebellar Cortex to Feed Back to Purkinje Cells and Interneurons. Neuron 91, 312–319. https://doi.org/10.1016/j.neuron.2016.05.037
Wizeman, J.W., Guo, Q., Wilion, E.M., Li, J.Y., 2019. Specification of diverse cell types during early neurogenesis of the mouse cerebellum. eLife 8, e42388. https://doi.org/10.7554/eLife.42388
Wright, K.M., Lyon, K.A., Leung, H., Leahy, D.J., Ma, L., Ginty, D.D., 2012. Dystroglycan Organizes Axon Guidance Cue Localization and Axonal Pathfinding. Neuron 76, 931–944. https://doi.org/10.1016/j.neuron.2012.10.009
Wu, W.C., Bradley, S.P., Christie, J.M., Pugh, J.R., 2022. Mechanisms and Consequences of Cerebellar Purkinje Cell Disinhibition in a Mouse Model of Duchenne Muscular Dystrophy. J. Neurosci. Off. J. Soc. Neurosci. 42, 2103–2115. https://doi.org/10.1523/JNEUROSCI.1256-21.2022
Wyeth, M.S., Zhang, N., Mody, I., Houser, C.R., 2010. Selective Reduction of Cholecystokinin-Positive Basket Cell Innervation in a Model of Temporal Lobe Epilepsy. J. Neurosci. 30, 8993–9006. https://doi.org/10.1523/JNEUROSCI.1183-10.2010
Xing, X., Zhang, J., Wu, K., Cao, B., Li, X., Jiang, F., Hu, Z., Xia, K., Li, J.-D., 2019. Suppression of Akt-mTOR pathway rescued the social behavior in Cntnap2-deficient mice. Sci. Rep. 9, 3041. https://doi.org/10.1038/s41598-019-39434-5
Yanagisawa, A., Bouchet, C., Bergh, P.Y.K.V. den, Cuisset, J.-M., Viollet, L., Leturcq, F., Romero, N.B., Quijano-Roy, S., Fardeau, M., Seta, N., Guicheney, P., 2007. New POMT2 mutations causing congenital muscular dystrophy: Identification of a

founder mutation. Neurology 69, 1254–1260. https://doi.org/10.1212/01.wnl.0000268489.60809.c4
Yang, B., Jung, D., Motto, D., Meyer, J., Koretzky, G., Campbell, K.P., 1995. SH3 domain-mediated interaction of dystroglycan and Grb2. J. Biol. Chem. 270, 11711–11714. https://doi.org/10.1074/jbc.270.20.11711
Yang, H., Song, D., Liu, Y., Chen, X., Zhu, Y., Wei, C., Fu, X., Liu, X., Yang, Z., Xiong, H., 2022. Seizures and EEG characteristics in a cohort of pediatric patients with dystroglycanopathies. Seizure 101, 39–47. https://doi.org/10.1016/j.seizure.2022.07.008
Yatsenko, A.S., Kucherenko, M.M., Xie, Y., Urlaub, H., Shcherbata, H.R., 2021. Exocyst-mediated membrane trafficking of the lissencephaly-associated ecm receptor dystroglycan is required for proper brain compartmentalization. eLife 10, 1–52. https://doi.org/10.7554/eLife.63868
Yoshida-Moriguchi, T., Campbell, K.P., 2015. Matriglycan: a novel polysaccharide that links dystroglycan to the basement membrane. Glycobiology 25, 702–713. https://doi.org/10.1093/glycob/cwv021
Yoshida-Moriguchi, T., Willer, T., Anderson, M.E., Venzke, D., Whyte, T., Muntoni, F., Lee, H., Nelson, S.F., Yu, L., Campbell, K.P., 2013. SGK196 is a glycosylation-specific O-mannose kinase required for dystroglycan function. Science 341, 896–899. https://doi.org/10.1126/science.1239951
Yuasa, S., Kawamura, K., Ono, K., Yamakuni, T., Takahashi, Y., 1991. Development and migration of Purkinje cells in the mouse cerebellar primordium. Anat. Embryol. (Berl.) 184, 195–212. https://doi.org/10.1007/BF01673256
Zaccaria, M.L., Di Tommaso, F., Brancaccio, A., Paggi, P., Petrucci, T.C., 2001. Dystroglycan distribution in adult mouse brain: A light and electron microscopy study. Neuroscience 104, 311–324. https://doi.org/10.1016/S0306-4522(01)00092-6
Zhang, B., Chen, L.Y., Liu, X., Maxeiner, S., Lee, S.J., Gokce, O., Südhof, T.C., 2015. Neuroligins Sculpt Cerebellar Purkinje-Cell Circuits by Differential Control of Distinct Classes of Synapses. Neuron 87, 781–796. https://doi.org/10.1016/j.neuron.2015.07.020
Zhang, C., Atasoy, D., Araç, D., Yang, X., Fucillo, M.V., Robison, A.J., Ko, J., Brunger, A.T., Südhof, T.C., 2010. Neurexins Physically and Functionally Interact with GABAA Receptors. Neuron 66, 403–416. https://doi.org/10.1016/j.neuron.2010.04.008
Zhang, X.M., Ng, A.H.L., Tanner, J.A., Wu, W.T., Copeland, N.G., Jenkins, N.A., Huang, J.D., 2004. Highly restricted expression of Cre recombinase in cerebellar Purkinje cells. Genesis 40, 45–51. https://doi.org/10.1002/gene.20062
Zheng, X., Wu, B., Liu, Y., Simmons, S.K., Kim, K., Clarke, G.S., Ashiq, A., Park, J., Wang, Z., Tong, L., Wang, Q., Xu, X., Levin, J.Z., Jin, X., 2023. Massively parallel in vivo Perturb-seq reveals cell type-specific transcriptional networks in cortical development. https://doi.org/10.1101/2023.09.18.558077
Zijlstra, M., Li, E., Sajjadi, F., Subramani, S., Jaenisch, R., 1989. Germ-line transmission of a disrupted β2microglobulin gene produced by homologous recombination in embryonic stem cells. Nature 342, 435–438. https://doi.org/10.1038/342435a0

Appendix A: Dag1 Conditional Knockout Phenotypes in the Literature

Table 0.1 *Dag1* Conditional Knockout Phenotypes in the Literature

Adapted from: Jahncke, J.N., Wright, K.M. (2023). “The many roles of dystroglycan in nervous system development and function”. Developmental Dynamics. 252(1): 61- 80. doi:10.1002/dvdy.516

Cre Line	Cre Timing	Cre Recombination Pattern	Developmental Phenotype(s)	Axon Guidance Phenotype(s)	Synaptic Phenotype(s)	References
Meox2^{Cre};Dag1^{cKO}	E5.5	Epiblast	Hydrocephalus, fused cortical hemispheres, fused cerebellar lobules, mismigrated cortical cells, granule cells, and Purkinje cells	*Not examined*	*Not examined*	(Li et al., 2011)
Sox2^{Cre};Dag1^{cKO}	E6.5	Epiblast	*Not examined*	Spinal commissure postcrossing randomization, discontinuous dorsal funiculus, misprojection and stalling of corticothalamic and thalamocortical axons of the internal capsule	*Not examined*	(Lindenmaier et al., 2019; Wright et al., 2012)
Wnt1^{Cre};Dag1^{cKO}	E7.5	Neural crest	*Not examined*	Normal spinal commissure postcrossing beahvior	*Not examined*	(Lindenmaier et al., 2019)

Cre Line	Cre Timing	Cre Recombination Pattern	Developmental Phenotype(s)	Axon Guidance Phenotype(s)	Synaptic Phenotype(s)	References
Dlx5/6^{Cre};Dag1^{cKO}	E9.5	LGE-derived interneurons of the ventral telencephalon	*Not examined*	Normal internal capsule axon targeting	*Not examined*	(Lindenmaier et al., 2019)
Foxg1^{Cre};Dag1^{cKO}	E10.5	Neuroepithelial cells and progeny in dorsal telencephalon	*Not examined*	Misprojection and stalling of corticothalamic and thalamocortical axons of the internal capsule	*Not examined*	(Lindenmaier et al., 2019)
Gbx2^{CreERT2};Dag1^{cKO}	E10.5 TAM	Thalamic neuronal precursor cells	*Not examined*	Normal internal capsule axon targeting	*Not examined*	(Lindenmaier et al., 2019)
Six3^{Cre};Dag1^{cKO}	E9.0	Retina and ventral forebrain	Abnormal cellular lamination in retina, disruptions in dendritic stratification of amacrine cells and retinal ganglion cells	Retinal ganglion cell axons send aberrant ipsilateral projections at the optic chiasm to the LGN, with some axons projecting to the contralateal eye	*Not examined*	(Clements et al., 2017; Clements and Wright, 2018)
Isl1^{Cre};Dag1^{cKO}	E9.0	Postmitotic retinal ganglion cells	Normal retina cellular lamination and dendrite stratification	Normal retinal ganglion cell axon tract projections	*Not examined*	(Clements et al., 2017; Clements and Wright, 2018)
Emx1^{Cre};Dag1^{cKO}	E10.5	Forebrain progenitors	Mismigrated cortical cells and hippocampal dentate gyrus	Abnormal targeting of CCK^{+} basket axons in hippocampal CA regions; misprojection of ascending	*Not examined*	(Jahncke et al., 2024; Pawlisz and Feng, 2011)

Cre Line	Cre Timing	Cre Recombination Pattern	Developmental Phenotype(s)	Axon Guidance Phenotype(s)	Synaptic Phenotype(s)	References
				thalamocortical internal capsule axons		
Nestin^{Cre};Dag1^{cKO}	E11.5	CNS and PNS neural stem cells	Hydrocephalus, fused cortical hemispheres, fused cerebellar lobules, mismigrated cortical cells, cerebellar granule cells, and hippocampal dentate gyrus	Abnormal targeting of CCK^{+} basket axons in hippocampal CA regions	Reduced amplitude and prolonged implicit time of the elecroretinogram b-wave	(Myshrall et al., 2012; Nguyen et al., 2014; Satz et al., 2010, 2009)
NEX^{Cre};Dag1^{cKO}	E11.5	Pyramidal neurons of the forebrain	Normal cellular migration throughout brain	Disappearance of CCK^{+} basket axons in hippocampal CA regions	Impaired LTP, loss of functional transmission from CCK^{+} basket cells onto CA1 pyramidal cells in hippocampus, loss of CCK^{+} basket cell markers (VGluT3, CCK, CB_1R)	(Früh et al., 2016; Miller and Wright, 2021; Satz et al., 2010)
Crx^{Cre};Dag1^{cKO}	E12.5	Retinal photoreceptors	*Not examined*	*Not examined*	Reduced amplitude and prolonged implicit time of the elecroretinogram b-wave	(Omori et al., 2012)

Cre Line	Cre Timing	Cre Recombination Pattern	Developmental Phenotype(s)	Axon Guidance Phenotype(s)	Synaptic Phenotype(s)	References
hGFAP^{Cre};Dag1^{cKO}	E13.5	Neuroepithelial cells in the CNS	Fused cortical hemispheres, fused cerebellar lobules, mismigrated cortical cells, cerebellar granule cells, and hippocampal dentage gyrus	*Not examined*	Impaired LTP	(Moore et al., 2002; Nguyen et al., 2014; Satz et al., 2010)
mAlpha6^{Cre};Dag1^{cKO}	P4	Cerebellar granule cells	Normal cellular migration throughout brain	*Not examined*	*Not examined*	(Nguyen et al., 2014)
L7^{Cre};Dag1^{cKO}	P6	Cerebellar Purkinje cells	Normal cellular migration throughout brain	*Not examined*	Decreased density of inhibitory synapses onto Purkinje cells, reduced sISPC amplitude, reduced sIPSC frequency, fewer presynaptic vesicles	(Briatore et al., 2020; Nguyen et al., 2014)

Appendix B: Nonspecific *GFAP*^{Cre} Recombination in Hippocampus and Cerebellum

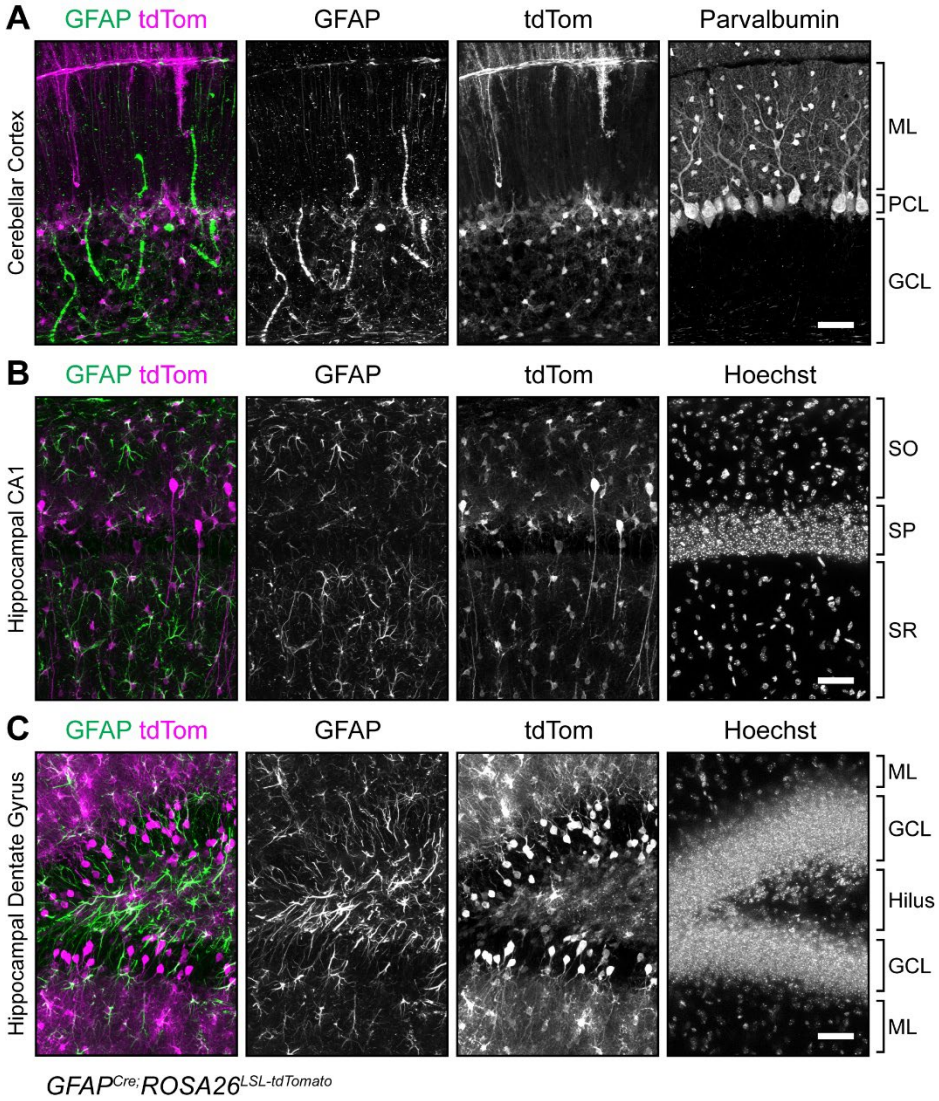

Figure 0.1 *GFAP*^{Cre} recombination in Hippocampal CA1 and Cerebellar Cortex

A *GFAP*^{Cre} line (B6.Cg-*Tg(Gfap-cre)77.6Mvs/2J*, Jax Stock #024098) (Gregorian et al., 2009) was crossed to a *ROSA26*$^{LSL-tdTomato}$ fluorescent reporter line (B6.Cg-*Gt(ROSA)26Sor*$^{tm14(CAG-tdTomato)Hze}$*/J*, Jax Stock #007914) (Madisen et al., 2010) to examine the *GFAP*^{Cre} recombination pattern. PFA perfused brains were blocked and sectioned at 70µm (**A**, cerebellum, sagittal) or 50µm (**B**, **C**, forebrain, coronal) and counterstained with mouse anti-GFAP (Millipore, Cat. No. MAB360, RRID: AB_2109815, 1:500) and Hoechst 33342 nucleic acid stain (Life Technologies, Cat. No. H3570, 1:10,000). Cerebellar slices were also counter stained with rabbit anti-Parvalbumin (Swant, Cat. No. PV27, RRID: AB_10000344, 1:1000) to visualize GABAergic cells in cerebellar cortex. Scale bars = 50µm. *Abbreviations: ML, Molecular Layer; PCL, Purkinje Cell Layer; GCL, Granule Cell Layer; SO, Stratum Oriens; SP, Stratum Pyramidale; SR, Stratum Radiatum; ML, Molecular Layer.*

Appendix C: Interneuron axon targeting in *GFAP^{Cre};Dag1^{cKOs}*

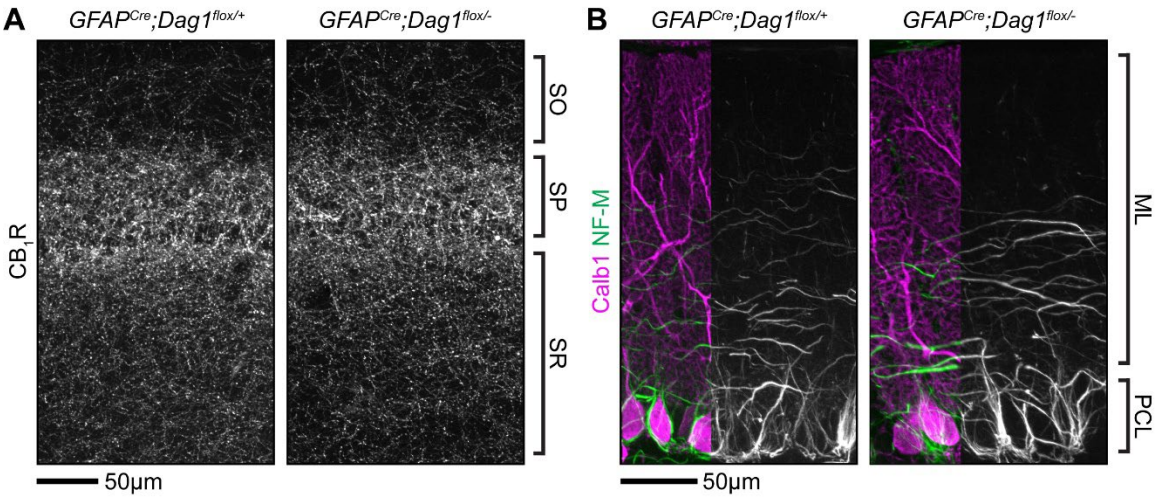

Figure 0.2 Interneuron axon targeting in *GFAP^{Cre};Dag1^{cKOs}*

GFAP^{Cre}, which should drive Cre recombination in astrocytes (see **Appendix B**: *GFAP^{Cre}* recombination), was crossed to *Dystroglycan* (*Dag1*) conditional mice to generate *GFAP^{Cre};Dag1^{cKOs}* (*flox/-*) and *GFAP^{Cre};Dag1^{Ctrls}* (*flox/+*). **(A)** Hippocampal sections were counterstained with guinea pig anti-CB_1R (Synaptic Systems, Cat. No. 258-104, RRID: AB_2661870, 1:500) to visualize CCK^+/CB_1R^+ basket cell axons, which appear to exhibit normal targeting in the cKO hippocampus. **(B)** Cerebellar sections were counterstained with chicken anti-Calbindin (Boster Bio, Cat. No. M03047-2, RRID: AB_2936235, 1:1000) to visualize Purkinje cells and mouse anti-Neurofilament M (DSHB, Cat. No. 2H3-s, RRID: AB_531793, 1:500) to visualize basket MLI axons, which appear normal in the cKOs. *Abbreviations: SO, Stratum Oriens; SP, Stratum Pyramidale; SR, Stratum Radiatum; ML, Molecular Layer; PCL, Purkinje Cell Layer.*

Appendix D: *Wnt1*^{Cre} Recombination in the Cerebellum

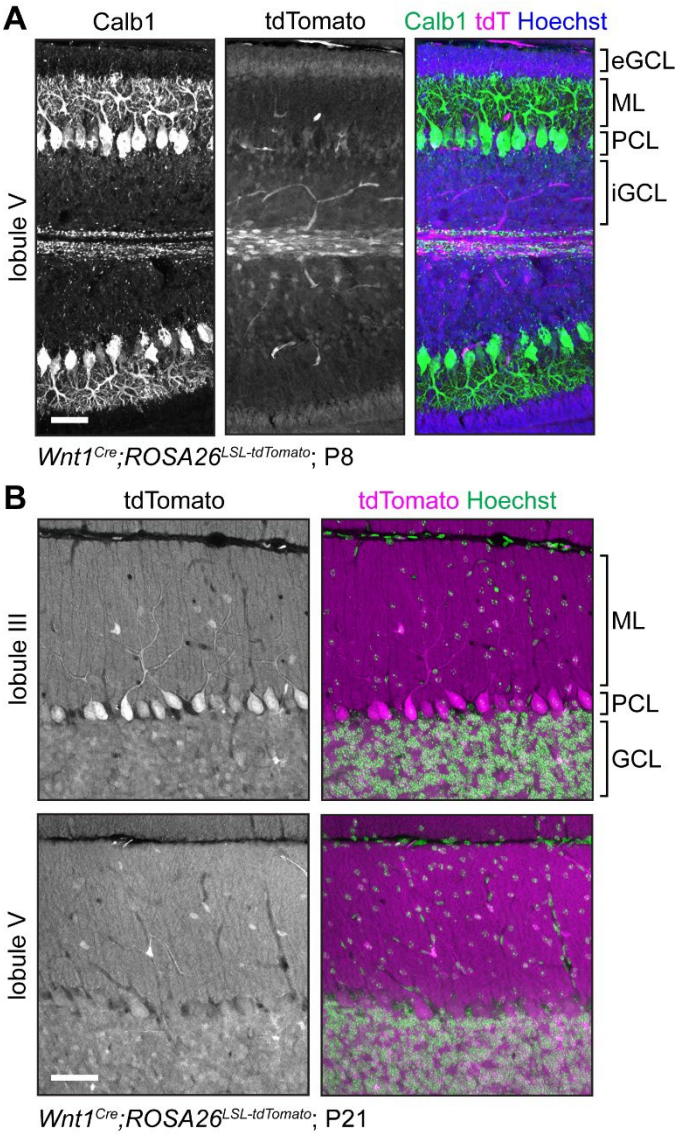

Figure 0.3 *Wnt1*^{Cre} recombination in the Cerebellum

A *Wnt1*^{Cre} line (129S4.Cg-E2f1$^{Tg(Wnt1\text{-}cre)2Sor}$/J, Jax Stock #022137) (Lewis et al., 2013) was crossed to a *ROSA26*$^{LSL\text{-}tdTomato}$ fluorescent reporter line (B6.Cg-*Gt(ROSA)26Sor*$^{tm14(CAG\text{-}tdTomato)Hze}$/J, Jax Stock #007914) (Madisen et al., 2010) to visualize the *Cre* recombination pattern of *Wnt1*^{Cre}. Paraformaldehyde fixed cerebellum samples were taken for analysis at P8 **(A)** and P21 **(B)**. **(A)** At P8, no tdTomato^{+} Purkinje cells were observed in lobule V. Scale bar = 50μm. **(B)** At P21, tdTomato^{+} Purkinje cells were observed in some lobules (ex. lobule III) and not others (ex. lobule V). Occasional tdTomato^{+} molecular layer interneurons were observed. Scale bar = 50μm. *Abbreviations: eGCL, External Granule Cell Layer; iGCL, Internal Granule Cell Layer; GCL, Granule Cell Layer; ML, Molecular Layer; PCL, Purkinje Cell Layer.*

Appendix E: Purkinje Cell Dendrite Morphology in *Pcp2^{Cre};Dag1^{cKOs}*

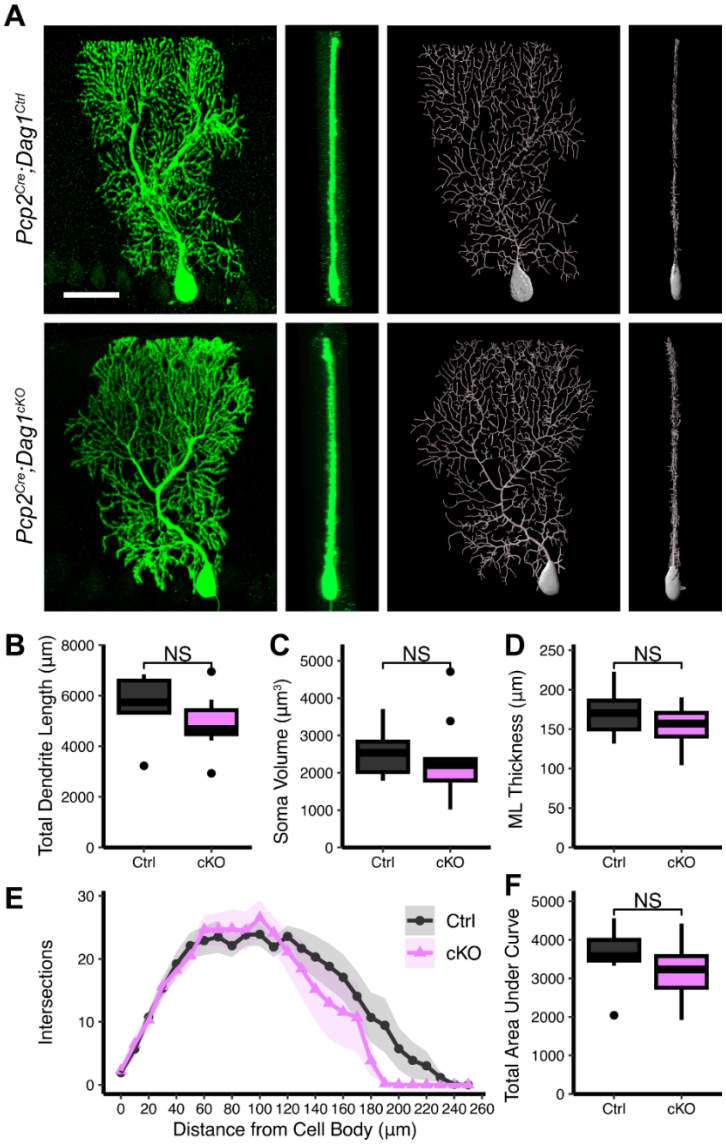

Figure 0.4 Purkinje cell morphology in *Pcp2^{Cre};Dag1^{cKOs}*

Pcp2^{Cre} (B6.Cg-*Tg(Pcp2-cre)3555Jdhu*/J, Jax Stock #010536) (Zhang et al., 2004), which drives recombination in Purkinje cells between P7-P14 (**Chapter 3**), was used to delete Dystroglycan from Purkinje cells coincident with synapse formation. **(A)** P0 pups were injected with AAV8-hSyn1-EGFP into the lateral ventricles (as described in **Chapter 3**) to achieve sparse fluorescent labeling of Purkinje cells for analysis at P30. Cells were imaged at 63X on a laser scanning confocal (Zeiss LSM 980) and reconstructed in Imaris 9.8 (Oxford Instruments). Confocal images are shown in green. Reconstructions are shown in grey. The *en face* view is shown on the left and the lateral view is shown on the right. Scale bar = 50µm. **(B-F)** Quantification of morphological features including **(B)** total dendritic length, **(C)** soma volume, **(D)** molecular layer thickness, and **(E-F)** Sholl analysis revealed no statistically significant differences between genotypes.

Appendix F: NF-M is reduced in *Calb1^{Cre};Dag1^{cKO}* MLI basket cells

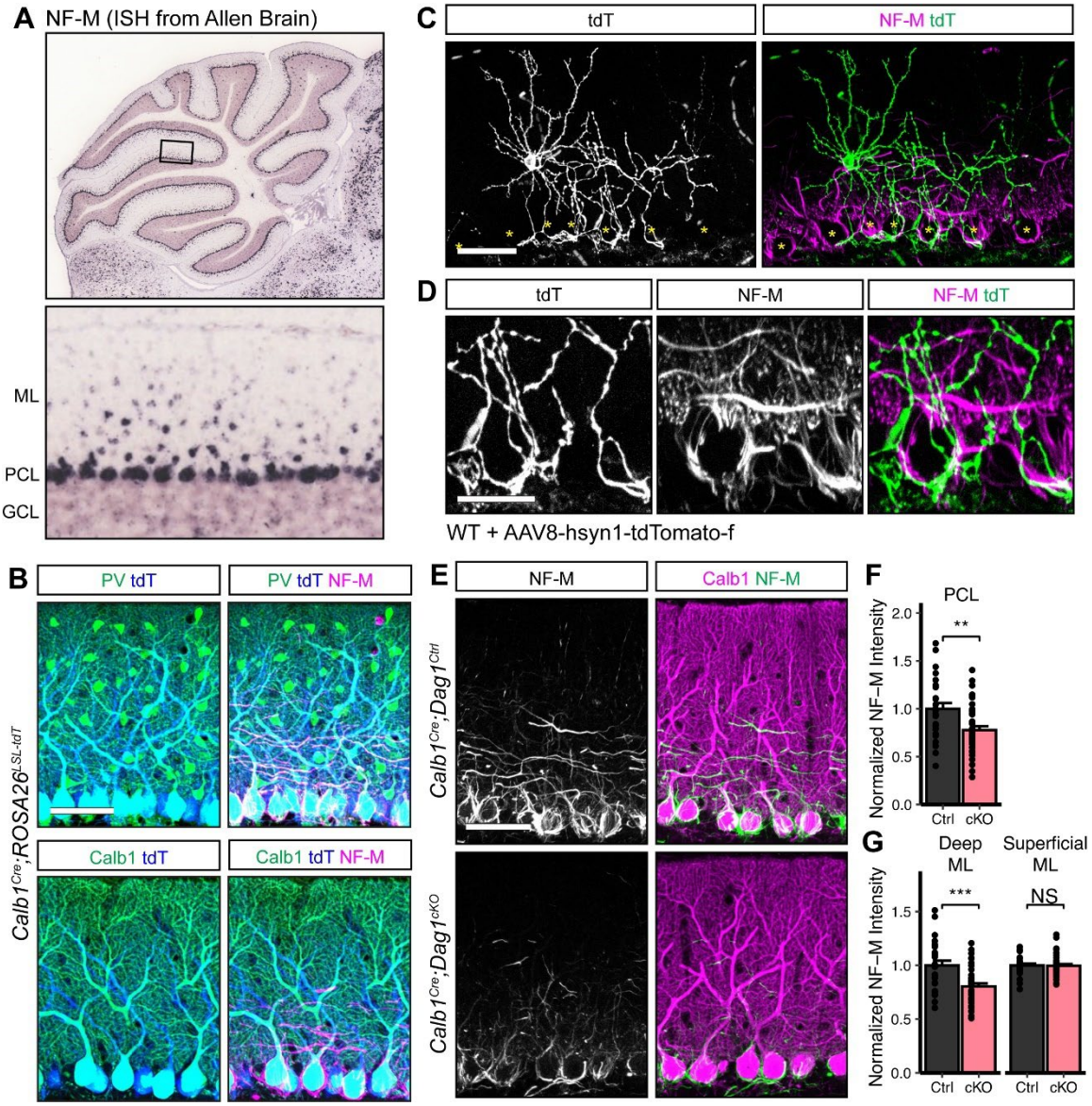

Figure 0.5 NF-M expression in cerebellar MLIs

(A) *In situ* hybridization (ISH) data from the Allen Mouse Brain Atals (Lein et al., 2007) indicates that NF-M is expressed by Purkinje cells and MLIs in the lower portion of the molecular layer, consistent with basket cell expression. **(B)** NF-M immunofluorescence colocalizes with MLI signal from Parvalbumin IHC but not *Calb1^{Cre}* driven tdTomato in Purkinje cells. Scale bar = 50μm. **(C)** The lateral ventricles of P5 wildtype (WT) mice were injected with AAV8-hsyn1-tdTomato-f (Addgene Cat. No. 104060) to drive sparse expression of membrane-tethered tdTomato. NF-M immunofluorescence co-localizes with some but not all basket cell axons. Asterisks denote the positions of Purkinje cell somas. Scale bar = 50μm. **(D)** Insets from images in **(C)**; scale bar = 25μm. **(E)** NF-M fluorescence in *Calb1^{Cre};Dag1^{cKOs}* and littermate controls. Scale bar = 50μm. **(F-G)** Quantification of NF-M intensity from images in **(E)**.

Appendix G: Exploring an indirect Dag1:Gephyrin interaction

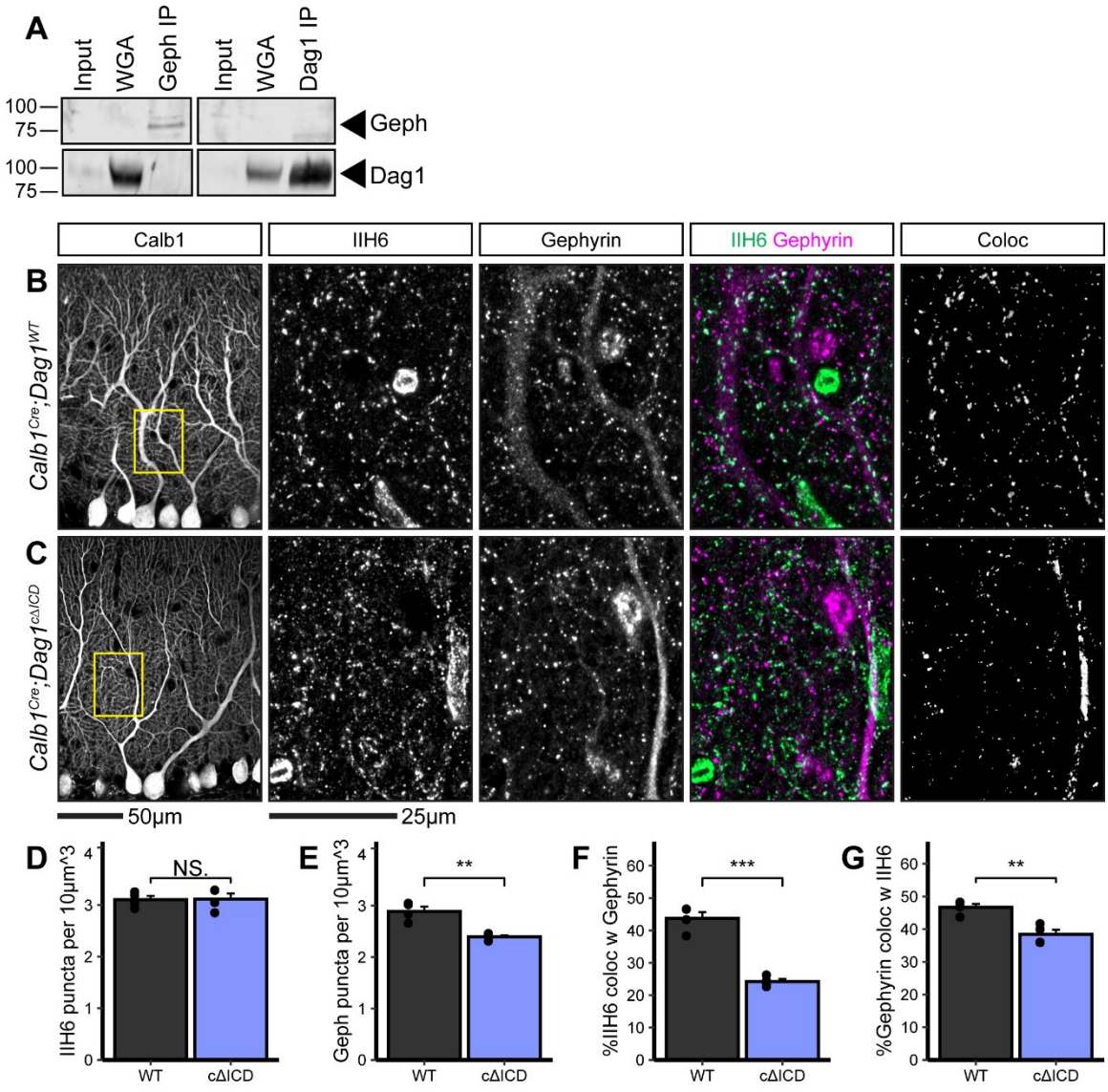

Figure 0.6 An indirect Dag1:Gephyrin interaction

(A) Whole brain lysate was used to generate a membrane fraction (WGA) and for immunoprecipitation using anti-Gephyrin (left) or anti-Dag1 (right). Resultant western blots were then probed for Gephyrin and IIH6 (Dag1). Neither Gephyrin nor Dag1 are abundant enough to appear in crude lysate (input). Gephyrin is not present in the membrane fraction whereas Dag1 is. The anti-Gephyrin antibody did not IP Dag1 and the anti-Dag1 antibody did not IP Gephyrin. **(B-C)** *Calb1^{Cre};Dag1^{cΔICD}* and littermate control cerebella immunostained for Calbindin to visualize Purkinje cells, IIH6 (Dag1, green), and Gephyrin (magenta). Far right panel indicates colocalized pixels. **(D-E)** Quantification of IIH6 **(D)** and Gephyrin **(E)** puncta densities. **(F-G)** Quantification of the colocalization between IIH6 and Gephyrin.

Appendix H: Synaptic localization of Dag1 in cytoplasmic deletion mutant.

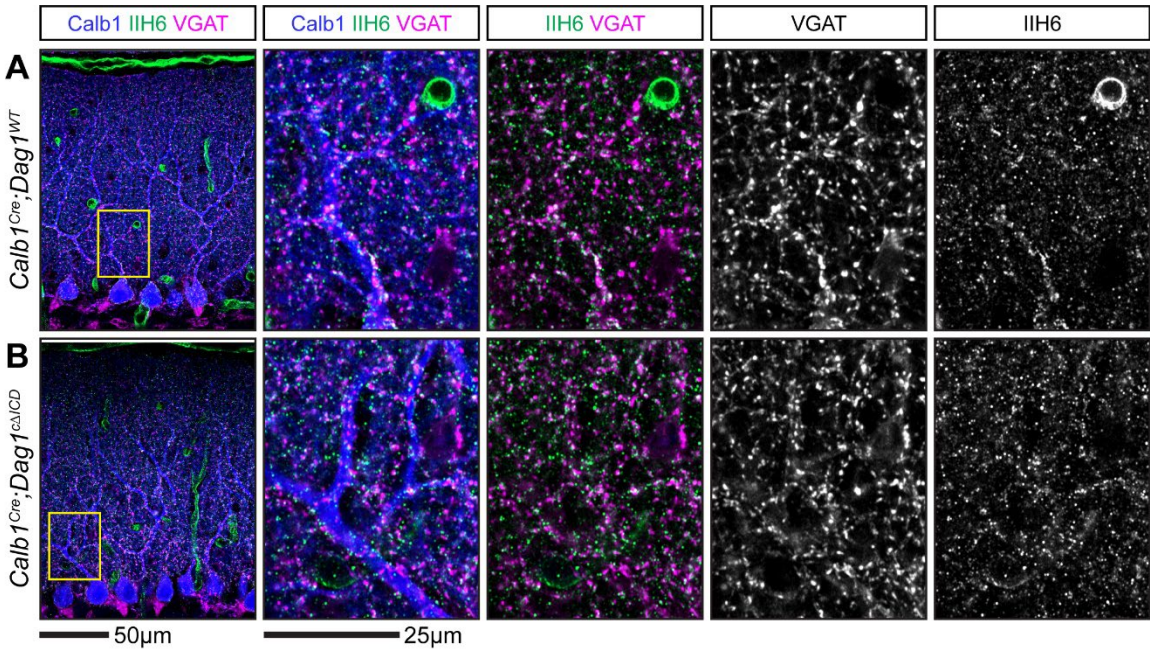

Figure 0.7 Dag1 retains synaptic localization in *Calb1^{Cre};Dag1^{cΔICD}* mutants

(A-B) *Calb1^{Cre};Dag1^{cΔICD}* and littermate control cerebella were immunostained for Calbindin (Calb1) to visualize Purkinje cells, IIH6 (glycosylated Dag1, green), and VGAT (magenta).

Appendix I: LG Domain containing protein RT-PCR primer sets

Table 0.2 RT-PCR Primer Sets (from **Chapter 5: Figure 5.1**).

Gene (Primer Set)	Amplicon Size	Fwd Primer	Fwd T_m	Rev Primer	Rev T_m
Agrn (1)	585	AGGCCTTGCTCCAACAGATCCA	60	TGCCACGTGCATTGCCATTGTA	60
Agrn (2)	550	TTCACAGCAGCGCCTTCTATGC	59.9	GAAGCATTTCTGGGTGCCGTGT	60
BC067074 (1)	541	TCATGACCTGAGAGCCGTGACC	60.1	CGGCTCTGTCGACCTGACTCAT	60.2
BC067074 (2)	315	GGAAGGTACACGGGGAAGGGTT	60	AGGTCTTCCCCTGCCACAGAAG	60
Celsr2 (1)	444	GCACCCAGAACTGAGTCAGGGA	60	AGGGAGGTCAGCCTGGTTGATG	60
Celsr2 (2)	601	CTCAGGCCGTTGTACTCCAGGT	60	TCAGATGGACCTTGGGGAAGCC	60
Celsr3 (1)	600	ACCACAGCATACTGGCCTTCCA	60	CACATCTTTGGGGTGGGCAAGG	60
Celsr3 (2)	593	CGCTCCTTTCCTCCCAGTTCCT	60	TGCCATAGTGCCGTTGTTTGCA	60
Cntnap1 (1)	616	ATCCCTGGCTGCAGATCGACTT	59.8	TCTCGGCCATATCGATCCACCC	59.8
Cntnap1 (2)	597	TGCTCAACACTGCAGGAGGCTA	60	CAGCTCGGACCAAATGCCACTC	60.2
Cntnap2 (1)	503	AGTTCAACCACATCGCCCCTCT	60	TAGGTGCCCTTGTGACGGAACA	59.9
Cntnap2 (2)	331	GAGCATGCAGCATTTTCGCACC	60	GAACCTCATGCCACTGCCCATC	59.9
Cntnap3 (1)	531	TCTCCAGCCTTCCTTCCACACC	60	AAACGCTCTCCAGGCATCAGGA	60
Cntnap3 (2)	522	TCCGGTCCCTTCAGGTGAATGG	60	GCTGGTGGAAGTGACCATCTGC	59.9
Cntnap4 (1)	564	ATTTTCTGGGAACGCGAACGCA	60	GCAGGTGCTGAGATCCCTCCAA	60.4
Cntnap4 (2)	640	AAGAGCCACAGTAACCCCTGGG	60	AGCCAATGCAGTCTCCTGGTCT	59.7
Cntnap5a (1)	489	CAGCACTGTGCCCTTGGTCATC	60.1	GTCCCTGAGCCTTCAGACAGCT	60
Cntnap5a (2)	468	CAGAGGGAGGCCATTTCCGACT	60.1	TGAGGTAGAGCAAGAGGGTGGG	59.2
Cntnap5b (1)	616	TATTTGCTGCTACCTGGCACCC	59	AGGTGGCTCCTGTGTAACCAGT	59.3
Cntnap5b (2)	513	CCCGGTGACCAAGAACACAAGC	60.3	ACAGGAGAAATGCTGGCATGGC	59.9
Cntnap5c (1)	480	AAGGGTGAGACTGATGCCCTGG	60	GCTGACAGAATGCCACATGCCA	60.1
Cntnap5c (2)	597	GAATTGGCCCCTTGCGTTGCTA	60.1	TCTCCACACACTTGCCCCCATT	60.2
Col18a1 (1)	631	TGGACCAGACTCCAACAGTGGC	60.5	GGAAGTGACAGGAGGTGGCTGA	60
Col18a1 (2)	456	AAGTTGGAGCAGATGGAGCCCA	60	AGCCAATTTCACCCTTGTGCCC	60

Gene (Primer Set)	Amplicon Size	Fwd Primer	Fwd T_m	Rev Primer	Rev T_m
Col24a1 (1)	598	CTGTGCCGTCATCGTCATGGTC	60	ATTCCTGCCGTGTGAGGAAGGT	60
Col24a1 (2)	621	CCAGAGGGTTTTCCGGGAGACA	60	GCCCGGTTTTCCTTGAACTCCC	60
Col5a1-201 (1)	475	GGTGCTCCAGGGACTCCTTCAA	60	TGTCGATCTCCAGCACCGTCTT	59.8
Col5a1-201 (2)	429	GCAGCTGTACCCTGAGTCTGGT	60	AGTGTCACAGTCGGGGCTGTAG	60
Crb1 (1)	534	ATGGGTCACAAGTGGCTCCCAT	60	CCCAGGCAGCCTGCTTTAACAT	59.5
Crb1 (2)	410	GGGATGGTCAGGGACACACTGT	60	CGGAGGCACACTCGTTGATGTC	59.9
Cspg4 (1)	377	TTCTTCGGGGAGAACCACCTGG	60	AGGTCAAGGCTTCCAGAGGAGC	60
Cspg4 (2)	536	TCACTGGGCCTTACTTCCCCAC	60	GAGGTCGAAGTGGAAGCCTCCT	59.8
Fat1 (1)	430	ACCGCCTGCTGGAGAATGAGAA	60	CACTCTTCGATGTGCGCGTAGG	60.1
Fat1 (2)	481	CAGCATCGAGGAAGGCAACGAG	60	TGTTGCCTCCACGGTGAGGTTA	59.9
Fat2 (1)	521	GCTACATGCGGTATAGGCCCCT	60	TCAGGGGAGGAGACACATGTGC	60
Fat2 (2)	673	CGACCCTGTCACGGGAGTTGTA	60	GTTCAACCCCAGGCAGTGTGTC	60
Fat3 (1)	541	TGTCCACCAGGGAAACTCGGAG	60	TAGAGCACACAGCCCAGCTTCA	60
Fat3 (2)	593	TGAGTGTCGAGGTCACCGATGG	60.1	CCCGTGTTCCCTGCTTCAATGG	60.1
Fat4 (1)	502	GGCAAGCACTGTGAGCTGAACA	60	ATGCACTGACACTGCTGCCATG	60.1
Fat4 (2)	659	CCCACCGGTGTTTCCAACAGAC	60	TGCTCGGGTCAGGTTGAAGACA	59.9
Gas6 (1)	573	CCAACCATCAACCACGGCATGT	60	CAACTGCCAGGACCACCAACTG	60
Gas6 (2)	556	AAGTCTTCGAGGAGGCCAAGCA	60	ACTCGTCCACATCTTGGCAGGT	60
Nell1 (1)	513	AGCATTGGTTTCTTGCTGGCGT	60	GACCTTGTGCCACTGTCCATCG	59.9
Nell1 (2)	502	GGGCTGAAGCATAATGGGCAGG	60	ACACCAGATCCACAGAGCAGCA	60
Nell2 (1)	471	ATTGCTGCCAATGTGTGTGCCT	60	GCAGACCATCCGTCGACACATG	60
Nell2 (2)	426	GCATCCACTGCTACAGCTGAGC	60	ATTAAGGTCCGGGCACTGAGCA	60
Nrxn1 (1)	575	CACAACGGGCTACACGCAAGAA	60.1	TACCTGACCGTCCATCCCGTTG	60.1
Nrxn1 (2)	357	GAGACCACCACAACCCTGGCTA	60	GACCCTTCATCCCGGTTCCTGT	60
Nrxn1 (3)	329	CTGCCAAAACTGGTCCATGCCA	60	GCTAAATCCGATGGCCAGCCTG	60
Nrxn2 (1)	492	TGCAGTGAAGAGGAACACCCCA	59.8	AATCCTCCTGCGTGTAGCCTGT	59.8

Gene (Primer Set)	Amplicon Size	Fwd Primer	Fwd T_m	Rev Primer	Rev T_m
Nrxn2 (2)	511	GCACATTGACCAGGGCACTGTT	60	AGAGTGGTGGCAGTGGTCTCAG	60
Nrxn3 (1)	595	TTGTGCGCTTCACCAGGAATGG	60	TGGGCTGAATGCTGGCTGTAGA	60
Nrxn3 (2)	480	TGGCCACACTGGATCCCATCAA	60	CGTGAACAGGAGGACTTGACGC	59.9
Slit1 (1)	620	AGAACATCCCACGGAACACCGA	60	GCAGCTGAATTCGCCCTTTTGC	59.9
Slit1 (2)	520	CCTGCCTCTGTGTTGAGGGCTA	60	TCGCTGTTGAGGGTGTAGTGCT	60
Slit2 (1)	536	GCTTCAGCAACATGACCCAGCT	59.8	CGGGGTCATTGTTACAGGTGCC	59.9
Slit2 (2)	426	CGTGGAACTCTATCGAGGGCGA	60	GGCAGGTCCCATGCACACATTT	60
Slit3 (1)	611	ACTGTGTGCCCGAGATGAACCT	60	TGGCCATCATTCACCGTCTCCA	60
Slit3 (2)	601	CTGCAGGAGCCTTCACCCAGTA	60	GATGCGGGCTAGCTTCTGGTTG	60
Tspear (1)	401	GCCGGAAAAGAACCAAAGGCCT	60	GATGCTGAACACCTCGATGCCC	60
Tspear (2)	430	TGAGGTGGACGGAGAGCACTTC	60	CTGAGCGGTGATGTTCAGCTCG	60
Ush2a (1)	550	TAATGGCTGTGGTGGGCCTGAT	60	CCCAGGGTTCCACGCTCTAACT	60
Ush2a (2)	506	AGAAGTCTTCCCTCCCAGCTGC	60	AAAGGTAGCCACGTCCCAGAGG	60

Appendix J: Dystroglycan immunoprecipitation mass spectrometry results

Table 0.3 Mass Spectrometry Results (From **Chapter 5: Figure 5.2**).

Table of proteomics results from the mass spectrometry experiment. Counts refers to the total number of MS/MS spectra matching the protein. Because larger proteins will show bias towards increased counts, the total counts were normalized to the molecular weight in the subsequent column. Results are displayed from highest to lowest normalized count. Unique reads refer to the total number of MS/MS spectra matching only that protein. The unique fraction is the fraction of MS/MS spectra that are unique to that protein; this table is filtered to only include results with a unique fraction above 0.75. *(Abbreviations: MW = Molecular Weight, AA = Amino Acids, Norm = Normalized, Frac = Fraction.)*

Gene	Uniprot ID	Description	MW (KDa)	Sequence Length (AA)	Counts (Total)	Counts (Norm to MW)	Unique Reads (Total)	Unique (Frac)
LAC1	P01843	Ig lambda-1 chain C region	11.57	105	368	31.81	368	1.000
IGH1M	P01869	Ig gamma-1 chain C region, membrane-bound form	43.39	393	1086	25.03	1086	1.000
CNTP1	O54991	Contactin-associated protein 1	156.31	1385	1210	7.74	1210	1.000
Q9Z1A1	Q9Z1A1	PB1 domain-containing protein	43.02	397	308	7.16	308	1.000
DAG1	Q62165	Dystroglycan	96.9	893	629	6.49	629	1.000
RPB2	Q8CFI7	DNA-directed RNA polymerase II subunit RPB2	133.91	1174	858	6.41	858	1.000
RPB1	P08775	DNA-directed RNA polymerase II subunit RPB1	217.17	1970	1210	5.57	1210	1.000
NECA2	Q91ZP9	N-terminal EF-hand calcium-binding protein 2	43.44	389	217	5	217	1.000
LV1C	P01725	Ig lambda-1 chain V region S178	11.65	110	53	4.55	53	1.000
MAP1A	Q9QYR6	Microtubule-associated protein 1A	300.14	2776	1297	4.32	1291	0.995
F120A	Q6A0A9	Constitutive coactivator of PPAR-gamma-like protein 1	121.64	1112	523	4.3	495	0.946
LYAG	P70699	Lysosomal alpha-glucosidase	106.25	953	324	3.05	324	1.000
GYS1	Q9Z1E4	Glycogen [starch] synthase, muscle	83.93	738	215	2.56	210	0.977
NUMBL	O08919	Numb-like protein	64.13	604	162	2.53	162	1.000
RPB3	P97760	DNA-directed RNA polymerase II subunit RPB3	31.44	275	60	1.91	60	1.000
G3P	P16858	Glyceraldehyde-3-phosphate dehydrogenase	35.81	333	58	1.62	51	0.879
CNTN1	P12960	Contactin-1	113.39	1020	183	1.61	183	1.000

Gene	Uniprot ID	Description	MW (KDa)	Sequence Length (AA)	Counts (Total)	Counts (Norm to MW)	Unique Reads (Total)	Unique (Frac)
MBP	P04370	Myelin basic protein	27.17	250	42	1.55	42	1.000
LAMC1	P02468	Laminin subunit gamma-1	177.3	1607	271	1.53	265	0.978
RPB9	P60898	DNA-directed RNA polymerase II subunit RPB9	14.52	125	21	1.45	21	1.000
DLG1	Q811D0	Disks large homolog 1	100.12	905	140	1.4	111	0.793
BIP	P20029	Endoplasmic reticulum chaperone BiP	72.42	655	100	1.38	91	0.910
TGO1	Q8BI84	Transport and Golgi organization protein 1 homolog	213.67	1930	285	1.33	285	1.000
HNRPU	Q8VEK3	Heterogeneous nuclear ribonucleoprotein U	87.92	800	116	1.32	116	1.000
H4	P62806	Histone H4	11.37	103	15	1.32	15	1.000
RC3H1	Q4VGL6	Roquin-1	125.38	1130	163	1.3	163	1.000
UBB	P0CG49	Polyubiquitin-B	34.37	305	43	1.25	43	1.000
AGRIN	A2ASQ1	Agrin	207.54	1950	255	1.23	255	1.000
A0A075B5V7	A0A075B5V7	Ig-like domain-containing protein	10.76	98	13	1.21	13	1.000
CN37	P16330	2',3'-cyclic-nucleotide 3'-phosphodiesterase	47.12	420	54	1.15	54	1.000
LAMB2	Q61292	Laminin subunit beta-2	196.58	1799	224	1.14	222	0.991
PLAK	Q02257	Junction plakoglobin	81.8	745	93	1.14	90	0.968
GRP75	P38647	Stress-70 protein, mitochondrial	73.46	679	84	1.14	84	1.000
DLG3	P70175	Disks large homolog 3	93.48	849	106	1.13	90	0.849
NID1	P10493	Nidogen-1	136.54	1245	149	1.09	148	0.993
HNRPK	P61979	Heterogeneous nuclear ribonucleoprotein K	50.98	463	52	1.02	52	1.000
MIA2	Q91ZV0	Melanoma inhibitory activity protein 2	156.46	1396	157	1	157	1.000
F120C	Q8C3F2	Constitutive coactivator of PPAR-gamma-like protein 2	119.72	1091	115	0.96	87	0.757
LAMB1	P02469	Laminin subunit beta-1	197.09	1786	181	0.92	179	0.989
GRL1A	Q6P6I6	DNA-directed RNA polymerase II subunit GRINL1A	41.24	366	37	0.9	37	1.000
RENT1	Q9EPU0	Regulator of nonsense transcripts 1	123.97	1124	104	0.84	102	0.981
ATPA	Q03265	ATP synthase subunit alpha, mitochondrial	59.75	553	48	0.8	48	1.000
ANXA2	P07356	Annexin A2	38.68	339	29	0.75	29	1.000

Gene	Uniprot ID	Description	MW (KDa)	Sequence Length (AA)	Counts (Total)	Counts (Norm to MW)	Unique Reads (Total)	Unique (Frac)
1433Z	P63101	14-3-3 protein zeta/delta	27.77	245	20	0.72	16	0.800
DPYL2	O08553	Dihydropyrimidinase-related protein 2	62.28	572	44	0.71	37	0.841
RPAP3	Q9D706	RNA polymerase II-associated protein 3	74.1	660	49	0.66	49	1.000
LAMA2	Q60675	Laminin subunit alpha-2	343.81	3118	207	0.6	207	1.000
RPAP2	Q8VC34	Putative RNA polymerase II subunit B1 CTD phosphatase Rpap2	68.53	614	41	0.6	41	1.000
GNAO	P18872	Guanine nucleotide-binding protein G(o) subunit alpha	40.08	354	24	0.6	19	0.792
AT1B1	P14094	Sodium/potassium-transporting ATPase subunit beta-1	35.19	304	21	0.6	21	1.000
NSF	P46460	Vesicle-fusing ATPase	82.61	744	49	0.59	49	1.000
K1107	Q80TK0	AP2-interacting clathrin-endocytosis protein	134.06	1239	78	0.58	78	1.000
KPBB	Q7TSH2	Phosphorylase b kinase regulatory subunit beta	123.89	1085	68	0.55	68	1.000
RPAB3	Q923G2	DNA-directed RNA polymerases I, II, and III subunit RPABC3	17.14	150	9	0.53	9	1.000
DLG4	Q62108	Disks large homolog 4	80.47	724	41	0.51	33	0.805
GUAD	Q9R111	Guanine deaminase	51.01	454	26	0.51	26	1.000
PGBM	Q05793	Basement membrane-specific heparan sulfate proteoglycan core protein	398.29	3707	198	0.5	198	1.000
FUBP1	Q91WJ8	Far upstream element-binding protein 1	68.54	651	34	0.5	34	1.000
H2A1B	C0HKE1	Histone H2A type 1-B	14.13	130	7	0.5	7	1.000
RECQ5	Q8VID5	ATP-dependent DNA helicase Q5	108.24	982	53	0.49	53	1.000
EAA2	P43006	Excitatory amino acid transporter 2	62.03	572	29	0.47	29	1.000
MA2C1	Q91W89	Alpha-mannosidase 2C1	115.69	1039	53	0.46	53	1.000
DESP	E9Q557	Desmoplakin	332.91	2883	146	0.44	146	1.000
KCRB	Q04447	Creatine kinase B-type	42.71	381	19	0.44	19	1.000
KPB1	P18826	Phosphorylase b kinase regulatory subunit alpha, skeletal muscle isoform	138.82	1241	57	0.41	57	1.000

Gene	Uniprot ID	Description	MW (KDa)	Sequence Length (AA)	Counts (Total)	Counts (Norm to MW)	Unique Reads (Total)	Unique (Frac)
AT2A2	O55143	Sarcoplasmic/endoplasmic reticulum calcium ATPase 2	114.86	1044	47	0.41	47	1.000
HNRL1	Q8VDM6	Heterogeneous nuclear ribonucleoprotein U-like protein 1	96	859	39	0.41	39	1.000
UBP5	P56399	Ubiquitin carboxyl-terminal hydrolase 5	95.83	858	38	0.4	38	1.000
HBA	P01942	Hemoglobin subunit alpha	15.09	142	6	0.4	6	1.000
ATPB	P56480	ATP synthase subunit beta, mitochondrial	56.3	529	22	0.39	22	1.000
RO52	Q62191	E3 ubiquitin-protein ligase TRIM21	54.17	470	21	0.39	21	1.000
CPSF2	O35218	Cleavage and polyadenylation specificity factor subunit 2	88.38	782	33	0.37	33	1.000
NID2	O88322	Nidogen-2	153.91	1403	56	0.36	55	0.982
EF2	P58252	Elongation factor 2	95.31	858	34	0.36	34	1.000
ENPL	P08113	Endoplasmin	92.47	802	33	0.36	29	0.879
ANXA1	P10107	Annexin A1	38.73	346	14	0.36	14	1.000
CALM1	P0DP26	Calmodulin-1	16.84	149	6	0.36	6	1.000
EGFLA	Q4VBE4	Pikachurin	110.73	1017	38	0.34	38	1.000
FIP1	Q9D824	Pre-mRNA 3'-end-processing factor FIP1	64.96	581	22	0.34	22	1.000
GLNA	P15105	Glutamine synthetase	42.12	373	14	0.33	14	1.000
CLH1	Q68FD5	Clathrin heavy chain 1	191.55	1675	62	0.32	62	1.000
EAA1	P56564	Excitatory amino acid transporter 1	59.62	543	19	0.32	19	1.000
BASP1	Q91XV3	Brain acid soluble protein 1	22.09	226	7	0.32	7	1.000
CPSF1	Q9EPU4	Cleavage and polyadenylation specificity factor subunit 1	160.82	1441	50	0.31	50	1.000
EWS	Q61545	RNA-binding protein EWS	68.46	655	21	0.31	21	1.000
LAMA4	P97927	Laminin subunit alpha-4	201.82	1816	61	0.3	61	1.000
LRP1	Q91ZX7	Prolow-density lipoprotein receptor-related protein 1	504.74	4545	140	0.28	139	0.993
NCAM1	P13595	Neural cell adhesion molecule 1	119.43	1115	33	0.28	33	1.000

Gene	Uniprot ID	Description	MW (KDa)	Sequence Length (AA)	Counts (Total)	Counts (Norm to MW)	Unique Reads (Total)	Unique (Frac)
MAP6	Q7TSJ2	Microtubule-associated protein 6	96.45	906	27	0.28	27	1.000
PYGB	Q8CI94	Glycogen phosphorylase, brain form	96.73	843	27	0.28	24	0.889
CMC1	Q8BH59	Calcium-binding mitochondrial carrier protein Aralar1	74.57	677	21	0.28	21	1.000
RUVB1	P60122	RuvB-like 1	50.21	456	14	0.28	14	1.000
ENOA	P17182	Alpha-enolase	47.14	434	13	0.28	13	1.000
DPYL3	Q62188	Dihydropyrimidinase-related protein 3	61.94	570	17	0.27	14	0.824
NECA1	Q8BG18	N-terminal EF-hand calcium-binding protein 1	40.93	352	11	0.27	11	1.000
GLYG	Q9R062	Glycogenin-1	37.4	333	10	0.27	10	1.000
TPM3	P21107	Tropomyosin alpha-3 chain	32.99	285	9	0.27	9	1.000
MYPR	P60202	Myelin proteolipid protein	30.08	277	8	0.27	8	1.000
SUCA	Q9WUM5	Succinate--CoA ligase [ADP/GDP-forming] subunit alpha, mitochondrial	36.15	346	9	0.25	9	1.000
TERA	Q01853	Transitional endoplasmic reticulum ATPase	89.32	806	21	0.24	21	1.000
RPAB1	Q80UW8	DNA-directed RNA polymerases I, II, and III subunit RPABC1	24.57	210	6	0.24	6	1.000
HS105	Q61699	Heat shock protein 105 kDa	96.41	858	22	0.23	22	1.000
NDEL1	Q9ERR1	Nuclear distribution protein nudE-like 1	38.37	345	9	0.23	9	1.000
Q792Z1	Q792Z1	Peptidase S1 domain-containing protein	26.22	246	6	0.23	6	1.000
LAMA1	P19137	Laminin subunit alpha-1	338.14	3083	76	0.22	76	1.000
HXK1	P17710	Hexokinase-1	108.3	974	24	0.22	24	1.000
UBA1	Q02053	Ubiquitin-like modifier-activating enzyme 1	117.81	1058	25	0.21	25	1.000
PSA	Q11011	Puromycin-sensitive aminopeptidase	103.32	920	22	0.21	22	1.000
SDHA	Q8K2B3	Succinate dehydrogenase [ubiquinone] flavoprotein subunit, mitochondrial	72.58	664	15	0.21	15	1.000
MAP1B	P14873	Microtubule-associated protein 1B	270.25	2464	54	0.2	48	0.889
NRX3A	Q6P9K9	Neurexin-3	173.43	1571	35	0.2	30	0.857

Gene	Uniprot ID	Description	MW (KDa)	Sequence Length (AA)	Counts (Total)	Counts (Norm to MW)	Unique Reads (Total)	Unique (Frac)
FND3A	Q8BX90	Fibronectin type-III domain-containing protein 3A	131.96	1198	27	0.2	27	1.000
RAB3A	P63011	Ras-related protein Rab-3A	24.97	220	5	0.2	5	1.000
NRX1A	Q9CS84	Neurexin-1	166.17	1514	31	0.19	26	0.839
KPYM	P52480	Pyruvate kinase PKM	57.84	531	11	0.19	11	1.000
RMP	Q3TLD5	Unconventional prefoldin RPB5 interactor	59.08	531	11	0.19	11	1.000
PIHD1	Q9CQJ2	PIH1 domain-containing protein 1	32.21	290	6	0.19	6	1.000
NCKP1	P28660	Nck-associated protein 1	128.78	1128	23	0.18	23	1.000
HS74L	P48722	Heat shock 70 kDa protein 4L	94.38	838	17	0.18	16	0.941
DCLK1	Q9JLM8	Serine/threonine-protein kinase DCLK1	84.15	756	15	0.18	15	1.000
ALDOA	P05064	Fructose-bisphosphate aldolase A	39.35	364	7	0.18	7	1.000
MTAP2	P20357	Microtubule-associated protein 2	199.13	1828	34	0.17	34	1.000
S12A5	Q91V14	Solute carrier family 12 member 5	126.27	1138	21	0.17	21	1.000
GSTP1	P19157	Glutathione S-transferase P 1	23.61	210	4	0.17	4	1.000
F8VPN4	F8VPN4	4-alpha-glucanotransferase	174.28	1532	28	0.16	28	1.000
ENAH	Q03173	Protein enabled homolog	85.84	802	14	0.16	14	1.000
TRI46	Q7TNM2	Tripartite motif-containing protein 46	83.43	759	13	0.16	13	1.000
ODP2	Q8BMF4	Dihydrolipoyllysine-residue acetyltransferase component of pyruvate dehydrogenase complex, mitochondrial	67.94	642	11	0.16	11	1.000
SNTB2	Q61235	Beta-2-syntrophin	56.38	520	9	0.16	9	1.000
PYC	Q05920	Pyruvate carboxylase, mitochondrial	129.68	1178	20	0.15	20	1.000
DDX3L	P16381	Putative ATP-dependent RNA helicase Pl10	73.14	660	11	0.15	11	1.000
HS12A	Q8K0U4	Heat shock 70 kDa protein 12A	74.87	675	11	0.15	11	1.000
ROA3	Q8BG05	Heterogeneous nuclear ribonucleoprotein A3	39.65	379	6	0.15	6	1.000
HNRPL	Q8R081	Heterogeneous nuclear ribonucleoprotein L	63.96	586	9	0.14	9	1.000
CPNE1	Q8C166	Copine-1	58.89	536	8	0.14	8	1.000
ELAV4	Q61701	ELAV-like protein 4	42.37	385	6	0.14	6	1.000

Gene	Uniprot ID	Description	MW (KDa)	Sequence Length (AA)	Counts (Total)	Counts (Norm to MW)	Unique Reads (Total)	Unique (Frac)
DSG1A	Q61495	Desmoglein-1-alpha	114.6	1057	15	0.13	15	1.000
G3X972	G3X972	Sec24-related gene family, member C (S. cerevisiae)	118.58	1096	15	0.13	15	1.000
Q8CFX3	Q8CFX3	Protocadherin 1	112.41	1038	15	0.13	15	1.000
CSKP	O70589	Peripheral plasma membrane protein CASK	105.11	926	14	0.13	14	1.000
PSMD2	Q8VDM4	26S proteasome non-ATPase regulatory subunit 2	100.2	908	13	0.13	13	1.000
HSP74	Q61316	Heat shock 70 kDa protein 4	94.13	841	12	0.13	11	0.917
SV2A	Q9JIS5	Synaptic vesicle glycoprotein 2A	82.65	742	11	0.13	11	1.000
GEPH	Q8BUV3	Gephyrin	83.28	769	11	0.13	11	1.000
NDUS1	Q91VD9	NADH-ubiquinone oxidoreductase 75 kDa subunit, mitochondrial	79.78	727	10	0.13	10	1.000
CAND1	Q6ZQ38	Cullin-associated NEDD8-dissociated protein 1	136.33	1230	17	0.12	17	1.000
PKP1	P97350	Plakophilin-1	80.89	728	10	0.12	10	1.000
ACON	Q99KI0	Aconitate hydratase, mitochondrial	85.46	780	10	0.12	10	1.000
AMPH	Q7TQF7	Amphiphysin	75.01	686	9	0.12	9	1.000
2AAA	Q76MZ3	Serine/threonine-protein phosphatase 2A 65 kDa regulatory subunit A alpha isoform	65.32	589	8	0.12	8	1.000
BACH	Q91V12	Cytosolic acyl coenzyme A thioester hydrolase	42.54	381	5	0.12	5	1.000
TPIS	P17751	Triosephosphate isomerase	32.19	299	4	0.12	4	1.000
UBR5	Q80TP3	E3 ubiquitin-protein ligase UBR5	308.35	2792	33	0.11	33	1.000
ITIH2	Q61703	Inter-alpha-trypsin inhibitor heavy chain H2	105.93	946	12	0.11	12	1.000
SYAC	Q8BGQ7	Alanine--tRNA ligase, cytoplasmic	106.91	968	12	0.11	12	1.000
AP180	Q61548	Clathrin coat assembly protein AP180	91.85	901	10	0.11	10	1.000
DTNA	Q9D2N4	Dystrobrevin alpha	84.07	746	9	0.11	9	1.000
SYN1	O88935	Synapsin-1	74.1	706	8	0.11	7	0.875
IGG2B	P01867	Ig gamma-2B chain C region	44.26	404	5	0.11	5	1.000
SPTN1	P16546	Spectrin alpha chain, non-erythrocytic 1	284.59	2472	28	0.1	28	1.000
SRCN1	Q9QWI6	SRC kinase signaling inhibitor 1	134.86	1250	14	0.1	14	1.000

Gene	Uniprot ID	Description	MW (KDa)	Sequence Length (AA)	Counts (Total)	Counts (Norm to MW)	Unique Reads (Total)	Unique (Frac)
E9PXQ7	E9PXQ7	Protocadherin 10	115	1057	12	0.1	12	1.000
C1TC	Q922D8	C-1-tetrahydrofolate synthase, cytoplasmic	101.2	935	10	0.1	10	1.000
NCDN	Q9Z0E0	Neurochondrin	78.89	729	8	0.1	8	1.000
VATA	P50516	V-type proton ATPase catalytic subunit A	68.33	617	7	0.1	7	1.000
MAG	P20917	Myelin-associated glycoprotein	69.39	627	7	0.1	7	1.000
PP2BA	P63328	Serine/threonine-protein phosphatase 2B catalytic subunit alpha isoform	58.64	521	6	0.1	5	0.833
SAP	Q61207	Prosaposin	61.42	557	6	0.1	6	1.000
MPCP	Q8VEM8	Phosphate carrier protein, mitochondrial	39.63	357	4	0.1	4	1.000
MARCS	P26645	Myristoylated alanine-rich C-kinase substrate	29.66	309	3	0.1	3	1.000
SPTB2	Q62261	Spectrin beta chain, non-erythrocytic 1	274.22	2363	24	0.09	24	1.000
EXOC4	O35382	Exocyst complex component 4	110.54	975	10	0.09	10	1.000
NEDD4	P46935	E3 ubiquitin-protein ligase NEDD4	102.7	887	9	0.09	9	1.000
AL1L1	Q8R0Y6	Cytosolic 10-formyltetrahydrofolate dehydrogenase	98.71	902	9	0.09	7	0.778
LMNA	P48678	Prelamin-A/C	74.24	665	7	0.09	7	1.000
SFPQ	Q8VIJ6	Splicing factor, proline- and glutamine-rich	75.44	699	7	0.09	7	1.000
CATD	P18242	Cathepsin D	44.95	410	4	0.09	4	1.000
AGK	Q9ESW4	Acylglycerol kinase, mitochondrial	46.98	421	4	0.09	4	1.000
H12	P15864	Histone H1.2	21.27	212	2	0.09	2	1.000
DCTN1	O08788	Dynactin subunit 1	141.67	1281	12	0.08	12	1.000
AP3B2	Q9JME5	AP-3 complex subunit beta-2	119.19	1082	9	0.08	9	1.000
EXOC1	Q8R3S6	Exocyst complex component 1	101.89	894	8	0.08	8	1.000
E41L1	Q9Z2H5	Band 4.1-like protein 1	98.31	879	8	0.08	8	1.000
MATR3	Q8K310	Matrin-3	94.63	846	8	0.08	8	1.000
DPP6	Q9Z218	Dipeptidyl aminopeptidase-like protein 6	91.26	804	7	0.08	7	1.000
GELS	P13020	Gelsolin	85.94	780	7	0.08	7	1.000
KPCB	P68404	Protein kinase C beta type	76.75	671	6	0.08	6	1.000

Gene	Uniprot ID	Description	MW (KDa)	Sequence Length (AA)	Counts (Total)	Counts (Norm to MW)	Unique Reads (Total)	Unique (Frac)
HEM6	P36552	Oxygen-dependent coproporphyrinogen-III oxidase, mitochondrial	49.71	443	4	0.08	4	1.000
SYT1	P46096	Synaptotagmin-1	47.42	421	4	0.08	4	1.000
K2C80	Q0VBK2	Keratin, type II cytoskeletal 80	50.66	452	4	0.08	4	1.000
QCR1	Q9CZ13	Cytochrome b-c1 complex subunit 1, mitochondrial	52.85	480	4	0.08	4	1.000
GCAA	P01863	Ig gamma-2A chain C region, A allele	36.39	330	3	0.08	3	1.000
GBB1	P62874	Guanine nucleotide-binding protein G(I)/G(S)/G(T) subunit beta-1	37.38	340	3	0.08	3	1.000
RAB3C	P62823	Ras-related protein Rab-3C	25.87	227	2	0.08	2	1.000
C1QA	P98086	Complement C1q subcomponent subunit A	25.97	245	2	0.08	2	1.000
UGGG1	Q6P5E4	UDP-glucose:glycoprotein glucosyltransferase 1	176.43	1551	12	0.07	12	1.000
MAP4	P27546	Microtubule-associated protein 4	117.43	1125	8	0.07	8	1.000
PDE2A	Q922S4	cGMP-dependent 3',5'-cyclic phosphodiesterase	105.62	939	7	0.07	7	1.000
DNM1L	Q8K1M6	Dynamin-1-like protein	82.66	742	6	0.07	6	1.000
TFR1	Q62351	Transferrin receptor protein 1	85.73	763	6	0.07	6	1.000
STXB1	O08599	Syntaxin-binding protein 1	67.57	594	5	0.07	5	1.000
PDIA1	P09103	Protein disulfide-isomerase	57.06	509	4	0.07	4	1.000
CH60	P63038	60 kDa heat shock protein, mitochondrial	60.95	573	4	0.07	4	1.000
DPYL5	Q9EQF6	Dihydropyrimidinase-related protein 5	61.52	564	4	0.07	4	1.000
KCJ10	Q9JM63	ATP-sensitive inward rectifier potassium channel 10	42.43	379	3	0.07	3	1.000
C1QB	P14106	Complement C1q subcomponent subunit B	26.72	253	2	0.07	2	1.000
TENR	Q8BYI9	Tenascin-R	149.59	1358	9	0.06	9	1.000
WDR33	Q8K4P0	pre-mRNA 3' end processing protein WDR33	145.27	1330	8	0.06	8	1.000
DDB1	Q3U1J4	DNA damage-binding protein 1	126.85	1140	8	0.06	8	1.000
KIF5C	P28738	Kinesin heavy chain isoform 5C	109.27	956	7	0.06	7	1.000
ACLY	Q91V92	ATP-citrate synthase	119.73	1091	7	0.06	7	1.000

Gene	Uniprot ID	Description	MW (KDa)	Sequence Length (AA)	Counts (Total)	Counts (Norm to MW)	Unique Reads (Total)	Unique (Frac)
OGT1	Q8CGY8	UDP-N-acetylglucosamine--peptide N-acetylglucosaminyltransferase 110 kDa subunit	116.95	1046	7	0.06	7	1.000
ARHG2	Q60875	Rho guanine nucleotide exchange factor 2	111.97	985	7	0.06	7	1.000
OPA1	P58281	Dynamin-like 120 kDa protein, mitochondrial	111.34	960	7	0.06	7	1.000
IMB1	P70168	Importin subunit beta-1	97.18	876	6	0.06	6	1.000
CNNM2	Q3TWN3	Metal transporter CNNM2	96.7	875	6	0.06	6	1.000
ITCH	Q8C863	E3 ubiquitin-protein ligase Itchy	98.99	864	6	0.06	5	0.833
PDC6I	Q9WU78	Programmed cell death 6-interacting protein	96.02	869	6	0.06	6	1.000
TGM3	Q08189	Protein-glutamine gamma-glutamyltransferase E	77.31	693	5	0.06	5	1.000
CPSF3	Q9QXK7	Cleavage and polyadenylation specificity factor subunit 3	77.5	684	5	0.06	5	1.000
SYN2	Q64332	Synapsin-2	63.37	586	4	0.06	3	0.750
ODPX	Q8BKZ9	Pyruvate dehydrogenase protein X component, mitochondrial	54	501	3	0.06	3	1.000
QCR2	Q9DB77	Cytochrome b-c1 complex subunit 2, mitochondrial	48.23	453	3	0.06	3	1.000
RUVB2	Q9WTM5	RuvB-like 2	51.11	463	3	0.06	3	1.000
D4AFX7	D4AFX7	J domain-containing protein	255.06	2248	12	0.05	12	1.000
A2MG	Q6GQT1	Alpha-2-macroglobulin-P	164.35	1474	9	0.05	9	1.000
VIGLN	Q8VDJ3	Vigilin	141.74	1268	7	0.05	7	1.000
HYOU1	Q9JKR6	Hypoxia up-regulated protein 1	111.18	999	6	0.05	6	1.000
EPHA4	Q03137	Ephrin type-A receptor 4	109.81	986	6	0.05	6	1.000
VPP1	Q9Z1G4	V-type proton ATPase 116 kDa subunit a1	96.47	839	5	0.05	5	1.000
VPS35	Q9EQH3	Vacuolar protein sorting-associated protein 35	91.71	796	5	0.05	5	1.000
AKAP5	D3YVF0	A-kinase anchor protein 5	79.4	745	4	0.05	4	1.000
PERM	P11247	Myeloperoxidase	81.18	718	4	0.05	4	1.000
TAU	P10637	Microtubule-associated protein tau	76.24	733	4	0.05	4	1.000
R3HCL	Q8BJM3	Coiled-coil domain-containing protein R3HCC1L	84.48	775	4	0.05	4	1.000

Gene	Uniprot ID	Description	MW (KDa)	Sequence Length (AA)	Counts (Total)	Counts (Norm to MW)	Unique Reads (Total)	Unique (Frac)
ADDA	Q9QYC0	Alpha-adducin	80.65	735	4	0.05	4	1.000
CSDE1	Q91W50	Cold shock domain-containing protein E1	88.79	798	4	0.05	4	1.000
GABT	P61922	4-aminobutyrate aminotransferase, mitochondrial	56.45	500	3	0.05	3	1.000
VATB2	P62814	V-type proton ATPase subunit B, brain isoform	56.55	511	3	0.05	3	1.000
Q91VA7	Q91VA7	Isocitrate dehydrogenase [NAD] subunit, mitochondrial	42.19	384	2	0.05	2	1.000
MYH10	Q61879	Myosin-10	228.99	1976	9	0.04	7	0.778
RRBP1	Q99PL5	Ribosome-binding protein 1	172.88	1605	7	0.04	7	1.000
UBP7	Q6A4J8	Ubiquitin carboxyl-terminal hydrolase 7	128.47	1103	5	0.04	5	1.000
NAC2	Q8K596	Sodium/calcium exchanger 2	100.71	921	4	0.04	4	1.000
SYIM	Q8BIJ6	Isoleucine--tRNA ligase, mitochondrial	112.8	1012	4	0.04	4	1.000
LONM	Q8CGK3	Lon protease homolog, mitochondrial	105.84	949	4	0.04	4	1.000
RN216	P58283	E3 ubiquitin-protein ligase RNF216	97.68	853	4	0.04	4	1.000
ICAM5	Q60625	Intercellular adhesion molecule 5	96.94	917	4	0.04	4	1.000
NLGN3	Q8BYM5	Neuroligin-3	91.16	825	4	0.04	3	0.750
NUCL	P09405	Nucleolin	76.72	707	3	0.04	3	1.000
HNRPQ	Q7TMK9	Heterogeneous nuclear ribonucleoprotein Q	69.63	623	3	0.04	3	1.000
PDIA6	Q922R8	Protein disulfide-isomerase A6	48.1	440	2	0.04	2	1.000
PLCB1	Q9Z1B3	1-phosphatidylinositol 4,5-bisphosphate phosphodiesterase beta-1	138.4	1216	4	0.03	4	1.000
NRCAM	Q810U4	Neuronal cell adhesion molecule	138.52	1256	4	0.03	4	1.000
CO6A1	Q04857	Collagen alpha-1(VI) chain	108.49	1025	3	0.03	3	1.000
PSMD1	Q3TXS7	26S proteasome non-ATPase regulatory subunit 1	105.73	953	3	0.03	3	1.000
INP4A	Q9EPW0	Inositol polyphosphate-4-phosphatase type I A	105.54	939	3	0.03	3	1.000
ITIH4	A6X935	Inter alpha-trypsin inhibitor, heavy chain 4	104.66	942	3	0.03	3	1.000
SYMC	Q68FL6	Methionine--tRNA ligase, cytoplasmic	101.43	902	3	0.03	3	1.000
SE1L1	Q9Z2G6	Protein sel-1 homolog 1	88.34	790	3	0.03	3	1.000

Gene	Uniprot ID	Description	MW (KDa)	Sequence Length (AA)	Counts (Total)	Counts (Norm to MW)	Unique Reads (Total)	Unique (Frac)
FLNA	Q8BTM8	Filamin-A	281.22	2647	5	0.02	5	1.000
IF4G3	Q80XI3	Eukaryotic translation initiation factor 4 gamma 3	174.89	1579	4	0.02	4	1.000
ZMYM2	Q9CU65	Zinc finger MYM-type protein 2	154.64	1376	3	0.02	3	1.000
CEIP2	Q5FWI3	Cell surface hyaluronidase	153.8	1383	3	0.02	3	1.000
CAPS1	Q80TJ1	Calcium-dependent secretion activator 1	153.11	1355	3	0.02	3	1.000
ASTN1	Q61137	Astrotactin-1	144.88	1302	3	0.02	3	1.000
SYIC	Q8BU30	Isoleucine--tRNA ligase, cytoplasmic	144.27	1262	3	0.02	3	1.000
SMRC2	Q6PDG5	SWI/SNF complex subunit SMARCC2	132.6	1213	3	0.02	3	1.000
SRGP3	Q812A2	SLIT-ROBO Rho GTPase-activating protein 3	124.42	1099	3	0.02	3	1.000
APBA2	P98084	Amyloid-beta A4 precursor protein-binding family A member 2	82.76	750	2	0.02	2	1.000
P3H1	Q3V1T4	Prolyl 3-hydroxylase 1	83.65	739	2	0.02	2	1.000
INT3	Q7TPD0	Integrator complex subunit 3	117.94	1041	2	0.02	2	1.000
IDE	Q9JHR7	Insulin-degrading enzyme	117.77	1019	2	0.02	2	1.000
XPO2	Q9ERK4	Exportin-2	110.45	971	2	0.02	2	1.000
COPB	Q9JIF7	Coatomer subunit beta	107.06	953	2	0.02	2	1.000
C1TM	Q3V3R1	Monofunctional C1-tetrahydrofolate synthase, mitochondrial	105.73	977	2	0.02	2	1.000
CTDP1	Q7TSG2	RNA polymerase II subunit A C-terminal domain phosphatase	104.55	960	2	0.02	2	1.000
EXOC2	Q9D4H1	Exocyst complex component 2	103.96	924	2	0.02	2	1.000
AUXI	Q80TZ3	Putative tyrosine-protein phosphatase auxilin	102.3	938	2	0.02	2	1.000
EP15R	Q60902	Epidermal growth factor receptor substrate 15-like 1	99.31	907	2	0.02	2	1.000
GRIA2	P23819	Glutamate receptor 2	98.66	883	2	0.02	2	1.000
EIF3B	Q8JZQ9	Eukaryotic translation initiation factor 3 subunit B	91.37	803	2	0.02	2	1.000
AP1G1	P22892	AP-1 complex subunit gamma-1	91.35	822	2	0.02	2	1.000

Gene	Uniprot ID	Description	MW (KDa)	Sequence Length (AA)	Counts (Total)	Counts (Norm to MW)	Unique Reads (Total)	Unique (Frac)
M4K2	Q61161	Mitogen-activated protein kinase kinase kinase kinase 2	91.26	821	2	0.02	2	1.000
SF3A1	Q8K4Z5	Splicing factor 3A subunit 1	88.54	791	2	0.02	2	1.000
HGS	Q99LI8	Hepatocyte growth factor-regulated tyrosine kinase substrate	86.01	775	2	0.02	2	1.000
E9PWQ3	E9PWQ3	Collagen, type VI, alpha 3	353.93	3284	4	0.01	4	1.000
DYHC1	Q9JHU4	Cytoplasmic dynein 1 heavy chain 1	532.04	4644	4	0.01	4	1.000
ANK2	Q8C8R3	Ankyrin-2	426.26	3898	4	0.01	4	1.000
PLXA4	Q80UG2	Plexin-A4	212.56	1893	2	0.01	2	1.000
TRIO	Q0KL02	Triple functional domain protein	347.86	3102	2	0.01	2	1.000
USP9X	P70398	Probable ubiquitin carboxyl-terminal hydrolase FAF-X	290.71	2559	2	0.01	2	1.000
SPT6H	Q62383	Transcription elongation factor SPT6	199.08	1726	2	0.01	2	1.000
ADCY5	P84309	Adenylate cyclase type 5	139.12	1262	2	0.01	2	1.000
MADD	Q80U28	MAP kinase-activating death domain protein	175.18	1577	2	0.01	2	1.000
SYEP	Q8CGC7	Bifunctional glutamate/proline--tRNA ligase	170.08	1512	2	0.01	2	1.000
LPPRC	Q6PB66	Leucine-rich PPR motif-containing protein, mitochondrial	156.61	1392	2	0.01	2	1.000
TPP2	Q64514	Tripeptidyl-peptidase 2	139.88	1262	2	0.01	2	1.000
GSLG1	Q61543	Golgi apparatus protein 1	133.73	1175	2	0.01	2	1.000